
MUMERICAL INVESTIGATIONS OF SPALLING IN
CONCRETE SUBJECTED TO FIRE

ABBAS MOHAMMED ABUBAKER

Thesis submitted for the degree of
Doctor of Philosophy



*School of Engineering
Geotechnics and Structures
Newcastle University
Newcastle upon Tyne
United Kingdom*

September 2022

Acknowledgments

First of all I would like to thank my first supervisor Dr. Colin T. Davie for his kind and generous support from the beginning of my PhD studies to date. He has been not only an ideal supervisor for me but also an academic role model throughout last four years. He never let me to feel abandoned, distressed, and unmotivated. I am very grateful for having him in this stage of my academic life and wish him best lucks in his life.

I want to thank Dr Enrico Masoero and Dr Amir Mofidi as second supervisors at early stages of my study for their contribution in my work.

Many thanks for my mother, my wife Shaida Al-Dalo, and my two lovely kids San and Lano for their continuous care and love and being patient with me throughout my studies.

I should thank all my colleagues at VOID Bureau for Engineering Consultancy especially Mr. Aryan M. Ahmad for his continuous logistic support relating to the bureau works we have undertaken together.

I would like to express my thanks to my close friends Mr. Hemen M. Ali, Dr. Jamal A. Hussein, Dr. Ali M. Salih, Dr. Hadi M. Ismail, for their logistic supports during early stages of my arrival in the UK.

Thanks for all my friends and family members who have been in contact with me throughout my study time and show their supports in different ways.

I want to thank Dr. Ako R. Hama and Prof. Jalal A. Saeed for their support as referees at first stages of my PhD applications.

Dedication

To my father's soul, I owe and miss him forever.

To my mother who has suffered to take care of us.

Abstract

Spalling of concrete subjected to elevated temperatures remains a controversial research area despite the pursuance of experimental investigation for more than a century. To date, experimental investigations have mostly been aimed at identifying spalling types, factors affecting spalling and methods to reduce spalling risk. However, numerous questions remain due to varied and sometimes contradictory results.

To address these inconsistencies, this work aimed to investigate how the test methodologies themselves may influence the results and spalling behaviour. To do this, a numerical model was developed in ABAQUS and employed to simulate a consistent set of experiments conducted with different test configurations. The study was extended to investigate factors such as sample size, restraints (including mechanical, self-restraint via the so called 'cold ring' effect and applied load) and load intensity.

Fundamentally, it was found that the boundary conditions of the test can have a significant influence on spalling behaviour due to their effect on the stress state in the samples. While mechanically restraining a sample can improve resistance to spalling, samples with the entire thickness restrained were found to have less resistance than those with only part of the thickness restrained. However, samples restrained through loading applied prior to heating tended to spall earlier than samples restrained mechanically. Increasing load intensity was found to worsen conditions for spalling while the position and eccentricity of loading can significantly vary the compressive regime in a sample. The influence of an unheated 'cold ring' around the sample was found to vary considerably with test configuration and in some cases had no effect on spalling. Sample thickness was found to be more significant, with thicker samples having less resistance to spalling than more flexible thinner samples.

In conclusion, reflecting real conditions relating to size, loading and restraints in the test set up is strongly recommended to ensure representative results.

Publications

- A. M. Abubaker and C. T. Davie, “A generalised model for direct prediction of stresses in concrete at high temperatures,” Magazine of Concrete Research, pp. 1–34, 2022.
- A Abubaker and C. Davie, “Underlying factors controlling experimental test outputs for concrete samples subjected to elevated temperatures”, accepted for 7th International Workshop on Concrete Spalling due to Fire Exposure, Berlin-Germany, October 2022
- A Abubaker and C. Davie, “Underlying physical phenomena controlling concrete spalling at elevated temperature : numerical investigations of spalling sensitivity to restraints“ (Under review)
- A Abubaker and C. Davie, “Underlying physical phenomena controlling concrete spalling at elevated temperature: numerical investigations of spalling sensitivity to sample size and test setup“, (in preparation)
- A Abubaker and C. Davie, “Underlying physical phenomena controlling concrete spalling at elevated temperature :numerical Investigations of spalling sensitivity to load intensity and testing set up “, (in preparation)
- A Abubaker and C. Davie, “Underlying physical phenomena controlling concrete spalling at elevated temperature : numerical investigations of spalling sensitivity to cold rim”, (in preparation)

Contents

1	Introduction	1
1.1	Introduction	1
1.2	Aims and objectives	2
1.3	Methodologies	2
1.4	Thesis novelty	4
1.5	Outline of the dissertation	5
2	Literature Review	7
2.1	Definition and historical overview of concrete spalling	7
2.2	Types of concrete spalling	9
2.3	Mechanisms of concrete spalling	10
2.4	Classification of literature concrete spalling tests	13
2.4.1	Heated unrestrained samples	13
2.4.2	Heated restrained samples	16
2.4.3	Loaded samples	21
2.4.4	Concluding remarks on experimental tests available in the literature	27
2.5	Modelling of concrete at high temperature	30
2.6	Temperature dependent properties of concrete	32
2.6.1	Concrete temperature dependent mechanical properties	32
2.6.2	Concrete temperature dependent thermal properties	39
2.6.3	Concrete temperature dependent deformation properties	42
2.6.4	Concluding remarks on modelling of concrete at high temperatures	45
3	Coupled Thermo-Mechanical Model	47
3.1	Introduction	47
3.2	ABAQUS FE model constitutive equations	47
3.2.1	Material properties	47
3.2.2	Modified transient strain equation	50
3.2.3	Concrete damage plasticity model	52
3.3	Model calibration	54
3.3.1	B Samples	57
3.3.2	A Samples	58
3.3.3	D Sample	60
3.3.4	Comparison of stress developed in A and D Samples	61
3.4	Conclusion	62

4	Preliminary Analyses and Preparations	64
4.1	Introduction	64
4.2	Common concrete spalling test setups	64
4.3	Mesh sensitivity analysis	65
4.4	Observed temperature and spalling of the heated samples	66
4.5	Hygro-thermo damage sensitivity analysis of concrete samples under effects of heating	67
5	Effects of Restraint on Concrete Behaviour and Spalling at High Temperatures	71
5.1	Introduction	71
5.2	Restraint configurations	71
5.3	Analysis results and discussions	72
5.3.1	Unloaded rectangular samples	73
5.3.2	Ring samples	78
5.3.3	Uniaxially loaded square samples	83
5.3.4	Biaxially loaded samples	88
5.4	Conclusions	91
6	Effects of Sample Size on Concrete Behaviour and Spalling at High Temperatures	94
6.1	Introduction	94
6.2	Size configurations	95
6.3	Analysis results and discussions	96
6.3.1	(A) Samples- unloaded unrestrained	97
6.3.2	(B) Samples - unloaded partially restrained	101
6.3.3	(C) Samples - eccentrically loaded samples	106
6.4	Conclusions	112
7	Effects of Load on Concrete Behaviour and Spalling at High Temperatures	114
7.1	Introduction	114
7.2	Load configurations	115
7.3	Analysis results and discussions	117
7.3.1	Axially loaded samples	117
7.3.2	Passively restrained rectangular Sample	121
7.3.3	Eccentrically loaded samples	125
7.4	Conclusions	129
8	Effects of Cold Rim on Concrete Behaviour and Spalling at High Temperatures	131
8.1	Introduction	131
8.2	Cold rim configurations	131
8.3	Analysis results and discussions	133
8.3.1	Unloaded restrained ring sample	134
8.3.2	Unloaded rectangular slabs	139

8.3.3	Uniaxially loaded slab	146
8.3.4	Biaxially loaded slabs	149
8.4	Conclusions	153
9	Conclusions	155

List of Tables

2.1	Concrete thermal conductivity models	39
2.2	Concrete specific heat models	40
2.3	Concrete mass loss models	40
3.1	Temperature dependent thermal properties	49
3.2	Detail of samples used in the model validation	56
4.1	Selected samples to be investigated	65

List of Figures

2.1	a) Rectangular sample tested in lab b) Wall of a garage after exposing to fire . . .	7
2.2	Types of spalling a) Explosive spalling, b) Surface spalling, c) Corner spalling .	9
2.3	Mechanisms of concrete spalling at elevated temperatures	11
2.4	Temperature range in thermo-chemical spalling mechanism	13
2.5	a) Non structural thick sample b) Non structural ring sample c) Structural sample-column d) Cylinder sample e) Entire building test f) Structural sample-beam g) Flat slab with column	14
2.6	Test setup of unrestrained unloaded sample	15
2.7	Various restrained samples from a) Large ring sample, b) Large ring sample test configuration, c) Small ring sample, and d) Rectangular prism sample	19
2.8	a) Concrete sample details with embedded pressure–temperature sensors, and b) The biaxial loading system configurations	27
2.9	Comparison of concrete compressive strength degradation models at high temperature	33
2.10	Concrete tensile strength degradation models at high temperature	35
2.11	Concrete elastic modulus degradation models at high temperatures	36
2.12	Comparison of concrete stress strain relationships at various temperatures . . .	39
2.13	Different thermal conductivity models from literature	41
2.14	Different thermal conductivity models from literature	41
2.15	Different thermal conductivity models from literature	42
2.16	Different expansion coefficient from literature	43
2.17	Comparison of different transient thermal models from literature	45
3.1	Spring model to represent end restraints used by Nielsen	50
3.2	Spring model with external loading	51
3.3	Yield surface in plane stress used by CDP model in ABAQUS	52
3.4	Behaviour of concrete under uniaxial compressive stress	53
3.5	Behaviour of concrete under uniaxial tension stress	54
3.6	Mesh sensitivity analysis	55
3.7	Schematic diagram of the samples used in the validation	56
3.8	Model and experimental results of B samples	58
3.9	Model and experimental results of B samples with 0.1 linear limit	58
3.10	Model and experimental results of A samples	60
3.11	Model and experimental results of D samples	61
3.12	Developed pure mechanical stress for D and A samples	62
4.1	Selected samples and test methodologies for parametric studies	66

4.2	Max principal stress at different heating times considering different mesh sizes through depth of a,b) S1 small unrestrained sample, c,d) S2 small restrained sample	67
4.3	a Temperature Profile for S1 Sample with 42MPa Compressive Strength at 30mm Depth from the Heated Surface b Temperature Profile for S6 Sample with 70MPa Compressive Strength at 50mm Depth from the Heated Surface	68
4.4	Spalling time and Maximum spalling depth for the Selected Samples a) Samples with 42MPa compressive Strength b) Samples with 70MPa compressive Strength	69
4.5	Gas Pressure through thickness of S5 Sample from Table 4.1 for different porosity an permeability values at spalling time (480 seconds)	70
5.1	Restraint configurations showing heated areas, mechanical restraints and loading	72
5.2	3D section showing the temperature profile in the unrestrained slab (configuration (A) at time of spalling (660 s)	73
5.3	3D sections of minimum and maximum principal stress profiles at time of spalling in a), b) configuration (A), c), d) configuration (B) & e), f) configuration (C)	74
5.4	a) Minimum and b) maximum principal stress profiles through the thickness of the rectangular slabs at center (configurations (A, B & C) at different times	75
5.5	3D sections of in-plane and out of plane stress profiles at time of spalling in a), b) configuration (A), c), d) configuration (B) & e), f) configuration (C)	76
5.6	Profiles across the centre line of the heated face showing displacements perpendicular to the face for restraint configurations (A, B & C) at different times	78
5.7	3D section showing the temperature profile in the ring slab (configuration (C) at closest time step to time of spalling (540 s)	79
5.8	3D sections of minimum and maximum principal stress profiles as close as possible to time of spalling in a), b) configuration (D) Case 1 & c), d) configuration (D) Case 2	80
5.9	a) Minimum and b) maximum principal stress profiles through the centreline thickness of the ring sample (configurations (D) Cases 1 & 2 at different times	81
5.10	3D sections of in-plane and out of plane stress profiles as close as possible to time of spalling in a), b) configuration (D) Case 1 & c), d) configuration (D) Case 2	82
5.11	3D Views showing developed in-plane stresses at the exposed surface of the ring samples under different testing scenario from Figure 5.1-D at time 1200 s	82
5.12	3D Views showing developed in-plane stresses at the exposed surface of the ring sample for scenario extended from Figure 5.11 at time 1200Sec	83
5.13	3D section showing the temperature profile in the uniaxially loaded slab (configurations (E) & (F) at time of spalling (360 s)	84
5.14	a,b Minimum and maximum principal stresses of E sample at the nearest time step to the first spalling time, c,d Minimum and maximum principal stresses of F sample at the nearest time step to the first spalling time	85

5.15	(a) Minimum and (b) Maximum principal stresses through thickness of the axially loaded square samples from Figure 5.1-E,F at different heating times	86
5.16	(a) Minimum and (b) Maximum principal stresses at mid-height, 60 mm from edge through the thickness of the axially loaded square samples (Configurations (E & F)) at time of spalling	87
5.17	a,b In-plane and out of plane stress profiles of E sample at the nearest time step to the first spalling time, c,d In-plane and out of plane stress profiles of F sample at the nearest time step to the first spalling time	88
5.18	3D section temperature Profile of the biaxially loaded samples with and without slits- G configuration	89
5.19	Temperature profiles at different depths of the bi-axially loaded sample	89
5.20	Minimum principal stresses through thickness of (G) configurations at different times	90
5.21	Simulated displacement results of a central point at the exposed surface through time for (G) configurations	91
6.1	Different sample sizes with various boundary conditions	97
6.2	a Original test set up of sample (A) with 400 mm thickness, b Temperature profile of sample (A) at first spalling incidence, and c, d Minimum and maximum principal stress at first spalling incidence respectively	98
6.3	a,c,e Minimum and b,d,f Maximum principal stress profiles through the thickness of the samples at their centre line, for all three sample thicknesses at different times	99
6.4	Displacement in meters toward the heating source: a,b,c for (A) Samples, and d,e,f for (B) Samples having 100mm, 200mm, 400mm thickness respectively at time step 720 seconds	100
6.5	Developed in-plane stress at the heated surface: a,b,c for the (A) samples, and d,e,f for the (B) samples having 100mm, 200mm, 400mm thickness respectively at time step 720 seconds	101
6.6	a Original test set up of sample (B) with 400 mm thickness, b Temperature profile of sample (B) at 620 seconds, c Minimum principal stress profile after 620 seconds, and d Maximum principal stress profile after 620 seconds	102
6.7	a,c,e Minimum and b,d,f Maximum principal stress profiles through the thickness of the samples at their centre line, for all three sample thicknesses at different times	103
6.8	Test set up and temperature profile of (C) sample at nearest time step to spalling	106
6.9	a,b,c,d Minimum principal stress of the (C) samples, and e,f,g,h Minimum principal stress of the (D) samples at different heating times through their thickness, having 1.30m, 3.50m, 4.00m, 6.00m heated span respectively	107
6.10	a,b,c,d Maximum principal stress of the (C) samples, and e,f,g,h Maximum principal stress of the (D) samples at different heating times through their thickness, having 1.30m, 3.50m, 4.00m, 6.00m heated span respectively	108

6.11	a,b,c,d Displacement of the (C) samples, and e,f,g,h Displacements of the (D) samples toward the heating source over the samples' height at different heating times, for samples with 1.30m, 3.50m, 4.00m, 6.00m heated span	109
6.12	a,b,c,d Developed in-plane stresses of (C) samples, and e,f,g,h Developed in-plane stresses of (D) samples over the height of the different size samples, with the direction of the initial applied load, at different heating times	110
7.1	Work program and sample boundary conditions	115
7.2	a,b,c Minimum principal stress and d,e,f Maximum principal stress at spalling time for A,B,C configurations shown in Figure 7.1 loaded to 12% of their compressive strength	118
7.3	a,b,c Minimum principal stress and d,e,f Maximum principal stress through thickness of the square sample loaded to 12%, 50%, 80% of their compressive strengths respectively	119
7.4	a,b Minimum principal stress and c,d Maximum principal stress at spalling time for D,E configurations shown in Figure 7.1	123
7.5	a Minimum principal stress and b Maximum principal stress through thickness of the restrained sample at different heating times	124
7.6	In-plane stresses at the exposed surface along a central axis with the length of the sample for restrained samples (D and E samples shown in Figure 7.1) at different time steps	125
7.7	Test set up and temperature profile of (F) Sample at nearest time step to spalling	126
7.8	a Minimum principal stress, and b Maximum principal stress of through thickness of the eccentrically loaded samples	127
7.9	Displacement at the exposed surface along a central axis passing through the height of the samples with front and rear eccentric loads at different time steps	128
8.1	Cold rim configurations showing heated areas, mechanical restraints, loading, and different hypothetical test scenarios	132
8.2	a) Temperature profile in time, 50 mm from the heated surface of the ring sample (configuration (A)), b) 3D section showing the temperature profile in the ring slab (configuration (A) at closest time step to time of spalling (540 s)	134
8.3	3D sections of minimum and maximum principal stress profiles as close as possible to time of spalling in a), b) configuration (A) Case 1 & c), d) configuration (A) Case 2	135
8.4	a) Minimum and b) maximum principal stress profiles through the centreline thickness of the ring sample (configurations (D) Cases 1 & 2 at different times .	136
8.5	In-plane stress at the exposed surface of A samples Case 1 & Case 2 at different times	138
8.6	In-plane stress as close as possible to time of spalling at the exposed surface of A samples a) Case 1, b) Case 2, c) Case 3, & d) Case 4	139

8.7	3D sections of minimum and maximum principal stress profiles as close as possible to time of spalling in a), b) configuration (B) Case 1 & c), d) configuration (B) Case 2	140
8.8	3D sections of minimum and maximum principal stress profiles as close as possible to time of spalling in a), b) configuration (C) Case 1 & c), d) configuration (C) Case 2	141
8.9	a) Minimum and b) maximum principal stress profiles through the centreline thickness of the B and C samples (Cases 1 & 2) at different times	142
8.10	In-plane stress at the exposed surface of a) B Samples Case 1 & Case 2 b) C samples for Case 1 & Case 2 at different times	143
8.11	In-plane stress as close as possible to time of spalling at the exposed surface of B samples a) Case 1, b) Case 2, c) Case 3, & d) Case 4	144
8.12	In-plane stress as close as possible to time of spalling at the exposed surface of C samples a) Case 1, b) Case 2, c) Case 3, & d) Case 4	145
8.13	a) 3D section showing the temperature profile in D sample without cold rim at closest time step to time of spalling (364 s), b) 3D section showing the temperature profile in D sample with cold at closest time step to time of spalling (351 s)	147
8.14	3D sections of minimum and maximum principal stress profiles as close as possible to time of spalling in a), b) configuration (D) without cold rim & c), d) configuration (D) with cold rim	148
8.15	a) Minimum and b) maximum principal stress profiles through the centreline thickness of the D samples with and without cold rims	149
8.16	Exposed surface displacements a) toward the heating source , b) transverse to the uniaxial loading direction for sample with no cold rim, and c) toward the heating source, d) transverse to the uniaxial loading direction for sample with cold rim .	150
8.17	a,b) 3D section temperature profile of the E samples with and without slits, c) Temperature profiles at different depths of the sample, and d) Sagging and hogging phase displacement of a central point at the exposed surface in time for the both tested E samples	151
8.18	Simulated displacement results of a central point at the exposed Surface in time for different configurations of the E sample group	151
8.19	Minimum principal stresses through thickness in times for a) Samples without slits, b) Samples with slits, c) Samples with cold rims, and d) Samples without cold rims	152

Chapter 1

Introduction

1.1 Introduction

Disintegration by spalling phenomenon is a devastating concrete failure upon its exposure to elevated temperatures. It affects crucially load bearing capacity of structural elements due to impairing strength of the concrete and exposing embedded reinforcements to the heating, thereby potential failure of the structure. Concrete exposure to elevated temperatures may be due to unanticipated accidents such as fire or due to functional requirements of the structures such as in nuclear plants and other industrial factories where heating is required for the production. Whatever the reason would be and considering the abrupt and continuous worldwide demand on construction starting from last century, thorough understanding of concrete behaviour under elevated temperatures has become a modern crucial requirement to save lives and assets in the same time.

It has been more than a century since identifying this failure and investigations have been pursued extensively in this area. Despite of undertaking numerous theoretical and experimental investigations, still there is no consensus among researchers regarding the concrete spalling due to involvement of numerous influencing factors and so many controversial questions. Regarding theoretical investigations, despite of developing abundant of models to capture the complex behaviour of the concrete when heated still many concerns in coupled interactions between chemical reactions and mechanical damages remain unsolved and debatable. On the other hand, results from experimental works have been inconclusive due to different and even contradicted outputs regarding the spalling. Therefore this area has remained an open research area theoretically and experimentally.

In this thesis a series of state of the art investigations have been conducted seeking for identifying reasons behind the lack of consensus regarding concrete behaviour and its spalling at elevated temperatures. Underlying influencing parameters, rather than those relating to the concrete properties as a material, have been highlighted and found to have crucial effects in controlling concrete behaviour and spalling, and thus test outcomes. This has been achieved through investigating parameters relating to boundary conditions, sample shape and size, load configuration, and other test related details. To achieve this, parametric studies have been conducted considering different experimental tests from the literature utilizing a sophisticated ABAQUS model newly developed in this work.

1.2 Aims and objectives

The aim of this thesis is to discover whether/how underlying physical phenomena rather than concrete properties relating to the test methodologies can control behaviour and spalling of concrete under elevated temperatures. The parameters include sample size, restraint types, degree of restraint, mechanical characteristics of the restraint, load types, load intensity, details of the load application (uniaxial or biaxial), load location with respect to the heating (eccentricity), and other test details relating to friction and fixity while the load applied between the loading platens at top and bottom of the sample.

The objectives of the thesis are

1. To identify and classify the most common literature test methodologies relating to concrete behaviours and spalling under effects of elevated temperatures
2. To select the most common methodologies to be investigated in details
3. To develop and validate a sophisticated numerical model capable of capturing coupled thermo mechanical behaviours of concrete under the effects of loads and elevated temperatures considering different boundary conditions.
4. To highlight the most important parameters relating to test methodologies which can significantly affect concrete behaviours and its spalling when subjected to elevated temperatures.
5. To determine effects of the each highlighted parameters: sample size, restraint types, degree of restraint, mechanical characteristics of the restraint, load types, load intensity, details of the load application (uniaxial or biaxial), load location with respect to the heating (eccentricity), and other test details relating to friction and fixity while the load applied between the loading platens at top and bottom of the sample on concrete behaviour and spalling when subjected to heating under different scenarios.
6. To compare the results of the different scenarios in terms of stress and displacement states
7. To conclude how the investigated parameters control test outputs

1.3 Methodologies

Since the nature of this doctoral thesis is to investigate, through parametric studies, different key parameters affecting concrete behaviour and spalling at elevated temperatures, each parameter has been dealt with separately. Each parameter has been investigated thoroughly in a separate chapter utilizing its own methodology presented there, however there is a holistic methodology based on which the entire thesis inventions have been conducted. This can be summarised as follow :

1. A thermo-mechanical finite element model in the framework of ABAQUS utilizing the concrete damage plasticity has been developed (all details are in Chapter 3)

2. A set of temperature dependent concrete property models from the literature have been incorporated into the ABAQUS model utilizing a MATLAB code developed for the data preparation. Furthermore, a novel numerical model to account for transient strain has been developed and incorporated into the ABAQUS model through modifying temperature dependant stress strain curve of concrete. Then the reliability of the whole developed ABAQUS model has been validated through recapturing a set of experimental results in terms of temperature, stresses, and displacements (all details are in Chapter 3).
3. A set of experimental tests from the literature have been selected to be adopted in the parametric studies throughout this thesis. The choices have been decided carefully to cover the most important parameters which are known to have effects on concrete behaviour and spalling when heated and intended to be investigated in this thesis. That is to include parameters like sample size, various types of restraints, and various types of loads. (all details are in Chapter 4).
4. An investigation has been conducted through a validated model [1] to find out whether the hygro-thermo reactions in the concrete are severe enough to affect results in this thesis, which are obtained considering only thermo- mechanical actions (see Chapter 4)
5. For each selected test from the literature, the given experimental results have been simulated first through the ABAQUS model, then parametric studies have been pursued considering different scenarios under the same test conditions.
6. To investigate restraint effects, available restraint configurations in the literature including mechanical restraints and load restraints have been considered. First, observed test results have been simulated, then parametric studies have been conducted through changing the restrained area over the sample's thickness, changing stiffness of the restraints through providing cold rims around the heated area or providing slits into the unheated portions of the samples, and providing different levels of frictions between the furnace walls and the samples (or between the loading platens and the samples). Then the stress states through the thickness of the samples and displacements toward the heating source have been compared for each category under considerations. Finally, the results between different categories have also been compared (detailed methodology give in Chapter 5).
7. To investigate sample size effects, different samples tested under different test methodologies have been considered. First, observed test results have been simulated, then parametric studies through changing the thickness or the heated span of the samples have been performed, then the stress states through the thickness of the samples and displacements toward the heating source have been compared (detailed methodology give in Chapter 6).
8. To investigate load effects, different configurations from the literature, namely loads from restraints, initially applied concentric static loads, and initially applied eccentric loads have been considered. First, observed test results have been simulated, then parametric studies

have been undertaken through changing restraint stiffness, load intensity, and changing the eccentric load position from one heated face to the cold face of the samples. Then the stress states through the thickness of the samples and displacements toward the heating source have been compared for each category under considerations. Finally, the results between different categories have also been compared (detailed methodology give in Chapter 7).

9. To investigate cold rim, which is special form of restraint, available cold rim tests from the literature have been considered. First, observed test results have been simulated, then parametric studies have been performed through simulating scenarios without cold rims, changing boundary conditions, incorporating loads, and changing cold rim stiffness. Then the stress states through the thickness of the samples and displacements at the exposed surfaces have been compared for each category under considerations. Finally, the results between different categories have also been compared (detailed methodology give in Chapter 8).

1.4 Thesis novelty

The novelties throughout this thesis can be categorised into three parts

1. Proposing a new sophisticated model which is :
 - (a) valid with for various boundary conditions capable to predict stress states at different temperatures under simultaneous effects of restraints and initial applied loads
 - (b) capable to capture real behaviour of columns and shear walls in high rise buildings where these elements are restrained and loaded at the same time.
 - (c) capable to be directly applied for normal strength and high strength concrete with no modification
 - (d) applicable to assist structural engineers to quantify stresses in heated members simply without performing complex finite element analyses
2. Performing holistic investigations on structural and non structural samples from the literature considering various parameters which resulted in:
 - (a) Identifying some literature results to be test specific which can not be generalized
 - (b) Identifying and evaluating some parameters, which are not relating to material properties of concrete, affecting concrete spalling and lead to get inconsistent test results: sample size and shape, restraints, load intensity, load type, and test setup details
 - (c) Highlighting some factors have caused literature disagreements about spalling: not considering real boundary conditions, low load intensity, not representative sample thickness

3. Providing suggestions for experimental works to get accurate results:
 - (a) Sample length, unlike its thickness, can be compromised during designing test set up for concrete under effects of heating
 - (b) Considering realistic boundary conditions in lab tests is a key point to get accurate results to be used in assessing real structural members
 - (c) When eccentricity exists, more than one scenario required in the investigations
 - (d) Considerations should be given to the sample shape because they could deviate results
 - (e) Unloaded samples are not recommended to be used in experimental tests unless they are identical to real cases where the concrete will be used as non structural non loaded elements.

1.5 Outline of the dissertation

The thesis consists of nine chapters as follow:

Chapter 1 presents brief introduction, aims and objectives, methodologies, and summary of thesis novelty.

Chapter 2 presents detailed literature review covering experimental works and modelling background of concrete at elevated temperatures.

Chapter 3 presents in detail steps undertaken in developing the novel ABAQUS thermo mechanical damage model. It also illustrates how it has been validated through samples tested under different test setups considering different boundary conditions.

Chapter 4 presents some preliminary preparations and analyses which will be applied throughout the thesis. Experimental test details which have been simulated in the thesis have been summarised. Parameters known arguably that have effects on concrete behaviour and its spalling while heated have been highlighted. Given temperature profiles in the experimental test reports have been reproduced confirming the versatility of the developed ABAQUS model. Mesh sensitivity analysis has been conducted to select mesh sizes without compromising analysis results. Finally, a hygro thermo analysis has been conducted to show if pore pressure may affect results of this thesis which are derived from thermo mechanical damage.

Chapter 5 investigates in details how restraints alter test outcomes of samples under effects of heating. Different types of restraints have been investigated covering mechanical restraint, self restraint, and load restraint. Mechanical characteristics of restraints and details through which restraints have been applied have been investigated.

Chapter 6 covers effects of sample size on altering test outcomes of concrete samples under effects of heating. Parametric studies conducted on different test setups through altering thickness or length of the sample. The test set ups have been chosen to cover unrestrained samples, restrained samples, and loaded samples.

Chapter 7 investigates how different load types, load intensities, the details through which the loads were applied can affect test outcomes. The chosen test cases cover axially loaded samples,

eccentrically loaded samples, and passively loaded samples through mechanical restraints. Parametric studies have been performed through altering load intensity, load eccentricity, and stiffness of the mechanical restraints in passively loaded samples.

Chapter 8 investigates in details to what extent cold rim, which has been understood to act as self restrainer, is effective in imposing stress to the samples and may alter test outputs accordingly. Parametric studies on different samples covering unrestrained samples, restrained samples, uniaxially loaded samples, and biaxially loaded samples have been performed.

Chapter 9 concludes the thesis.

Chapter 2

Literature Review

2.1 Definition and historical overview of concrete spalling

During the course of their existence, concrete structures may be subjected to extreme heating for a variety of reasons, including the necessity of the structure for its intended purpose, as in factories and nuclear power plants, or unexpected accidents like fire. Through concrete spalling, abnormal heating can seriously harm buildings and other structures.

Concrete thermal spalling can be defined as a failure mode following concrete exposure to a severe, often unintentional, thermal load such as fire that is characterised by disintegration of concrete pieces from the structural elements violently or non-violently [2, 3]. It significantly impairs concrete strength, reduces the concrete member cross section, and exposes the embedded reinforcements to the direct flame which may trigger fatal failure of the entire structure and potential loss of lives. Figure 2.1 shows spalling of concrete illustrating all these damages for a tested sample and a real case garage wall.

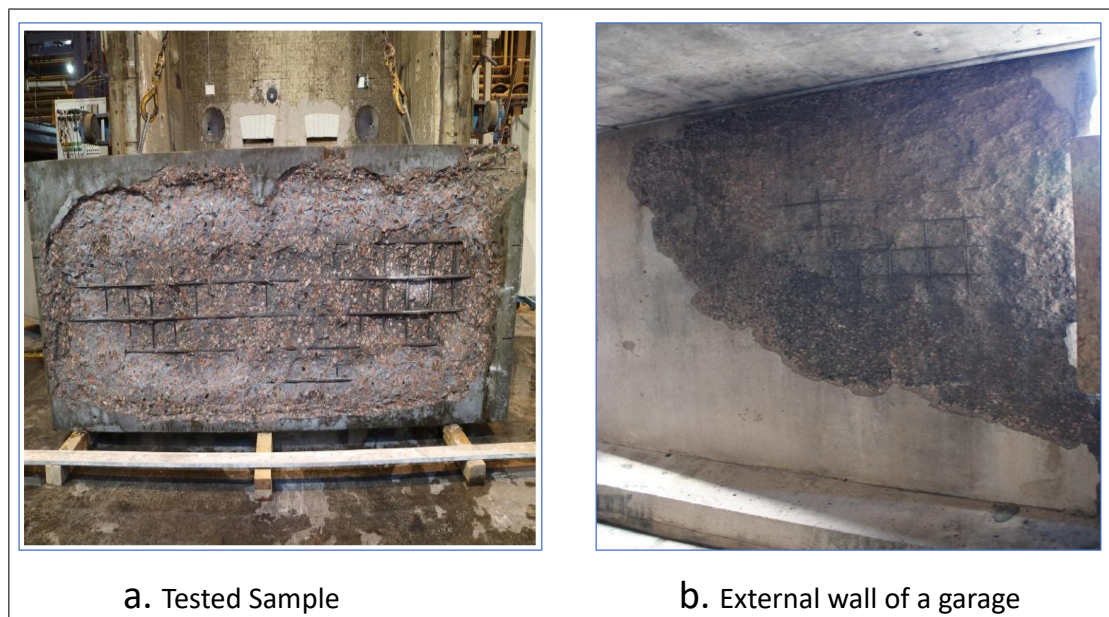


Figure 2.1: a) Rectangular sample tested in lab [4] b) Wall of a garage after exposing to fire [5]

Concrete spalling history investigations could be dated back to 1854 when concrete spalling under heating effects was discussed in a publication by Barret cited in [6] illustrating that flint aggregate is unstable under effects of fire and therefore would make concrete to split and yield accordingly. Afterwards, heated concrete spalling research area has witnessed significant advancement mile stones. In 1866 rapid cooling of concrete building during fire fighting was found to be a cause of spalling even in building designed to be fire resistant as recorded by

Ingle cited in [6]. Investigations afterwards incorporated effects of reinforcement and how it can improve fire resistance of concrete as it was conducted by Hyatt in 1877. Additionally effects of concrete compressive strength and moisture content has been found to be effective in the same era. Between 1905 -1918, some key observations and advancements were identified, namely liquid water coming out from unexposed cold portions of concrete was observed, effects of age on concrete spalling was recognised, and early classification of spalling types have been initiated [6].

There were numerous instances of concrete spalling in the last century which made investigations to be pursued and to establish robust codes and standards having a focus on fire and concrete. The Ronan Point collapse in London in 1968 was one of the most noteworthy accidents[7]. The concrete panels cracked and collapsed as a result of a fire that was started by an explosion in a gas cooker. Precast concrete panel use in high-rise structures has come under further attention as a result of this incident. The 1967 fire at McCormick Place in Chicago is another noteworthy incident [8]. The roof and several levels were destroyed when the fire broke out when the McCormick Place convention centre was being built. Concrete spalling caused by concrete being exposed to fire was identified as the cause of the collapse. New materials and methods for concrete structure fireproofing were created as a result of this catastrophe. In the Joelma building in Sao Paulo, Brazil, a severe event of concrete spalling as a result of fire happened in 1974, killed 189 people and more than 320 were injured [9]. An electrical problem caused the structure to catch fire, and the high temperatures produced extensive concrete spalling, which led to the building collapsing. Due to this tragedy, fire safety was given more consideration while designing buildings and new fire-resistant materials were created.

In this period a number of significant findings and theories can be identified from intensive investigations around the world. In 1961 Moisture Clog Theory was formulated which associates spalling with the role of moisture content in moving moisture inside the porous medium of the concrete creating a saturated layer inside the concrete which prevents further movement and causes tensile failure of the concrete as it will be discussed later. At the same era investigations were advanced to higher levels covering pre-stressed concrete fire resistance, identifying explosive spalling which is accompanied by energy release, and incorporating different fibre types aiming to improve fire resistance of concrete [6].

Experimental investigation on spalling were pursued along side development of numerical modelling to understand the complex behaviour of spalling. Numerous models and spalling theories have been proposed along side identifying different types of spalling and their controlling parameters. However, with these huge efforts have spent in this area, there are no standardized methods to quantify or predict the spalling phenomena accurately. Additionally, there are still neither complete understanding nor consensus among researchers regarding the spalling mechanisms and its governing factors. It therefore remains an open area research to be studied experimentally and theoretically.

2.2 Types of concrete spalling

In the literature, several different types of concrete thermal spalling can be identified based on the spalling location, its depth, whether it is internal or external, whether it is non-violent or explosive spalling, and many other considerations. In general spalling types can be categorised into four main types: 1) explosive spalling, 2) surface spalling, 3) corner spalling, and 4) aggregate spalling as shown in Figure 2.2 [10, 11].

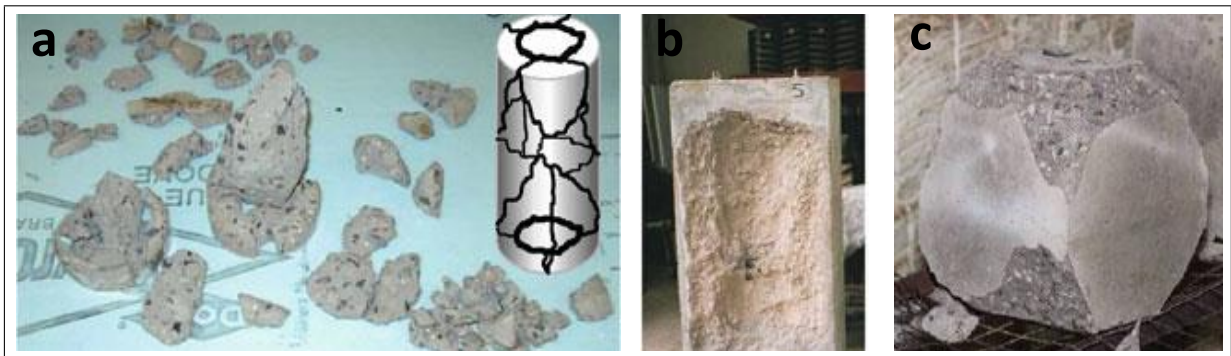


Figure 2.2: Types of spalling a) Explosive spalling, b) Surface spalling, c) Corner spalling [10]

The most hazardous concrete spalling is explosive spalling which is accompanied by huge energy release [2]. High explosive energy causes concrete fragments to fly at high speeds, increasing the number of casualties and causing damage to the environment, including breaking nearby windows, as well as allowing more oxygen to reach the fire area and escalating the severity of the fire. Additionally, explosive spalling might endanger the stability of the entire structure and result in complete structural collapse. This prompts major questions regarding research into the phenomena and developing strategies for preventing concrete spalling. It has been justified through excessive pore pressure within the concrete which causes explosive spalling when free and mixed water inside the concrete begins to evaporate and move, inside the concrete porous medium, upon concrete exposure to fire. If the concrete has a low permeability, the pore pressure begins to build up and causes stresses to be introduced into the concrete's internal structure. With an increase in temperature, vapour stresses can accumulate to high levels. If these stresses are greater than the concrete's tensile strength, a local failure occurs, releasing high energy and causing a chain reaction of microstructural failure in nearby portions. Finally, the violent explosion of concrete occurs [2, 12].

Surface spalling has been argued to be more specific to normal strength concrete rather than high performance concrete. It might also be claimed that concrete layers that explode out of a structural element or fall off are examples of surface spalling, a subset of explosive spalling. According to Lennon cited in [6], there is a high safety margin in the design values of the fire resistance for ordinary concrete elements, so the influence of fire spalling on the safety of the structure is frequently minimal for ordinary low strength concrete as the spalling rarely amounts to more than slight surface flaking.

Corner spalling could be more specific to corners of beams and columns which may spall after being exposed to fire for a prolonged period of time (greater than 30 minutes). This behaviour

has been observed in numerous instances in actual flames, and it is frequently easy to break corners with the fingers after a fire. It has been noted that this phenomena is triggered by the development of concrete cracks combined with thermal stresses in the surface, leading to a crack pattern where the corner falls off because of its weight. As long as the corner spalling does not expose the embedded reinforcements to the direct flame, the overall load bearing capacity will remain intact [3].

Aggregate spalling is the phenomena in which individual pieces of aggregate rupture and form minute craters on the surface without affecting the load-bearing capability. Water inclusions in aggregates like flint and sandstone may be the cause, however the effect is localised close to the stone and has, generally, no structural relevance [3, 13].

It has been noted that explosive, surface, and aggregate spalling typically takes place during the first 20-30 minutes of the concrete part being exposed to high temperatures. Due to the requirement of a specific temperature gradient, corner spalling is typically seen between 30 to 90 min of exposure to high temperatures. When reinforcement bars along the concrete's edges are heated, the likelihood of corner spalling increases [10, 14].

2.3 Mechanisms of concrete spalling

As discussed before, there is no agreement among researchers regarding spalling and its exact physical causes. Different theories have been established to explain spalling which are favorite differently among researchers. The most common theories are pore pressure spalling, thermal stress spalling, thermal cracking spalling, and thermo-chemical spalling [10, 13].

First, pore pressure mechanism illustrated in Figure 2.3-a associates spalling with the migration of air, vapour and liquid water inside the concrete body while subjecting to elevated temperatures. This is after occurrence of hygro thermo reactions inside the concrete which triggers moisture transportation through sample's depth via the concrete porous medium. Tensile stress develops due to the pore pressure inside the concrete which reaches the highest value at a saturated layer within the concrete body named moisture clog layer. The intensity of the developed stress depends on the permeability and the moisture content of the concrete mix, and it causes spalling upon surpassing tensile strength capacity of concrete [10]. Many researchers have incorporated this effect in the investigations [1, 15, 16, 17].

Second, thermal stress spalling mechanism illustrated in Figure 2.3-b associates spalling with the development of severe compressive stresses close to the exposed face due to restrained thermal expansion and tensile stresses at the deeper cooler portions of the sample [10]. Many researchers have relied on this mechanism in the investigations for example [18, 19, 20, 21, 22] considering that effects of pore pressure may not have decisive effects on the results.

The focus of the previous two methods are mainly on explosive spalling for which there is huge uncertainty about location and time of its occurrence among researchers. Therefore, third method, thermal cracking theory, associates spalling by internal cracking mainly due to quick decomposition of hydrated cement components [23]. This leads to crack formation between

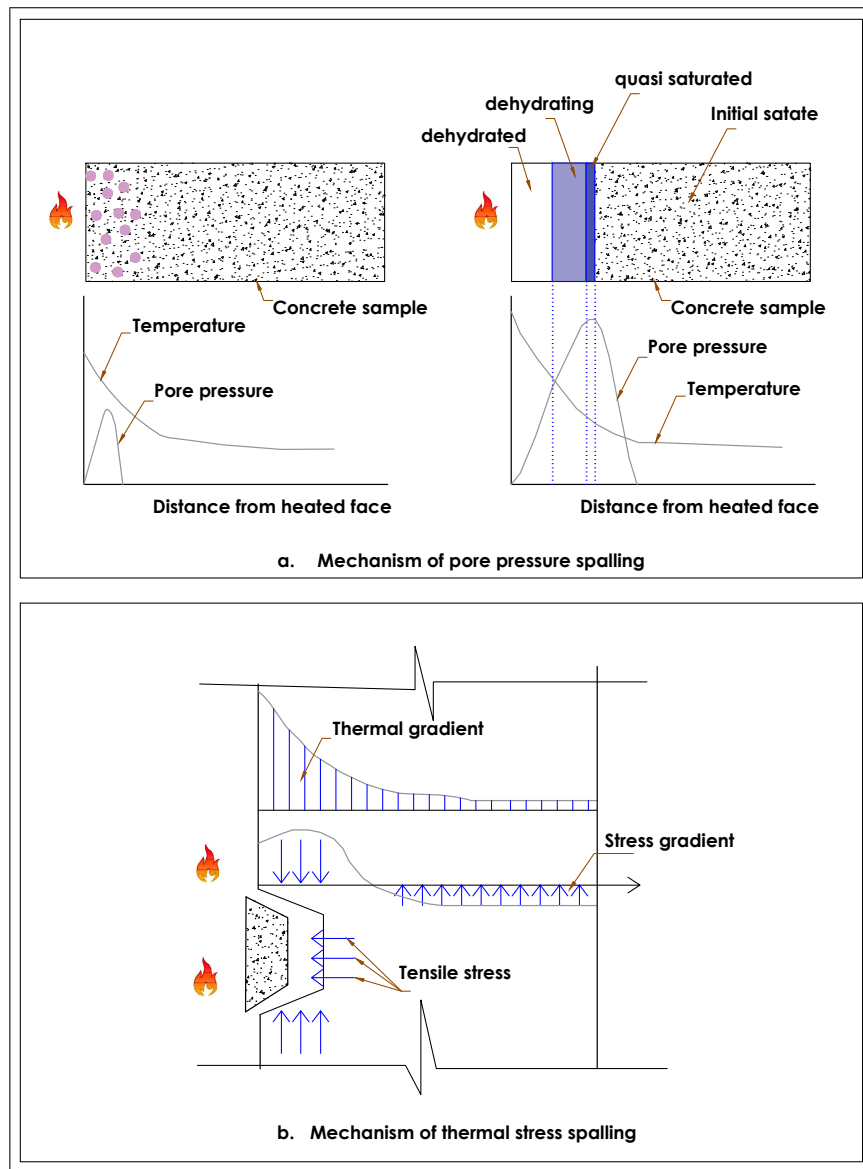


Figure 2.3: Mechanisms of concrete spalling at elevated temperatures [10]

cement mortar and the aggregate particles and hence causes spalling occurrence.

Numerous unloaded and unrestrained concrete specimens that have cracked demonstrate that pore pressure build-up, which depends mainly on permeability and moisture content, is the primary cause of the observed spalling. However, the pore pressure spalling theory can hardly be used to explain the spalling of concrete cover in columns that happened at the intermediate or late stages of the fire during the fire endurance tests. Comparable cover spalling, however, has been seen in concrete columns loaded in concentric compression at room temperature before the columns reach their maximum capacity. This suggests that while pore pressure alone cannot cause this form of fire-induced spalling, initial applied compressive stress and thermal stress produced via restricted thermal dilatation can cause spalling [13].

Additionally, it is clear during fire, heating starts to conduct through concrete body from the exposed surface, and spalling starts from the exposed surface too. Therefore, it can be argued that efficiency of pore pressure as a main spalling trigger may be questionable. Main moisture part nearby the heated surface would evaporate/migrate toward the heating once heating

started, and the thermal expansion leads to crack occurrence at the exposed surface. This eases moisture discharge and undermines severity of pore pressure, deeper in the concrete. This argument is also true for the thermal cracking theory because spalling initiating from the surface may ease formation of internal cracking in deeper portions. Unlike these two methods, the mechanism of thermal theory can be more justifiable because the mechanical behaviour and associated developed stresses at the exposed surface, where the spalling starts, have been taken into consideration as spalling triggers.

Apart from the aforementioned three main spalling theories which are mostly relating spalling to physical actions happen during the heating, thermo-chemical spalling theory [13] focuses on chemical reactions inside the concrete mixture. It focuses on two types of spalling which are sloughing-off spalling that occurs at extremely high temperatures and post-cooling spalling.

Sloughing-off spalling results from severe cement-aggregate bond breakdown and happens at extremely high temperatures. The breakdown of calcium hydroxide, calcium-silicate-hydrates, and calcareous aggregate, among other materials, is a significant source of degradation in the aggregate-cement bond. When the temperature is high, aggregates expand while cement paste contracts. This variation reduces the bond between the aggregates and the cement paste even further [13].

Post-cooling spalling occurs when in calcareous aggregate, calcium carbonate breaks down and releases calcium oxide at a high enough temperature. The air's moisture is absorbed by hot concrete after it has cooled, eventually penetrating deep into the material. The surface concrete layer expands (44% more in volume) as a result of a reaction between the newly formed calcium oxide and the moisture absorbed by the concrete. Rehydration-related expansion causes significant cracking in the concrete, which then results in the pieces falling to the ground. If there is enough calcium oxide in the deeper concrete region and enough moisture from the ambient air, post-cooling spalling may happen gradually. But compared to thermo-hydral spalling, this sort of progressive spalling occurs much more slowly. The progressive post-cooling spalling may take a few weeks to complete. The understanding of the precise post-cooling spalling mechanism is still somewhat limited. However, it shortens the useful life of concrete structures and might even cause them to collapse. Therefore, it is essential to learn more about the mechanism of concrete's post-cooling spalling [13].

Sloughing-off spalling and post-cooling spalling are mostly about the chemical reactions inside deeper portions of the concrete at high temperatures where severe chemical reactions should take place. They can both be correlated with concrete's maximum temperature, meaning that thermo-chemical spalling happens when the maximum temperature in concrete surpasses a certain threshold. The complete dehydration of concrete and the decarbonation of calcium carbonate are connected to the threshold temperature for thermo-chemical spalling. As shown in Figure 2.4 calcium carbonate commonly decomposes between 700 °C and 900 °C. Concrete typically completely dehydrates when the temperature rises beyond 800 °C. Therefore, it is assumed that 700 °C is the threshold temperature for thermo-chemical spalling. In particular for calcareous concrete, thermo-chemical spalling is prone to happen when concrete temperature

surpasses. For concrete samples assessed as materials rather than structural members, this

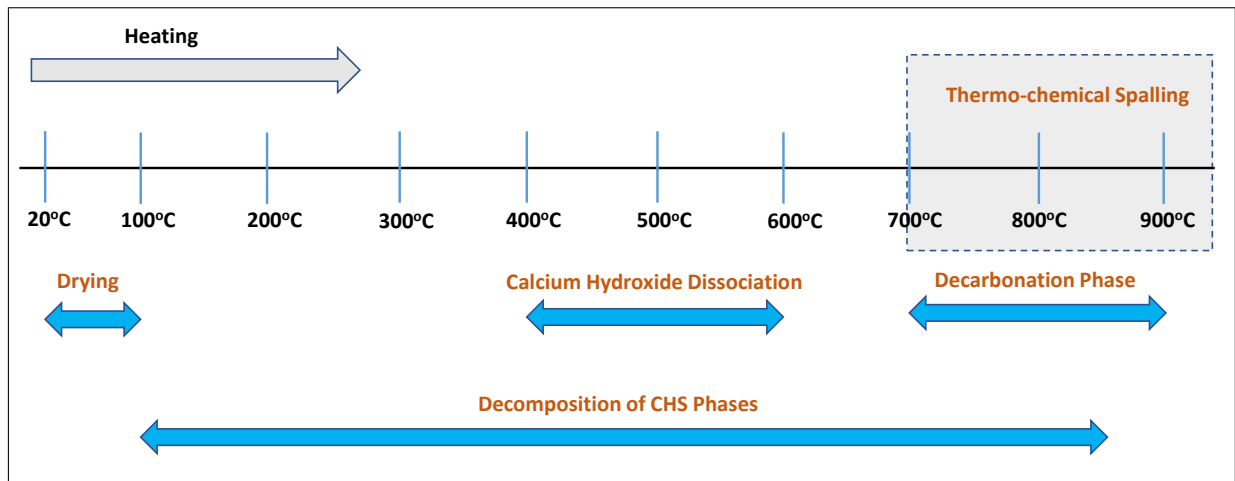


Figure 2.4: Temperature range in thermo-chemical spalling mechanism [13]

mechanism is conceptually comprehensible. However, from a structural and practical standpoint, spalling close to the exposed surface typically occurs earlier and at lower temperatures than those required by this theory, undermining the integrity of the concrete even before chemical reactions. For the interior of the concrete body to be affected, a much longer fire duration and greater temperature are needed per this theory. Since the mechanical behaviour and produced stresses at the exposed surface, where the spalling starts, have been taken into account as spalling triggers, the mechanism of thermal theory can be more justified for shallower spalling at the cover region, as was previously mentioned.

2.4 Classification of literature concrete spalling tests

Depending on whether they were loaded before heating or not, the samples experimentally tested in the literature can generally be classified as either non-structural samples or structural samples. These can be further broken down into three groups, including heated without load samples (unrestrained samples), restrained then heated samples (loaded through restrains when the heating progresses), and loaded then heated samples (initially loaded samples prior to heating). Different scale samples considering different boundary conditions, load types, restraints, and test setups have been employed. Some examples are shown in Figure 2.5 incorporating non structural samples with different sizes, various structural member samples, and even complete building sample.

2.4.1 Heated unrestrained samples

Majority of real case concrete members are usually loaded through dead load and live loads. However, still different scale unloaded samples in the literature can be found which have been aimed for different purposes such as measuring temperature dependent mechanical properties of concrete [28], investigating spalling mechanisms under sole effects of heating [15], identifying

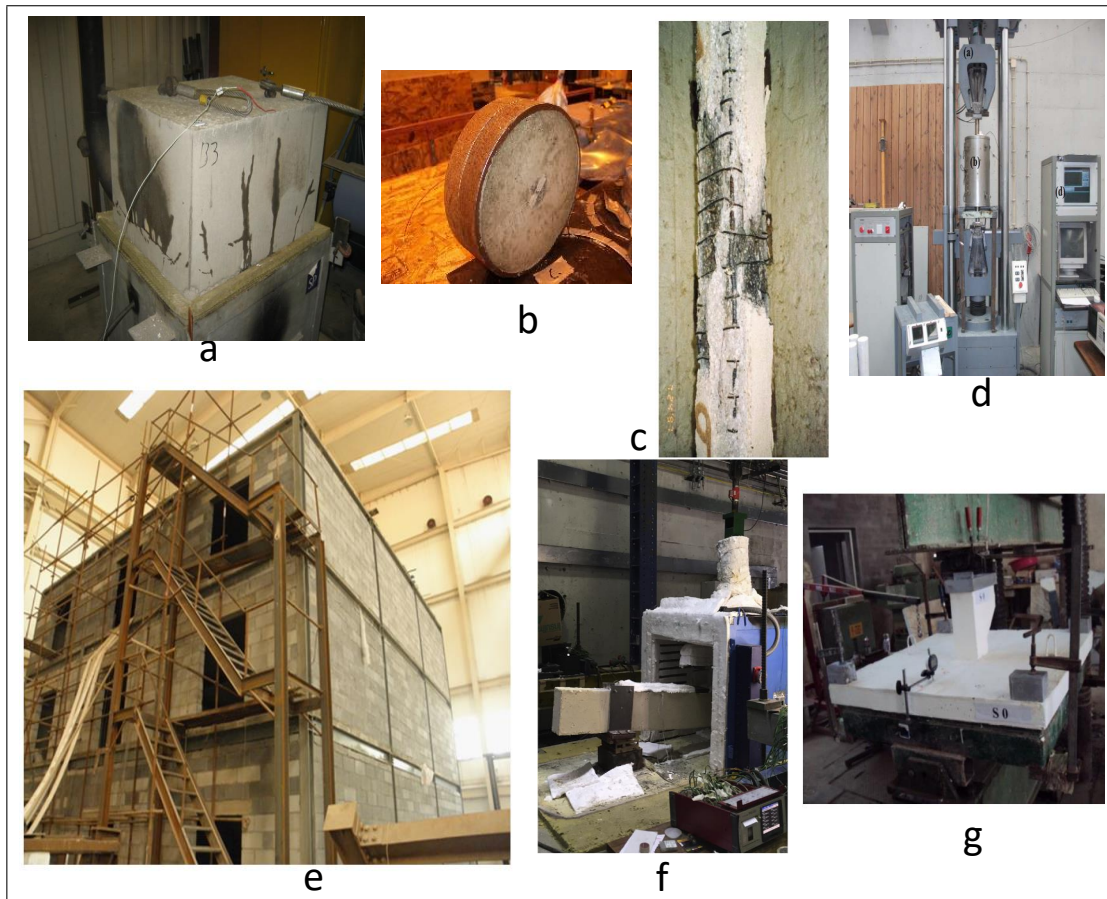


Figure 2.5: a) Non structural thick sample [4] b) Non structural ring sample [4] c) Structural sample-column [24] d) Cylinder sample [25] e) Entire building test [18] f) Structural sample-beam [26] g) Flat slab with column [27]

spalling types, investigating methods to mitigate spalling in concrete mixture through adding fibre [29], and understanding chemical reactions inside concrete triggered by heating [30]. In a work conducted in [31] aiming to measure residual mechanical properties and spalling of high performance concrete (HPC), small cylinders without loading during heating exposure were tested. The 102 x 204 mm cylinders were heated to steady state thermal conditions at a target temperature, and residual mechanical properties were assessed when the specimens cooled to ambient temperature. The four HPC mixtures used to create the test specimens had water-to-cementitious material ratios ranging from 0.22 to 0.57, and their room-temperature compressive strengths ranged from 51 MPa to 93 MPa. In two of the four HPC combinations, silica fume was present. The specimens were heated at a rate of 5 °C/min to a maximum core temperature of 450°C. According to the results of the experiments, HPCs with greater initial strengths (lower w/cm) and silica fume retain more residual strength after being exposed to high temperatures than those with lower initial strengths (higher w/cm) and no silica fume. Modulus of elasticity variations are not as noticeable. However, HPC specimens with lower w/cm and silica fume had a higher risk of explosive spalling.

When explosive spalling occurred, the specimens' core temperatures were measured to be between 240°C and 280°C, which is higher than the temperatures at which the majority of the chemically bound water had already been released from the concrete matrix. The sudden,

dramatic disintegration of the test specimen into very small fragments that project outward at high velocity, along with evidence of a more restrictive heat-induced mass loss process experienced by the exploded specimens, have been considered as justifications to support the theory that internal pore pressure buildup is the main cause for the explosive spalling. However, the occurrence of explosive spalling coincident with the specimen's maximum thermal gradient suggests that the accumulation of strain energy brought on by thermal stress may also have played a supporting role in the explosive spalling mechanism. Since the aggregates expand with rising temperature while the cement paste contracts, it is unclear whether this secondary role delays or contributes to the explosive spalling mechanism.

It is worth mentioning here that specimen size and the test set up might have significant contribution in getting these results. While the cylindrical samples were too small and therefore prone to spalling violently, the testing set up in which the entire surfaces of the samples subjected to heating was another conducive factor. The cylinder was put in totally heated environment equally affecting the entire sample surface unlike other samples in some other tests where the heating was targeted only through a face. These justifications can be supported by results seen in [4] in which thick rectangular slabs with dimensions 600 x 500 x 400 mm and compressive strength 40 MPa to 70 MPa were tested in unloaded, unrestrained state under effects of heating as shown in Figure 2.6. Three concrete mixes used in their fabrications, fibre content 1.0 kg per

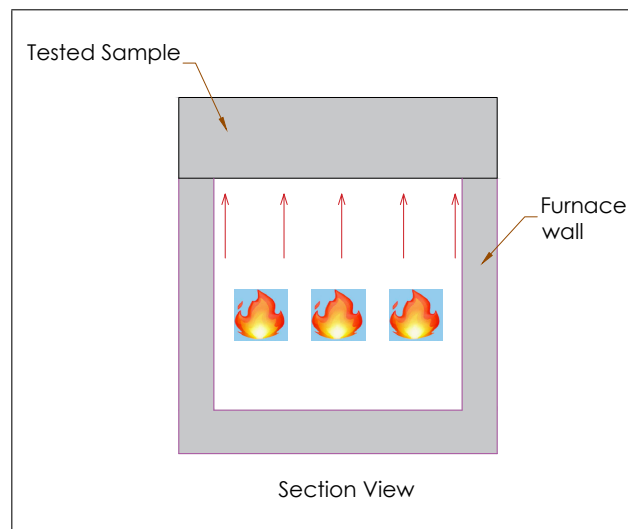


Figure 2.6: Test setup of unrestrained unloaded sample [4]

cubic meter was added only for a mixture. The samples were put on an oven and heated through lower surfaces up to temperature 350 °C, after 60 minutes, 30 mm away from the exposed surface. The samples fabricated with the fibrous concrete mixture did not spall while others experience several spalling incidents, happened intermittently and each accompanied by a bang. In all samples, including those that did not spall, water was observed on all vertical sides of the samples. While the fibre content prevented spalling, observing water without spalling may question if the spalling of the cylindrical samples was triggered solely by the pore pressure. Furthermore, it seems logical that in the spalled samples fabricated with the mixture without fibre, the thickness of the sample prevented the sample from complete disintegration.

Contradicting to these results, in another test experiment even slab sample with fibre content spalled [32]. The test incorporates slab sample, cast monolithically with beam, thinner than previous test case with dimension 4500 x 1500 x 200 mm. The test set up is similar to the 400 mm samples discussed before, that is unloaded and heated from the lower face, covering both the slab and beam areas. The compressive strength of the mixture is 93 MPa, the temperature reached around 500 °C after 60 minutes, 40mm from the heated surface. Alongside with this samples, a column sample fabricated with the same concrete mixture was also tested. According to the reported results, the slab specimen had the worst spalling state comparing to the beam, cast monolithically with it, and to the column sample. This is justified by the one-sided heating condition and natural convection result in the maximum temperature gradient. Because of the one-sided heating, vapour that forms at the bottom of the slab can rise to the top and finally escape into the atmosphere, causing a dramatic drop in temperature at the surface. The temperature increase at the bottom of the slab is most strongly influenced by natural convection in the furnace, which also causes the temperature difference between the bottom and top of the slab to widen. While these justifications are reasonable, other parameters such as thickness of the slab, heating rate, exposed area, fiber type and content, and boundary conditions need to be considered whether may have effects on obtaining these different results in comparison to the 400 mm samples discussed before.

Finally, through comparing rectangular samples to the cylinder samples discussed earlier, more differences in boundary conditions can be highlighted. As mentioned before, the entire surface of the cylinder was subjected to the heating source, however only lower surface of the rectangular slabs was subjected to the heating such that a cold rim left along the perimeter of the sample where the sample put on the wall. While rectangular samples were intended to be tested unloaded and unrestrained, these cold rims have been considered by some researchers to act as self restrainer imposing stress to the heated portion [33]. This issue has not been investigated in detail in the literature and has been mostly intended to ease experimental investigations rather than being a matter of investigations. Therefore, more investigations are still necessary to fully understand its effects on behaviour and spalling of concrete under effects of heating.

2.4.2 Heated restrained samples

As in previous category, numerous experimental investigations can be observed in the literature in which various restrained samples were employed for different investigation aims. The main difference between this categories and previous one is the involvement of external stresses developed passively through restraint reactions preventing expansion of the sample, after exposing to elevated temperatures. Therefore, here a more complicated stress states, combined between effects of the heating and mechanical stresses, control concrete behaviour and its spalling.

Restraints can be observed in different configurations in the literature, applied on various sample consisting of structural members like beams or non structural samples confined through steel rings or steel sections. Axial restraints provided for reinforced concrete beams during fire exposure test can be observed in [34]. Six reinforced concrete beams were tested for fire

resistance as part of the experimental investigation. While two of these beams were constructed with normal strength concrete, the other four were made of high strength concrete. All of the beams had a rectangular cross section measuring 406 x 254 mm and with 3960 mm long. At 28 days and the day of testing, the concrete's average compressive cylinder strength was 52.2 and 58.2 MPa for NSC and 93.3 and 106 MPa for HSC, respectively.

In order to simulate the temperature, stresses, end restraints, and heat transfer that a structural part could experience during a fire, a test furnace has been specifically created. The fire chamber of the furnace is 2.44 m in width, 3.05 m in length, and 1.68 m in height. It is supported by a steel framework and four steel columns. Different load levels can be applied for each beam as the furnace can accommodate two beams at once. The testing of one of the two beams is possible under axial restraint support settings, whereas the testing of the other beam is required under simply supported end conditions. The loading frame's and the axial restraint system's rigidity for axially restricting the beam was found to be about 13 kN/mm. Because there are no rotational restraints provided by the axial restraint system at the ends of the beam, the restrained tested beams are free to rotate at the support.

All beams were put to the test with two point loads that were each placed 1.4 metres from the end supports. Each of the two-point loads for each beam was 50 kN, or 55% of the beam capacity. About 30 minutes prior to the start of the fire test, the load was applied, and it was kept in place until a point where no more increase in the beam's deflection could be measured. This was chosen as the initial circumstance for the beam's deflection. During the test, the beam was exposed to heat that was carefully managed so that the average furnace temperature closely matched the desired temporal temperature curve. When the hydraulic jack, which has a stroke of 250 mm, was unable to continue supporting the load, the beams were declared to have failed, and the tests were stopped.

The deflection response of the tested beams was used to estimate the impact of axial restraint on the fire response of RC beams. Even though a beam with the designation (Beam B4) reported to have lower rebar and concrete temperatures than a beam with the designation (Beam B2), the former had a larger mid-span deflection. This is mostly due to the axial restraint that Beam B2 experienced. A counterbalancing bending moment is created by the axial force created by restricting the thermal expansion of an RC beam, which is similar to arch-action. Reduced deflections are the result of the bending moment cancelling out the applied load's moment.

While the effects of restraints can be seen from this experimental work, the results may be not accurate enough if compared to real case restraint scenario. Restraint states of beams in reinforced concrete frames is rigid enough and not provide rotations as it was allowed in this test. Therefore, end moments would develop at ends result in providing more stiffness against mid-span deflection. This means that results obtained from this test could be too conservative. Additionally, comparing to uniformly distributed load, the state of point load is rather theoretical rather than being so common in buildings. Therefore, in performing similar tests, considering different load type, stiffer restraints with rotation prevented, would provide more accurate results.

Responding to these considerations, other researchers conducted tests on beams with end

restraints axially and rotationally restrained [26]. The tested beams had a rectangular cross-section of 100 mm x 250 mm and were made of normal strength concrete with 25.85 MPa. Samples with different end restraints, mixed between either axially restrained or axially plus rotationally restrained, were considered. During testing, the specimens were subjected to a load level equal to 50% of the load bearing capacity of the RC beams at ambient temperature. For the test specimens, this value roughly equated to 34.2 kN. In order to prevent instrumentation damage from the high temperatures that generated throughout the test, the load level of 50% was chosen for shorter test duration. The load levels in actual RC beams used in buildings range between 20 and 50 % of the load bearing capacity's design value at room temperature. Two stiffness values, one lower and one higher were considered for the axial and rotational restraints. The key finding of this study is that the RC beam's fire resistance rises when thermal restraint (either axially only or axially + rotationally) is imposed. For instance, when introducing the lower degree of axial constraint, there may be an increment of 18%, and when introducing axial and rotational restraint, there could be an increment of 100%. This again suggests that the calculated fire resistance may be excessively conservative if the thermal restraint is not taken into consideration in the design of the RC beams. Another important observation is that, the addition of restraint increases beam stiffness under the effects of the heating. For instance, the beam without axial and rotational restraint required around 74 minutes to achieve a vertical displacement at midspan of 60 mm. The lower level of axial restraint is introduced, and the duration is raised by 16%. The increase was 108% for the more severe level of axial and rotational constraint.

While in these beam samples restraint effects were investigated with existence of applied load, applied transversely producing flexural moment, another type of restraint without involvement of load can be observed in the literature. It consists of very thick steel or steel sections confining samples with different shapes such as ring or prism shapes. In an experimental investigation conducted in [4], four passively restrained samples through steel rings were tested. Two ring samples with dimensions (Diameter x Height) (610 x 300 mm) and (300 x 100 mm) respectively, and two rectangular prism sample with dimensions (Length x Width x Thickness) (600 x 500 x 400 mm) and (600 x 500 x 300 mm) respectively. These configurations are shown in Figure 2.7. The compressive strength of the smaller ring and the prism sample is 42 MPa while the larger ring sample fabricated with 70 MPa concrete mixture. For each configuration, several samples were fabricated from concrete mixtures with and without fibre. For samples created from fibrous concrete no spalling were observed for all samples. Interestingly, all samples fabricated from the concrete mixture with no fiber content spalled except small ring samples. The reason for this is not clear and no clear justification was provided. However, it could be related to the test setup especially there is difference in the exposure area between the big and small ring. For the latter, the entire surface exposed to the heating, however the big ring sample was put on the oven such that unheated zone along its circumference, where the sample sits on the oven walls, has left unaffected by the heating (Figure 2.7-b,c). While recently in some literature investigations cold rim has been investigated, still more investigations are necessary considering different parameters and scenarios. A cold rim is an unheated area surrounding the heated area of a sample that is

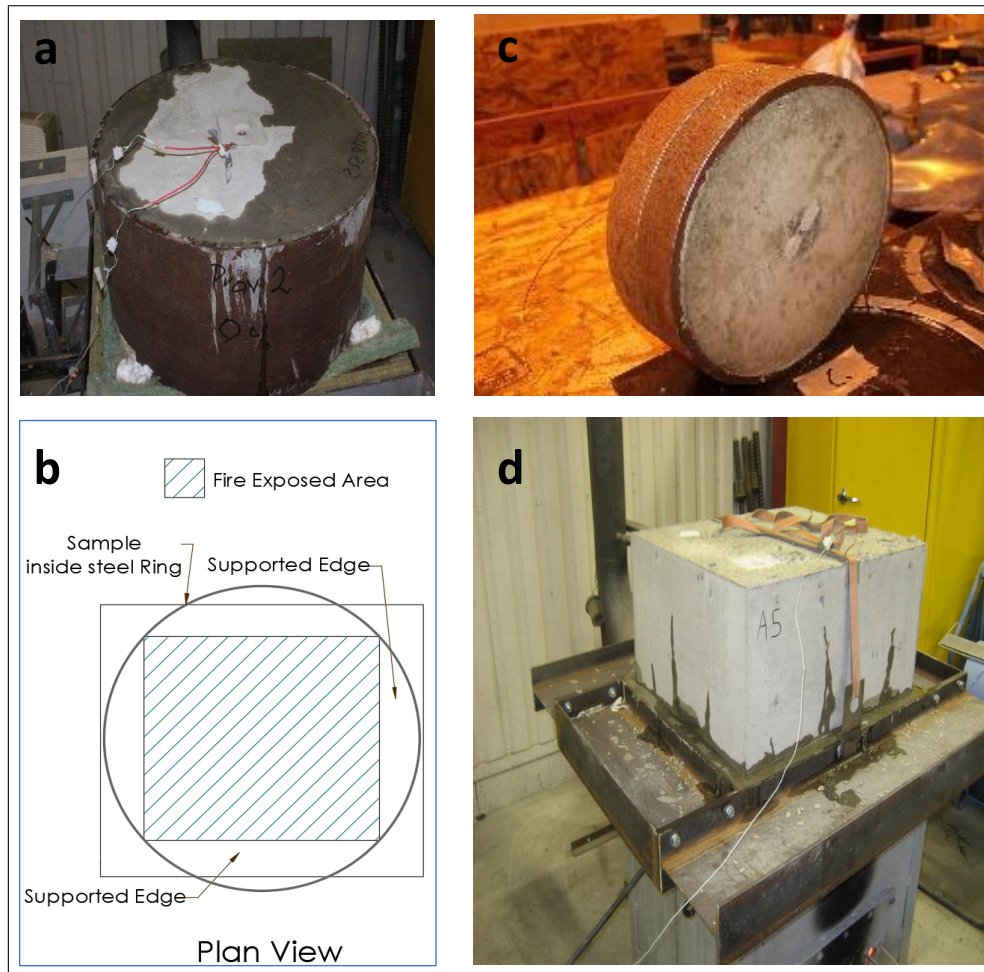


Figure 2.7: Various restrained samples from [4] a) Large ring sample, b) Large ring sample test configuration, c) Small ring sample, and d) Rectangular prism sample

considered may act as a self restrainer imposing stresses in the heated concrete and therefore triggering spalling [33]. In a real structure, cold rims might appear where a structural element is partially exposed to fire. However, in experimental works they can be found in different configurations for different purposes.

In some experiments, the cold rim was not the investigation aim, it was provided to ease the experimental process where the sample necessarily rests on the walls of a furnace and the periphery is consequently unheated e.g [4, 3, 22, 35, 36]. However, there are some tests in which cold rim was investigated considering different test setups. For example, in some tests cold rims have been modeled accompanied by initial applied biaxial compression load [37, 38]. However, in [33] cold rims were provided in two different ways based on the size of the samples. In the unloaded slab samples cold rims were provided through isolating a circumferential rim around the heated portion from the heating source at sitting area where the sample rest on the furnace walls. However, in the smaller samples cold rims were provided through directing small flame to affect only central portion of the exposed area of the sample.

The observations from these investigations can not be easily compared due to adopting different concrete mix, sample sizes, and test setups, therefore further investigations are required. Regarding observations observed in [37, 38] in which thin slab samples were tested under biaxial

load to investigate cold rim effects, even though different behaviours were observed with different test configurations, it can be argued if they are due to the mechanical characteristics of the cold rim or due to its heating status or both. Additionally, some of the observed behaviour of the samples, specifically their deflections, that may influence spalling, could be test specific for these thin samples under biaxial loading and might not be applicable for thicker samples. Considering results from [33], different concrete mixes were used in producing the tested samples which means samples are not identical in terms of modulus of elasticity and compressive strength. Therefore, some of the observed results might relate to this mix inconsistency. Furthermore, while all small samples spalled, all larger tested slab samples did not spall. The effectiveness of the cold rim was justified by spalling termination once the cold rim spalled, therefore in the samples that did not spall, the effectiveness of the cold rim as a restraint cannot be confirmed. Additionally, all of similar size samples were tested using only one test methodology. All large samples put on the oven, and small samples through directing small flames into central portion of the exposed surfaces. Other parameters such as restraint and load were not considered. Therefore, it cannot be ruled out that observed results are specific only to this test set up. Above all, the concrete was considered 'cold' up to temperatures of 200°C although this temperature could be enough to cause considerable expansion reducing any restraint effect that the rim might have.

In this thesis, through taking into consideration the various test methodologies mentioned above, along with other hypothetical scenarios where necessary to incorporate more parameters, thorough investigations will be conducted to determine whether the observed results in the cold rim tests have been due to the cold rim or due to other underlying physical phenomena arising from test set up, sample size and shape or boundary conditions. To achieve this, different tests from literature will be simulated under different scenarios and the results will be compared in term of stress states and displacements.

To sum up, restraint is an inclusive parameter from literature investigations. It is cited to improve resistance against spalling in beams samples [39, 40]. These findings are based on comparison of results of restrained and unrestrained beam samples with the same test configuration, comparisons that consider degree of restraint and the mechanical characteristics of the restraint are not so well reported. Due to involvement of flexure in beam samples, results may not be comparable with samples restrained through different settings such as passive restraints through steel rings or external loading which are available in the literature. Additionally, some artifact details in specific test ups designed for passively restrained samples may arise questions regarding test outcomes. Leaving unheated area at the exposed surface attached to the restraints where the sample sits on the oven such as in [4] may affect test results comparing to the case if the entire surface heats without any cold zones. Furthermore, from a structural point of view, restraint due to applied loads rather than mechanical restraint may be considered. Loaded spalling tests can be found in literature such as in [4, 28] and typically it is reported that loaded samples are more vulnerable to spalling than unloaded restrained samples. This suggests that the influence of restraint on spalling behaviour depends on the type and specific characteristics of the restraint which needs to be investigated. Given that, in a real structure, members may be

restrained through a combination of applied loads and a wide range of mechanical restraint from adjoining members, it is important that these distinctions are understood. Therefore a chapter in this thesis examines closely the details of the configuration and characteristics of the restraints applied in spalling tests and investigates the extent to which they affect test outputs. In addition to this, consideration is also given whether other underlying physical phenomena arising from test set up, sample size, boundary conditions and load intensities may be affecting the results of experimental tests focused on the role of restraint.

2.4.3 Loaded samples

This category covers wide range of the literature experimental works in which the samples were loaded prior exposing to the heating, and the load maintained throughout the test. Loaded structural member samples like beams, slab, and columns, and non structural members like cylinders and prisms can be observed with different sizes and test configurations.

Loaded beams were usually tested in the literature to investigate behaviour and determine residual capacity of damaged members. In an experimental work conducted in [41], normal strength concrete is used to construct twelve RC beams. The variables for the studies are time, beam size, and loading, which stand for the duration of the fire exposure, cross-section size, and initial load level, respectively. The specimens have dimensions of 250 x 400 x 5000 mm, 300 x 500 x 5000 mm, and 350 x 650 x 5000 mm. The tests' results show that the concrete has a mean compressive strength of 25.08 MPa and a mean tensile strength of 2.98 MPa after 28 days of curing.

Different load values of 40, 60, and 80% of the nominal moment capacity (M_n) of the beams were applied, corresponding to 4, 7, 23, and 9.65 ton-forces for small beams, 10, 88, and 10.9 ton-forces for middle beams, and 28, 99 ton-forces for large beams, respectively. The number of rebars is adjusted based on the cross-section sizes, and all beams are designed to have the same reinforcing ratio. All beams are simply supported with an effective span of 4700 mm and put through a four-point loading system prior to heating. There are 1200 mm between each loading point. Designated load level applied to the beams and maintained then three surfaces on each beam are heated in accordance with the ISO 834 standard time-temperature curve. The samples are kept for a week after the fire test. All beams are put through the four-point bending test for the residual strength test until the beam manifests failure.

According to the experimental findings, temperatures measured by thermo couples vary based on their location within the beam section and range from 100 to 600 °C. Temperature distributions rise with increasing load levels, which is consistent with crack growth brought on by loading. As the load level rises, the beams' deflection during the fire tests increases. However, as the cross section grows, the maximum deflection of the beams during fire tests reduces nonlinearly. Because the temperatures of the reinforcing bars did not reach 500 °C for the strength of steel to be decreased to 50% of its original strength, discrepancies in the maximum loads between all specimens from the residual strength tests of the fire-damaged beams are not statistically significant. As the load or exposure time to fire increases, the stiffness and ductility

decrease. As the cross section size grows, the beams' ductility and stiffness improve with respect to various cross-sectional sizes.

It should be emphasised that the test methodology adopted in this experiment could influence and alter test outcomes which may question if they are representing actual building scenarios. Despite the fact that the compressive strength of all samples of different sizes of concrete is the same, keeping reinforcement ratio regardless of the beam cross section caused delayed failure of beams with smaller cross sections. Simply supported beams loaded under a four point load simplify the experiment setup, although this is far from real scenarios in buildings. Beam boundary conditions in real cases are usually restrained through adjacent members and the loading conditions are uniformly distributed loads. Additionally, in reality, beams are seldom single spanned, continuous beams run over several supports and cast monolithically with slabs are common cases in buildings. Most importantly, in continuous statically indeterminate beams, redistribution of moments between different zones of the beams prolong their resistance time under the combined effects of the mechanical and thermal loading. This is meanwhile no redistribution in single spanned statically determinate simply supported beam is possible. Due to disregarding boundary conditions, results from this test may not be accurate enough to be used in assessment of real cases. Additional research is required to determine the relative importance of various affecting elements, such as test set up, cross-sectional size, load level, and duration exposed to fire, for the fire-damaged RC beams.

In investigating behaviour of continuous statically indeterminate beams, six reinforced concrete T-beams with 500 MPa nominal yield strength steel reinforcing bars were fabricated and tested in both the environment and under fire [21]. The continuous beam configuration consisted of two beams, each 1.86 m length, simply supported, loaded through a central point load on each span. The beam dimensions are identical with 150 mm width and 250mm depth including 80mm slab thickness. All samples were cast using concrete with measured cube compressive strength at ambient temperature 64.5 MPa after 28 days. Five of the tested samples had the same reinforcement ratio of 0.7% but various load ratios, with the load ratios being 0.3, 0.5, and 0.7, respectively (defined as the applied load in the fire test to the ambient temperature capacity). Only one specimen had a reinforcement ratio of 1.0% but subjected to the same loading ratio. The middle support was inside the furnace and it was suspended to prevent failure and also to increase the precision of measurements for the support reactions. The temperature of the furnace matched the ISO-834 standard fire curve. Fire exposure occurred during the experiment on the bottom side of the continuous T-shape beam flange and three sides of the T-stem. The ends of the beam were insulated, and the topside of the beam was in contact with air at room temperature. Six tests were conducted, including two at room temperature to determine the beams' maximum capacity and four fire tests exposed to the ISO 834 standard fire.

For beams tested at ambient temperature, with increasing load, a plastic hinge formed at the central support of the continuous beam. The mid-span part of the beam's tensile reinforcement yielded as the applied load was increased further, and concrete crushing was seen at the mid-span section's flange. This could mean that the second plastic hinge is forming or that the beam is

failing. In the time between the first plastic hinge forming at the mid-support and the second plastic hinge forming at the mid-span of the beam, the steel reinforcement strain continued to rise but did not reach the fracture strain. This indicates that the plastic analysis of the beam may imply limitless moment redistribution.

For beams tested for heating effects, water vapour started to develop at around 8 minutes after fire exposure and persisted until 90 minutes into the fire test. This shows the varying times it takes for the exposed side and the unexposed side of the concrete piece to reach the temperature at which water vaporises, which is roughly 100 °C. The sagging moment resistance initially outweighed the hogging moment resistance because the sagging reinforcement was greater. Due to the reinforcement in the sagging zone being at higher temperatures, the sagging moment capacity reduced more quickly with increased fire exposure than the hogging moment capacity. The middle support section moment resistance increased to exceed the mid-span cross-section after around 60 minutes. The plastic hinge mechanism's formation sequence was different at ambient temperature and in a fire as a result of this difference in relative section resistance. All test specimens were found to suffer flexural failure along with total failure of the plastic hinge mechanism. Based on changes in the reaction forces, extensive redistribution of internal forces was seen, allowing load transfer from the mid-span to the mid-support such that a full plastic hinge mechanism could emerge. This process prolongs resistance, especially there was no fracture in the reinforcement.

Comparing these results with those for the simply supported beams, it is clear that test set up has significantly altered the outcomes. Redistribution of moments and plastic hinge formation can significantly prolong resistance of beams, which is not happening in single spanned simply supported beams. Even though results of the continuous beams are more comparable with real cases, still more investigations can be pursued reflecting more aspects close to real cases. This may include load type through using uniformly distributed load rather than point loads, and testing beams with larger cross sections and larger spans.

Apart from beam samples which are flexural members and mostly their tension face exposed to the heating, other members loaded axially in compression such as column, walls, and slabs profoundly cover the literature with different shapes and test configurations. Eight reinforced concrete columns were tested for fire resistance as part of the experimental programme in [42]. Two of these columns were constructed with high strength concrete with 63 MPa compressive strength, while the remaining six columns were composed of conventional strength concrete with 34 MPa compressive strength. Each column measured 2800 mm in length and had a 300 mm square cross section. There were eight 16 mm longitudinal bars in each column. At varied intervals ranging from 50 mm to 200 mm, the bars were secured using 10 mm ties, by adding more cross ties, two columns were given more confinement. A yield strength of 569 MPa was present in the primary reinforcing bars and ties. By securing the top and bottom of the columns to the loading frame's steel girders, the columns were put into the furnace. For each test, the columns' end conditions were maintained as fixed-fixed. At the ends of the columns, 100 x 100 x 12 mm angles that were bolted to the girders were used to create fixity. The top girder was

left free to move and was designed to rest on the column. The load on the columns was applied using a hydraulic jack that was fastened to another steel girder fixed to the loading frame. The columns were tested with fixed supports and a concentric axial load 40% of the design load. The column's exposed length was 2000 mm. About 60 minutes prior to the fire test, the columns were subjected to the axial load. The column was subjected to the standard fire under controlled conditions so that the temperature profile closely matched the desired fire curve. Over the course of the test, the load was kept constant.

According to the test results, although it is not taken into account in design rules, the arrangement of ties and the confinement of columns significantly affect how well NSC and HSC columns behave in the event of a fire. In NSC columns as opposed to HSC, the effect of confinement is more pronounced. In NSC and HSC columns, respectively, a 50% increase in confinement boosted fire resistance by 12 and 3.5%, respectively. When the hydraulic jack was unable to support the load any longer, the columns were considered to have failed. In the end, all eight columns buckled and failed in compression. Comparatively speaking, NSC columns expanded less than HSC columns. Depending on the degree of confinement, the spalling pattern changed. While there was no spalling in the NSC columns, which had confining tie spacing of 50, 75, 100, and 150 mm, respectively, later in the test, significant spalling was seen in the NSC and HSC columns, which had confining tie spacing of 150, 200, and 150 mm, respectively. However, there was less spalling in the HSC column with additional cross ties than there was in the column without cross ties.

Although numerous parameters were taken into account for this work, many additional points can be made that may have an impact on test results. Columns in real cases are frequently eccentric for a variety of reasons, so using concentric force in the tests may not adequately represent them. Eccentric loads are typically imposed on columns where beams with different spans meeting on the column. Column positions in relation to the building can also make them eccentric. Contrary to interior columns, where moments from opposite sides of the column may significantly reduce eccentricity, corner columns are typically susceptible to biaxial moments and consequently eccentric loads. Additionally, difference in live and dead loads in adjacent spans meeting on the column can also cause eccentricity, this is particularly in high rise buildings where difference in loading at any floor may cause eccentricity.

Emphasising on effects of eccentricity, eleven RC column specimens were tested in [43], six of which were made of low strength concrete (25 to 28 MPa) and five of which were made of high strength concrete (55 to 64 MPa). Each column specimen was 3150 mm in height and had a 300 mm square cross-section. This cross-section was chosen in order to efficiently incorporate various reinforcing systems and up to eight longitudinal bars with 40 mm covers. In all of these examples, the overall longitudinal reinforcement area was maintained quite consistently. For both longitudinal and transverse reinforcing bars, average yield tensile strength was between 491.5 MPa to 499.5 MPa. Seven columns have uniform transverse reinforcement with 150mm spacing. For the he rest five columns, the column's centre and end zones, the transverse reinforcement was spaced 150 mm center-to-center and 75 mm center-to-center, respectively.

The furnace's heating zone contained the column's central section with transverse reinforcement spaced 150 mm apart. This heating zone has a height of 2175 mm and it begins 500 mm from the base of the column. The columns were tested in a specially constructed column fire furnace with internal hot zone dimensions of 2.175 m in height, 1 m in width, and 1 m in depth. The furnace has the ability to apply the intended fire exposure and an axial load concurrently. For each specimen, the end support conditions were fixed bottom and pinned top. The goal was to produce lower bound values for lateral stiffness under eccentric loads. Additionally, the column was thought of as a continuous supported column, similar to a frame where beams frame the column and provide lateral translation constraint. As a result, any column section drift caused by vertical forces is disregarded. Furthermore, with pinned support at the top, it was discovered that giving eccentricity was practically advantageous.

The ISO-834 fire curve was applied to each column specimen and maintained as closely as feasible. At eccentricities ranging from 0 to 40 mm, eccentric loads were applied. To transfer the load eccentrically, a steel ball with a diameter of 60 mm was put in the desired grooves at a certain off-set from the loading mechanism's centre line. The imposed static load was equal to 33% of the column's maximum axial design capacity. About 30 minutes before to the fire's ignition, the load was applied, and it was kept at that level until the fire started in the furnace chamber. Due to the restriction on the column's thermal expansion during the fire, thermal (compressive) stresses that develop cause an increase in compressive loads. As soon as the load began to decrease, it was maintained. When the column could no longer support the loads, the test was terminated when the loads began to fall suddenly.

According to the experimental findings, increasing load eccentricity from 20 to 40 mm causes more spalling, which causes an exponential decline in fire resistance by 43%. Spalling is reduced by more longitudinal bars, especially mid-perimeter bars, which helps to boost fire resistance by 100% with doubling of longitudinal bars. Even a reduction in transverse reinforcement spacing from 300 mm to 150 mm for eccentric loads results in a 123% increase in fire resistance. Further loss in fire resistance occurs for explosively spalled high-strength columns due to local weakening of longitudinal reinforcement caused by early (10 min) and lasted up to 58 min deep spalling. The likelihood of a global column element buckling increases with a load eccentricity of 40 mm.

Even though these results conclude that spalling can be affected by load eccentricity significantly, more investigations considering different test methodologies may still be necessary. The adopted test set up is not accurate enough in reflecting end restraints, especially at the top of the columns. The eccentric load was applied through a steel ball which cannot represent real boundary conditions where column end are restrained to rotate and laterally translate at the same time. Columns in buildings are usually loaded through dead and live loads and restrained against rotational and transnational deformations at the same time through adjacent beams, in this test up the load is considered but only with lateral restraint. Additionally, in real cases there is possibility of partial exposing of columns to the fire depending on location of the fire and the column. Therefore, investigating column behaviours and spalling under eccentric load transferring through the

heated portion of the column may be different from a case if it transfers through the cold portion column. In addition to these concerns, other factors such as reinforcement details, load ratio, column size, column shape, and column height may also affect test outputs and therefore impose questions if they can be used in assessing members in relation to concrete heat spalling.

Another type of investigation available in the literature is uniaxially loaded large slabs (walls) tested vertically while subjected to heating. This configuration differs from column in which buckling is possible in both directions. Here bending is restricted to happen in one direction because the other direction is significantly longer. In a test conducted in [4], square slab 500 x 500 x 250 mm and rectangular slab 600 x 500 x 300 mm were tested under combined effects of uniaxial load and heating. The load was applied concentrically on the former but eccentrically for the latter. The compressive strength of the square and rectangular slabs was 42 MPa and 70 MPa respectively. Unlike to the column cases discussed above, here both end restraints are not fixed and are free to displace rotationally. The square samples were loaded up to 12% of their compressive strength while this was 9.6% for the rectangular slabs.

According to the test results, for the eccentrically loaded sample 70 mm spalling observed after 420 seconds whereas 9mm depth spalling observed for the concentrically loaded sample after 360 seconds. Even though the compressive strength of the eccentric sample is much higher than the concentric sample and both are loaded approximately to the same loading ratio, the former spalled deeper. This could be triggered by the test set up, the eccentric load has changed the stress state through the sample thickness which may change the behaviour of the sample on exposing to the heating. It is shown in the test that eccentric load located nearby the hot face, therefore more investigations are required to clarify if the eccentric load put on the rear cold face. Most importantly, end restraints are free to rotate and applied load intensity is too low in both cases, more investigations considering intenser loads are still necessary.

In a completely different test configuration, slab samples loaded biaxially can be observed in a work conducted by Lo Monte et al [37]. The test's objective is to evaluate the spalling sensitivity of heated concrete slabs subjected to biaxial membrane compression. Emphasising on explosive spalling, vertical deflection, temperature and pore pressure were monitored throughout the test. Square concrete slabs with 800 mm side, and 100 mm thickness were used. In order to maintain a low temperature in the outer 100 mm concrete rim in contact with the hydraulic jacks, heating is applied to the bottom face of a 600 x 600 mm central window. There are sixteen radial slits cut into the cold rim to disrupt its mechanical continuity since it may impact how the load is transmitted. All sample and instrumental details are shown in Figure 2.8. The slab is set within the loading system, which consists of eight hydraulic jacks mounted to the exterior restraint steel frame and has a maximum capacity of 1000 kN per axis. The aforementioned configuration was used to conduct more than 30 tests. Different concrete mixtures with compressive strengths ranging from 40 to 125 MPa, various types of aggregate, and the inclusion or exclusion of one or more forms of fibre have been studied. In every instance, the fire curve was ISO 834-1, and the slab thickness was 100 mm.

The applied load level was 10 MPa, and the greatest spalling depth at the end of the test

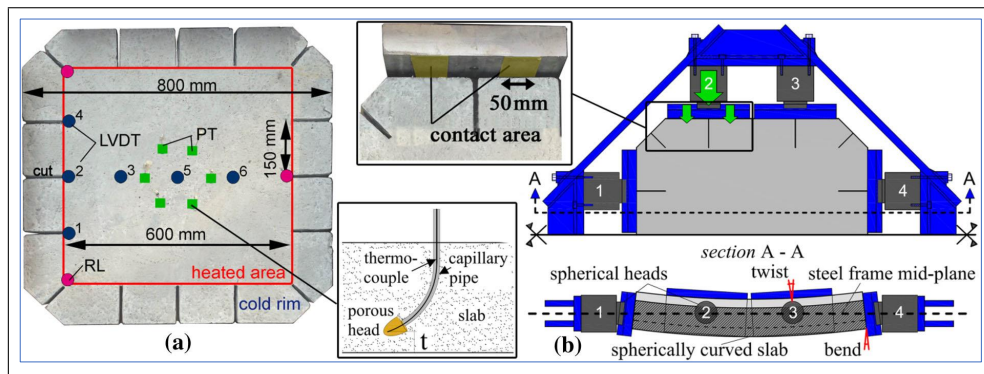


Figure 2.8: Adopted from [37], a) Concrete sample details with embedded pressure–temperature sensors, and b) The biaxial loading system configurations

was greater than 50 mm. Spalling was so severe that the slab collapsed after 34 minutes, demonstrating that the hogging bending moment had caused the unreinforced slab's bending carrying limit to be reached. Results indicate that, to some extent depending on the concrete mix, spalling severity rises with external compression. The influence of load on normal-strength concrete is evident: spalling depth dramatically rises with load in the low stress range (0–5 MPa), but tends to stabilise for higher compression. The impact of applied load is minimal in ultra high-performance concrete, on the other hand. It has been demonstrated through testing that polypropylene fibre successfully prevents spalling because the pore pressure is reduced. However, steel fibre appears to cause more stable fracture propagation and to keep pore pressure values comparable to or greater than in ordinary concrete.

It is worth mentioning that some results obtained in this investigation are test specific and therefore may not be generalised. During the early stages of the test, the mid span deflection of the samples increased appreciably, displacing toward the heating source. With heating pursuance and the degradation of the concrete, the stiffness centre shifted upward to the cooler zone resulting in reversing the displacement state, this time away from the heating source. This behaviour would not be observed if thicker samples were tested. This implies that size (thickness) of the sample can be another factor in altering test outputs.

2.4.4 Concluding remarks on experimental tests available in the literature

It is clear that the nature of the undertaken experimental investigations to date has been generally aimed at identifying spalling types, highlighting factors affecting spalling, and methods to reduce spalling risk. The implications behind adopting various test methodologies, which have led to different and even contradicted results, have not been well considered. Furthermore, disregarding the real member boundary conditions can be clearly observed in test setups in the experimental investigations. As a result, despite highlighting some parameters affecting concrete behaviour upon heating, findings through these investigations have been inconclusive and therefore insufficient to produce a standardized method to be followed in the tests relating to investigating concrete behaviour under effects of elevated temperatures.

Regarding parameters affecting concrete spalling at elevated temperature, numerous factors

have been highlighted from the experimental works which can be classified generally into three main categories, material characteristics, structural characteristics and fire characteristics. Material characteristics include material properties such as strength, mix ingredients (for example cement content, additives, moisture content, fibres), and aggregate type, while structural characteristics focus on specimen size, lateral reinforcement, degree of restraint, load intensity and load configuration. Fire characteristics relate to fire intensity and rate of heating [44].

Even though some of these parameters have been investigated individually in the literature, the findings are inconclusive and many concerns can be highlighted. For example, sample size has been decided based on practical considerations or the limitations of the laboratory without a focus on the implications the chosen size may have on the test outputs. On the other hand, lack of standardized method in testing concrete samples has given freedom to laboratories and researchers to choose various sample sizes utilizing different test set ups. As discussed before, small non-structural element samples like very thin, small plates, cubes and cylinders have been used in [45, 15, 46, 47, 28]. Meanwhile larger samples in the form of a single structural member like beam, column and slab have been used in [48, 19, 20, 22]. In macro level studies, continuous beams such as in [21] and even entire buildings [18] have been tested to facilitate a testing environment closer to the real structures in terms of size, boundary conditions and loads.

Regarding test setups, while in many experimental works samples were tested under the sole effect of heating with no applied load and no external mechanical restraints, e.g. [45, 4], in some other tests initial applied load prior heating was provided e.g. [39, 49, 28, 4, 24, 37]. In other studies samples were tested with the presence of mechanical restraints only [50, 4]. Above all these, other differences in terms of load intensity, whether it is concentric or eccentric load, and whether it is biaxial or uniaxial load can be found in the literature.

As a result of this scattered sample patterns, contradicted results can be observed in the literature. According to [44] the risk of explosive spalling of concrete increases with sample size, however it was found in [45] that thinner, unloaded, unrestrained samples spalled sooner and in a more destructive way than thicker samples and it was advised to pursue investigations for larger scale samples considering load and restraints. In a detailed work [4], conducted by a group of researchers for the sake of defining small or medium size samples to be used in tests relating to assessing fire spalling of concrete, different size samples with different geometries, utilizing different test set ups were investigated. Although it was found that some small samples correlated with larger samples in their fire resistance, it was reported that they are not sufficient to represent the real behaviour of concrete in real life situations because of significant differences in boundary conditions and sizes. From this test, different concrete behaviours were clearly observed between different size samples with the same material properties but tested in different test set ups. While some samples experienced spalling, some did not spall at all. To examine sample size effects on the behaviour and spalling of concrete while heated, still thorough investigations are necessary covering common test configurations and various boundary conditions.

Inconclusive and contradicted results can be also observed in investigating load effects from the literature. In spite of the differences mentioned between samples loaded through initially

applied load or passively loaded from restraints upon heating, the applied load intensity, on the other hand, could be another key factor to be questioned. As discussed before, some tests have been conducted under low intensity load such as 9.60% or 12% of the concrete strength such as in [4] meanwhile in other tests restraints have been provided instead of initial applied load where the load develops gradually only with the heat progress and expansion prevention from end restraints. These test methodologies are questionable, on one hand low loaded members would not well represent members in real structures knowing that compression members are usually loaded to a severer load ratio to achieve an economic design. Under low intensity load the concrete strength is well below yield limits prior testing, therefore it can contribute more in resisting heat effects which accordingly affects concrete behavior, specifically stress states and therefore spalling potential and test outcomes.

For the restraint samples on the other hand, the transient strain effect which is mainly a function of the applied load might not be well represented by the restrained samples accurately (transient strain will be discussed with more details in later sections). The load generation is gradual comparing to the real case scenario where the intensive initial loads are already there in addition to restraints from adjacent members. This is in addition to that the concrete here is fully intact at the ambient temperature and therefore resists heating effects more effectively, with its full strength, which results in observing very conservative results and may not represent reality, especially if the results would intend in assessing loaded structural members. In reality, structural members are often exposed to stresses from different applied loads and end restraint effects from adjoining beams or slabs. Therefore some researchers recommended to test heated samples in conjunction with loading [39, 49] to get more realistic outputs without giving particular recommendation on the load intensity and its type.

Apart from load intensity, inconsistency in testing set up relating to the type of the load could be another reason behind literature disagreement about spalling. For example, as mentioned above, in some tests loads were applied passively through mechanical restraint of the sample [4, 50] while in others uniaxial loads with different intensities were applied prior heating [28, 4, 24] and in others biaxial loads were applied [37]. Additionally, different methods can also be seen in applying the loads such as concentric loading [24], eccentric loading [43], and pre-stress technique through embedded bars [51].

The final concern in loaded sample investigations is the specific details through which the loads have been applied which may significantly affect the test results. For example, whether the tests were load or displacement controlled and how is the status of frictional resistance between the loading platens and the concrete body. Similarly in passively restrained samples, how the types and stiffness of the restraint may alter test outcomes.

To sum up, literature experimental tests have been conducted without specific consideration for the effects that the test set up could have on the observed behaviours. It is possible this has been a reason behind different test outcomes and hence a lack of consensus in the literature. Therefore, one of the most important question which will be investigated throughout this thesis is whether underlying parameters relating to test methodologies like sample size, restraints

(including mechanical, self-restraint via the so called ‘cold ring’ effect and applied load), and load intensity may control test outcomes and have been a reason of the literature contradicted results.

2.5 Modelling of concrete at high temperature

Understanding concrete’s performance in fire situations or other high temperature environments requires modelling the material’s behaviour at these temperatures. Concrete experiences a number of physical and chemical changes at high temperatures that have a substantial impact on its mechanical characteristics. In modeling concrete at higher temperature many steps and factors need to be considered.

1. Thermal analysis to study temperature distribution within the concrete structure is required. Finite element analysis which takes into account elements including heat conduction, convection, and radiation is crucial to show the temperature profile of the concrete during a fire through modelling the heat transport mechanisms.
2. Concrete’s properties alter with temperature, including thermal conductivity, specific heat capacity, and thermal expansion are required. These characteristics can be empirically calculated or measured experimentally. The numerical models are then updated to appropriately reflect the behaviour of concrete at high temperatures by include the temperature-dependent material properties.
3. Strength degradation with temperature is another key parameter in modeling concrete. This can be modelled by taking into account the chemical changes, thermal cracking, and spalling that take place inside the material. Different mathematical models and empirical provisions have been established to explain how concrete loses strength at high temperatures.
4. Concrete is a porous material that experiences mass loss at high temperatures as a result of the evaporation of chemically and physically bonded water. The thermal characteristics and mechanical behaviour of concrete are impacted by the loss of moisture content. To precisely forecast how concrete would react to high temperatures, moisture flow and evaporation need to be considered.
5. Structural response: The interplay of thermal impacts and mechanical behaviour determines how concrete structures react in hot environments. When considering both thermal and mechanical loading, the structural response can be simulated using finite element analysis. The model needs to take into consideration thermal stresses, thermal expansion, and the impact of strength deterioration on structural integrity.
6. Experimental validation: It is essential to check the numerical models’ predictions against actual data from experiments. Concrete specimens or full-scale structures can be subjected

to high-temperature testing, which can yield data for model calibration and verification. The accuracy and dependability of the modelling technique can be increased by comparing the projected results with experimental measurements.

The behaviours of concrete at high temperatures have been studied mainly using two different methods: thermo mechanical models and hygro-thermo mechanical models. Both models seek to represent the complicated relationships between concrete's mechanical characteristics, moisture content, and temperature, but they vary in complexity and level of detail.

The main focus of thermo mechanical models is on the thermal behaviour of concrete exposed to high temperatures. They take into account the methods of internal heat transport and how they affect the mechanical characteristics of concrete, such as strength, stiffness, and creep. These models frequently include simplified assumptions, such as the behaviour of materials being isotropic and ignoring the effect of moisture content. The behaviour of concrete structures in fire situations has been extensively studied using thermo-mechanical models [52].

Hygro-thermo-mechanical models, on the other hand, take into account the additional impact of moisture on the behaviour of concrete at high temperatures. These simulations take into account the interaction of heat transfer, moisture transport, and mechanical deformation. They take into account concrete's hygroscopic and thermal expansion as well as the impact of moisture content on its mechanical characteristics. Particularly suitable for applications where moisture plays a large role including concrete subjected to high temperatures in humid settings. The concrete is modelled as a three-phase system with solid, liquid, and gas phases in a fully coupled hygro-thermo mechanical formulation. The solid skeleton is thought to have isotropic elastic-damage behaviour, and other major thermo-mechanical behaviour is taken into account along with material degradation brought on by mechanical and thermal loads. Adsorbed water that is physically attached to the surface of the solid skeleton is thought to be a part of the liquid phase, and its behaviour is examined when necessary. Dry air and water vapour, both of which are expected to behave as ideal gases, are thought to make up the gas phase [1].

To choose between these two model types, the exact conditions and study aims will determine whether to use thermo-mechanical or hygro-thermo-mechanical models. Thermo-mechanical models are appropriate in situations when moisture effects can be ignored or are of minor concern, they are simpler to use and more computationally efficient. On the other hand, hygro-thermo-mechanical models provide a more thorough study by taking into account the effect of moisture on concrete's reaction to high temperatures. Although more difficult and computationally demanding, they offer a more accurate representation of actual conditions.

Following this pattern, parallel to experimental investigations, numerous numerical model e.g. [1, 28, 52, 53, 54, 55] and many others can be found in the literature which were established aiming to understand complex behaviour of concrete spalling.

It is very challenging to design a model capable of simulating and predicting concrete behaviour under abnormal heating effects. Numerous temperature dependent parameters such as thermal expansion, conductivity, concrete degradation in tension and compression, specific heat, modulus of elasticity, stress strain behaviour in tension and compression, and many others should

be taken into consideration. For each of these parameters various equations have been proposed which are affecting modeling outputs upon choosing one over the other. In the following sections, these parameters have been discussed and summarized.

2.6 Temperature dependent properties of concrete

Concrete's temperature dependent characteristics, which have a considerable impact on how the material responds to high temperatures, can generally be divided into three groups. They are temperature dependent mechanical properties, temperature dependent thermal properties, and temperature dependent deformation properties [56].

2.6.1 Concrete temperature dependent mechanical properties

Compressive strength, tensile strength, elastic modulus, and concrete stress strain response are main mechanical properties of concrete affected by heating.

2.6.1.1 Compressive strength

The fundamental concern in fire resistance design is the compressive strength of concrete at high temperatures. Concrete's compressive strength at room temperature is influenced by the water-cement ratio, the transition zone between the aggregate and the cementitious paste, the curing environment, the type and size of the aggregate, and the types of admixtures [57]. These elements, along with the rate and duration of heating, have a significant impact on compressive strength degradation at high temperatures [58]. To determine concrete's compressive strength at high temperatures, several models have been suggested as summarised in Equations 2.1 through 2.5 and compared graphically in Figure 2.9.

Equation 2.1 is from Yang et al. [52] which considers three range of concrete degradation. It considers concrete to remain intact up to 450°C , afterwards sudden disintegration takes place which ends to complete strength loss at 874°C .

$$\begin{aligned} f_c(T) &= f'_c & 0 \leq T \leq 450^{\circ}\text{C} \\ f_c(T) &= f'_c[2.011 - 2.353(T - 20)/1000] & 450^{\circ}\text{C} \leq T \leq 874^{\circ}\text{C} \\ f_c(T) &= 0 & T > 874^{\circ}\text{C} \end{aligned} \quad (2.1)$$

In contrast to this equation, Equation 2.2 from Lie et al.[59] considers concrete degradation early on, however considers complete strength loss at lower temperature 700°C .

$$\begin{aligned} f_c(T) &= f'_c(1 - 0.001T) & T \leq 500^{\circ}\text{C} \\ f_c(T) &= f'_c(1.375 - 0.00175T) & 500^{\circ}\text{C} \leq T \leq 700^{\circ}\text{C} \\ f_c(T) &= 0 & T > 700^{\circ}\text{C} \end{aligned} \quad (2.2)$$

In Equation 2.3 suggested by Hertz[60], where concrete degradation has been related to different aggregate types, siliceous aggregate has been considered to degrade more rapidly with

temperature rise (Figure 2.9).

$$f_c(T) = f'_c / [1 + T/T_1 + (T/T_2)^2 + (T/T_8)^8 + (T/T_{64})^{64}] \quad (2.3)$$

For Siliceous aggregate: $T_1 = 15,000$, $T_2 = 800$, $T_8 = 570$, and $T_{64} = 100,000$, Light weight aggregate: $T_1 = 100,000$, $T_2 = 1100$, $T_8 = 800$, and $T_{64} = 940$, Other aggregates: $T_1 = 100,000$, $T_2 = 1080$, $T_8 = 690$, and $T_{64} = 1000$.

Equation 2.4 proposed by Li and Purkiss [53] takes middle range among others considering early degradation just beyond ambient temperature.

$$f_c(T) = f'_c [0.00165(T/100)^3 - 0.03(T/100)^2 + 0.025(T/100) + 1.002] \quad (2.4)$$

Equation 2.5 suggested by Kodur et al. [61], it considers more significant deterioration early on, then a stable zone between $100 - 400^\circ\text{C}$, and its last range takes middle range close and parallel to the Equation 2.4 (Figure 2.9).

$$\begin{aligned} f_c(T) &= f'_c [(1.0 - 0.003125(T - 20))] & T < 100^\circ\text{C} \\ f_c(T) &= 0.75 f'_c & 100^\circ\text{C} \leq T \leq 400^\circ\text{C} \\ f_c(T) &= f'_c (1.33 - 0.00145T) & T > 400^\circ\text{C} \end{aligned} \quad (2.5)$$

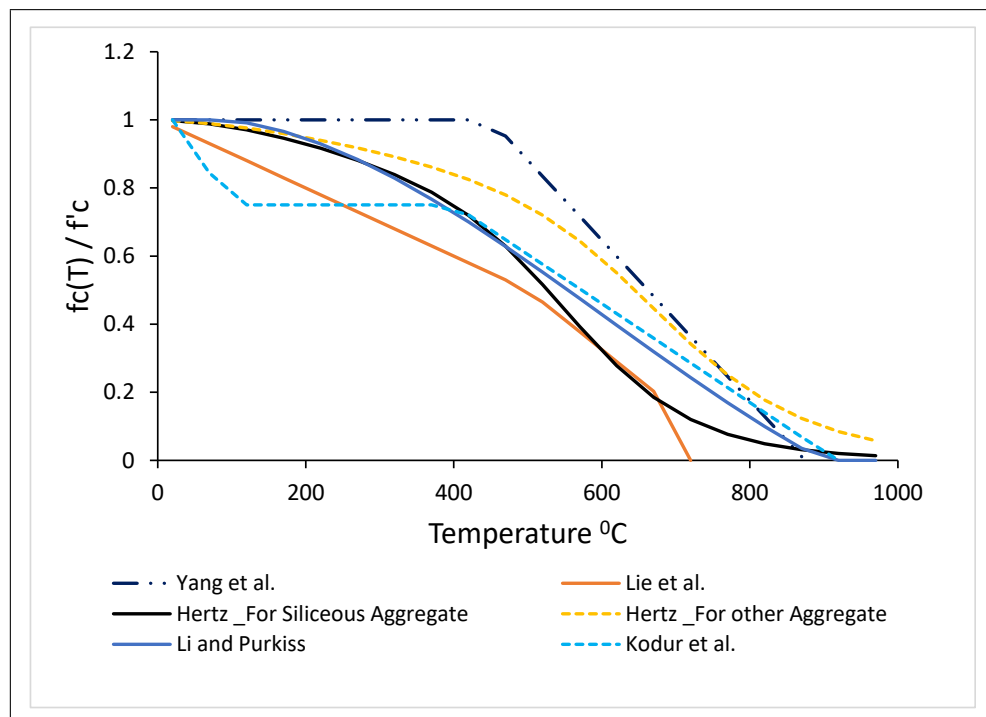


Figure 2.9: Comparison of concrete compressive strength degradation models at high temperature

Generally speaking, as clear from Figure 2.9, 25% difference which is increasing with temperature, reaching around 40% at 400°C , can be observed between lower and upper limits. These differences are high enough to deviate numerical investigation outputs upon selecting one option over the other. One reason may be different test set ups adopted in experimental

investigations from which the data were extracted to derive these equations. Throughout this thesis, test set up effects on test outcomes will be investigated considering literature experiments tested under different scenarios.

2.6.1.2 Tensile strength

In comparison to compressive strength, there are far fewer research on the tensile strength of concrete at high temperatures. Because concrete's tensile strength is substantially lower than its compressive strength, which is only around 10% of its compressive strength, calculations for strength at normal temperatures frequently ignore this factor. However, from the perspective of fire resistance, it is a crucial feature. Tensile stresses are typically the cause of concrete cracking, and the continuation of microcracking frequently results in structural damage to the member under tension. Therefore, knowledge of concrete's temperature-dependent tensile strength is essential to understand the spalling caused by fire [56, 62]. Equations 2.6 through 2.11 which are plotted in Figure 2.10 have been adopted widely in the literature.

Equation 2.6 suggested by Yang et al. [52] relates tensile strength degradation with compressive strength deterioration. It has widest stable range assuming that concrete remain intact up to 450°C. and it takes upper limit comparing to other models (Figure 2.10).

$$f'_t(T) = 0.09f_c(T) \quad (2.6)$$

Where $f_c(T)$ is from Equation 2.1

However, Equation 2.7, proposed by Bazant et al. cited in [62], relates the degradation as function of temperature consisting of three ranges. It takes middle range between upper and lower limit up to around 450°C then starts to decline, reaching lower limit at higher temperatures.

$$\begin{aligned} f'_t(T) &= -0.000526T + 1.01052 & 20^\circ\text{C} \leq T \leq 400^\circ\text{C} \\ f'_t(T) &= -0.00252T + 1.8 & 400^\circ\text{C} \leq T \leq 600^\circ\text{C} \\ f'_t(T) &= -0.0005T + 0.6 & 600^\circ\text{C} \leq T \leq 1000^\circ\text{C} \end{aligned} \quad (2.7)$$

Similar to Equation 2.6, Terro [52] suggested tensile degradation dependant on compressive strength reduction.

$$f'_t(T) = f'_t[f_c(T)/f'_c], \quad f'_t = f'_c/10 \quad (2.8)$$

From Chang et al. [63] again the deterioration has been related to temperature increase. It takes lower limit throughout the entire temperature range (Figure 2.10).

$$\begin{aligned} f'_t(T) &= f'_t(1.05 - 0.0025T) & 20^\circ\text{C} \leq T \leq 100^\circ\text{C} \\ f'_t(T) &= 0.8f'_t & 100^\circ\text{C} \leq T \leq 200^\circ\text{C} \\ f'_t(T) &= f'_t(1.02 - 0.0011T) \geq 0 & 200^\circ\text{C} \leq T \leq 800^\circ\text{C} \end{aligned} \quad (2.9)$$

Li and Guo Equation reported in [64] considers linear decrease in the tensile strength, runs

mostly along with the lower limit comparing to other models.

$$f'_i(T) = f'_i(1 - 0.001T) \quad 20^\circ\text{C} \leq T \leq 1000^\circ\text{C} \quad (2.10)$$

Bastami et al. Equation [62] considers highest degradation after around 600°C .

$$\begin{aligned} f'_i(T) &= f'_i(1.02 - 0.00098T) \leq 1 & 20^\circ\text{C} \leq T \leq 300^\circ\text{C} \\ f'_i(T) &= f'_i(0.965 - 0.0001T - 9 \times 10^{-7}T^2 \\ &\quad - 3 \times 10^{-9}T^3 + 3.2 \times 10^{-12}T^4) & 300^\circ\text{C} \leq T \leq 900^\circ\text{C} \\ f'_i(T) &= 0 & T \geq 1000^\circ\text{C} \end{aligned} \quad (2.11)$$

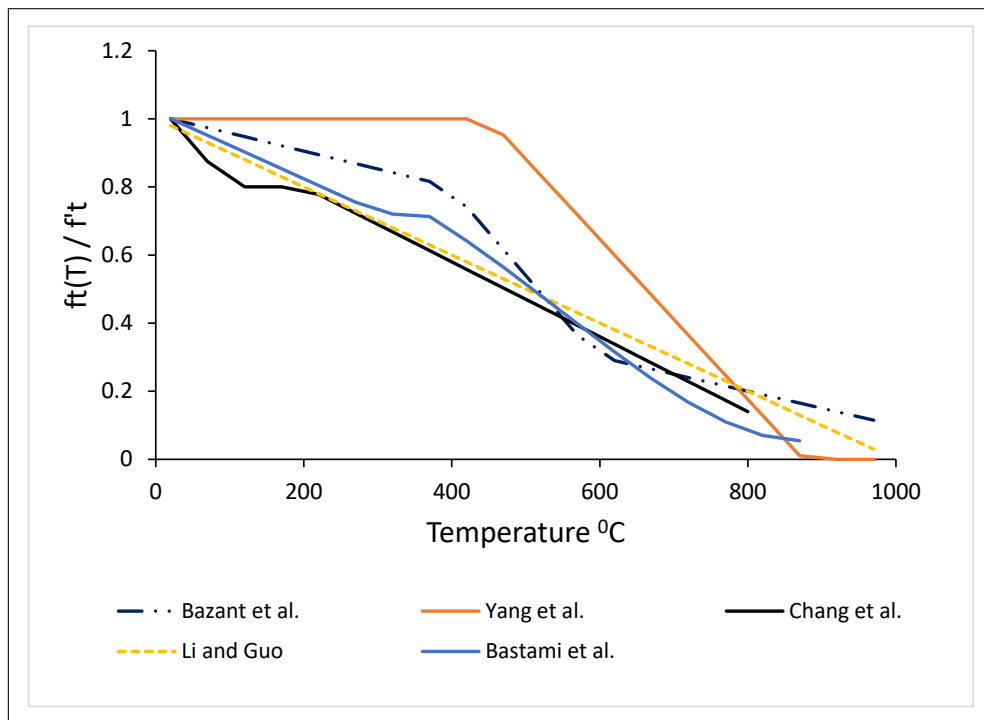


Figure 2.10: Concrete tensile strength degradation models at high temperature

2.6.1.3 Elastic modulus

The modulus of elasticity of the concrete is influenced mainly by the same parameters affecting compressive strength. It decreases with increasing temperature due to disintegration of hydrated cement products and deterioration of bonds in the microstructure of cement paste. The extent of elastic modulus deterioration depends on moisture content loss, high temperature creep, and aggregate type [56]. The most commonly used models have been summarised below and plotted graphically in Figure 2.11. Anderberg and Thelandersson [28] derived a mathematical equation incorporating ϵ_{max} which is strain at peak stress:

$$E(T) = \frac{2f_c(T)}{\epsilon_{max}} \quad (2.12)$$

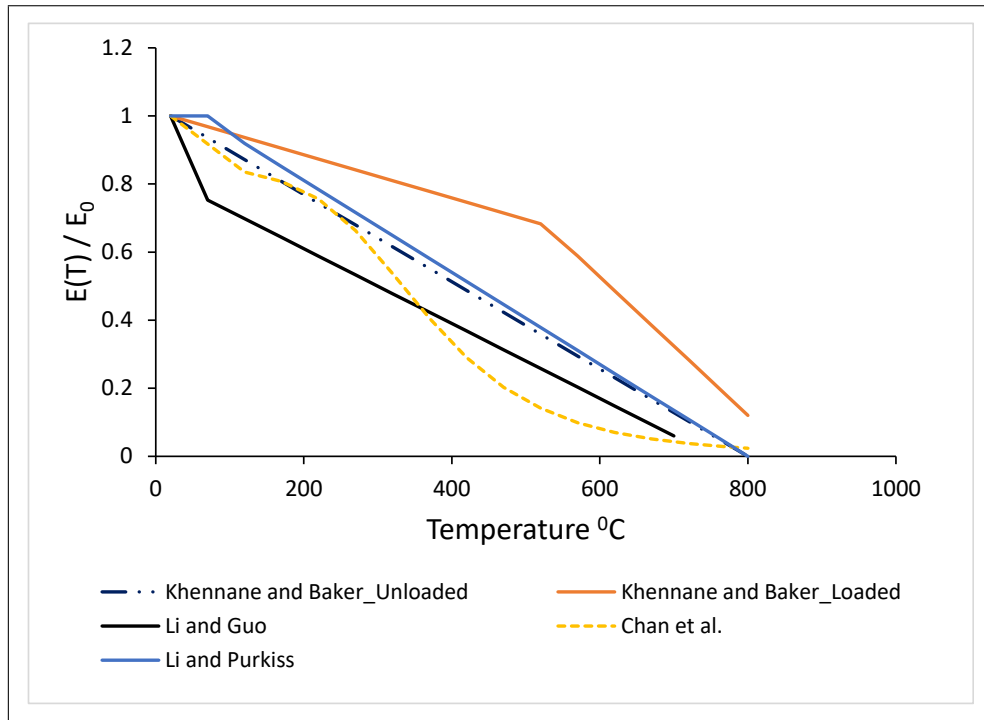


Figure 2.11: Concrete elastic modulus degradation models at high temperatures

Where, as explained in [65, 62]

$$\varepsilon_{max} = 0.00000167T + 0.002666 \geq 0.003, \quad T \leq 800^{\circ}\text{C} \quad (2.13)$$

Based on the experimental data from [28], Khennane and Baker proposed two equations based on the adopted test methodologies [65]. Equation 2.14 is for unloaded samples meanwhile Equation 2.15 is for samples loaded prior heating and throughout the test.

For unloaded sample:

$$E(T) = E_0(-0.001282T + 1.025641) \quad 20^{\circ}\text{C} \leq T \leq 800^{\circ}\text{C} \quad (2.14)$$

For preloaded sample:

$$\begin{aligned} E(T) &= E_0(-0.000634T + 1.012673) \quad 20^{\circ}\text{C} \leq T \leq 525^{\circ}\text{C} \\ E(T) &= E_0(-0.002036T + 1.749091) \quad 525^{\circ}\text{C} \leq T \leq 800^{\circ}\text{C} \end{aligned} \quad (2.15)$$

As it can be seen from Figure 2.11, the unloaded samples degrade more significantly comparing to loaded samples under effects of heating. The loaded samples takes the upper limit among all other models. This is also another indication emphasising on test set up effects on concrete behaviour observed in literature tests.

Equation 2.16 proposed by Li and Guo cited in [64] takes the lower limit range among other models up to around 450°C . It has been derived up to 700°C which is the lowest range comparing to other models.

$$\begin{aligned} E(T) &= E_0 \quad 20^{\circ}\text{C} \leq T \leq 60^{\circ}\text{C} \\ E(T) &= E_0(0.83 - 0.0011T) \quad 60^{\circ}\text{C} \leq T \leq 700^{\circ}\text{C} \end{aligned} \quad (2.16)$$

Equation 2.17 derived by Chang et al. [63] takes middle strip of the range up to around 300°C, then it starts to decline significantly, afterwards it takes lower limit among other models up to 800°C.

$$\begin{aligned} E(T) &= E_0(-0.00165T + 1.033) & 20^\circ\text{C} \leq T \leq 125^\circ\text{C} \\ E(T) &= E_0/[1.2 + 18(0.0015T)^{4.5}] & 125^\circ\text{C} \leq T \leq 800^\circ\text{C} \end{aligned} \quad (2.17)$$

Li and Purkiss [53] equation (Equation 2.18) is very similar to Equation 2.14. While the former is derived for any samples, the latter is assigned just for unloaded samples as discussed before. This is again emphasising on literature inconsistency regarding concrete behaviours at elevated temperature.

$$\begin{aligned} E(T) &= E_0 & 20^\circ\text{C} \leq T \leq 60^\circ\text{C} \\ E(T) &= E_0[(800 - T)/740] & 60^\circ\text{C} \leq T \leq 800^\circ\text{C} \end{aligned} \quad (2.18)$$

2.6.1.4 Stress strain relationship

As clarified in previous sections, different models are available to predict degradation of concrete properties such as compressive strength, tensile strength, and modulus of elasticity under effects of heating. This has been reflected in the proposed stress strain relationships in tension and compression.

In terms of compressive stress strain relationships, Equation 2.19 is proposed by Lie [66]

$$\sigma_c = \begin{cases} f_c(T) \left[1 - \left(\frac{\epsilon_{max} - \epsilon_c}{\epsilon_{max}} \right)^2 \right] & \epsilon_c \leq \epsilon_{max} \\ f_c(T) \left[1 - \left(\frac{\epsilon_c - \epsilon_{max}}{3\epsilon_{max}} \right)^2 \right] & \epsilon_c > \epsilon_{max} \end{cases} \quad (2.19)$$

where ϵ_c is concrete strain at different temperatures, f'_c is the compressive strength at ambient temperature, $f_c(T)$ which is the temperature dependent compressive strength given by Equation 2.1, and the strain at ultimate compressive strength at different temperatures, ϵ_{max} , is given by

$$\epsilon_{max} = 0.0025 + (6T + 0.04T^2) \times 10^{-6} \quad (2.20)$$

From Kodur et al. [61] the following equation has been proposed

$$\sigma_c = \begin{cases} f_c(T) \left[1 - \left(\frac{\epsilon_{max} - \epsilon_c}{\epsilon_{max}} \right)^H \right] & \epsilon_c \leq \epsilon_{max} \\ f_c(T) \left[1 - \left(\frac{30(\epsilon_c - \epsilon_{max})}{(130 - f'_c)\epsilon_{max}} \right)^2 \right] & \epsilon_c > \epsilon_{max} \end{cases} \quad (2.21)$$

Where

$$\epsilon_{max} = 0.0018 + (6.7f'_c + 6T + 0.03T^2) \times 10^{-6} \quad (2.22)$$

$f_c(T)$ is per Equation 2.5 and $H = 2.28 - 0.012f'_c$.

In EN1992-1-2 [67], the ascending part of the curve proposed to be

$$\sigma_c = \frac{3\epsilon_c f_c(T)}{\epsilon_{max}(2 + (\epsilon_c/\epsilon_{max})^3)} \quad \epsilon_c \leq \epsilon_{max} \quad (2.23)$$

Parameters $f_c(T)$ and ε_{max} are tabulated in the code. For the descending part, linear or non-linear equations based on the same given tabular data can be established.

From Anderberg and Thelandersson [28] the following equation proposed which incorporates elastic modulus.

$$\sigma_c = \begin{cases} E(T) \left[\varepsilon_c - \frac{\varepsilon_c^2}{(2\varepsilon_{max})} \right] & \varepsilon_c \leq \varepsilon_1, \\ E(T) \left[\varepsilon_1 - \frac{\varepsilon_1^2}{(2\varepsilon_{max})} \right] - 880(\varepsilon_c - \varepsilon_1) & \varepsilon_c > \varepsilon_1 \end{cases} \quad (2.24)$$

Where $E(T)$ is per Equation 2.12, ε_{max} is per Equation 2.13, and $\varepsilon_1 = \varepsilon_{max}(1 - 880/E(T))$.

In terms of stress strain relationship in tension, very limited number of equations are available in the literature. From Yang et al. [52]

$$\begin{aligned} \sigma_t &= E(T)\varepsilon_t & \varepsilon_t &\leq \varepsilon_{tk} \\ \sigma_t &= f'_t(T) - \frac{0.1f'_t(T)}{\varepsilon_{tk}}(\varepsilon_t - \varepsilon_{tk}) & \varepsilon_{tk} &< \varepsilon_t \leq 2\varepsilon_{tk} \\ \sigma_t &= 0.9f'_t(T) & \varepsilon_t &> 2\varepsilon_{tk} \end{aligned} \quad (2.25)$$

where $f'_t(T) = 0.09f_c(T)$, $\varepsilon_{tk} = \frac{f'_t(T)}{E(T)}$, and $f_c(T)$ is from Equation 2.1.

From Bastami et al.[62]

$$\begin{aligned} \sigma_t &= f'_t(T)E_o & \varepsilon_t &\leq \varepsilon_{tk} \\ \sigma_t &= f'_t(T)(\varepsilon_{tk}/\varepsilon_t)^{0.75} & \varepsilon_t &> \varepsilon_{tk} \end{aligned} \quad (2.26)$$

where $f'_t(T)$ is suggested to be obtained from Equation 2.11

To clarify how stress strain curves are different in the literature, compressive stress strain curves are compared numerically in Figure 2.12 for a hypothetical 40 MPa concrete material. While at ambient temperature the presented models are close, with increasing temperature the ultimate strength is significantly different for each model. Up to 200°C, Lie, EN1992-1-2, and Andeberg equations consider strength to remain intact, however Kodur considers around 30% reduction of the ultimate strength. With further increasing temperature to 400°C, only Lie and Andeberg equations consider strength to remain intact, however Kodur and EN1992-1-2 consider around 30% reduction of the strength. At 600°C all equations consider significant strength reduction, 34% according to Lie and Andeberg equations and 56% per Kodur and EN1992-1-2 Equations. It can also be noted with increasing temperature, strain corresponding to ultimate strength (ε_{max}) increases significantly, having different values per each model. Again, all of these inconsistencies show that the various equations were derived using data taken from tests with various test ups. Therefore, when testing concrete under the effects of heating, taking into account test set up effects on test outputs is a critical element that has not been well researched in the literature.

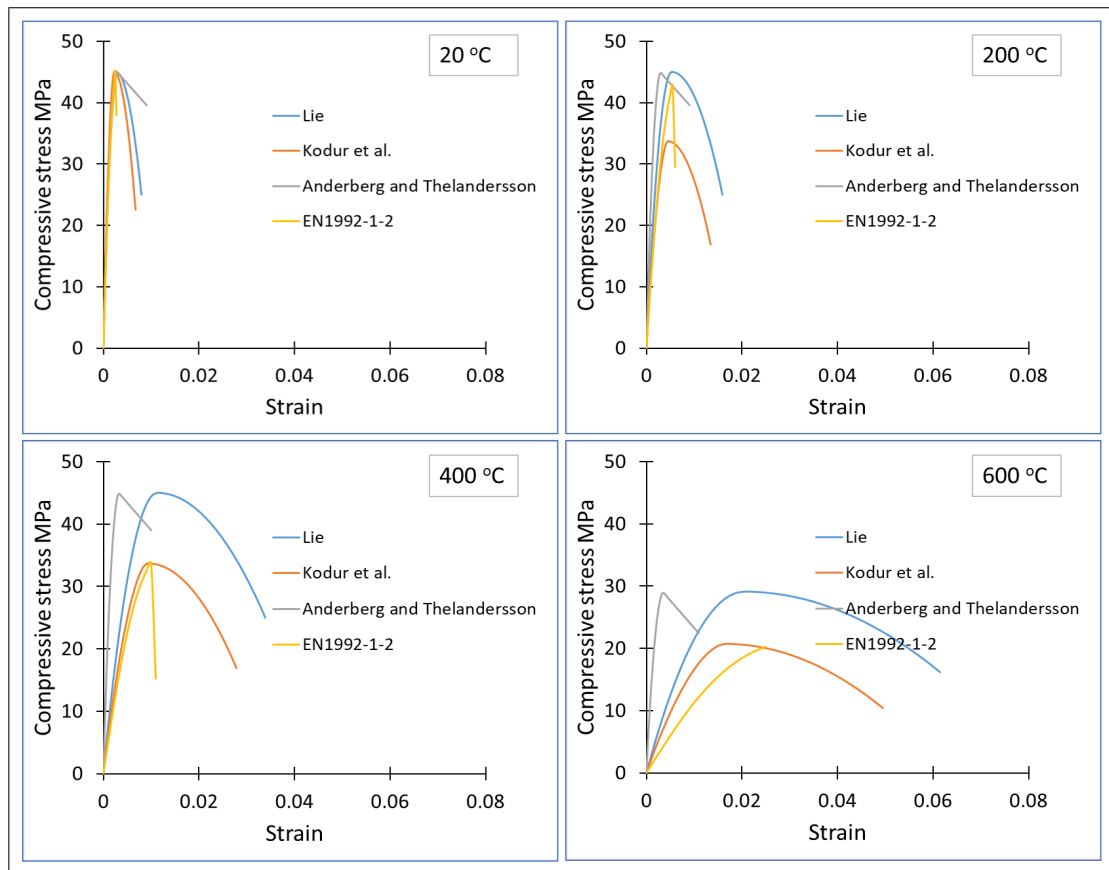


Figure 2.12: Comparison of concrete stress strain relationships at various temperatures

2.6.2 Concrete temperature dependent thermal properties

Thermal conductivity, specific heat (or heat capacity), and mass loss are thermal properties that control temperature dependent characteristics of concrete structures. Aggregate type, amount of moisture in the mix, and composition of the concrete all have a significant impact on these characteristics. For each property, several models have been proposed in the literature as summarised in Tables 2.1, 2.2, 2.3 respectively.

Table 2.1: Concrete thermal conductivity models

References	Function	Range
1.(Kodur et al.(2004)) Siliceous Aggr. Carbonate Aggr.	$k_c = (2 - 0.0011T) * 0.85$ (W/m°C) $k_c = (2 - 0.0013T) * 0.85$ $k_c = (2.21 - 0.002T) * 0.85$	$0^\circ\text{C} \leq T \leq 1000^\circ\text{C}$ $0^\circ\text{C} \leq T \leq 300^\circ\text{C}$ $300^\circ\text{C} \leq T \leq 1000^\circ\text{C}$
2.(EN1992-1-2) Upper limit all Agg. Lower limit all Agg.	$k_c = 2 - 0.2451(T/100) + 0.0107(T/100)^2$ $k_c = 1.36 - 0.136(T/100) + 0.0057(T/100)^2$	$20^\circ\text{C} \leq T \leq 1200^\circ\text{C}$ $20^\circ\text{C} \leq T \leq 1200^\circ\text{C}$
3.ASCE Manual 1992 Siliceous Aggr. Carbonate Aggr.	$k_c = -0.000625T + 1.5$ $k_c = 1$ $k_c = 1.35$ $k_c = -0.001241T + 1.7162$	$20^\circ\text{C} \leq T \leq 800^\circ\text{C}$ $T \geq 800^\circ\text{C}$ $20^\circ\text{C} \leq T \leq 293^\circ\text{C}$ $T \geq 293^\circ\text{C}$

Table 2.2: Concrete specific heat models

References	Function	Range
1.(Eurocode 2 (2004))	$C_p(T) = 900$ (J/kg °C) $= 900 + (T - 100)$ $= 1000 + (T - 200)/2$ $= 1100$	$20^\circ\text{C} \leq T \leq 100^\circ\text{C}$ $100^\circ\text{C} \leq T \leq 200^\circ\text{C}$ $200^\circ\text{C} \leq T \leq 400^\circ\text{C}$ $400^\circ\text{C} \leq T \leq 1200^\circ\text{C}$
2.ASCE Manual 1992 Siliceous Aggr. Carbonate Aggr.	$C_p(T) = (0.005T + 1.7) \times 10^6 / \rho$ ρ density (J/kg °C) $= 2.7 \times 10^6 / \rho$ $= (0.013T - 2.5) \times 10^6 / \rho$ $= 2.7 \times 10^6 / \rho$ $C_p(T) = 2.566 \times 10^6 / \rho$ (J/kg °C) $= (0.1765T - 68.034) \times 10^6 / \rho$ $= (25.00671 - 0.05043T) \times 10^6 / \rho$ $= 2.566 \times 10^6 / \rho$ $= (0.01603T - 5.44881) \times 10^6 / \rho$ $= (0.16635T - 100.90225) \times 10^6 / \rho$ $= (176.07343 - 0.22103T) \times 10^6 / \rho$ $= 2.566 \times 10^6 / \rho$	$20^\circ\text{C} \leq T \leq 200^\circ\text{C}$ $200^\circ\text{C} \leq T \leq 400^\circ\text{C}$ $400^\circ\text{C} \leq T \leq 500^\circ\text{C}$ $T \geq 600^\circ\text{C}$ $20^\circ\text{C} \leq T \leq 400^\circ\text{C}$ $400^\circ\text{C} \leq T \leq 410^\circ\text{C}$ $410^\circ\text{C} \leq T \leq 445^\circ\text{C}$ $445^\circ\text{C} \leq T \leq 500^\circ\text{C}$ $500^\circ\text{C} \leq T \leq 635^\circ\text{C}$ $635^\circ\text{C} \leq T \leq 715^\circ\text{C}$ $715^\circ\text{C} \leq T \leq 785^\circ\text{C}$ $T \geq 785^\circ\text{C}$
3.(Kodur et al.(2004)) Siliceous Aggr. Carbonate Aggr.	$C_p(T) = (0.005T + 1.7) \times 10^6 / \rho$ ρ density (J/kg °C) $= 2.7 \times 10^6 / \rho$ $= (0.013T - 2.5) \times 10^6 / \rho$ $= (10.5 - 0.013T) \times 10^6 / \rho$ $= 2.7 \times 10^6 / \rho$ $C_p(T) = 2.45 \times 10^6 / \rho$ (J/kg °C) $= (0.026T - 12.85) \times 10^6 / \rho$ $= (0.0143T - 6.295) \times 10^6 / \rho$ $= (0.1849T - 120.11) \times 10^6 / \rho$ $= (-0.263T + 212.4) \times 10^6 / \rho$ $= 2 \times 10^6 / \rho$	$20^\circ\text{C} \leq T \leq 200^\circ\text{C}$ $200^\circ\text{C} \leq T \leq 400^\circ\text{C}$ $400^\circ\text{C} \leq T \leq 500^\circ\text{C}$ $500^\circ\text{C} \leq T \leq 600^\circ\text{C}$ $600^\circ\text{C} \leq T \leq 635^\circ\text{C}$ $20^\circ\text{C} \leq T \leq 400^\circ\text{C}$ $400^\circ\text{C} \leq T \leq 475^\circ\text{C}$ $475^\circ\text{C} \leq T \leq 650^\circ\text{C}$ $650^\circ\text{C} \leq T \leq 735^\circ\text{C}$ $735^\circ\text{C} \leq T \leq 800^\circ\text{C}$ $800^\circ\text{C} \leq T \leq 1000^\circ\text{C}$

Table 2.3: Concrete mass loss models

References	Function	Range
1.(Eurocode 2 (2004))	$\rho(T) = \rho(20^\circ\text{C})$ $\rho(T) = \rho(20^\circ\text{C})(1 - 0.02(T - 115)/85)$ $\rho(T) = \rho(20^\circ\text{C})(0.98 - 0.03(T - 200)/200)$ $\rho(T) = \rho(20^\circ\text{C})(0.95 - 0.07(T - 400)/800)$	$20^\circ\text{C} \leq T \leq 115^\circ\text{C}$ $115^\circ\text{C} \leq T \leq 200^\circ\text{C}$ $200^\circ\text{C} \leq T \leq 400^\circ\text{C}$ $400^\circ\text{C} \leq T \leq 1200^\circ\text{C}$
2.(Lie et al. (1996))	$\rho(T) = \rho(20^\circ\text{C})(0.9987 - 0.00003992T)$	$0^\circ\text{C} \leq T \leq 1000^\circ\text{C}$

To visualize the differences between various models, graphical representation of conductivity, specific heat, and mass loss are shown in Figure 2.13, Figure 2.14, and Figure 2.15 respectively.

For conductivity (Figure 2.13), wide range difference can be observed between proposed equations. EN1992-1-2 proposed lower and upper limits, however Kodur and ASCE equations

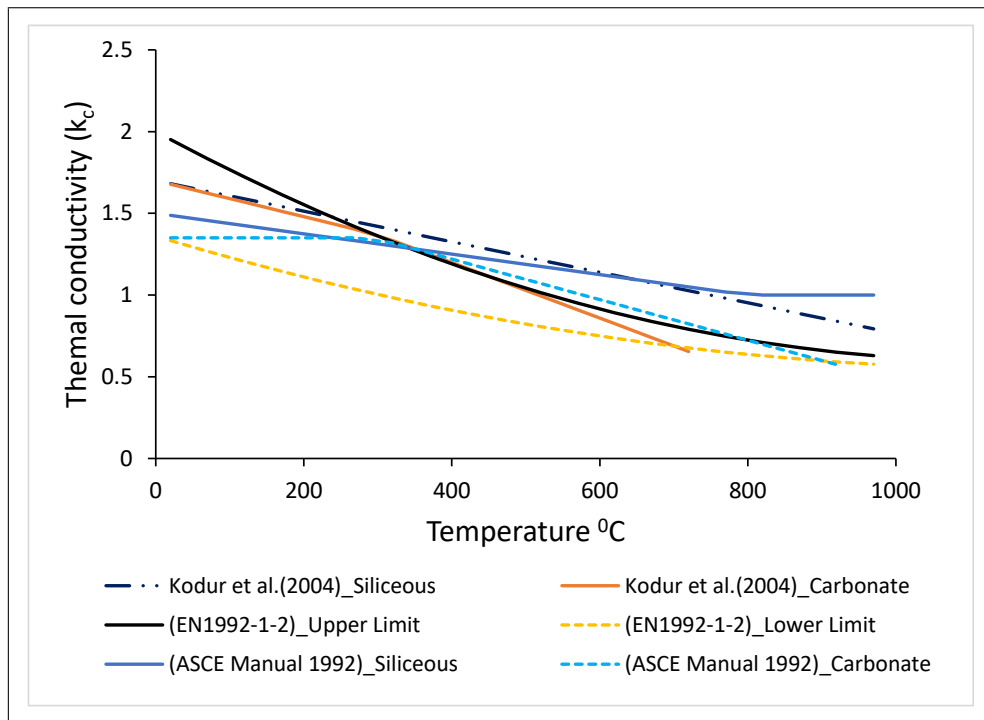


Figure 2.13: Different thermal conductivity models from literature

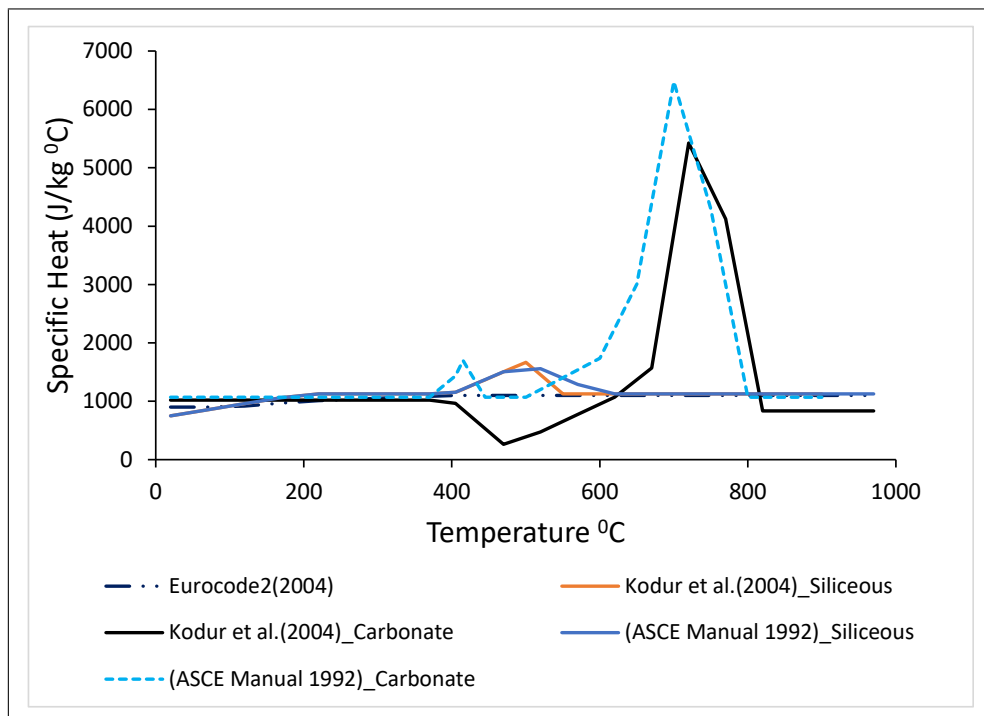


Figure 2.14: Different specific heat models from literature

proposed different equations based on aggregate types. The lower limit of EN1992-1-2 is lower than all other equations, while its upper limit is surpassed by other equations after around 350°C.

In terms of specific heat (Figure 2.14), Kodur and ASCE models are close for siliceous aggregate types, however, a difference can be seen for carbonate aggregate, where the specific heat is 20% higher according to the ASCE model at 700°C. For both equations, carbonate aggregate shows a significant difference with siliceous aggregate between 600°C and 800°C.

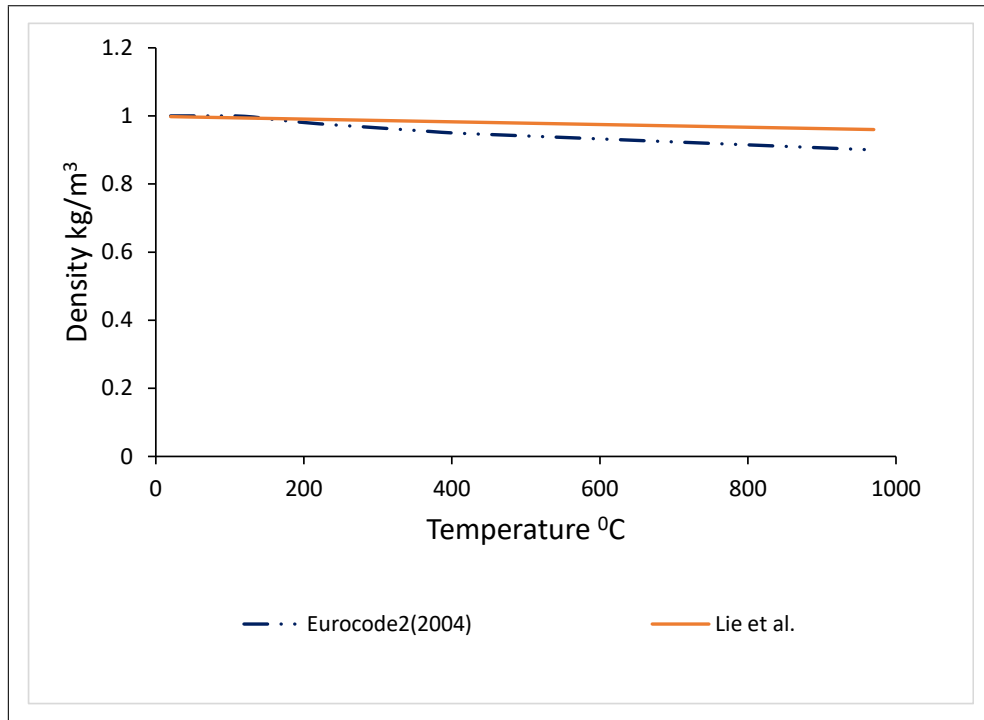


Figure 2.15: Different thermal conductivity models from literature

For the mass loss property (Figure 2.15), comparing to conductivity and specific heat, the two presented models, (Eurocode 2 (2004)) and (Lie et al. (1996)) [68]), are close in predicting mass loss.

2.6.3 Concrete temperature dependent deformation properties

Thermal expansion and creep of the concrete at high temperatures are the deformation characteristics that govern the fire performance of reinforced concrete members. Furthermore, the transient strain has found to be a crucial part of total strain in structural concrete components that are exposed to fire and loading simultaneously [56].

When subjected to heating, concrete undergoes strain consisting of components from four different sources which can be mathematically written as [67]

$$\varepsilon_{total} = \varepsilon_{th}(T) + \varepsilon_{\sigma}(T, \sigma) + \varepsilon_{tr}(T, \sigma) + \varepsilon_{cr}(T) \quad (2.27)$$

Where: ε_{total} is the total strain, $\varepsilon_{th}(T)$ is free thermal strain, $\varepsilon_{\sigma}(T, \sigma)$ is the mechanical strain, $\varepsilon_{tr}(T, \sigma)$ is transient thermal strain or load-induced thermal strain, $\varepsilon_{cr}(T)$ is the time dependent creep strain, T is the temperature and σ is the mechanical stress.

The time dependant creep strain, $\varepsilon_{cr}(T)$, is significantly smaller than the other strain components and can be neglected when considering rapid temperature increase. For example, it was observed in [28] that it did not exceed 5% of total strain in a 3 hour heating period.

Free thermal strain, $\varepsilon_{th}(T)$, is an important component of the total strain of concrete at elevated temperatures. It is expressed as the product of the coefficient of thermal expansion and change in temperature. However, to represent it within a model, many linear and non

linear equations may be found in the literature. These can be very different in the values they produce, e.g. [69, 61, 70] (Figure 2.16). Some of these equations are specified for concrete with

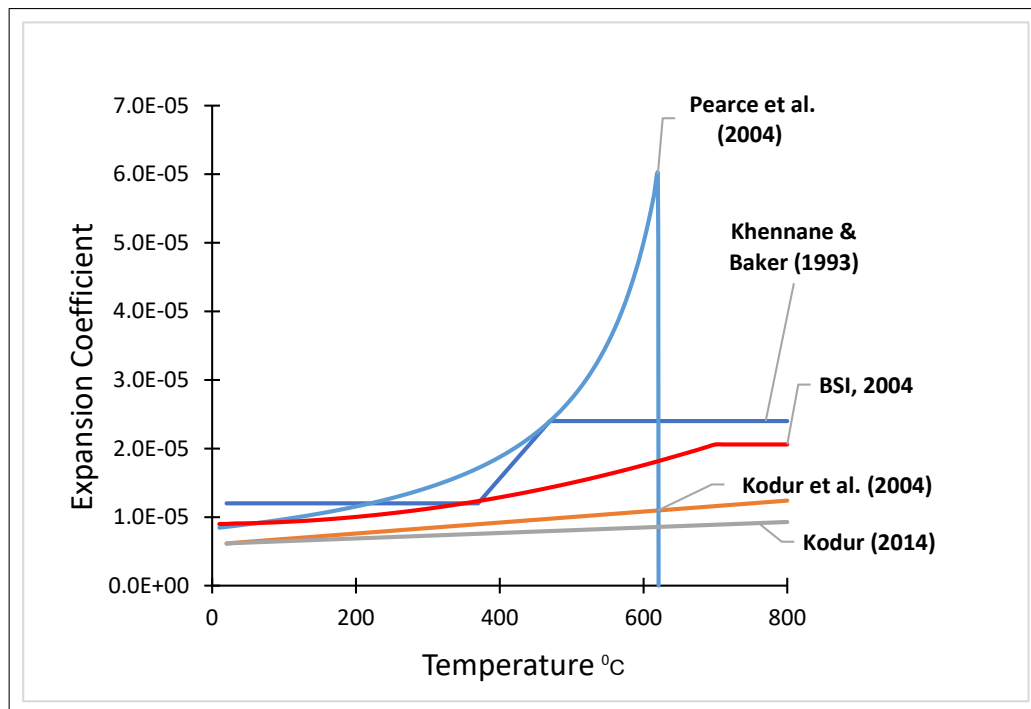


Figure 2.16: Different expansion coefficient from literature

particular aggregate types [68] while others have been defined generally [61]. Employing one of these equations over another can lead to very significantly different results being produced. Additionally, it is not often clear whether the defined equations are relevant for free thermal expansion where there are no external stresses or for stress-dependent thermal expansion where there are external mechanical stresses affecting the concrete during heating [71]. These issues can lead to significant uncertainty in the calculation of the strain in concrete subjected to elevated temperatures and it is important that consideration is given to the choice of an appropriate function.

In terms of mechanical strain $\epsilon_{\sigma}(T, \sigma)$, a thermally dependent stress-strain relationship must be defined considering the degradation in material properties such as compressive strength and elasticity that occur when concrete is heated. As shown previously (Figure 2.12), various stress-strain equations have been proposed aiming to capture this relationship at various temperatures considering various parameters for example [28, 66, 72] and many others. As with free thermal strain, employing one equation over another impacts the outcomes from the model, and it is again important that an appropriate function, consistent with other parts of the model is chosen.

However, the most important component of the total strain is the transient thermal strain $\epsilon_{tr}(T, \sigma)$ which has been found to be greater than both the mechanical strain and creep strain [28]. Transient strain develops under stressed concrete in compression while temperature increases. It can be defined as the main part of the total strain in stressed concrete when heated that can not be developed otherwise [28]. If TTS is not well considered in problems involving thermo-mechanical loading, and especially in compression members like columns and shear walls, the

results may be significantly inaccurate [71, 73]. This irrecoverable strain occurs only under the first heating of stressed concrete and is a function of temperature and the magnitude of the applied mechanical compressive stress.

Since transient thermal strain cannot be measured directly, it has to be found by quantifying differences in total strains between comparable heated test samples with and without compressive stresses applied prior to heating [28, 71]. Therefore, based on experimental results with varying methodologies, numerous linear and nonlinear equations have been proposed in the literature. Some of these equations are summarised below and compared numerically in Figure 2.17 for a hypothetical concrete mix with 40 MPa compressive strength.

From Nielsen et al. [74] a linear equation has been proposed

$$\varepsilon_{tr} = \beta \times T \times \sigma / f'_c, \quad \beta = 0.000038 \quad (2.28)$$

From Diederichs cited in [53] the following nonlinear equation is proposed

$$\varepsilon_{tr} = \sigma / f'_c [3.3 \times 10^{-10}(T - 20)^3 - 1.72 \times 10^{-7}(T - 20)^2 + 0.0412 \times 10^{-3}(T - 20)] \quad (2.29)$$

Unlike to these equations, Terro [55] proposed an equation taking into consideration the aggregate types, the aggregate volume inside the mixture, and the load level. The equations are derived considering concrete mixture with 65% aggregate and load level 30% of its ambient strength.

For light weight aggregate:

$$\varepsilon_{tr} = (43.87 - 2.73T - 6.35 \times 10^{-2}T^2 + 2.19 \times 10^{-4}T^3 - 2.77 \times 10^{-7}T^4) \times 10^{-6} \quad (2.30)$$

For gravel aggregate:

$$\varepsilon_{tr} = 1.48 \times 10^{-6}(1098.5 - 39.21T + 0.43T^2) - 1.48 \times 10^{-9} \quad (2.31)$$

$$(2.44T^3 - 6.27 \times 10^{-3}T^4 + 5.95 \times 10^{-6}T^5)$$

For different stress levels beyond 30% of its ambient strength, the Equation 2.30 and Equation 2.31 are multiplied by $(0.032 + 3.226 \times \sigma / f'_c)$. Similarly for concrete mixes having different aggregate content the equations can be multiplied by $(3.05 \times V_a / 100)$.

Yu-ye et al. [75] suggested the following generalised equation regardless of aggregate type or stress level.

$$\varepsilon_{tr} = \sigma / f'_c [72 \times (T / 1000)^2 - (T / 1000)] \times 10^{-3} \quad (2.32)$$

As it can be seen from Figure 2.17, there are differences in predicting transient strain, incorporating these different values into models can significantly alter the overall outputs.

It may be seen that restrictions relating to the associated test set-ups have been reflected in the development of these equations. For example, the majority of equations have been derived from tests where the samples had been stressed to a certain percentage of their strength at ambient temperature prior to heating. As a consequence, many researchers have derived functions that

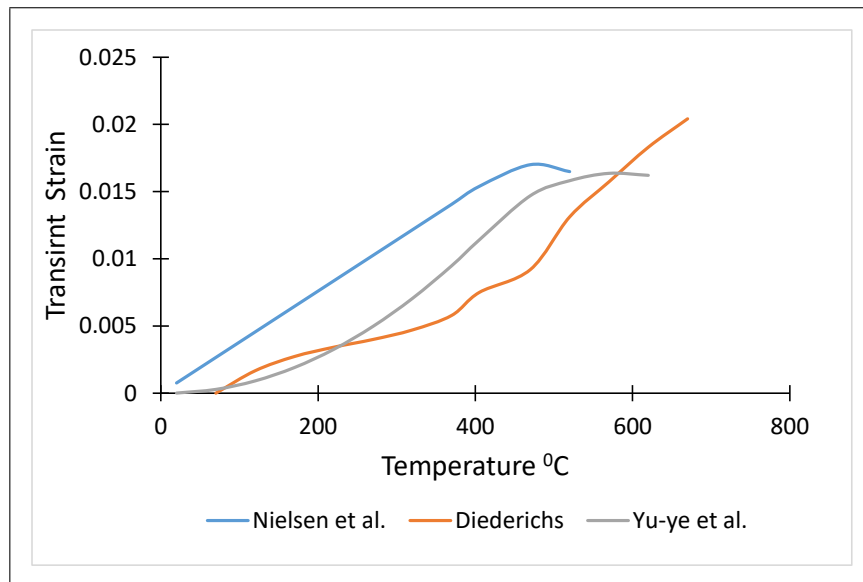


Figure 2.17: Comparison of different transient thermal models from literature

relate transient strain to the initial applied stress (load), concrete compressive strength at ambient temperature, and temperature e.g. Anderberg *et al.* [28], Diederichs cited in [53], the Guo and Shi model cited in [52, 74]. Others incorporate more parameters such as aggregate type and moisture content, e.g. Schneider [54], Terro [55].

Generally, to apply these equations directly to quantify the transient thermal strain at any temperature, prior knowledge of the applied stresses and the concrete strength at ambient temperature is required. Therefore, they cannot be applied easily for cases where there are no initial applied loads such as for restrained samples, where loads leading to transient strain only develop once thermal expansion begins to push against the restraint. On the other hand, equations derived for restrained samples, such as that proposed by Nielsen [74], cannot be applied for cases where there is external loading. While almost all columns and walls in buildings are stressed from different dead and live loads, the passive load technique through restraints may not represent this accurately. On the other hand, these members are also stressed from adjoining members like beams or slabs which act as restraints which are not considered in the models derived on initial applied load. Therefore, the combination of both cases, namely existing of initial load and restraining from adjoining members may be more accurate to capture real behaviours of these members while heated.

2.6.4 Concluding remarks on modelling of concrete at high temperatures

Apart from existing different spalling theories disputing on considering or disregarding hygro-thermal effects as mentioned before, another main challenge in numerical modelling is capturing temperature dependant properties of concrete in the analysis accurately.

It may be seen that restrictions relating to the associated test set-ups have been reflected in the development of models derived to capture parameters required in thermo mechanical analysis. Therefore, it is challenging to numerical modeller to select a particular model over the other

because of substantial difference in their outcomes.

To address concerns relating to inconsistent models available for heated concrete properties, it is crucial to investigate underlying parameters relating to test methodologies such as sample size, restraints, test set up details, and load which have not well investigated in the literature.

Chapter 3

Coupled Thermo-Mechanical Model

3.1 Introduction

For the purpose of investigations throughout this thesis, a novel theoretical model capable of quantifying the stress causing transient thermal strain (TTS) in heated concrete has been proposed in this chapter. It can be used in finite element models or as a direct design equation to help structural designers in assessing the stress developed during heating of concrete members caused by combined actions of mechanical loads, heating fluxes and end restraints. The model classifies heated concrete problems into three categories; concrete members heated to a certain temperature then loaded; concrete members stressed to a certain level and then heated to a certain temperature under load; concrete members heated with fully restrained ends with or without external loading. The new TTS equation has been incorporated in a novel coupled thermo-mechanical finite element model in the framework of ABAQUS. Material models capable of capturing the constitutive behaviour and specifically the degradation of material properties experienced by concrete exposed to elevated temperatures, have been selected from the literature and have been adapted to include TTS and, where absent, temperature dependence. The FE model, along with the developed stress equation, has been calibrated against experimental results in which samples were tested under various loading configurations and boundary conditions. It has been shown to successfully reproduce the results for all of the studied cases. Furthermore, in exploring these scenarios a number of observations were made. Firstly, it was found that the stress developed under restraint is lower than under applied preload, but that stress relaxation in part due to TTS is higher in preloaded samples. Secondly, the limit of elastic behaviour appears to be reduced in samples subject to free thermal expansion compared to those under restraint. Finally, while free thermal expansion is critical to the overall stress-strain response there is evidence that the choice of an equation from the scattered literature instead of another can alter results significantly.

3.2 ABAQUS FE model constitutive equations

3.2.1 Material properties

In this work material models capable of capturing the constitutive behaviour and specifically the degradation of material properties experienced by concrete exposed to elevated temperatures, have been selected from the literature. These have been adapted to include TTS and, where absent, temperature dependence.

Considering the stress-strain response in compression, the curve proposed by Lie [66] has been adopted as it includes temperature dependency through consideration of the degradation of the compressive strength of the concrete, and it is applicable over a wide range of concretes from Normal Strength to High Performance.

$$\sigma_c = \begin{cases} f_c(T) \left[1 - \left(\frac{\varepsilon_{max} - \varepsilon_c}{\varepsilon_{max}} \right)^2 \right] & \varepsilon_c \leq \varepsilon_{max} \\ f_c(T) \left[1 - \left(\frac{\varepsilon_c - \varepsilon_{max}}{3\varepsilon_{max}} \right)^2 \right] & \varepsilon_c > \varepsilon_{max} \end{cases} \quad (3.1)$$

where the temperature dependent compressive strength, $f_c(T)$, is given by

$$\begin{aligned} f_c(T) &= f'_c & 0 \leq T \leq 450^\circ\text{C} \\ f_c(T) &= f'_c [2.011 - 2.353(T - 20)/1000] & 450^\circ\text{C} \leq T \leq 874^\circ\text{C} \\ f_c(T) &= 0 & T > 874^\circ\text{C} \end{aligned} \quad (3.2)$$

and the strain at ultimate compressive strength, ε_{max} , is given by

$$\varepsilon_{max} = 0.0025 + (6T + 0.04T^2) \times 10^{-6} \quad (3.3)$$

noting that ε_c is concrete strain and f'_c is the compressive strength at ambient temperature.

The equivalent stress-strain relationship in tension is given by[52]

$$\begin{aligned} \sigma_t &= E(T)\varepsilon_t & \varepsilon_t \leq \varepsilon_{tk} \\ \sigma_t &= f'_t(T) - \frac{0.1f'_t(T)}{\varepsilon_{tk}}(\varepsilon_t - \varepsilon_{tk}) & \varepsilon_{tk} < \varepsilon_t \leq 2\varepsilon_{tk} \\ \sigma_t &= 0.9f'_t(T) & \varepsilon_t > 2\varepsilon_{tk} \end{aligned} \quad (3.4)$$

where $f'_t(T) = 0.09f_c(T)$ and $\varepsilon_{tk} = \frac{f'_t(T)}{E(T)}$.

For the modulus of elasticity the equation from Anderberg and Thelandersson [28] has been adopted since it is temperature dependent and compatible with Lie's stress-strain model.

$$E(T) = \frac{2f_c(T)}{\varepsilon_{max}} \quad (3.5)$$

For Poisson's ratio, few equations are available in the literature, the temperature dependent function from Bahr *et al.* [76] has been adopted

$$\nu = 0.204e^{-0.002T} \quad 0 \leq T \leq 500 \quad (3.6)$$

Regarding concrete expansion at different temperatures, the equation from [61] will be adopted since, as shown in Figure 2.16, it is between upper and lower limits from literature.

$$\alpha = (0.008 \times T + 6) \times 10^{-6} \quad (3.7)$$

As discussed before, TTS is irrecoverable strain occurs only under the first heating of stressed concrete and is a function of temperature and the magnitude of the applied mechanical com-

pressive stress. The irrecoverable nature of transient strain has been accounted for in the model developed in this thesis through adding the strain directly to the stress strain curve and amending the modulus of elasticity accordingly. Therefore, Equations 3.1 and 3.5 must be modified, firstly, as per the work of Youssef and Moftah [72] and Al Hamd *et al.* [27], the strain at peak compressive stress, ϵ_{max} , on the temperature dependant stress strain curves is shifted by an amount equal to ϵ_{tr} such that

$$\sigma_c = \begin{cases} f_c(T) \left[1 - \left(\frac{\epsilon_{max} + \epsilon_{tr} - \epsilon_c}{\epsilon_{max} + \epsilon_{tr}} \right)^2 \right] & \epsilon_c \leq \epsilon_{max} \\ f_c(T) \left[1 - \left(\frac{\epsilon_c - (\epsilon_{max} + \epsilon_{tr})}{3(\epsilon_{max} + \epsilon_{tr})} \right)^2 \right] & \epsilon_c > \epsilon_{max} \end{cases} \quad (3.8)$$

Secondly, for consistency, the ϵ_{max} term in the elasticity equation is modified in a similar way such that

$$E(T) = \frac{2f_c(T)}{(\epsilon_{max} + \epsilon_{tr})} \quad (3.9)$$

In considering concrete damage the damage parameters described by Birtel and Mark [77] have been employed. These are again compatible with the rest of the model and have the advantage of capturing damage beyond the yield strength rather than the ultimate strength. These parameters are here modified for temperature dependence through the incorporation of the degradation of elasticity and strength with increasing temperature.

$$d_c = 1 - \frac{\sigma_c E_{cT}^{-1}}{\epsilon_c^{pl}(1/b_c - 1) + \sigma_c E_{cT}^{-1}}, \quad d_t = 1 - \frac{\sigma_t E_{cT}^{-1}}{\epsilon_t^{pl}(1/b_t - 1) + \sigma_t E_{cT}^{-1}} \quad (3.10)$$

where d_c is the concrete damage parameter in compression and d_t is the concrete damage parameter in tension. ϵ_c^{pl} is the plastic strain in compression, which is determined proportional to the inelastic strain such that $\epsilon_c^{pl} = b_c \epsilon_c^{in}$ where $\epsilon_c^{in} = \epsilon_c - \sigma_c E_{cT}^{-1}$ and $0 < b_c < 1$. Similarly, $\epsilon_t^{pl} = b_t \epsilon_t^{in}$ where $\epsilon_t^{in} = \epsilon_t - \sigma_t E_{cT}^{-1}$. Functions for temperature dependent auxiliary parameters such as density, conductivity and specific heat are given in Table 3.1.

Table 3.1: Temperature dependent thermal properties

Property	Function	Range
Thermal Conductivity (Kodur et al. (2004))		
Siliceous Aggregate	$k_c = (2 - 0.0011T) * 0.85$ (W/m°C)	$0^\circ\text{C} \leq T \leq 1000^\circ\text{C}$
Carbonate Aggregate	$k_c = (2 - 0.0013T) * 0.85$	$0^\circ\text{C} \leq T \leq 300^\circ\text{C}$
Carbonate Aggregate	$k_c = (2.21 - 0.002T) * 0.85$	$300^\circ\text{C} \leq T \leq 1000^\circ\text{C}$
Specific Heat (Eurocode 2 (2004))		
	$C_p(T) = 900$ (J/kg °C)	$20^\circ\text{C} \leq T \leq 100^\circ\text{C}$
	$C_p(T) = 900 + (T - 100)$	$100^\circ\text{C} \leq T \leq 200^\circ\text{C}$
	$C_p(T) = 1000 + (T - 200)/2$	$200^\circ\text{C} \leq T \leq 400^\circ\text{C}$
	$C_p(T) = 1100$	$400^\circ\text{C} \leq T \leq 1200^\circ\text{C}$
Density (Eurocode 2 (2004))		
	$\rho(T) = \rho(20^\circ\text{C})$	$20^\circ\text{C} \leq T \leq 115^\circ\text{C}$
	$\rho(T) = \rho(20^\circ\text{C})(1 - 0.02(T - 115)/85)$	$115^\circ\text{C} \leq T \leq 200^\circ\text{C}$
	$\rho(T) = \rho(20^\circ\text{C})(0.98 - 0.03(T - 200)/200)$	$200^\circ\text{C} \leq T \leq 400^\circ\text{C}$
	$\rho(T) = \rho(20^\circ\text{C})(0.95 - 0.07(T - 400)/800)$	$400^\circ\text{C} \leq T \leq 1200^\circ\text{C}$

3.2.2 Modified transient strain equation

As discussed before, transient strain can not be quantified directly from experimental works, the difference between strains in two identical stressed (in compression) and unstressed samples has been considered as transient strain, albeit after subjecting samples to heating. To derive an equation capable to capture load and restraint effects in heated concrete without conducting laboratory test, mathematical derivation is required. Nielsen's equation (Equation 3.11) [74] has been considered in this thesis to quantify transient strain after performing amendments to consider external load effects too. The main rational behind selecting this equation is Nielsen's mathematical derivation for the stresses causing transient strain in end restrained samples. This derivation will be extended in this thesis to capture end restraint and external load effects simultaneously.

$$\varepsilon_{tr} = \beta \times T \times \sigma / f'_c \quad (3.11)$$

Equation 3.11 is a linear temperature dependant equation directly proportional to the applied compressive stress/strength ratio and temperature. Therefore, as with other commonly used models (e.g. [74, 28, 52, 53, 54, 55]), in order to apply this equation, stresses during heating need to be known or quantified. In most cases in literature where this kind of model is employed, the stresses are typically due to external mechanical loading, rather than end restraints, applied prior to heating and maintained during heating. However, there are also more realistic scenarios in which the developed stresses could be due to a combination of both externally applied loads and end restraints, such as in the case of columns in multi storey buildings that are restrained by slabs at top and bottom, and are stressed by imposed loads at the same time. Therefore, Neilsen's equation has been extended here to a novel formulation that can be used directly to predict the developed stresses under any of the mentioned circumstances.

In Nielsen's derivation, an external restraint against thermal deformation was modelled in a uniaxial concrete member by a linear spring, its stiffness remaining intact during heating as shown in Figure 3.1.

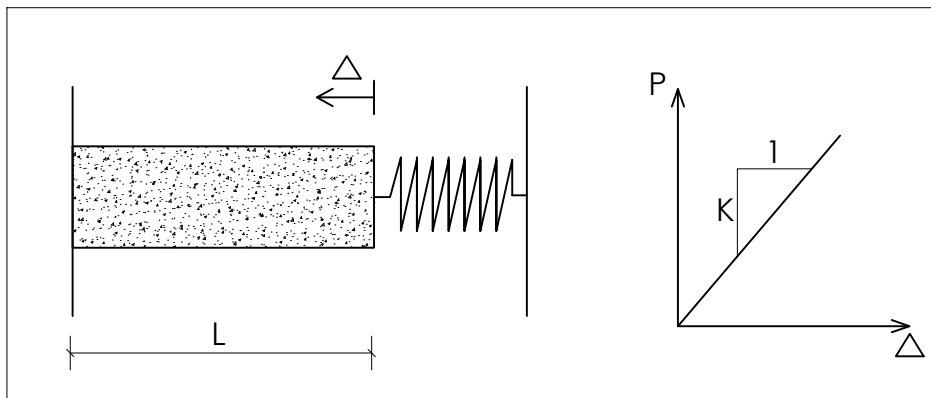


Figure 3.1: Spring model to represent end restraints used by Nielsen [74]

Upon heating of the member, compressive stresses build up causing deformation in the spring.

The strain compatibility equation between both the member and the spring is as follows:

$$\epsilon_{tot} = fts + \epsilon_{tr} + \epsilon = \frac{-\Delta}{L} \quad (3.12)$$

where fts is pure thermal strain, $\epsilon_{tr} = \beta T \sigma / f'_c$ is transient strain and $\epsilon = \sigma / E(T)$ is pure mechanical strain. The negative sign on the right hand side of the equation is due to the sign convention from Figure 3.1. Substituting these into Equation 3.12 and considering that $\sigma = P/A$ & $K = P/\Delta$, the following equation was derived by Nielsen [74]

$$\frac{\sigma}{E_0} = \frac{-fts}{\frac{1}{\rho} + \frac{E_0}{E(T)} + \beta T \frac{E_0}{f'_c}} \quad (3.13)$$

where $\rho = KL/(AE_0)$ is stiffness ratio between the spring and concrete member, which was found to be equal to 2, and $\beta = 0.000038$. It may be noted that in compression, only elastic mechanical strains are included.

Now extending this formulation so as to be valid for cases where external loads are applied as shown in Figure 3.2, potentially in addition to end restraints, the strain compatibility may be written as:

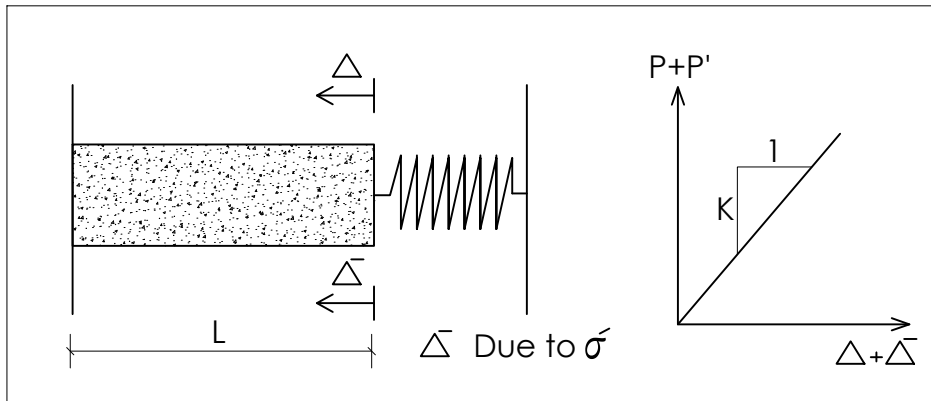


Figure 3.2: Spring model with external loading

$$fts + \epsilon_{tr} + \epsilon' + \epsilon = \left(\frac{-\Delta - \Delta'}{L} \right) \quad (3.14)$$

Where fts is pure thermal strain, $\epsilon_{tr} = \beta T (\sigma + \sigma') / f'_c$ is the transient strain (resulting from both externally applied stress σ' and stress developed during heating due to end restraints σ), $\epsilon' = \sigma' / E_0$ is the initial strain due to the externally applied stress, $\epsilon = \sigma / E(T)$ is the pure mechanical strain developed due to heating, and considering that $\sigma = P/A$, $\sigma' = P'/A$ & $K = (p + p') / (\Delta + \Delta')$, the equation can be expanded to

$$fts + \frac{\beta T (\sigma + \sigma')}{f'_c} + \frac{\sigma'}{E_0} + \frac{\sigma}{E(T)} = -\frac{\sigma' A}{KL} - \frac{\sigma A}{KL} \quad (3.15)$$

Substituting $E_0 = 2f'_c / \epsilon_{max20}$ & $E(T)$ as Equation 3.9, taking $\rho = KL/(AE_0)$ and simplifying

the equation to a quadratic form in terms of σ , the following expression can be obtained.

$$\sigma = \frac{-B + \sqrt{B^2 - 4AC}}{2A} \quad (3.16)$$

Where

$$A = \frac{\beta T}{2f'_c f_c(T)} \quad (3.17)$$

$$B = \frac{\beta T}{f'_c} + \frac{\varepsilon_{max}(T)}{2f_c(T)} + \frac{\beta T \sigma'}{2f'_c f_c(T)} + \frac{\varepsilon_{max20}}{2\rho f'_c} \quad (3.18)$$

$$C = f_{ts} + \frac{\beta T \sigma'}{f'_c} + \frac{\sigma' \varepsilon_{max20}}{2f'_c} + \frac{\sigma' \varepsilon_{max20}}{2\rho f'_c} \quad (3.19)$$

This generalised equation for σ may then be used to solve the transient strain equation (3.11) for any loading scenario while accounting explicitly for the degradation in strength and stiffness with temperature.

3.2.3 Concrete damage plasticity model

The finite element implementation in ABAQUS employs the concrete damage plasticity model (CDP) based on the yield function proposed by Lubliner *et al.* [78] considering modifications proposed by Lee and Fenves [79] (Figure 3.3). The CDP is a continuum, plasticity-based damage

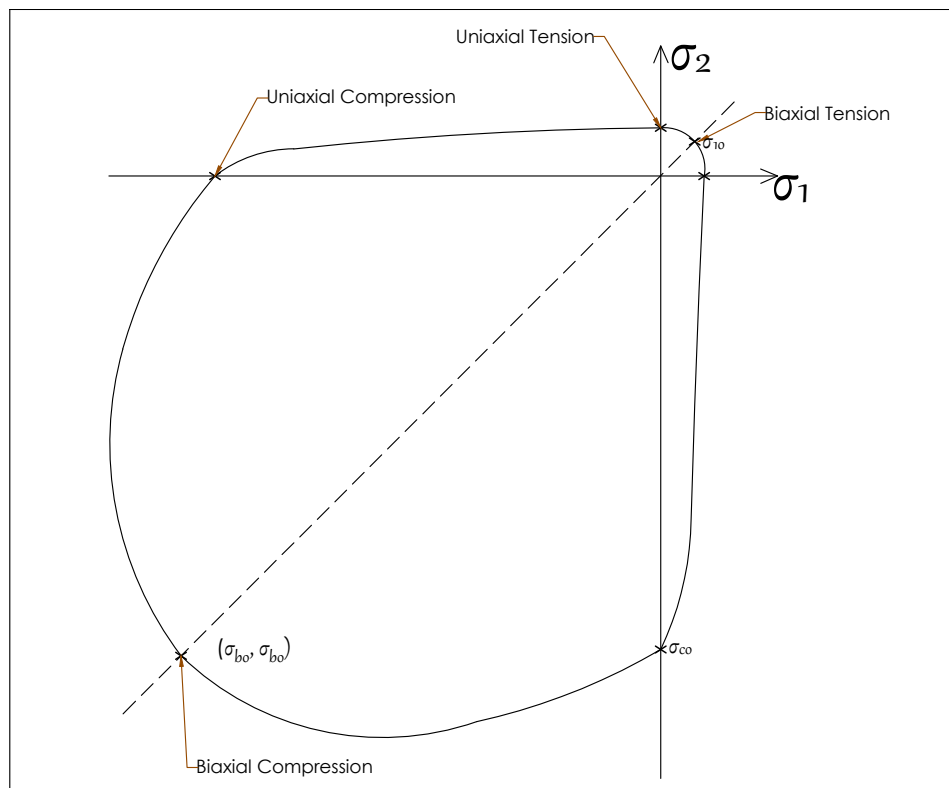


Figure 3.3: Yield surface in plane stress used by CDP model in ABAQUS [80]

model for concrete that takes into account two possible failure mechanisms; compressive crushing and tensile cracking. In order to study problems concerning concrete at elevated temperatures, it

is necessary to provide constitutive relationships accounting for both mechanical and thermal degradation of the concrete material in compression and tension.

For compressive crushing, firstly, the uniaxial compressive stress strain behaviour for concrete outside the elastic range is required. Compressive stress data in the form of a function of inelastic (crushing) strain ($\tilde{\epsilon}_c^{in}$) and temperature (T) are provided, noting that hardening data are input in terms of an inelastic strain ($\tilde{\epsilon}_c^{in}$) instead of plastic strain ($\tilde{\epsilon}_c^{pl}$). The former can be found from the total strain minus the elastic strain corresponding to the undamaged material, $\tilde{\epsilon}_c^{in} = \epsilon_c - \epsilon_{0c}^{el}$, where $\epsilon_{0c}^{el} = \sigma_c/E_0$ (see Figure 3.4). Secondly, unloading data are provided in terms of the thermally dependent compressive damage, d_c and the crushing strain $\tilde{\epsilon}_c^{in}$. The inelastic strain is converted to plastic strain using the relationship [80]

$$\tilde{\epsilon}_c^{pl} = \tilde{\epsilon}_c^{in} - \frac{d_c}{(1-d_c)} \frac{\sigma_c}{E_0} \quad (3.20)$$

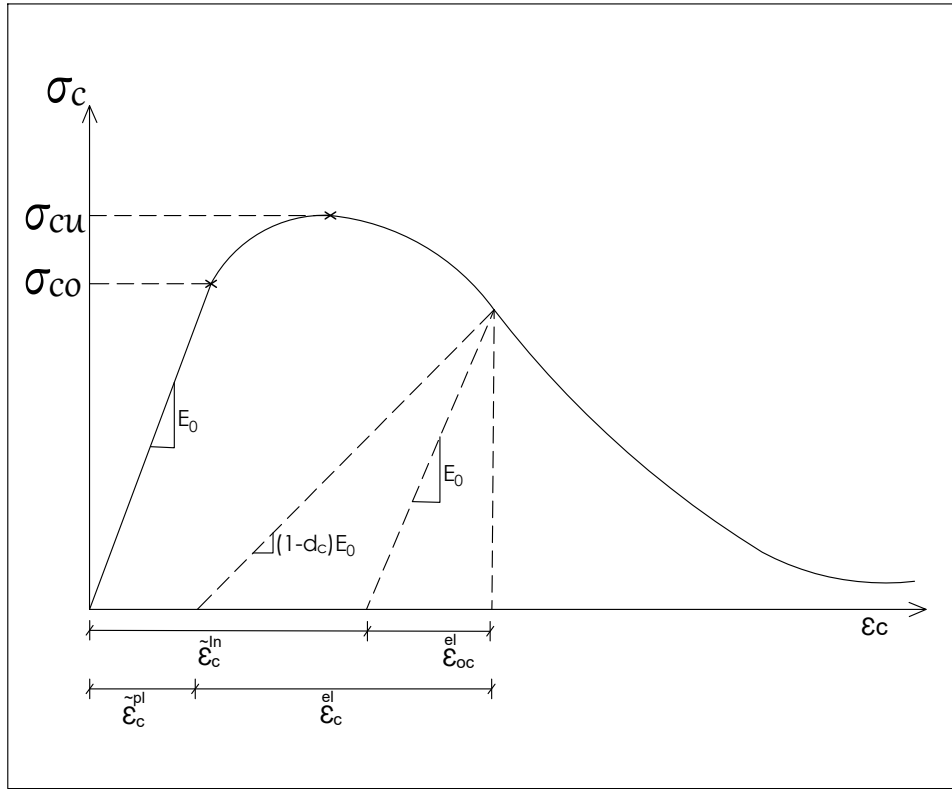


Figure 3.4: Behaviour of concrete under uniaxial compressive stress [80]

For tensile cracking, post failure stress is defined as a function of cracking strain ($\tilde{\epsilon}_t^{ck}$) and temperature (T). The cracking strain is given as the total strain minus the elastic strain corresponding to the undamaged material $\tilde{\epsilon}_t^{ck} = \epsilon_t - \epsilon_{0t}^{el}$, where $\epsilon_{0t}^{el} = \sigma_t/E_0$ (see Figure 3.5). Unloading data are provided in terms of the thermally dependent tensile damage, d_t , and the cracking strain, $\tilde{\epsilon}_t^{ck}$. The cracking strain is converted to plastic strain using the relationship [80]

$$\tilde{\epsilon}_t^{pl} = \tilde{\epsilon}_t^{ck} - \frac{d_t}{(1-d_t)} \frac{\sigma_t}{E_0} \quad (3.21)$$

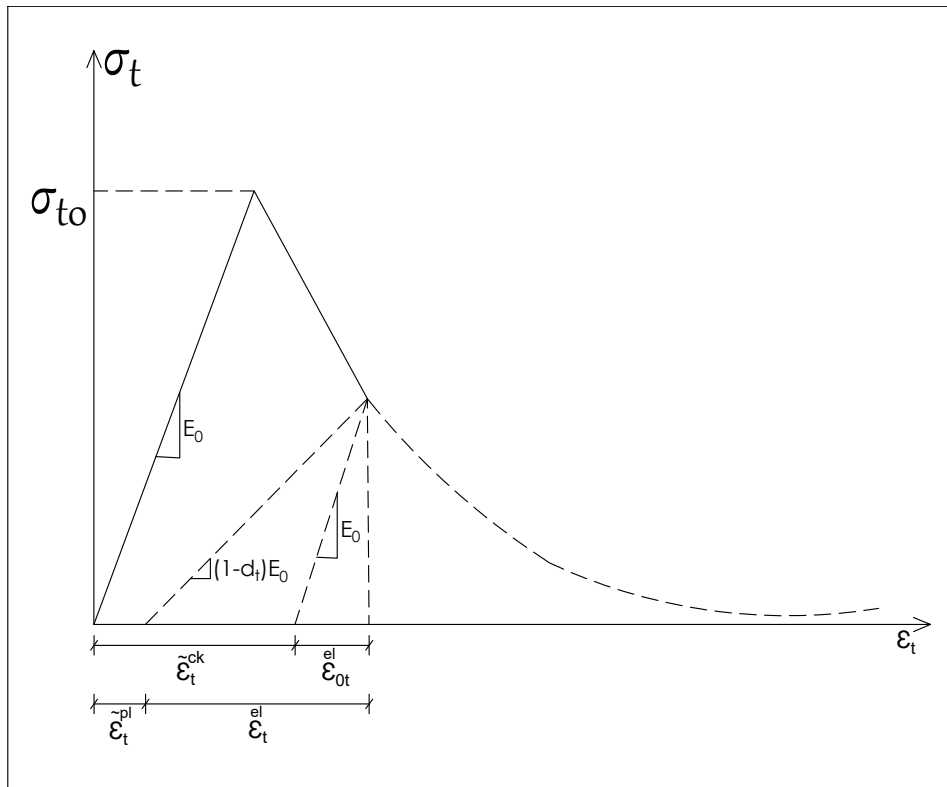


Figure 3.5: Behaviour of concrete under uniaxial tension stress [80]

3.3 Model calibration

In order to demonstrate the validity of the model and the need to capture the generalised loading scenarios available in the literature, it has been calibrated against the most common cases available in the literature prior pursuing to parametric studies. Considering that the main theme of this thesis is to investigate how test methodologies have affected test results in heated concrete investigations, different test scenarios representing structural and nonstructural elements (loaded and unloaded samples) have been considered in the calibration process. This makes the model to be applied confidently on various test methodologies from the literature while performing parametric studies in next chapters.

In general, literature test scenarios can be classified into three main categories. First category consists of tests in which unloaded samples were heated directly without involvement of any mechanical loading prior and during heating e.g.[4, 28]. This scenario is less common in reality as almost all structural elements would be loaded from self weight, dead load, and live loads. Unloaded sample investigations are available in the literature, despite controversies accompanied them, to quantify temperature dependant concrete properties. To perform thorough parametric studies, this scenario will be considered in the calibration of developed model in this thesis.

Second category consists of stressed sample with initial applied load prior heating e.g. [4, 24, 28, 37, 43, 51], the test proceeded through heating the sample while the initial applied

load maintained throughout the test duration. This categories is very compatible to the real cases in which coupled effects of mechanical and thermal loading have been incorporated.

Third category consists of samples heated while they were loaded passively only through restraints at both ends without incorporating other mechanical load e.g. [4, 50]. Again it is less common in reality, however it will be considered in the calibration process to expand application of the developed model.

After careful literature exploration, a set of sample tests matching aforementioned three categories, representing structural and non structural elements (loaded and unloaded samples), conducted by Anderberg & Thelandersson [28], have been chosen for the model calibration. The rationale for selecting this test set is the consistency of the samples. They are identical in size, applied heating curve, material used in their fabrication, and therefore temperature dependent material properties. They are different only in the test methods compatible to the three categories motioned above. The samples consisted of concrete cylinders (height 150 mm and diameter 75mm) having a 10 mm diameter hole at the centre for instrumentation purposes. While performing analysis, consistent mesh size and thermal boundary conditions have been considered in the model calibration for the samples. Regarding mesh size, mesh sensitivity analysis shown in Figure 3.6 has been conducted. Three mesh sizes, 2.5mm, 5mm, and 10mm has been investigated. Results for both smaller meshes coincide meanwhile the larger size mesh results deviate especially at higher temperatures. Therefore, 5mm mesh has been decided to be used for all samples in the calibration process without affecting the results. In terms of thermal boundary conditions, for heat convection a coefficient of $25W/(m^2K)$ was used for the exposed sides, while for radiation the emissivity of the exposed surfaces was set at 0.8 [81]. The

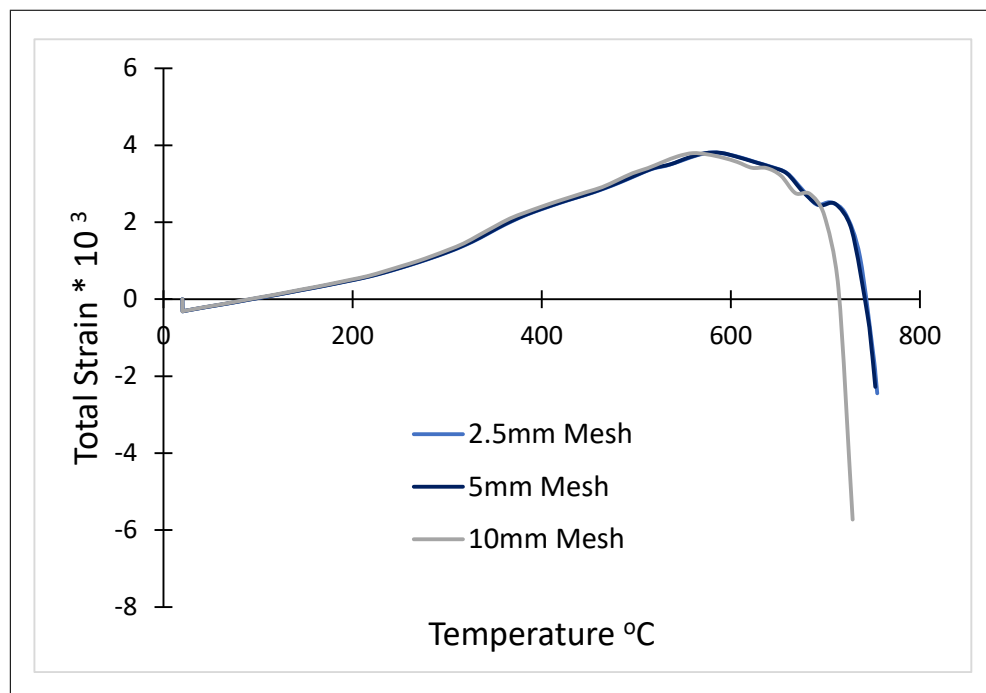


Figure 3.6: Mesh sensitivity analysis

Experimental test results, reported by Anderberg & Thelandersson as A, B and D Samples [28], were reproduced using the developed ABAQUS FE model (Figure 3.7 & Table 3.2). In order to

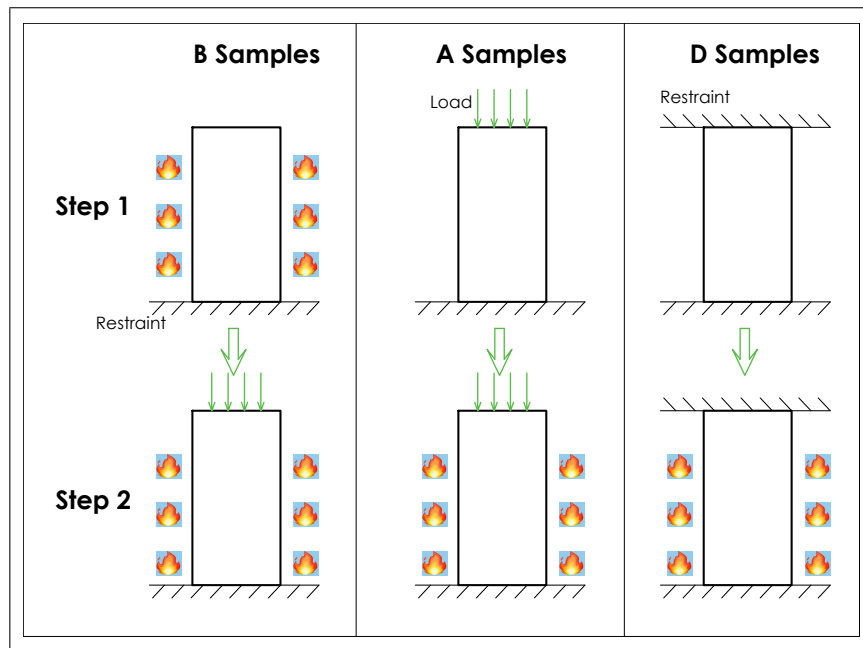


Figure 3.7: Schematic diagram of the samples used in the validation

present the findings in the most logical way these will be considered here in the order B, A, D, moving from post-loaded to pre-loaded samples.

B Samples (heating then loading) were heated to and held at a constant temperature (for 2 hrs until the whole specimen body reached uniform temperature) then stressed gradually at a constant rate of 0.23MPa/s until failure.

A Samples (loading then heating) were stressed to a given percentage of their ambient compressive strength, then heated at a constant rate of 5°C/min to 800°C or failure, whichever comes sooner.

D Samples (heating under restraint) were restrained at both ends, with no externally applied stress, that were then heated at a constant rate of 5°C/min to 800°C. Table 3.2 summarises the heating and loading scenarios that have been analysed for each test series.

Table 3.2: Detail of samples used in the model validation

No	Type	Temperature °C	Heating Rate °C. min ⁻¹	Stress During Heating %	Loading Rate MPa. s ⁻¹	Cube Strength MPa
1	B	20	-	0	0.23	51.3
2	B	185	-	0	0.23	50.0
3	B	265	-	0	0.23	51.9
4	B	400	-	0	0.23	50.0
5	B	500	-	0	0.23	53.5
6	B	645	-	0	0.23	53.2
7	A5	800	5	0	-	55.1
8	A6	800	5	0.225	-	58.4
9	A7	800	5	0.350	-	52.4
10	A8	800	5	0.450	-	64.0
11	A9	800	5	0.675	-	58.4
12	D1	800	5	0	-	46.7

3.3.1 B Samples

Given that the experimental samples were held for 2 hrs at the target temperature in order to ensure uniform temperature throughout the body, the problem could be modelled as a static analysis considering the target temperature as a predefined field boundary condition. Through this, reduced analysis time has been achieved without compromising the results. For the purpose of analysis, a 5 mm mesh of standard 3D stress elements (C3D8R - 8-noded linear bricks with reduced integration and hourglass control) with linear geometric order and three degrees of freedoms at each node was used. Mechanical boundary conditions were applied with vertical restraint to the base of the sample and horizontal restraint to the central hole to prevent laterally movement. The static load was applied at the top of the sample as in Table 3.2 (Figure 3.7).

The results of the model analysis versus experimental results are shown in Figure 3.8. In general, there is good agreement between the experimental and model results between 20°C and 400°C. However, the model result at 500°C underestimates the experimental curve results up to 35% of the sample's ambient compressive strength before switching to overestimate the experimental results as the strain increases. This is likely because the concrete undergoes significant and rapid degradation to its material properties around this temperature that the model struggles to capture. Furthermore, the free thermal expansion equation choice from scattered literature (Figure 2.16) which shows extensive variability especially, as noted in [56], in the range above 300°C, has affected the results.

It is worth mentioning that throughout this thesis, concrete behaviour investigations for unloaded samples have been considered at first spalling time at which the temperature ranges between 150°C to 300°C depending on the sample type and the test configuration. Up to around 475°C the developed model could capture the experimental results accurately covering the investigations conducted in this thesis. Considering this and that B sample scenario (heated then loaded) is representing nonstructural rather than structural members (loaded then heated) which are not common in reality, the model performance can be considered to be accurate especially it returns at temperatures above 500°C and the results at 650°C again agree well with the experimental results.

During the analysis of the B samples (heating then loading), the linear limit to which the concrete remains in the elastic range was assigned to be $0.3f'_c$ to fall within the range $0.3f'_c$ to $0.45f'_c$ found in literature (Khennane & Baker [65]). However the validation results clearly show that using this limit causes unrealistic sharp transitions in the curves. To address this, the elastic limit was reduced to $0.1f'_c$ and as can be seen in Figure 3.9 the results improved significantly. This suggests that the transition into plastic behaviour occurs earlier than previously thought and this indicates that unloaded samples may behave quite differently to loaded samples at elevated temperatures.

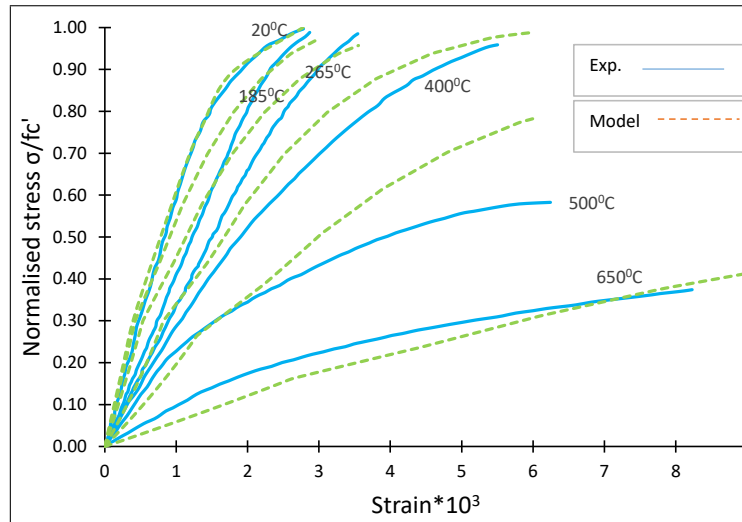


Figure 3.8: Model and experimental results of B samples

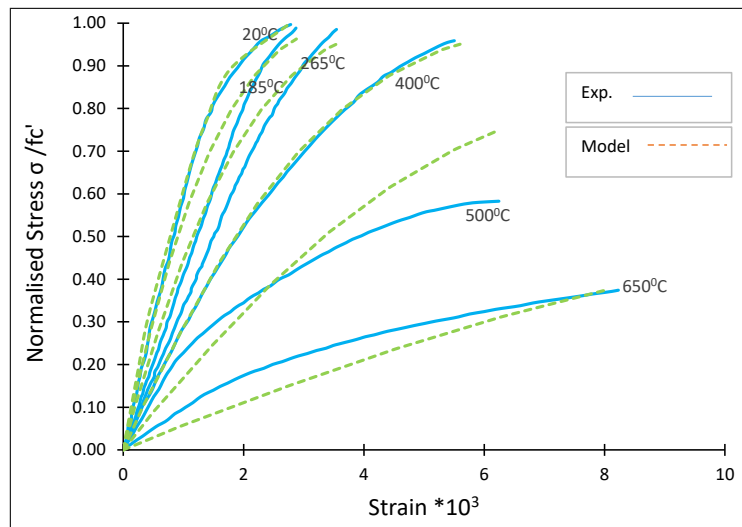


Figure 3.9: Model and experimental results of B samples with 0.1 linear limit

3.3.2 A Samples

To analyse this problem, a fully coupled thermal-stress analysis was employed. Similar to the B samples (heating then loading), a 5 mm mesh of standard coupled temperature displacement elements (C3D8T - 8-noded thermally coupled bricks with trilinear displacement and temperature) with linear geometric order and four degrees of freedoms at each node was used. Mechanical boundary conditions were applied as for the B Samples (heating then loading) although the axial load was applied before heating. For the thermal boundaries, heat was considered to transfer from the atmosphere to the specimen surfaces through convection and radiation mechanisms using the interaction interface facilities of ABAQUS. As discussed before, for heat convection, a coefficient of $25W/(m^2K)$ was used for the exposed sides, while for radiation the emissivity of the exposed surfaces was set at 0.8 [81]. Internal to the specimen, the heat transfers through conduction for which the auxiliary functions can be found in Table 3.1. A heat flux was applied over the height of the sample according to the heating rates given in Table 3.2.

As discussed previously, choices of the temperature dependent concrete properties from the

literature affect the simulation results. For example, although many functions exist in literature to describe the free thermal expansion these show extensive variability especially, as noted in [56], in the range above 300°C, and the choice of function has a significant effect on the predicted results. On the other hand, the complexity of the coupled thermo mechanical problem and involvement of too many parameters makes numerical modelling further challenging. Therefore, calibration process for coupled thermo mechanical problem may require to reproduce experimental results as it can be seen in some numerical simulations e.g.[37] in which stiffness and thermal expansion have been calibrated.

Throughout this thesis, concrete behaviour investigations for loaded samples have been considered at first spalling time at which the temperature is below 200°C depending on the sample type and test configuration. Up to around 285°C the developed model could capture the experimental results with no calibration.

However to provide accuracy for some hypothetical loaded sample cases beyond this range, which will be used in next chapters, a modification was conducted in order to maintain results beyond first spalling temperature at a good fit against experimental results. β parameter in Equation 3.11 has been set to be a constant value (0.000038) to simplify the model as suggested by [74]. This has been followed in this thesis up to 285°C, afterwards it has been calibrated such that to be varied with temperature in a similar way conducted in [70]. The calibration has been done through trial and error, and the best fit can be represented by Equation 3.22.

$$\beta = \begin{cases} 0.000038 & T \leq 285^{\circ}C \\ 2.057 \times 10^{-5} \times e^{(0.001654 \times T)} & T > 285^{\circ}C \end{cases} \quad (3.22)$$

It is possible that the model predictions could be further improved if for every stress level a separate β parameter equation had been derived but for practical simplicity a single function has been used here.

This function was employed for all A Sample (loading then heating) analyses except A5 where there was no external load applied. This is consistent given that the A5 sample can be considered within the B Sample (heating then loading) scenario of heating then loading (albeit with zero load). Similarly, it was found that it was necessary to consider an elastic limit of $0.1f'_c$ for the unloaded A5 sample, whereas a value of $0.3f'_c$ (as determined by Khennane & Baker [65]) was found to be more appropriate for the pre-loaded samples A6 to A9. This again suggests a significant influence of load level in the thermo-mechanical behaviour of concrete.

The model results versus experimental results are shown in Figure 3.10. As can be seen, generally, the model results are in good agreement with the experimental results and show an improvement over the results of other models (e.g. [65, 82]).

This improvement may be seen to be the result of the new formulation for the calculation of the stress causing transient strain Equation 3.16, which, rather than assuming a constant stress, accounts for the degradation of strength and stiffness with increasing temperature due to the effects of both the externally applied load and the restraint provided by the machine platens

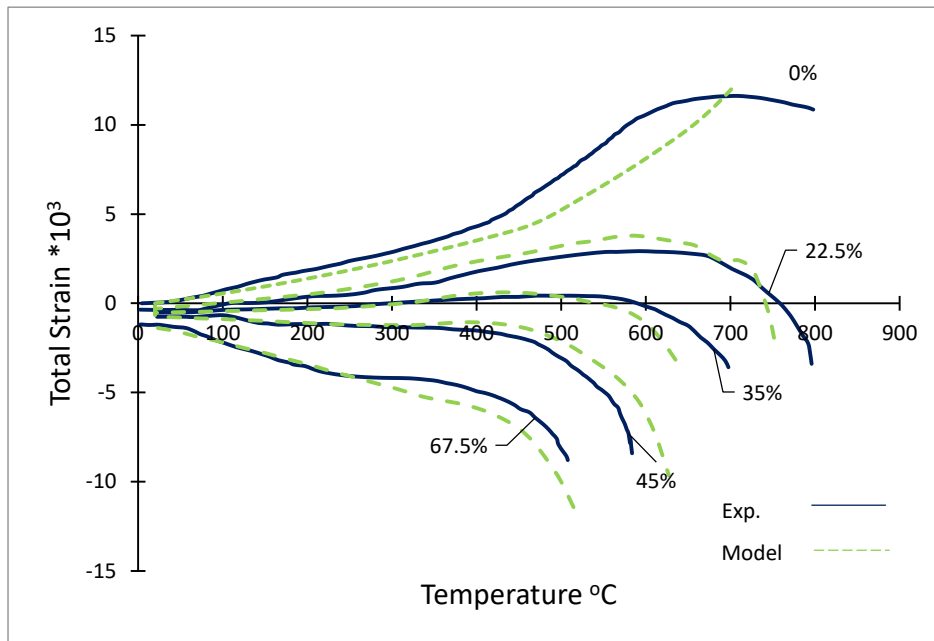


Figure 3.10: Model and experimental results of A samples

(something not explicitly considered by other models). By substituting it into the adopted linear equation for transient strain Equation 3.11, it is able to capture what is in fact non-linear behaviour.

It is recognised that, similar to the results for the B Samples above (heating then loading), the model results tend to drift from the experimental results at very high temperatures. Again, this effect is likely because of the significant and rapid degradation of the concrete material properties and it seems to increase with increasing load, which again goes to indicate the influence of load on the behaviour of the concrete at elevated temperatures. The match could perhaps be improved with an even more specific β function varying with load intensity, however, the drift is small for what is a generalised model, simplified for practical purposes, and then it can be seen that the overall behaviour is captured very well and better than by other models.

3.3.3 D Sample

As for the A Samples (loading then heating), a fully coupled thermal-stress analysis was employed for the D Sample and again a 5 mm mesh of 8-noded C3D8T elements was used. Mechanical and thermal boundary conditions were also as for the A Samples with the exception that the top of the sample was now restrained vertically with no external load applied.

Again, it was found that an elastic limit of $0.3f'_c$ was appropriate for this restrained, self-loaded sample. However, unlike A Samples (loading then heating), it was found that good results without calibration can be obtained suggesting that transient strain is more effective in the externally loaded samples. In restrained samples transient strain development lags due to slower stress evolution from restraints, however in the loaded sample the stress is already available and affecting the overall samples behaviour more effectively.

The model results in comparison with experimental results are presented in Figure 3.11. Overall the model captures the trend and magnitude of the experimental results very well and

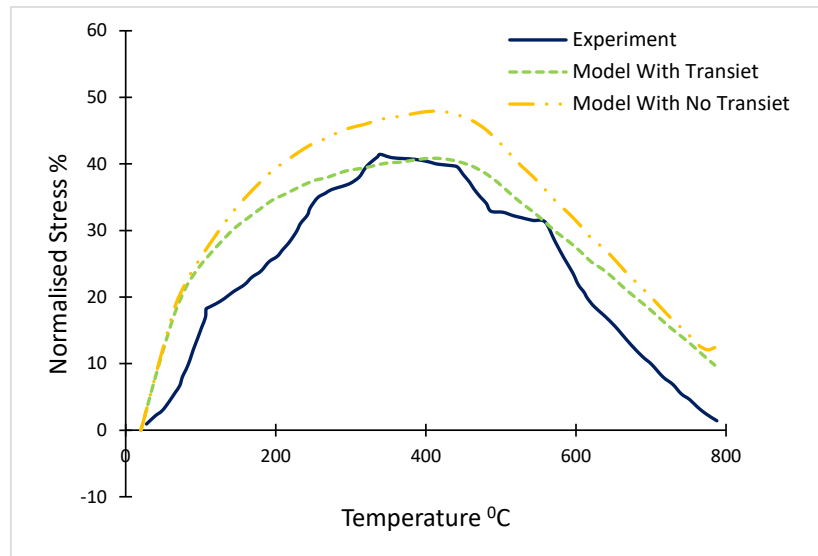


Figure 3.11: Model and experimental results of D samples

particularly the peak stress and the descending branch are in good agreement. However, from ambient temperature to about 300°C the model tends to slightly over predict the experimental results. This is similar to observations made by other studies that have looked at this type of problem (e.g. [69, 65, 82] and this deviation has been attributed to the neglect of hygral effects which are found to have significant effect within that temperature range. While this is a possibility, it can also be attributed here to the low intensity of the stresses that developed inside the sample during heating in this range compared to the pre-loaded A Samples (loading then heating). Although the D Sample analysis (heating under restraint) was set up in a similar way to the A Sample analysis in order to capture the transient strains developed by the external loading that developed during heating, in the early stages of this problem it in fact behaves more closely to a B Sample (heating then loaded). This is confirmed when the model results run without the transient strain equation switched on (also shown in Figure 3.11) are considered. It can be seen that there is no difference in the model results up to around 100°C and then only a little difference up to around 200°C. This suggests that this transient strain model (and others from the literature) under estimates the transient strain until the stress gradually increases to near peak value where transient strains become more significant. This may be related to the limited data available in the literature to inform the models with regard to transient strains developed under low loads.

3.3.4 Comparison of stress developed in A and D Samples

As discussed before, it appears that transient strain development differs depending on whether it is induced by an initial applied load (as in the A Samples) or a passive load through end restraints

(as in D Samples). This may question if restraint samples could be representative sample of real structural members loaded through imposed dead and live loads.

By considering Equation 3.16, the stresses developed in, and inducing transient strains in, the A (loading then heating) and D samples (heating under restraint) can be compared. Significant differences can be observed in Figure 3.12, in the case of the D samples (heating under restraint), the mechanical stress peaks at just 18% of the concrete compressive strength f'_c at ambient temperature regardless of f'_c value. This can be seen in the figure where results for D samples

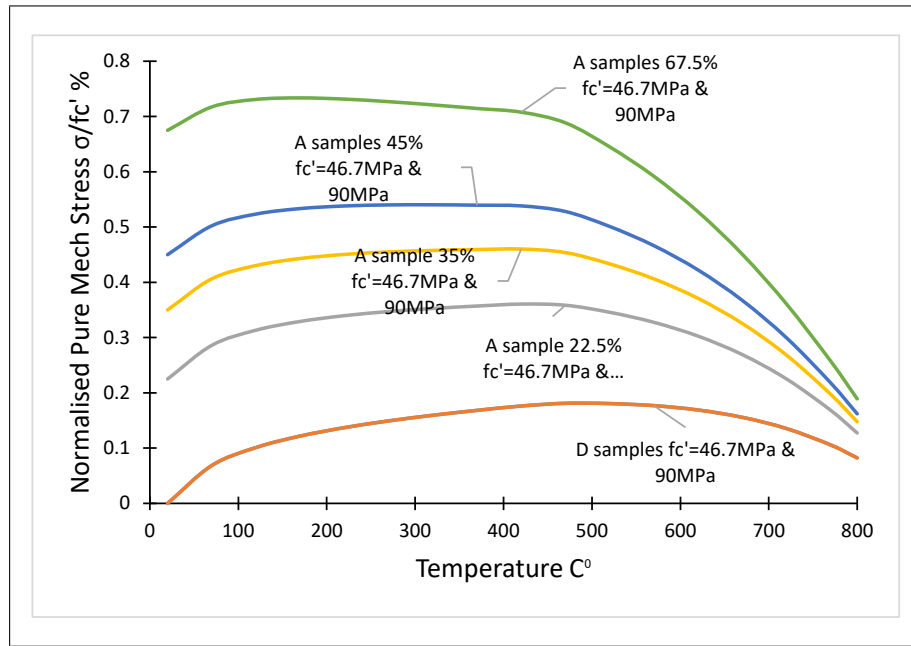


Figure 3.12: Developed pure mechanical stress for D and A samples

with $f'_c = 46.7$ MPa and 90 MPa coincide. This is clearly lower than even the least loaded of the A samples (loading then heating) where the peak mechanical stress varies according to the initial applied stress and reaches significantly higher values relative to initial compressive strength. However, it may be noted that the increase in stress from initial conditions is more significant in the restrained sample (increasing from 0-18% f'_c) than in the loaded samples as the transient strain effect becomes more pronounced (e.g. in the A sample initially loaded to 67.5% f'_c the stress increases to just 73%). Similarly, it may be noted that the stress relaxation is much greater in the preloaded samples where, in all cases, the stress drops below the pre-load value as the temperature reaches 500-700 °C. These results indicate that the validity of the test results from a restrained sample may not be a good reference to assess structural members severely stressed prior heating through initially applied load, this will be investigated more in next chapters considering different test set ups and boundary conditions.

3.4 Conclusion

A novel equation has been proposed that is capable of predicting developed stresses causing transient strain during heating of loaded and/or fully restrained concrete members. The equation

has been embedded in a new thermo-mechanical finite element model implemented in ABAQUS. The model has been validated against test results from the literature with different boundary conditions and loading-heating scenarios covering 'heating without restraint then loading', 'preloading then heating with restraint' and 'heating with restraint but no external load'.

The model was found to perform well in all scenarios in the prediction of strains and stresses with temperature. It can thus be seen as a versatile and robust formulation capable of capturing complex combinations of loading and restraint that may be found in real structural scenarios such as column members in high rise buildings. It has the advantage over other models that it considers a more realistic variable stress input to the transient strain equation compared to the constant values used in some previous equations. Furthermore, the stress equation itself may be used as a design tool for engineers to assess the stress developed in a member at any temperature under different boundary conditions.

It is noted that the model performs less well in reproducing experimental results at extreme high temperatures where concrete experiences significant and rapid degradation of its material properties, this is more particularly in unloaded free to expand samples. However, the overall performance of this generalised model is good and it remains an improvement over previous models.

In exploring the application of the model to different loading-heating scenarios several outcomes may be noted. Firstly, the stress evolution in the samples considered under each scenario is quite different and could not be captured without the adaptations made here. The stress developed under end restraint cannot be neglected but is generally lower than that developed under an externally applied preload, while the stress relaxation under increasing temperatures for higher preloads is much greater than under restraint alone.

Secondly, the stress limit below which the concrete behaves in a linear elastic manner appears to be significantly reduced under free thermal expansion without load (heat then load) compared to samples with end restraint (with or without external preloads). This then has a notable effect on the thermally dependent stress-strain response.

Finally, as may be expected, it has been found that for initially loaded samples, unlike to end restrained sample, results could not be captured accurately at higher temperature without calibration. This suggests that the stress intensity, pace of its evolution, and its type (whether directly applied or passively through end restraints) can have detrimental effects on concrete behaviour at elevated temperatures.

Chapter 4

Preliminary Analyses and Preparations

4.1 Introduction

Before moving on to the more in-depth parametric research in the following chapters, some initial setups and analyses have been done in this chapter. First, in this section, details of two experimental test sets from the literature have been selected in order to highlight factors to be employed in parametric research throughout the rest of this thesis. Second, a mesh sensitivity analysis has been carried out to identify various relevant mesh sizes that may be applied evenly across the samples' thickness in order to ease the numerical computations and guarantee that the outcomes are unaffected. Then the capability of the ABAQUS model has been re-proved again in re-simulate the given temperature results for the selected samples. Finally, an analysis has been performed to show that to what extent the hygro-thermo reactions inside concrete could alter the results of this thesis which are based on only thermo mechanical damages.

4.2 Common concrete spalling test setups

As discussed previously, the samples have been tested in the literature can be considered to represent either non-structural samples or structural samples depending on whether they were loaded prior heating or not. As discussed in Chapter 3, these can be further divided into three categories based on heating scenarios adopted in the tests. Generally there are three heating scenarios in the literature, heated without load samples (unrestrained samples), restrained then heated samples, and loaded then heated samples (initially loaded samples prior heating). These scenarios designated in the previous chapter, while calibrating the model, as B Samples, D samples, and A samples respectively.

For the parametric studies conducted in this thesis, each parameter has been investigated thoroughly through considering this three pattern of samples, as it was also done in the previous chapter for the model calibration. Therefore, a test set from the literature [4] which incorporates these three methodologies considering different sizes, shapes, loads, and boundary conditions, has been chosen. The test was conducted by a research team from different universities in which six concrete mixes were used in preparing 59 samples in 9 different shapes and sizes. In the experimental work, different spalling ratios observed for some samples meanwhile for some others spalling did not occur at all. The loaded samples from this set are loaded uniaxially, therefore two samples from the work of Lo Monte and Felicetti [37] have been chosen to incorporate biaxially loaded samples to the investigations too.

The samples have been selected carefully to cover the most important parameters which are

known arguably to have effects on concrete behaviour and spalling and intended to be investigated in this thesis. That is to include parameters like sample size, various types of restraints, and various types of loads. The selected samples can be classified into six groups, unrestrained rectangular samples, partially restrained rectangular samples, concentrically loaded samples, eccentrically loaded samples, fully restrained ring samples, and biaxially loaded samples. Each group will be investigated in details in next chapters under different scenarios considering different parameters. Properties and dimensions of the selected samples from both [4] and [37] are summarized in the Table 4.1 and the test set ups are shown in Figure 4.1.

Table 4.1: Selected samples to be investigated

No.	Sample Shape and Dimensions(m)	Loading/ Restraint Status	f'_c (MPa)	Mix Detail
S1	Rectangular Slab 0.60*0.50*0.40	Unrestrained	42	W/C= 0.4, No Fibres
S2	Rectangular Slab 0.60*0.50*0.40	Partially restrained	42	W/C= 0.4, No Fibres
S3	Square Slab 0.50*0.5*0.25	Loaded concentrically	42	W/C= 0.4, No Fibres
S4	Rectangular Slab 3.10*1.20*0.30	Loaded eccentrically	70	W/C= 0.4, No Fibres
S5	Rectangular Slab 0.60*0.50*0.30	Partially restrained	70	W/C= 0.4, No Fibres
S6	Ring Sample 0.61 D, 0.30 T	Fully restrained	70	W/C= 0.4, No Fibres
S7	Square Slab 0.80*0.80*0.10	Loaded biaxially	60	No Fibres

4.3 Mesh sensitivity analysis

Even though there are little recommendations in literature regarding mesh size such as one suggested by Bazant and Oh [83], they are not suggesting meshing size as much as they are providing maximum meshing size limit. It is numerically demanding to apply single size mesh across the samples thickness. Therefore, before starting detailed investigations, a mesh sensitivity analysis has been conducted to determine different appropriate mesh sizes that could be used uniformly across the samples' thickness in order to simplify the numerical calculations and ensure that the results are not affected. For this purpose, several simulations for two different samples, namely S1 Small Unrestrained Slab and S2 Small Restrained Slab, have been repeated many times with various mesh sizes until no appreciable difference was observed between subsequent analyses. For each sample, maximum principal stress states at different heating times have been shown in Figure 4.2, which are obtained from simulations with different mesh sizes. It can be observed that the meshing size could deviate results especially in the first 25mm from the heating source. Based on this, 2.5mm mesh size for the first 25mm portion from the heating source and more coarser sizes (5mm, 10mm, 20mm) for the rest of the sample depth have been

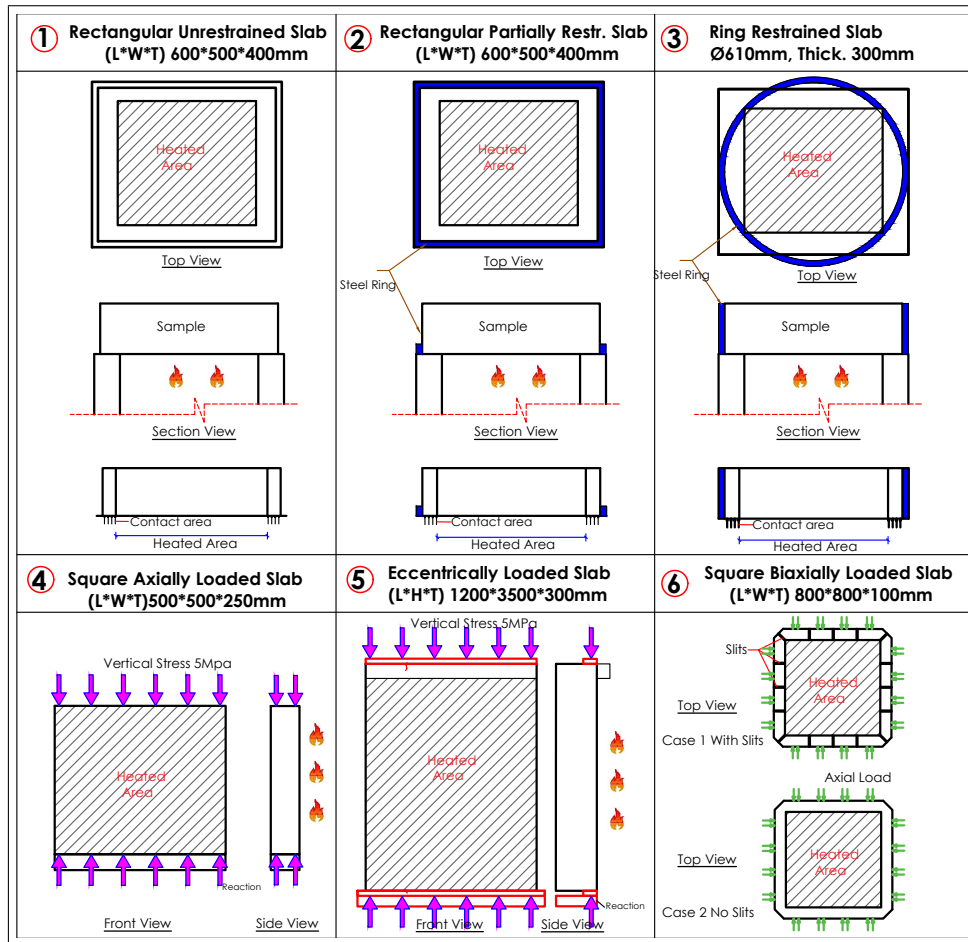


Figure 4.1: Selected samples and test methodologies for parametric studies

found to give high quality results without overly compromising computational performance. This pattern has been followed in all simulations undertaken in this thesis.

4.4 Observed temperature and spalling of the heated samples

In the selected experimental work discussed earlier, to measure the temperature of the heated concrete, some isolated thermo couples were installed on the heated surface and inside the samples at different distances from the heated surfaces. The thermo couples on the heated surface were out of order during the heating, however the inner thermo couples survived. Figure 4.3 shows the capability of the developed ABAQUS model in capturing the observed temperature at different thickness for various samples having different compressive strengths. Concerning concrete spalling, some samples spalled with various patterns in different temperatures and times meanwhile some others did not spall at all. The spalling depth and occurrence time for each sample are measured and reported in the report. Results of the selected series from the test report have been presented in Figure 4.4 and they will be used in discussions at next chapters.

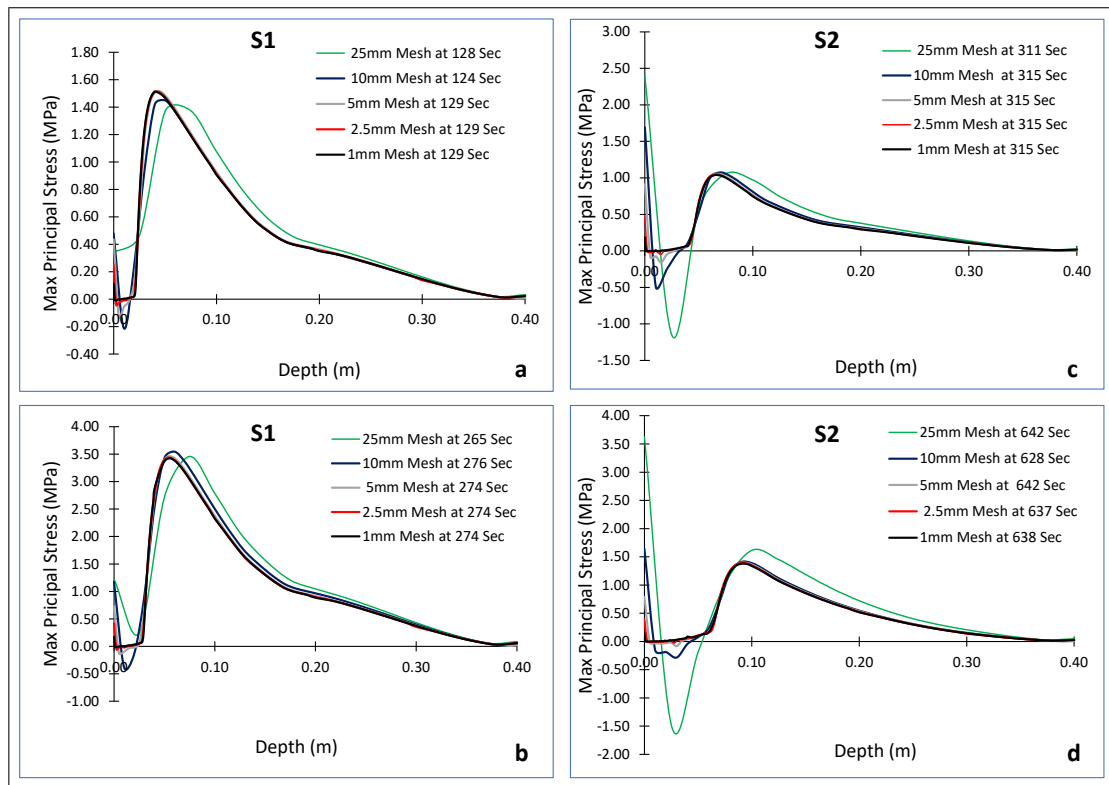


Figure 4.2: Max principal stress at different heating times considering different mesh sizes through depth of **a,b)** S1 small unrestrained sample, **c,d)** S2 small restrained sample

4.5 Hygro-thermo damage sensitivity analysis of concrete samples under effects of heating

The developed ABAQUS model which has been developed in Chapter 3 and applied in this thesis is a coupled thermo mechanical model without considering chemo-hygro-thermo reactions inside the concrete. As discussed before, one of the spalling mechanisms which has been highlighted in the literature is pore pressure mechanism which associates spalling with the migration of air, vapour and liquid water inside the concrete body while subjecting to elevated temperatures[10]. Many researchers incorporated this effect in the investigations [1, 15, 16, 17] meanwhile others did not include these effect in the investigations for example [19, 20, 21, 22, 18] and many others. Therefore, in this section the implications of pore pressure might have on the analysis results conducted in the thesis has been investigated.

To begin with the investigation, sample S5 from Table 4.1 has been considered which is rectangular partially restrained sample as shown in Figure 4.1 having 70 MPa compressive strength. A validated model [1] has been used for the hygro thermo investigation which is capable to captures the strong coupling between the independently considered solid, liquid, and gas fields inside the heated concrete, assuming concrete as a multi-phase system. The solid skeleton is thought to have isotropic elastic-damage behavior, and other important thermo-mechanical behaviour is taken into consideration along with material degradation under mechanical and thermal loading. Adsorbed water that is physically attached to the surface of the solid skeleton

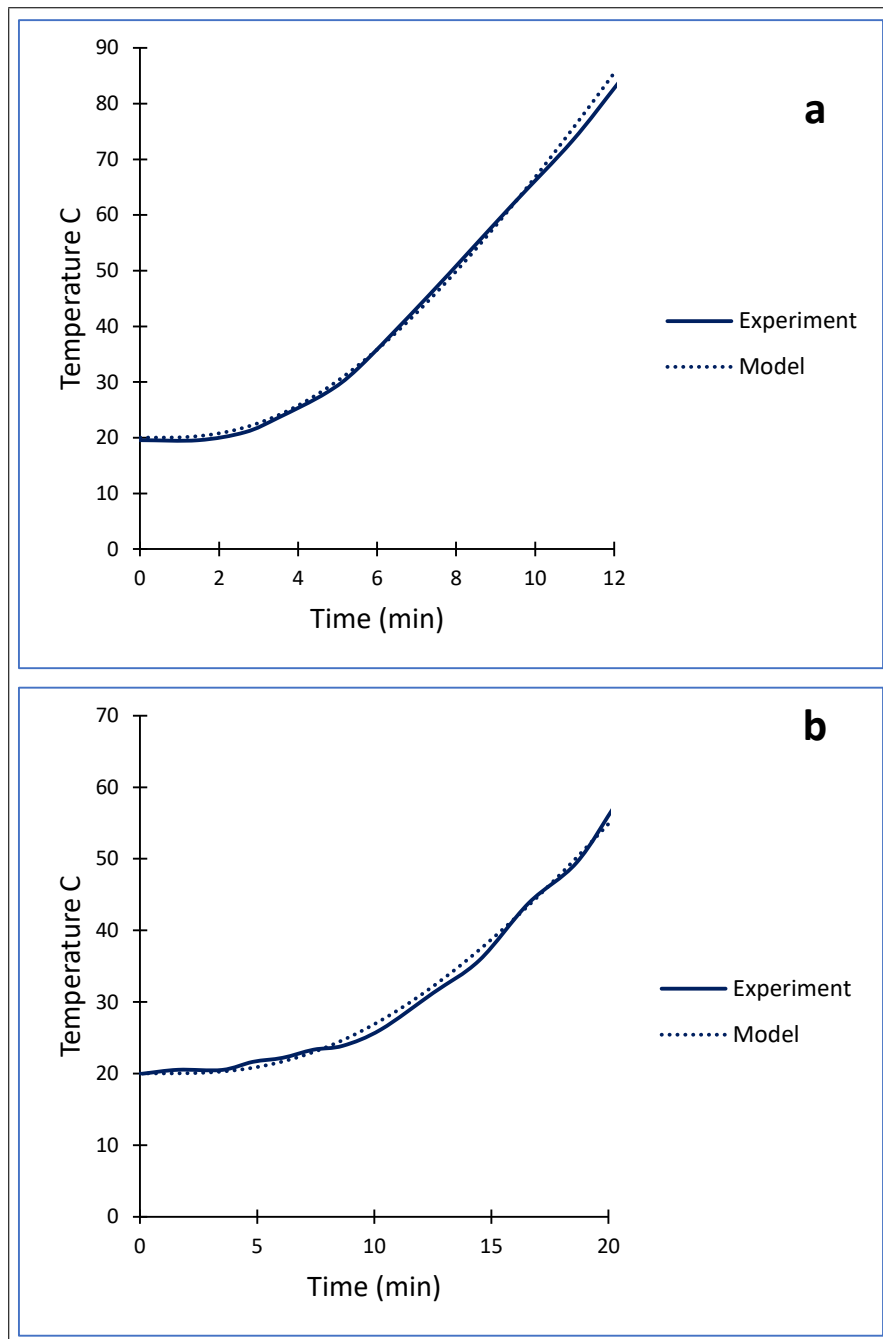


Figure 4.3: **a** Temperature Profile for S1 Sample with 42MPa Compressive Strength at 30mm Depth from the Heated Surface **b** Temperature Profile for S6 Sample with 70MPa Compressive Strength at 50mm Depth from the Heated Surface

is considered as a part of the liquid phase, and its behaviour is addressed when necessary. Dry air and water vapor, both of which are accounted as ideal gases, are considered to generate the gas phase. In order to accurately describe the fluid transport processes in concrete, heat and mass transfer of the fluid phases are modelled in a coupled manner. This illustrates, in particular, the redistribution of liquid and the increases in pore pressure and vapour content associated with the application of elevated temperatures. To perform analysis, each of moisture content, permeability and porosity parameters should be known to provide sufficient input data along with other concrete temperature dependent properties. The moisture content given in the test report

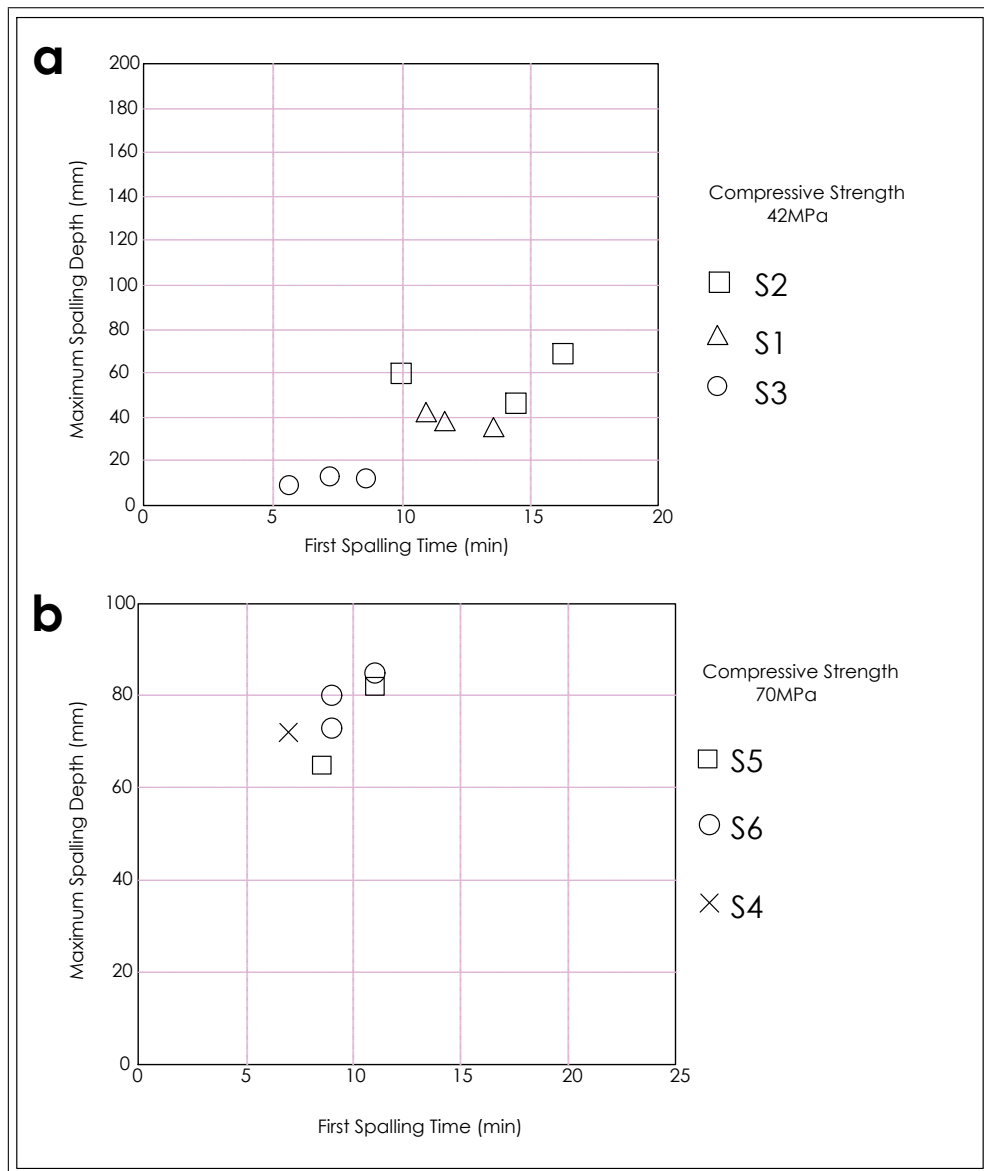


Figure 4.4: Spalling time and Maximum spalling depth for the Selected Samples from [4] **a**) Samples with 42MPa compressive Strength **b**) Samples with 70MPa compressive Strength

as 4%, however permeability and porosity are not given, therefore they have been chosen from literature. Very wide range for permeability and porosity can be found from the literature, Davie et al [84] summarizes the literature ranges for ordinary and high strength concrete, porosity ranges from 5% to 16% and permeability from $10^{-16}m^2$ to $10^{-22}m^2$.

First, the model has captured the temperature profile accurately identical to the ABAQUS results shown in Figure 4.3-b. Second, according to the given results shown in Figure 4.4-b, the selected S5 sample' first spalling is at 8 minutes with 63 mm depth. Therefore, the pore pressure at this heating time considering different porosity and permeability values has been investigated. For porosity, 10%, 12.5%, and 15% has been considered which for the given 4% moisture content, saturation degree values of 57.6%, 69.1%, and 86.4% would be achieved respectively. For each porosity value, two permeability scenarios $10^{-19}m^2$ and $10^{-21}m^2$ have been chosen within the literature range in performing the parametric studies. The results of the parametric study at spalling time (480 seconds) have been shown in Figure 4.5 in which

developed gas pressure for the first 40 mm from the heated surface have been shown only to visualize the peaks clearly.

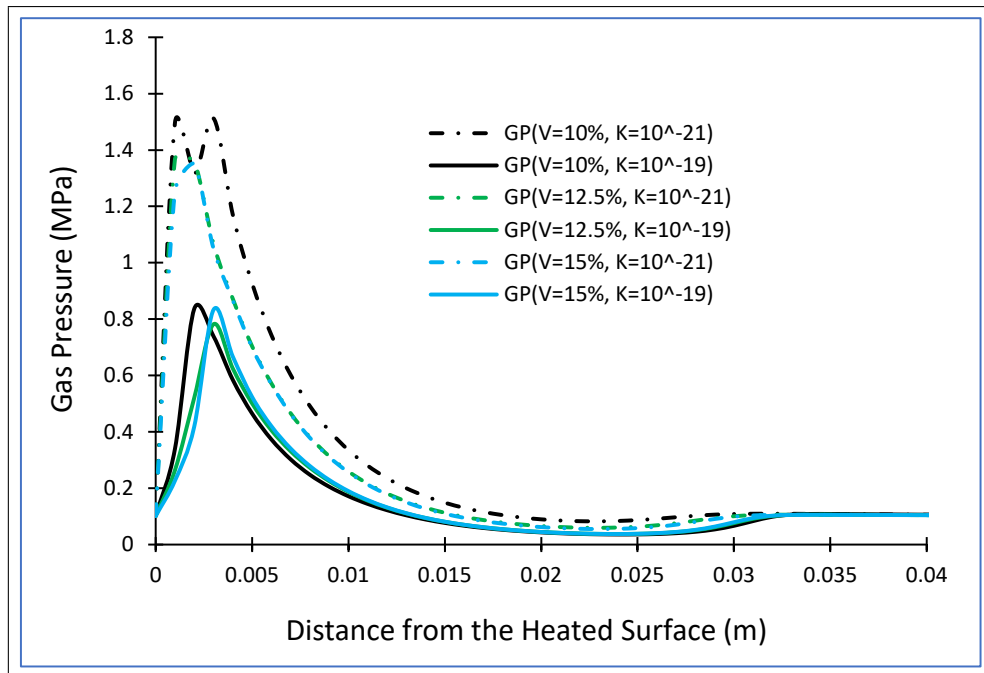


Figure 4.5: Gas Pressure through thickness of S5 Sample from Table 4.1 for different porosity and permeability values at spalling time (480 seconds)

As it is clear, the developed stresses peak almost identically at around 3mm from the heated surface for the same permeability value regardless of the porosity magnitude. At this very shallow depth from the heated surface, the pore pressure is not effective enough due to migration of the concrete moisture under the effect of the heating toward the outside of the concrete and evaporation occurrence. This can be evidenced by the low peaks developed, even for the smallest permeability and porosity, reaching 1.5 MPa which is well below the yielding value of concrete at tension ($0.09 \times 70MPa = 6.30MPa$). Based on these observations, it seems that the developed pore pressure stresses would have negligible effects on the results at the spalling time. While these results imply that the behaviour of the samples would be controlled by thermo mechanical effects, they give more confidence at the same time regarding the reliability of the observed results throughout this thesis.

Chapter 5

Effects of Restraint on Concrete Behaviour and Spalling at High Temperatures

5.1 Introduction

Throughout this chapter effects of underlying restraint parameters on concrete behaviour and its spalling have been investigated in detail to find out to what extent they may alter test outputs. While it is widely reported in the literature that restraint improves concrete fire resistance of beam samples, this investigation considered the details of the way in which the restraints have been applied in other types of samples in terms of degree of restraint, the method of application, their stiffness, and their type (i.e. mechanical restraint, self-restraint or restraint by loading). To do this, experimental tests with various sample types and test set ups were simulated via the developed ABAQUS coupled model developed in Chapter 3. As well as analysing the original test configurations, parametric studies were conducted to determine the influence of various aspects of the test configuration. The results showed that the test outputs are very sensitive to the precise way in which restraints have been applied, and it is likely that some of the results that have been reported in the literature are specific to the test set ups under consideration and cannot be generalized for other testing set ups.

5.2 Restraint configurations

To perform thorough investigations relating to restraint effects, it is crucial to choose samples covering structural and non structural elements and falling within the three main literature sample categories previously discussed in Chapter 3, namely heated unloaded samples, restrained then heated samples, and loaded then heated samples. Therefore, from the selections made in Chapter 4 and shown in Figure 4.1, four sample configurations, which were selected from [4], have been recalled in this chapter. The samples are an unloaded, unrestrained rectangular sample (Figure 5.1-A), an unloaded, rectangular sample laterally restrained by a 50 mm high steel frame around the base of its perimeter (Figure 5.1-B), an unloaded, circular sample laterally restrained by a steel ring around the full height of its circumference (Figure 5.1-D) and a square sample restrained by a uniaxial load (Figure 5.1-E). Additionally, two square samples, restrained by biaxial loading were chosen from the work of Lo Monte and Felicetti [37](Figure 4.1). These vary in that one has a series of slits cut into the unheated outside of the slab, perpendicular to the edge (Figure 5.1-G). The dimensions and test set ups for these samples from the literature are shown in the figure and the concrete used in these samples covers a wide range of compressive

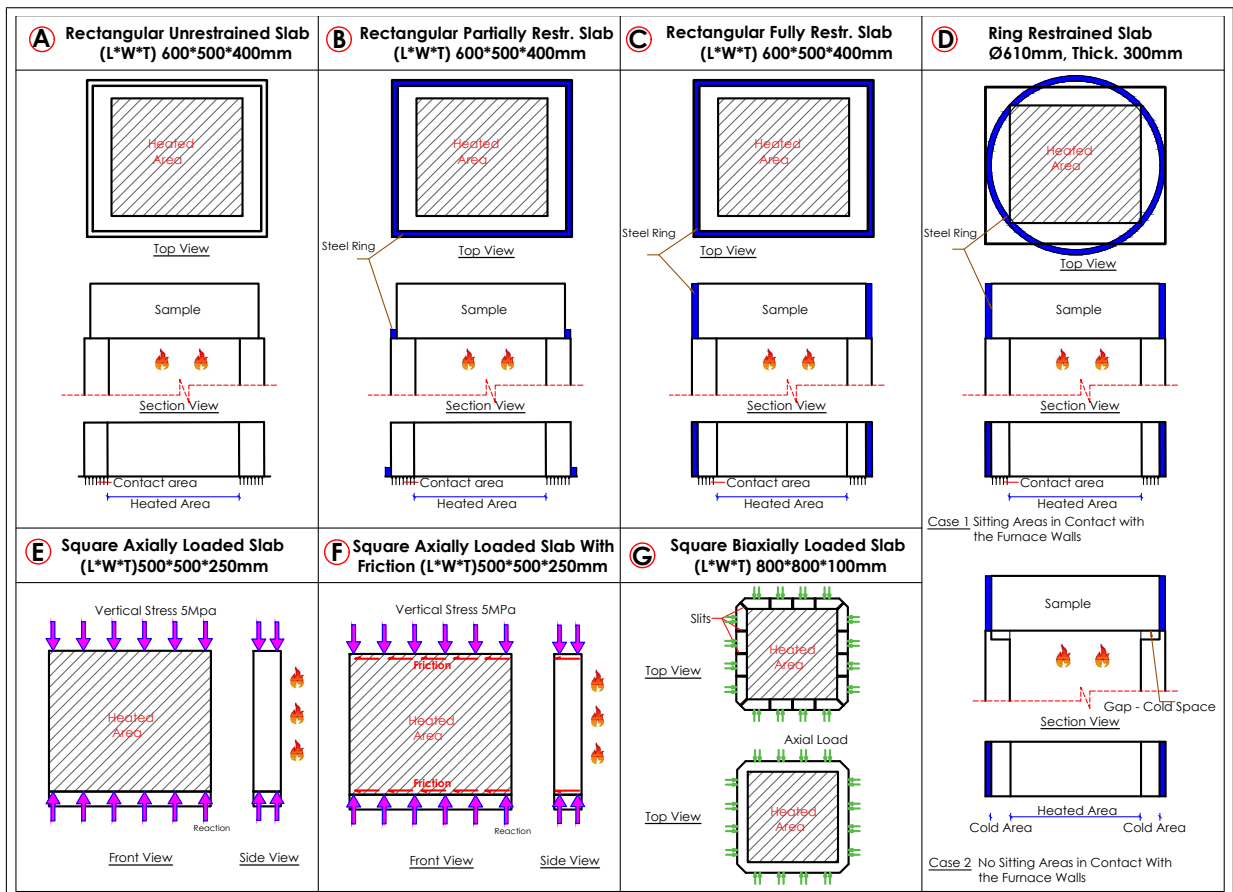


Figure 5.1: Restraint configurations showing heated areas, mechanical restraints and loading

strengths, 42 MPa for both unloaded rectangular samples (A & B) and the loaded square sample (E), 70 MPa for the circular sample (D) and 60 MPa for the biaxially loaded samples. All samples were exposed to the standard ISO834 fire curve through the surfaces shown as the hatched areas in Figure 5.1.

Furthermore, a number of the testing scenarios described above were extended to allow for parametric studies. First, test configuration (B) has been extended to include lateral restraint over its full thickness (Figure 5.1-C). Second, test configuration (D) has been extended to include two cases where frictional restraint related to the areas of the unheated, underside of the sample that rest on the walls of the furnace could be investigated (Figure 5.1-D). Third, test configuration (E) has been extended to consider the effects of friction between the loading platens at top and bottom of the sample (Figure 5.1-F).

5.3 Analysis results and discussions

Concrete spalling is known to begin from faces exposed directly to the heating source and continues toward the inner portions of the sample depending on the duration and the severity of the heating. Therefore, the investigations in this work are based on consideration of the stress and displacement states through the thickness of the samples and at the heat exposed surfaces. The developed ABAQUS model in Chapter 3 published in [85] has been employed in the analysis.

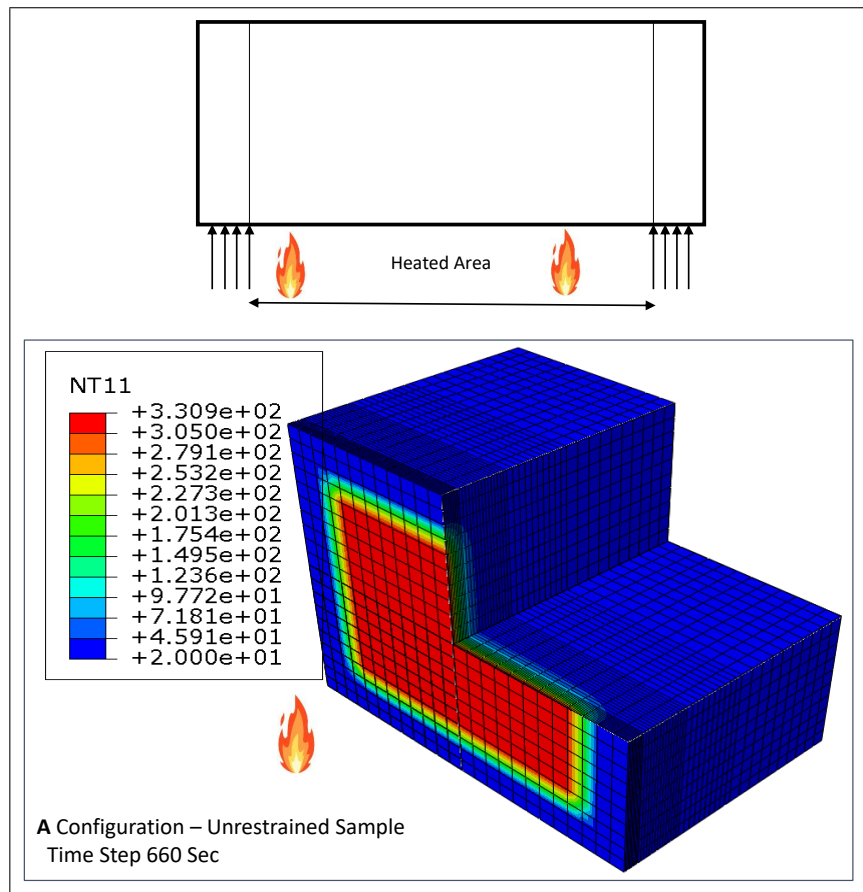


Figure 5.2: 3D section showing the temperature profile in the unrestrained slab (configuration (A) at time of spalling (660 s)

5.3.1 Unloaded rectangular samples

The unloaded, unrestrained and restrained thick, rectangular slab samples shown in Figure 5.1-A,B,C are identical in terms of geometry and material properties but different in boundary conditions and in the ways they have been restrained. Experimental results reported in [4] give temperature profiles in time at different locations through the thickness of the samples. It is clear from Figure 4.3-a that the model is able to capture the temperature in the slabs very well. The surface temperature at the centre of the fire exposed area at the time of spalling for configuration (A) (reported as 660 seconds) is predicted to be 331°C (Figure 5.2). For configuration (B) (time of spalling 600 seconds) is 304°C .

In terms of location of the spalling, it is noted in the experiments, as might be expected, to start from the fire exposed surface and deepen through the thickness in time. The depth of first spalling of the unrestrained and restrained samples (A) & (B) are reported to be 40 mm and 60 mm respectively. Cut-away views showing the minimum and maximum principal stresses at approximately these times for both tested samples (A) & (B) and the extended numerical only scenario (C) have been presented in Figure 5.3. Plots showing maximum and minimum principal stress profiles through the thickness of the samples at their centrelines, at different times, are shown in Figure 5.4.

As can be seen, the general trend in all of these sample configurations is for a highly

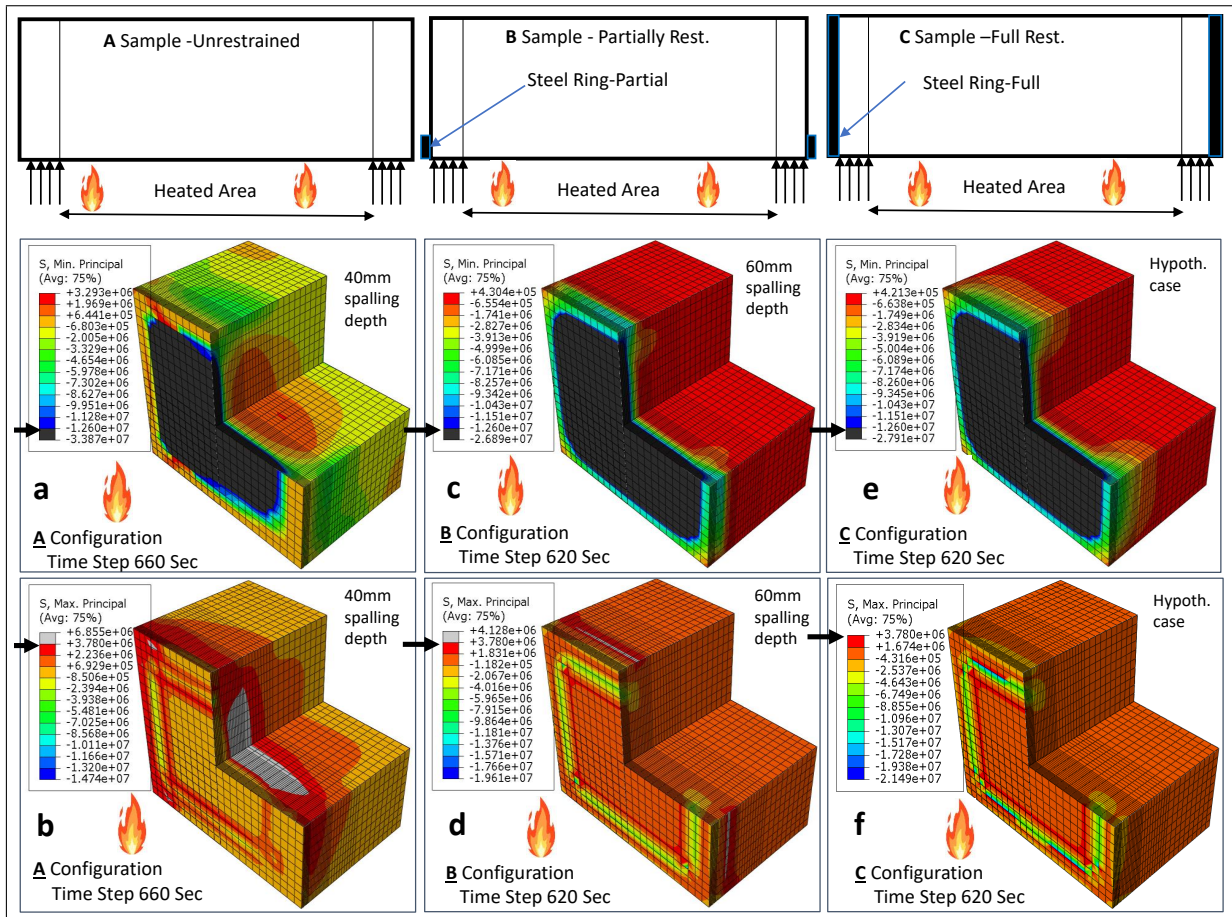


Figure 5.3: 3D sections of minimum and maximum principal stress profiles at time of spalling in a), b) configuration (A), c), d) configuration (B) & e), f) configuration (C)

compressive zone to develop in the hot region nearest to the fire exposed surface, with a dominantly tensile zone developing immediately behind it, deeper in the samples. Beyond that, some compressive stresses are seen in the zone nearest the cold top of the samples.

In the hot compressive zone, the stress values in all three configurations, up to 25mm from the exposed surfaces are significantly higher than the compressive yielding limit of the concrete (shown as black - Figure 5.3-a,c,e). Compressive yielding limit is the stress beyond which the concrete experiences plastic deformation which is consistently considered $0.3f'_c$ ($0.3 \times 42 \text{ MPa} = 12.6 \text{ MPa}$) as discussed in Chapter 3. The stress intensity for the unrestrained sample (configuration (A)) is much higher than in the two restrained samples (configurations(B) & (C)), which have almost the same stress intensity. However, the area of the yielded zone at the exposed surface of sample (A) is smaller than those on the the restrained samples (B) & (C). It worth mentioning that minimum principal stresses aligned to the in-plane stress components as shown in Figure 5.5-a,c,e. Furthermore, all mentioned observations can also be seen for all samples, namely front face yielded area in compression followed by deeper tensile area with the highest tension stress for configuration (A).

The observed differences between unrestrained and restrained rectangular samples can be attributed to the effects of the restraints increasing the stiffness of the samples against the lateral displacement that tends to occur due to thermal expansion. Therefore, stresses concentrate along

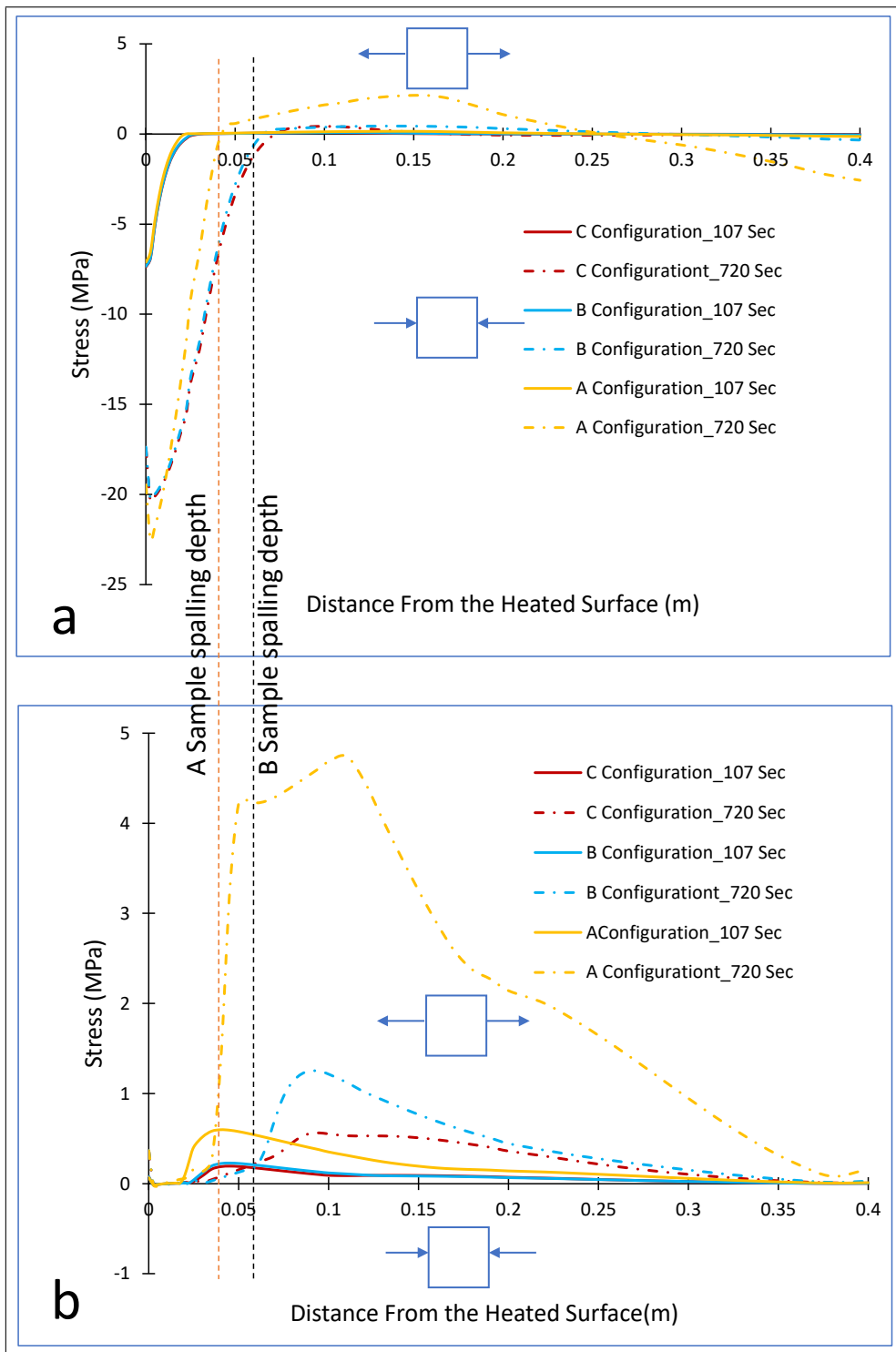


Figure 5.4: a) Minimum and b) maximum principal stress profiles through the thickness of the rectangular slabs at center (configurations (A, B & C) at different times

the circumferential areas and even into the cold rim beyond the fire exposed area of the samples. Conversely, the unrestrained sample has more freedom to expand laterally resulting in higher deformations in the central heated area, causing higher stress values.

Considering the stress profiles through the centre of the samples (Figure 5.4-a), the results show that in the early stages of heating the samples behave almost identically in this zone whereas at later stages, around 7 minutes, the compressive stress profiles in the restrained and

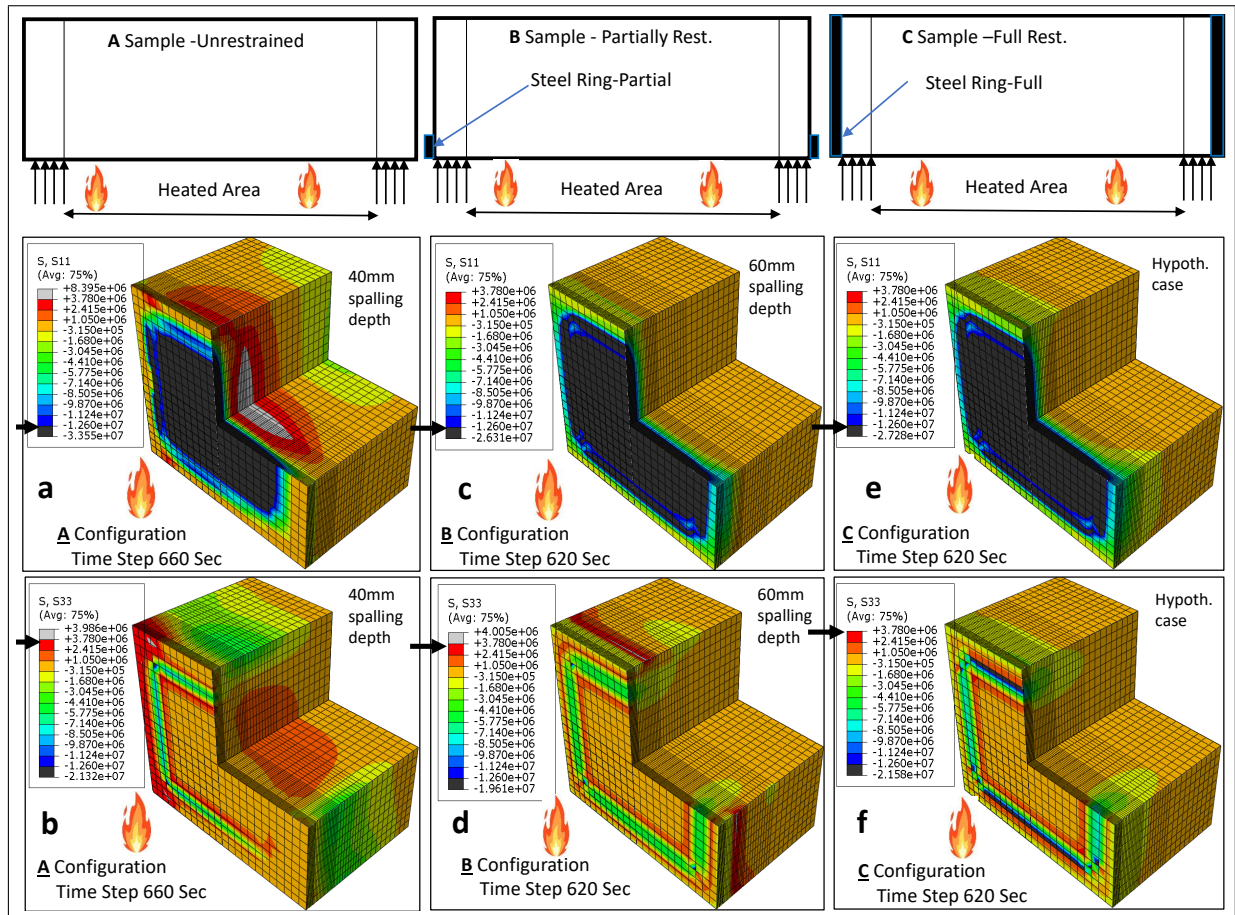


Figure 5.5: 3D sections of in-plane and out of plane stress profiles at time of spalling in a), b) configuration (A), c), d) configuration (B) & e), f) configuration (C)

unrestrained samples diverge. While there is negligible difference between the compressive stress states of the partially and fully restrained samples (B) & (C), the compressive stress zone in the unrestrained sample is narrower and peaks $\sim 12\%$ higher.

Looking now at the tensile zone, a region with an intensity exceeding the tensile yielding limit of the concrete can be seen in the centre of the (A) sample (shown as grey - Figure 5.3-b), between $\sim 30\text{mm}$ and $\sim 110\text{mm}$ from the hot surface. Tensile yielding limit is the stress limit beyond which the concrete fail in tension which is consistently considered $0.09f'_c$ ($0.09 \times 42 \text{ MPa} = 3.78 \text{ MPa}$) as discussed in Chapter 3. This high tensile stress is absent from both the restrained configurations (B) & (C) (Figure 5.3-d,f) although Figure 5.4 shows that they do also have a tensile stress regime. In contrast, a strip around the outside of the partially restrained (B) sample, just above the restraint frame, can be seen to have exceeded the tensile yield limit. This did not happened at all in the fully restrained (C) sample. As it has been observed in minimum principal stresses, maximum principal stresses aligned to the vector stresses but this time with the out of plane stress component. All mentioned observations can also be seen for all samples as shown in Figure 5.5-b,d,f including the higher tensile zone toward the fire for configuration (A) which is at yielding limit, it will exceed the limit upon superimposing with tension stress from other direction.

The reasons behind these different behaviours are again related to the restraints in controlling

the way that the samples deform. The restrained samples have been stiffened by the restraints, which limits lateral displacement of the exposed surfaces while the hot portion of the unrestrained (A) sample has more freedom to displace laterally, resulting in higher tensile stresses developing at depth in the colder regions of the sample. For the partially restrained (B) sample, the region just above the 50mm thick restraint frame is free to displace laterally and thus a tensile stress concentration develops at this discontinuity.

Looking at the stress profiles in time (Figure 5.4 -b), it can be seen that the high tensile stresses in the unrestrained (A) sample start to develop from early on, while the difference between the profiles in (B) & (C) becomes evident only later (after around 7 minutes of heating). While the difference between the tensile stress in (B) & (C) remains relatively small, the tensile stress in the unrestrained (A) sample is around five times higher.

Noticeable in all three configurations is a sharp switch between a compressive and a tensile regime and it is this that seems to correspond with spalling both in time and depth. From Figure 5.4 it is clear that, around the time of spalling (660-840 s for configuration (A) and 600-1020 s for configuration (B)) the transition to a fully tensile regime occurs at almost exactly the 40 mm spalling depth reported for (A) and the 60 mm depth reported for (B). The switch is most severe in the unrestrained (A) configuration and shows a slower transition in the two restrained configurations demonstrating that restraint both reduces the magnitude of the stresses and reduces the stress gradients within the samples, thereby reducing the likelihood of spalling. It seems the spalling occurrence is dependant on whether during this switch both or either of compressive and tensile limits have been surpassed. In this case, for all samples, compressive stresses have surpassed the compressive yielding limit (12.6MPa) at the exposed surfaces where the spalling starts meanwhile for the unrestrained (A) configuration, the tensile limit has been surpassed too. Corresponding to this, in addition to spalling at the surface due to compressive yielding, the tensile stress in the unrestrained (A) configuration makes the sample to experience shallower spalling (40mm) meanwhile in other sample the spalling depth is (60mm).

The effects of the restraint can also be seen in the displacement profiles of the samples. Figure 5.6 shows the displacements across the centre line of the heated face of the samples, perpendicular to the face, at different times. At the early stages of heating the samples showed very similar behaviour. However, after around 10 minutes and more obviously after 20 minutes, the fully restrained (C) sample shows larger displacements than the unrestrained or partially restrained samples. A possible reason to this is the freedom that each sample possessed to displace throughout its thickness. In the case of the fully restrained sample, the heated concrete could displace only axially toward the fire source while the partially restrained and unrestrained samples had more freedom to displace laterally, which results in lower axial deflections. Although not a significant issue in the case of these thick slab samples, this behaviour could be important for samples that are more sensitive to bending or tension stresses either due to having large bending spans or due to external loading.

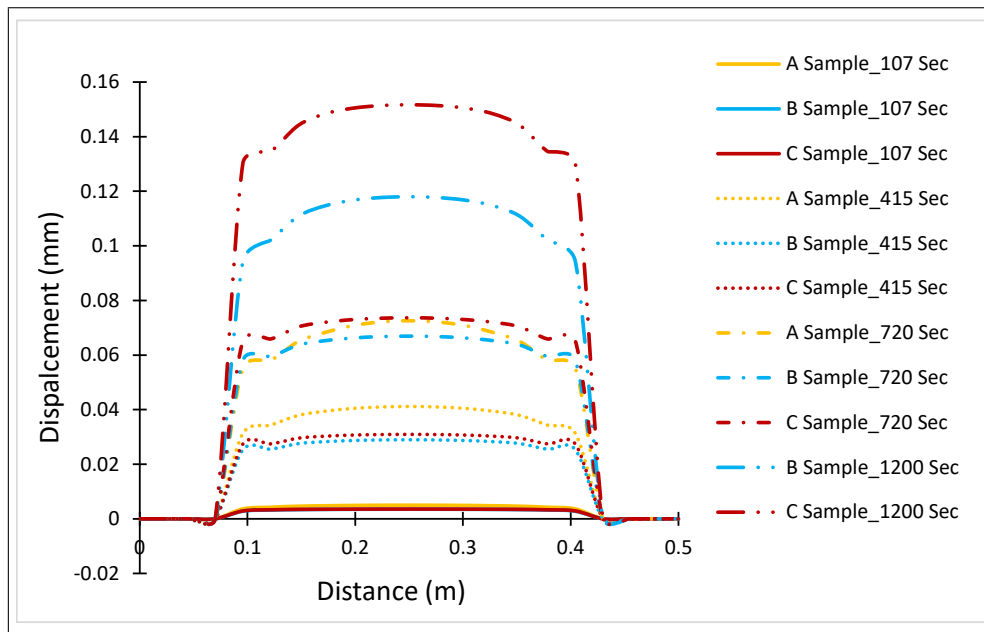


Figure 5.6: Profiles across the centre line of the heated face showing displacements perpendicular to the face for restraint configurations (A, B & C) at different times

5.3.2 Ring samples

The ring sample configuration (D) is shown in (Figure 5.1-D). This configuration consists of a steel ring that restrains the sample over its full height, similar to the fully restrained rectangular configuration (C). Very stiff restrained has been considered as per the tested sample, with this extreme restraint condition and even in very high temperatures, as discussed in Section 2.4.4 Chapter 3, the developed stress did not exceed 18% of the concrete compressive strength. Here more investigations have been pursued incorporating different geometry samples and test set ups. Broadly, the behaviour in terms of the compressive and tensile regions and the sharp transition between them are similar to the results seen with configuration (C) and so the focus here is on the influence of the frictional restraint that may be derived from the contact between the sample and the walls of the furnace on which it rests. The frictional restraint is directly proportional to the contact characteristics of the surfaces and the sample's weight. Therefore, samples with more weight provide more frictional restraint around the contact area, which may affect the overall response to heating. To investigate this, in addition to simulating the experimental test scenario shown as Case 1 in Figure 5.1-D, another simulation, shown as Case 2, has been incorporated. Case 2 has the same heating area and steel ring restraint as Case 1 but artificially removes the contact, and therefore friction, with the furnace walls.

Experimental results for configuration (D-Case 1) reported in [4] show that first spalling took place after 540 seconds of exposure to the ISO834 fire curve. As with the rectangular configurations (A-C), the model is shown to capture the thermal behaviour of the experiment very well (Figure 4.3-b). The temperature reached at the centre of the exposed area was predicted to be just over 150°C at this time (Figure 5.7).

Three spalling depths were reported for the ring samples. The, first and second, which

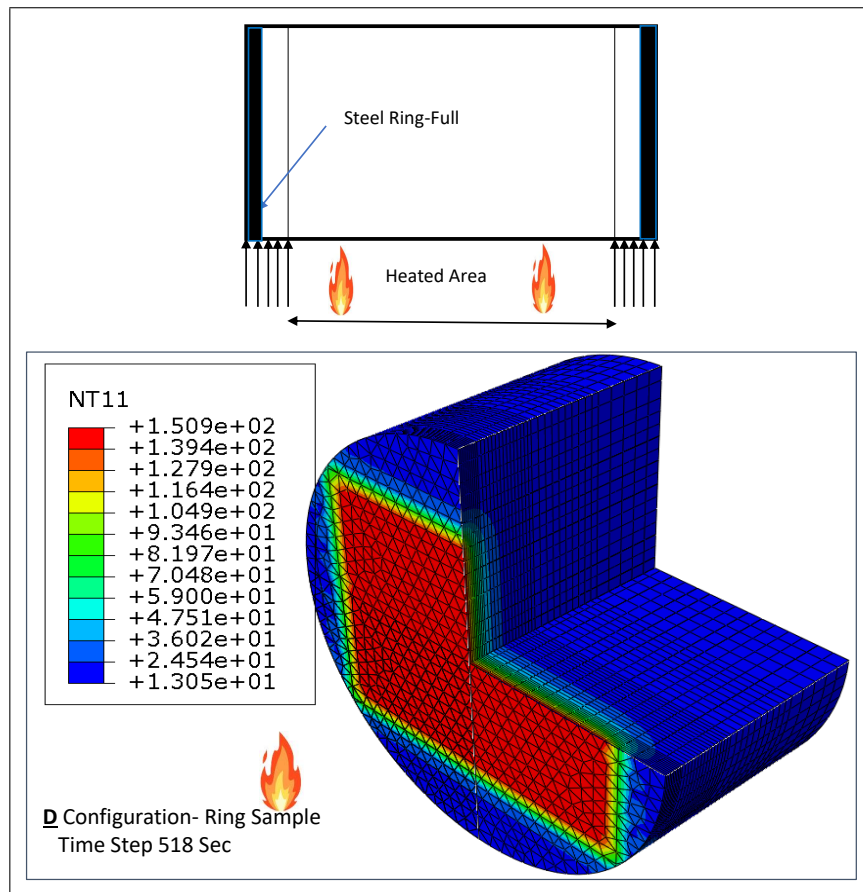


Figure 5.7: 3D section showing the temperature profile in the ring slab (configuration (C)) at closest time step to time of spalling (540 s)

both took place at 540 seconds were 73 mm and 80 mm respectively while the third, which took place at 660 seconds, was 85 mm. Cut-away views showing the minimum and maximum principal stresses for the two cases of configuration (D), as close as possible to 540 seconds are presented in Figure 5.8. Plots showing maximum and minimum principal stress profiles through the thickness of the samples at their centrelines, at different times, are shown in Figure 5.9.

As in the rectangular samples discussed in the previous section, the recorded spalling depths match well with the sharp transition from compression to tension seen in the stress profiles through the thickness of the samples (Figure 5.9). However, these profiles show almost no difference in the compressive stresses developed with or without the frictional restraint of the physically supported area of the sample, indicating that it has little effect on the stress state at the centre of the sample.

Again similar to the rectangular samples, the cutaway contour plots (Figure 5.8-a,c) both show severe areas of yielded concrete extending through to the outside of the furnace walls. For these samples the compression yielding limit is $0.3f'_c$ ($0.3 \times 70 \text{ MPa} = 21 \text{ MPa}$), higher than the rectangular samples but it has been surpassed earlier. In contrast to the stress profiles at the centre of the samples, the unsupported sample shows higher magnitude stresses suggesting that the restraint provided by the contact with the walls of the furnace helps limit the stress development. The higher stresses seen in the unsupported sample develop out towards the edges in the locations where the support restraint has been removed artificially. The same pattern can be observed if

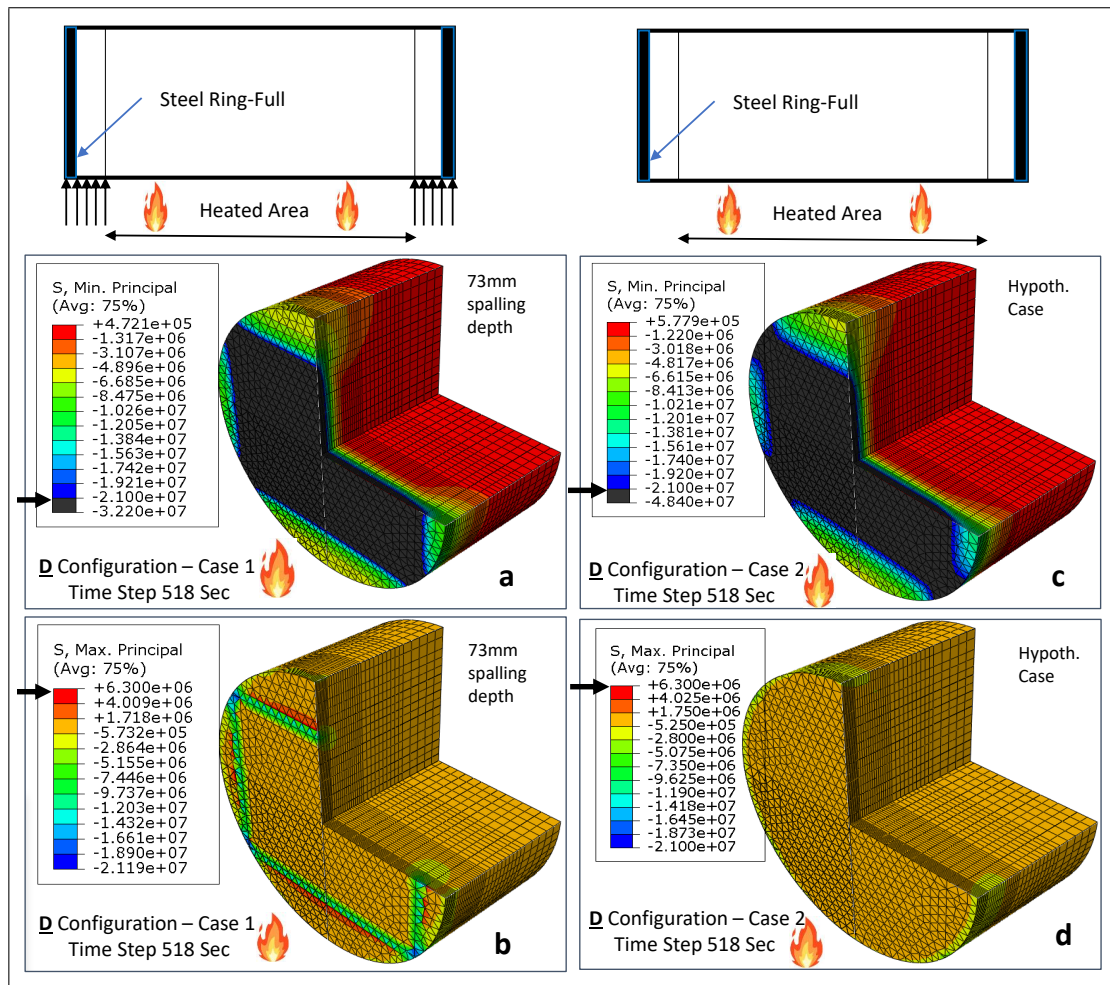


Figure 5.8: 3D sections of minimum and maximum principal stress profiles as close as possible to time of spalling in a), b) configuration (D) Case 1 & c), d) configuration (D) Case 2

in-plane stress components compared as shown in Figures 5.10- a) & c). This is even better seen after spalling occurrence in plots of in-plane stress (Figure 5.11) where the yielded zone can be seen to be larger and the magnitudes are higher. Whereas Figures 5.8- b) & d) show no severe tensile stresses surpassing tensile yielding limit $0.09 f'_c$ ($0.09 \times 70 \text{ MPa} = 6.3 \text{ MPa}$), it shows the ring of compressive stresses where the sample rests on the furnace. It disappears and a ring of compression instead developing at the outside of the sample where the steel restraining ring is (same can be seen from vector stresses shown in Figures 5.10- b) & d). Effects on tensile stresses are also visible in Figure 5.9 b), this time through the centre of the samples, where it can be seen that the stresses peak higher without the restraining effect of the furnace walls. Although the magnitudes are relatively low, this effect increases both the magnitude of the stress and the severity of the transition between compression and tension. As discussed for rectangular samples, the spalling may associate with this transitioning and whether the concrete yielding limits in compression or tension have been surpassed. Therefore, it seems ring samples mostly spalled due to compression failure starting from the exposed surface since the tensile stresses have been reduced by the effects of the ring restraints, and this is more pronounced in the samples with friction.

Thus, the effect of frictional restraint resulting from the test configuration, where a sample is

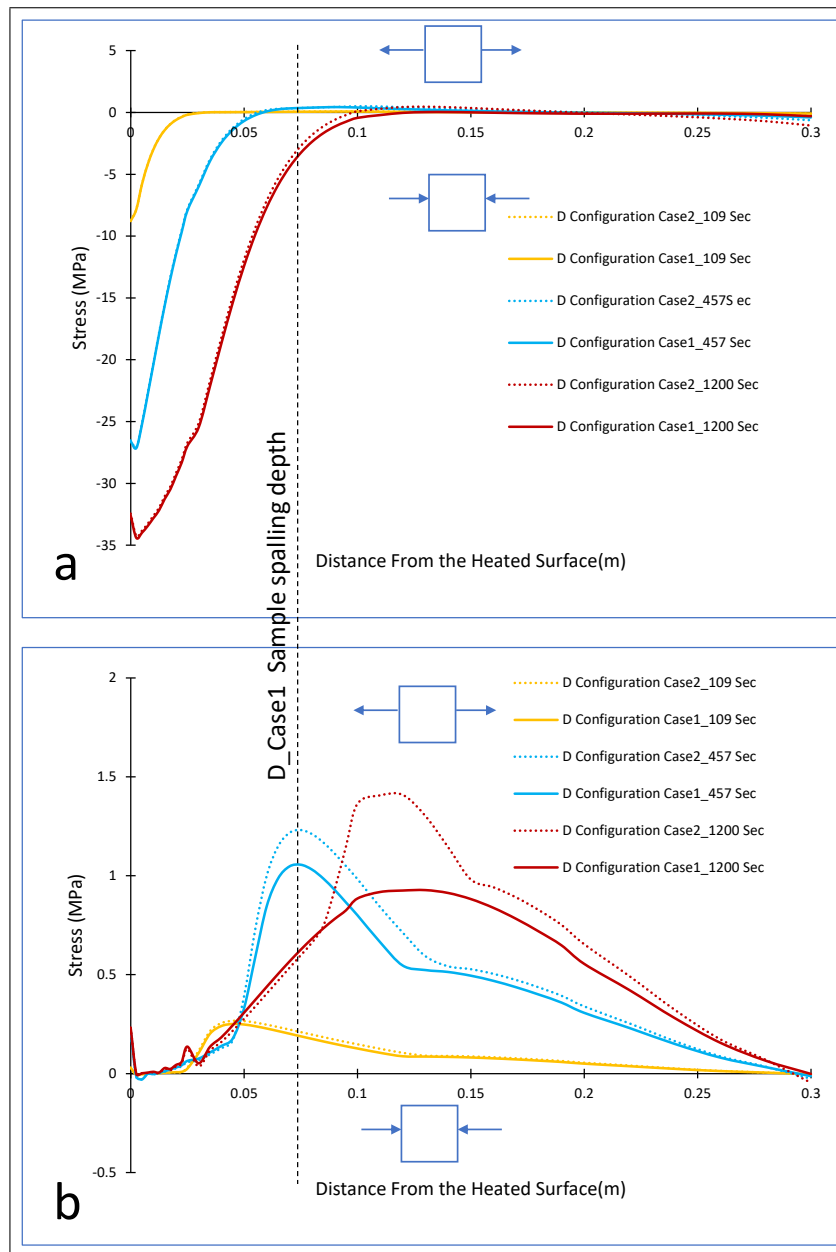


Figure 5.9: a) Minimum and b) maximum principal stress profiles through the centreline thickness of the ring sample (configurations (D) Cases 1 & 2 at different times

seated on the walls of a furnace can be seen to influence the stress state, and by extension, to reduce the risk of spalling in the samples. Moreover, it is the relative stiffness of that restraint that seems to be important. In the unsupported sample, where there is only the very stiff restraint provided by the steel ring on the outside of the sample, high stresses are concentrated in these areas. But, where frictional restraint is also present due to the walls of the furnace, stresses seem to be dissipated similar to how a less stiff, spring boundary would act.

In relation to a sample resting on the sides of a furnace, it is also often noted in literature (e.g. [3, 37, 33]) that the supported areas are unheated and that the resulting 'cold ring' around the sample may apply restraint through differential thermal expansion. To demonstrate that this is not the effect being seen here, the same numerical tests were conducted with heating applied to the whole surface. As can be seen in Figure 5.12, the results are very similar to those seen

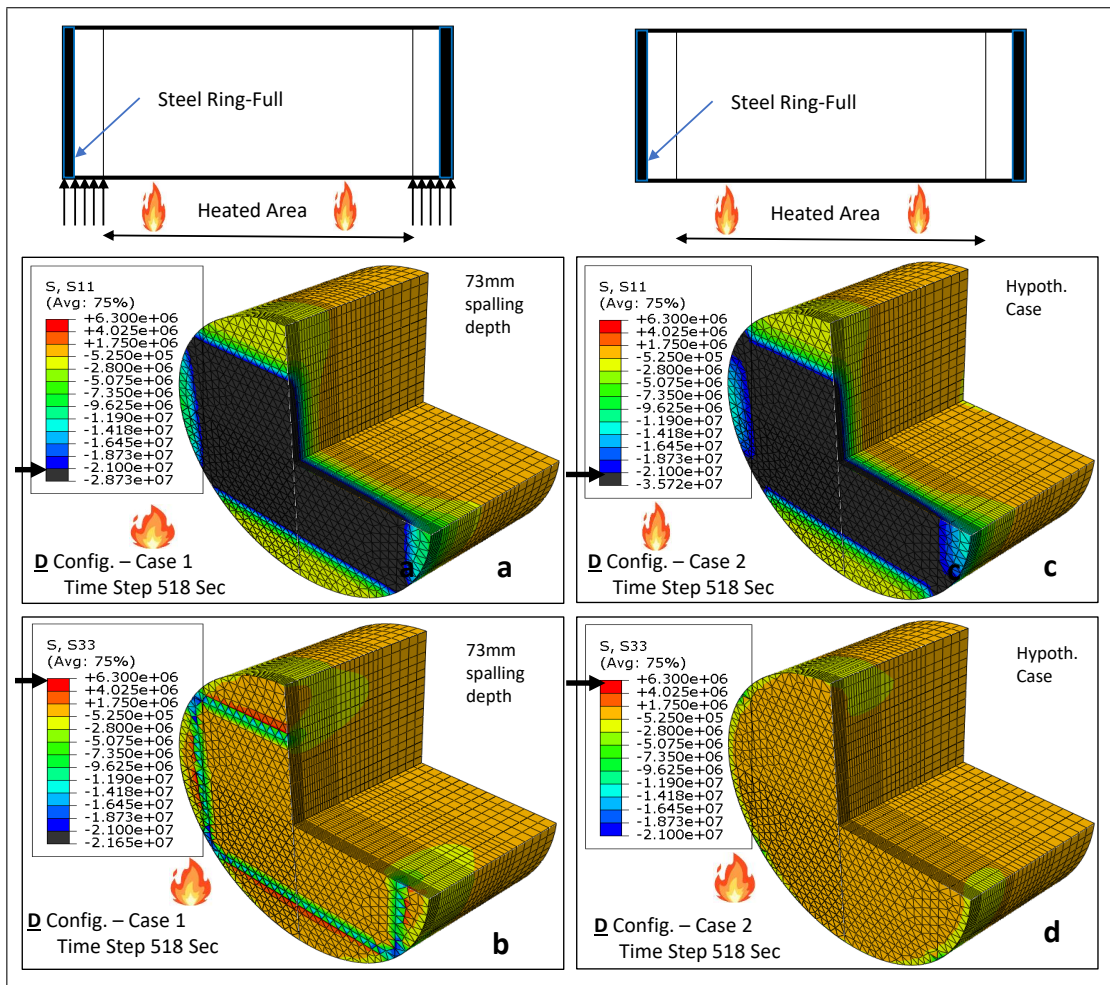


Figure 5.10: 3D sections of in-plane and out of plane stress profiles as close as possible to time of spalling in a), b) configuration (D) Case 1 & c), d) configuration (D) Case 2

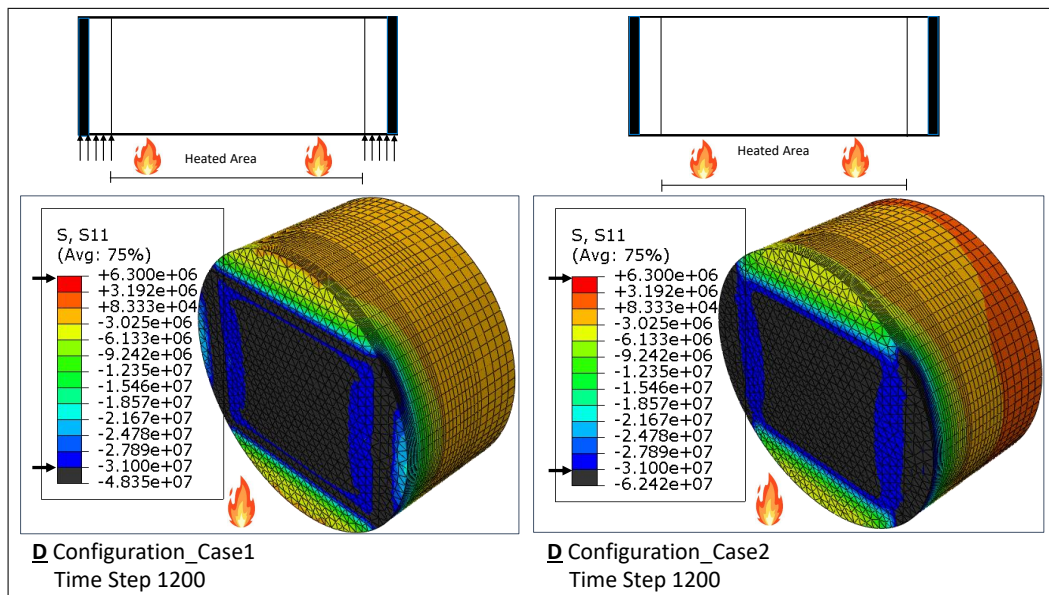


Figure 5.11: 3D Views showing developed in-plane stresses at the exposed surface of the ring samples under different testing scenario from Figure 5.1-D at time 1200 s

above in Figure 5.11 even far beyond the spalling time. Although, as is to be expected, the area of high compressive stresses is larger, the stresses are lower when frictional restraint is present

(Figure 5.12 a) and in fact there is almost no difference in the magnitude of the stresses with or without a 'cold ring'. ('Cold ring' effects are explored in more detail in a separate chapter).

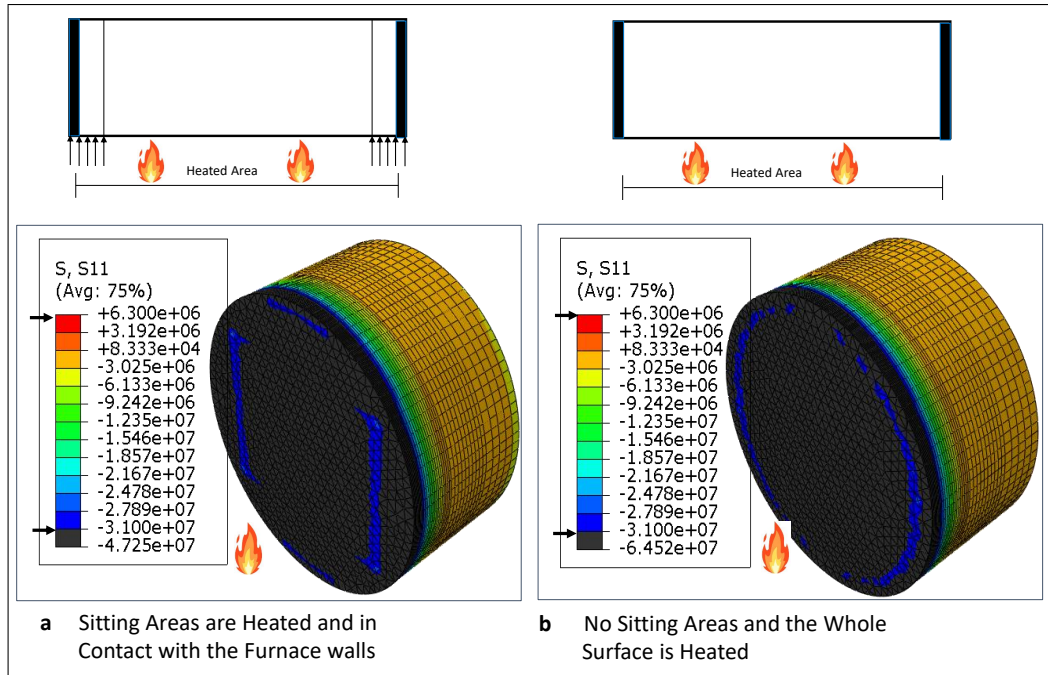


Figure 5.12: 3D Views showing developed in-plane stresses at the exposed surface of the ring sample for scenario extended from Figure 5.11 at time 1200Sec

5.3.3 Uniaxially loaded square samples

The samples discussed so far are all restrained mechanically without applied external loading. To investigate the effect of restraint by applied load, square samples loaded uniaxially and uniformly with a pressure of 5MPa were modelled (Figure 5.1-E,F). Configurations (E) & (F) are identical with the exception that, since the true properties of the the loading plattens is not known, the plattens in (E) are considered to be frictionless while the plattens in (F) are considered to generate full friction at the top and bottom (indicated by red horizontal arrows in Figure 5.1-F). Thus, in addition to investigating the effects of restraint by applied load, the influence of test set up in applying the load can be investigated. During analysis, displacement controlled technique has been considered for both cases, that is equivalent displacement at ambient temperature resulted by the load has been applied as boundary conditions.

According to the reported experimental test results ([4]), the sample first spalled after 360 seconds of exposure to the ISO834 fire curve with a depth of 9 mm, followed by two more spalls at 540 and 640 seconds with 10 and 11 mm depths respectively. This sample was the same concrete mix as the unloaded rectangular samples previously discussed (Configuration (A)) and therefore had the same temperature dependent material properties. The temperature at first spalling was predicted to be 195°C at the exposed surface (Figure 5.13). As before, 3D section views of minimum and maximum principal stresses for both configurations at time of spalling are presented (Figure 5.14) along with profiles of maximum and minimum principal stress through the thickness of the samples at their centrelines, at different times (Figure 5.15).

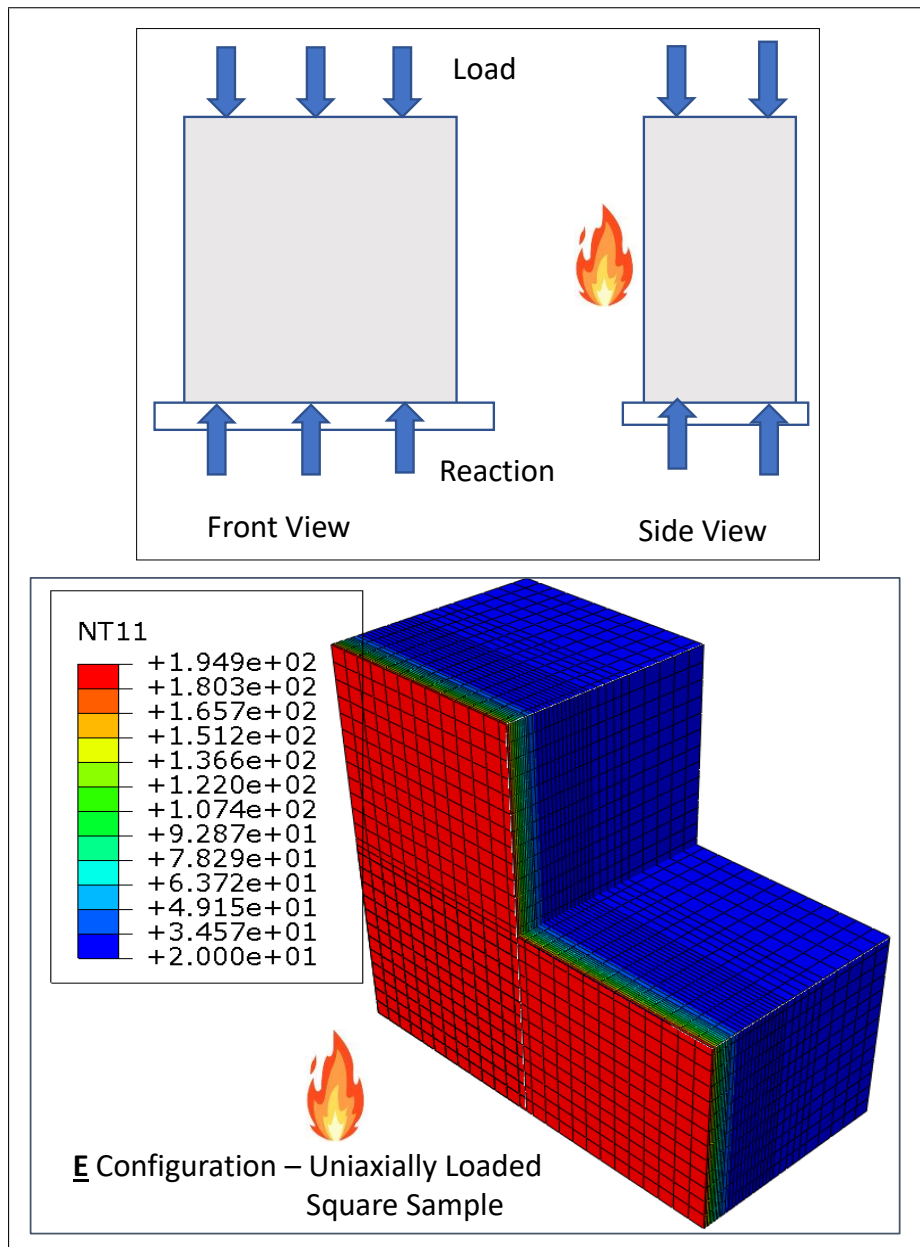


Figure 5.13: 3D section showing the temperature profile in the uniaxially loaded slab (configurations (E) & (F) at time of spalling (360 s)

In contrast to the mechanically restrained samples (Configurations (B) to (D)) it may be noted that, due to the applied load, the starting condition for these samples is to have a significant compressive minimum principal stress through their thickness and over their full height. The applied load essentially offsets the stress state from that produced by mechanical restraint (Figure 5.15 - a)).

Nonetheless, the pattern of stresses remains similar to the previous cases, with a strong compressive zone and yielding concrete near the fire exposed face (Figure 5.14 a,c - shown in black) and a significant tensile zone immediately behind it. However, because of the initial stress offset, the transition from one zone to the other is even more severe than in previous cases with a discontinuity between the minimum and maximum principal stresses. While the compressive yielding limit $0.3f'_c$ ($0.3 \times 42 \text{ MPa} = 12.6 \text{ MPa}$) has been severely surpassed, the tensile stress

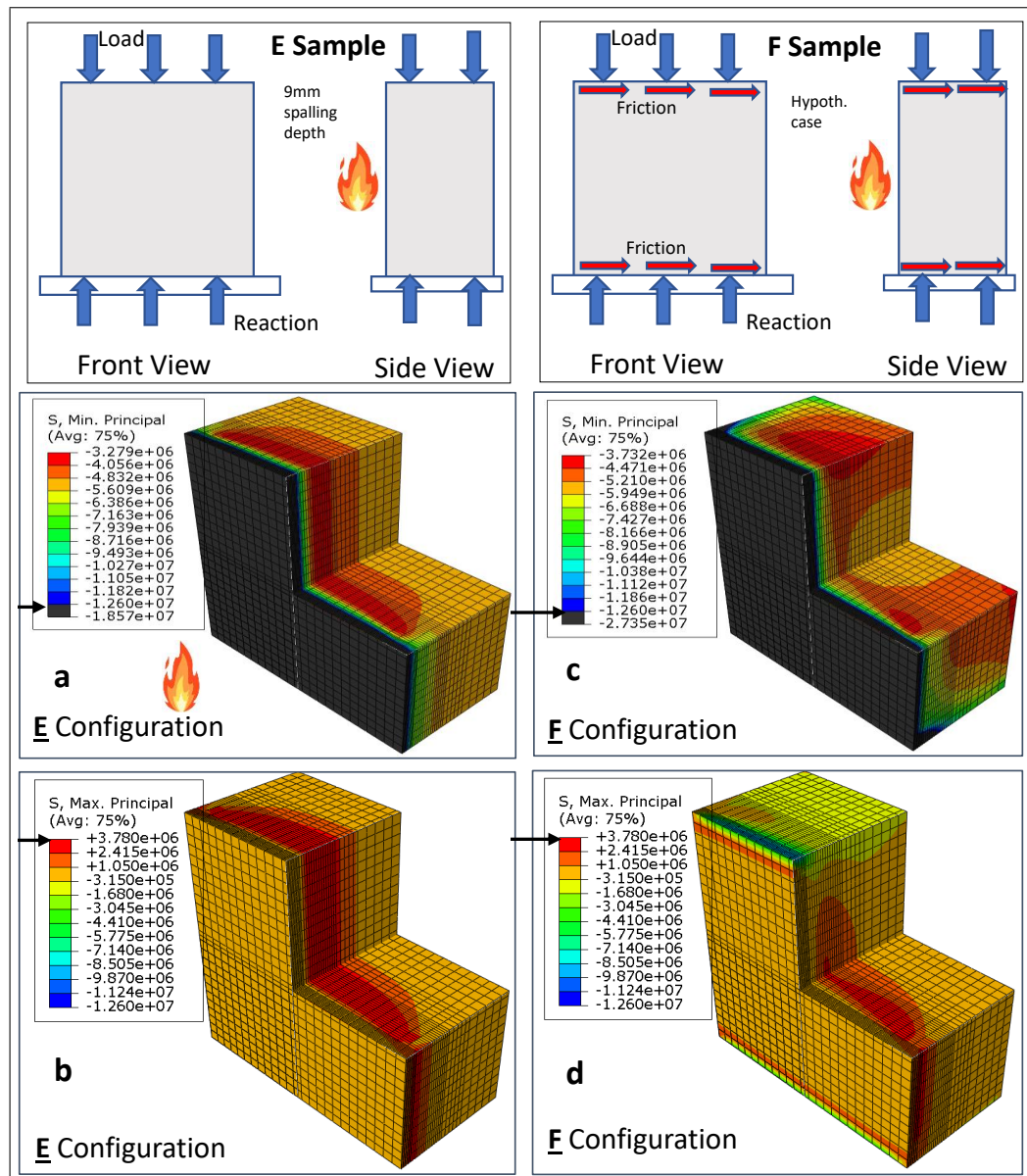


Figure 5.14: **a,b** Minimum and maximum principal stresses of E sample at the nearest time step to the first spalling time, **c,d** Minimum and maximum principal stresses of F sample at the nearest time step to the first spalling time

are close to the yielding limit $0.09f'_c$ ($0.09 \times 42 \text{ MPa} = 3.78 \text{ MPa}$) and non uniformly distributed behind the exposed surface (Figure 5.15 - b and Figure 5.14 b,d).

However, unlike previous cases, where the most severe stresses occurred along the centreline of the samples, the transition from compression to tension in that location does not match well with the reported spalling depth for this sample configuration. In this case it can be seen in Figure 5.14 that a more severe stress state exists out towards the lateral edges of the sample, probably due to the freedom the sample has to expand in that direction. This is even more clear when plotted as a stress profile through the thickness of the sample at mid-height, 60 mm from the edge (Figure 5.16) where it can be seen that tensile stresses develop close to the fire exposed face in the same location that compressive stresses are present thus developing an extremely steep stress gradient in the region that spalling was identified.

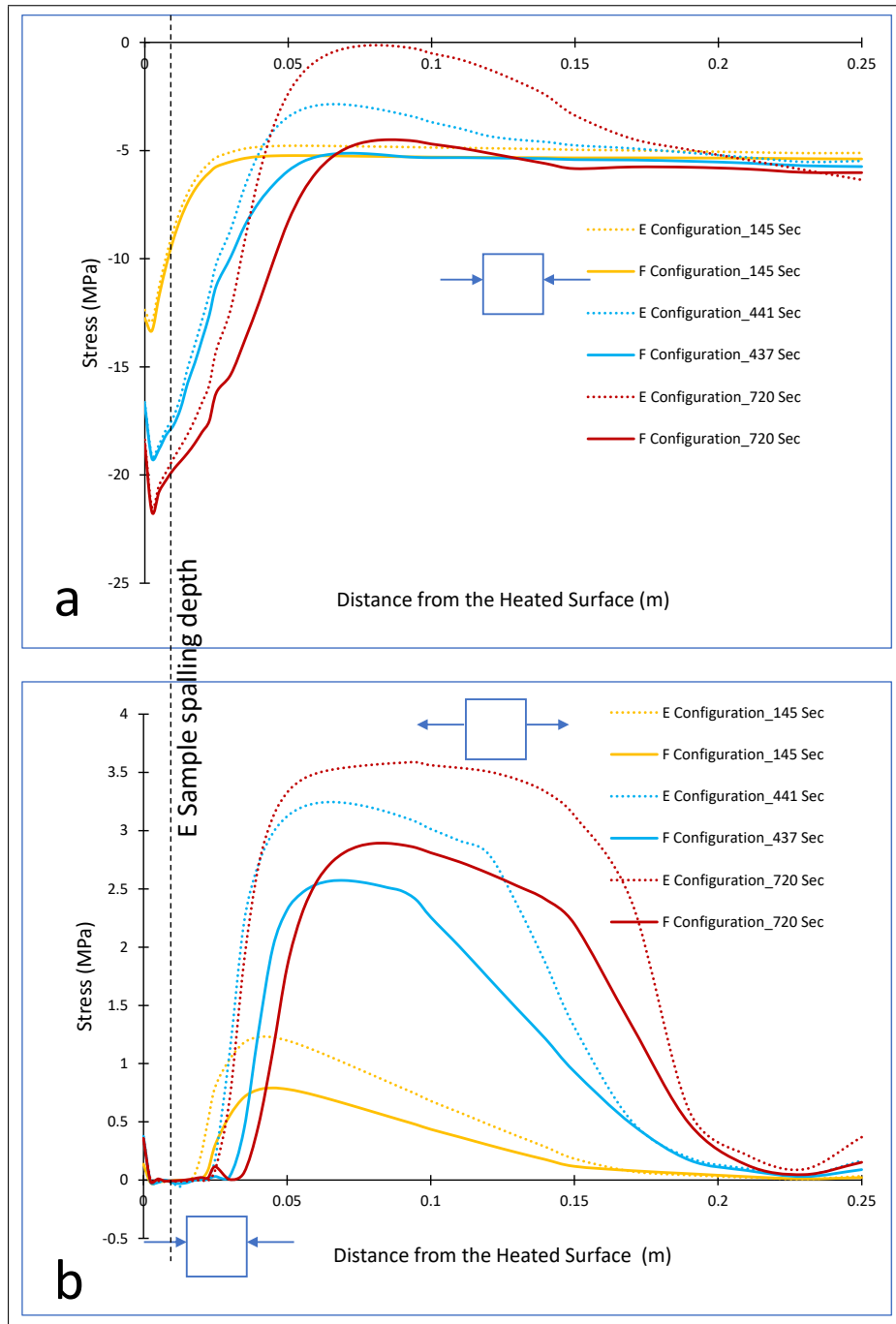


Figure 5.15: (a) Minimum and (b) Maximum principal stresses through thickness of the axially loaded square samples from Figure 5.1-E,F at different heating times

In addition to the steep gradients, it is notable that the stresses in both configuration are much higher than those observed in the restrained rectangular (Configuration (C)) and ring (Configuration (D)) samples. This indicates that restraint via uniaxial loading is likely to put samples in a worse situation from a spalling point of view, than restraint via mechanical fixings. Indeed, it may also be noted that the spalling time for the loaded samples are much earlier than for the restrained rectangular and ring samples.

Due to the presence of the initially applied load, the principal stress states are not aligned with the vector stresses as observed in rectangular and ring samples. To further explain differences stemming from initially applied load over the restrained samples, in-plane and out of plane

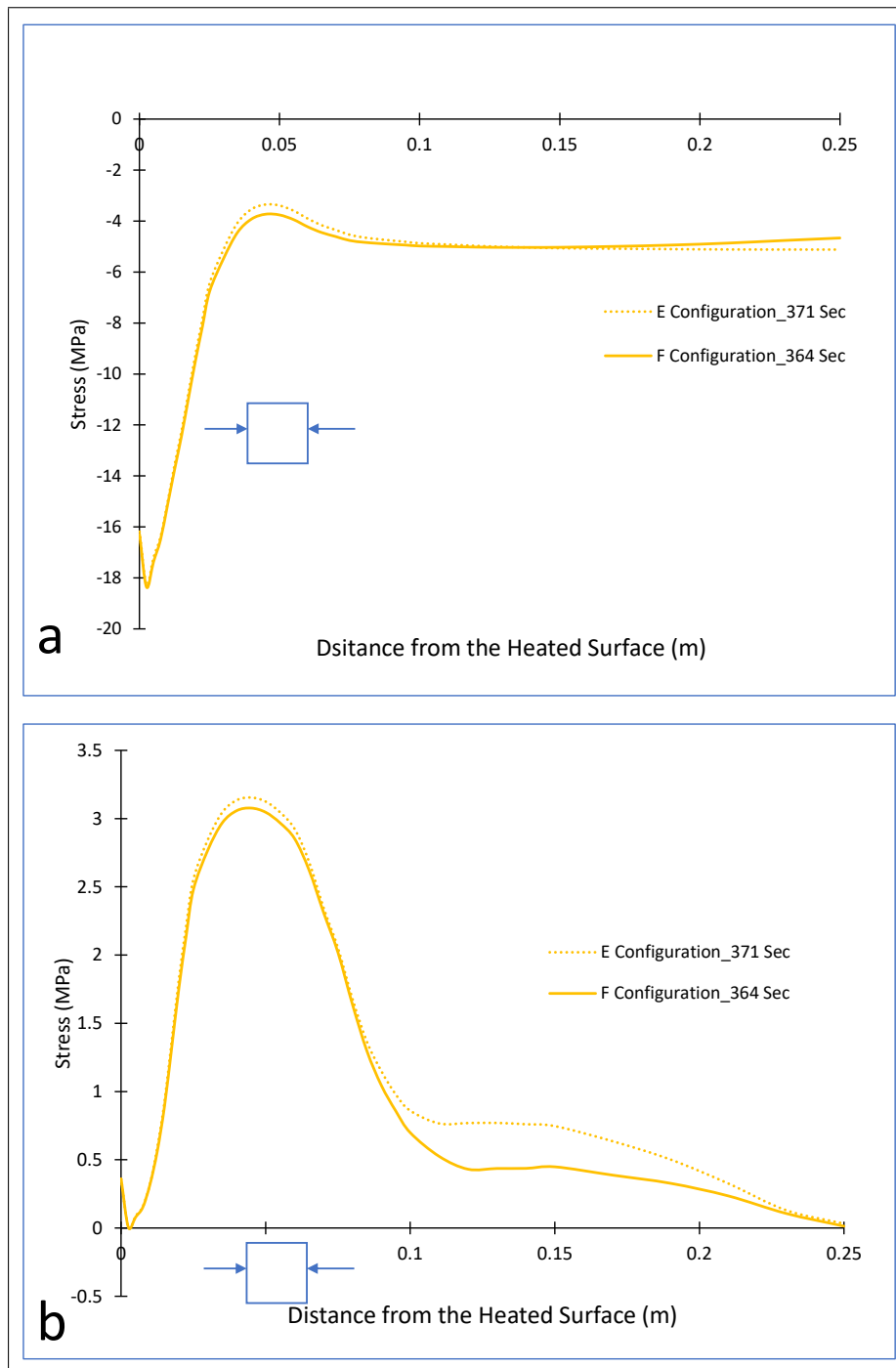


Figure 5.16: (a) Minimum and (b) Maximum principal stresses at mid-height, 60 mm from edge through the thickness of the axially loaded square samples (Configurations (E & F)) at time of spalling

stress states have been presented in Figure 5.17. In-plane stresses at the exposed surface tend to decrease toward the edges of the samples Figure 5.17-a,c, more noticeably in the sample without friction effects. However no noticeable difference can be observed for out of plane stresses Figure 5.17-b,d. While this alters severity of the stress transitioning from compression to tension, the exposed surface has yielded in compression and spall accordingly.

Considering the frictional restraint of the plattens in more detail, it can be seen that the effect of friction is to limit the development of tensile stresses. This can be seen in both Figure 5.15

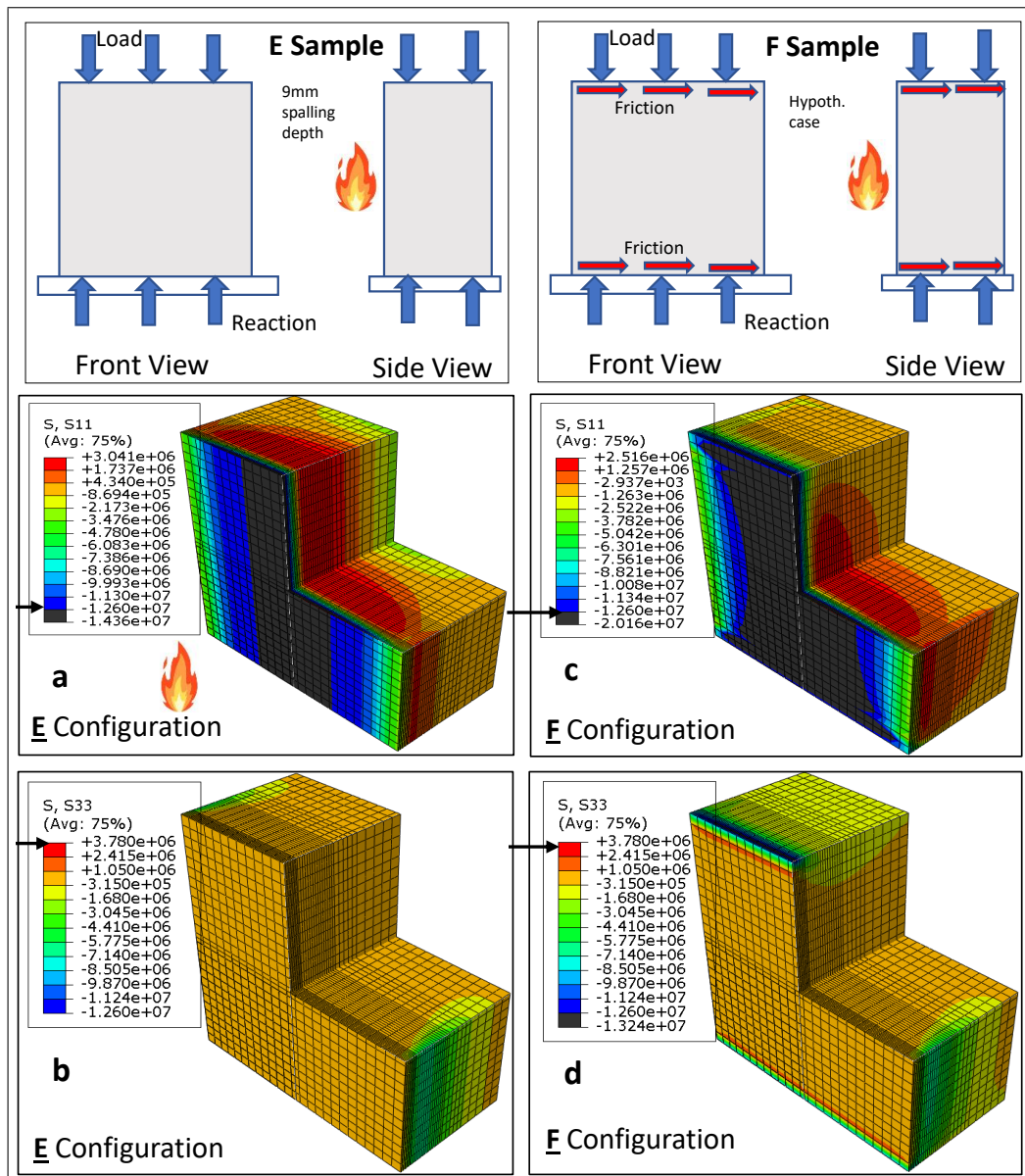


Figure 5.17: **a,b** In-plane and out of plane stress profiles of E sample at the nearest time step to the first spalling time, **c,d** In-plane and out of plane stress profiles of F sample at the nearest time step to the first spalling time

- b), where the tensile peaks are reduced when friction is considered, and in Figure 5.15 - a), where the compressive stresses tend to shift across the offset gap to be less compressive when no friction is considered. This finding is consistent with the observations in relation to Configuration (D) and again, shows the effect that test set up can have on the behaviour of the samples with friction limiting tension but maintaining the compressive offset in the principal stress space and creating a more severe stress gradient and potentially worse conditions for spalling.

5.3.4 Biaxially loaded samples

To extend the investigation to biaxially loaded samples, two cases from [37] and shown in Figure 5.1-G are investigated. These thin, square slab samples are identical except that one has radial slits around its circumference designed to limit the restraint effects of the outer zone,

which is unheated and rests on the walls of the furnace (c.f. Configuration (D)), by cutting its mechanical continuity for transmitting load. The test set ups and temperature profiles after 7200 seconds of heating are shown in Figure 5.18. The model’s ability to capture the experimentally reported temperature profile at different depths in the sample is demonstrated in Figure 5.19 and the maximum temperature at the exposed surface was found to reach 910°C.

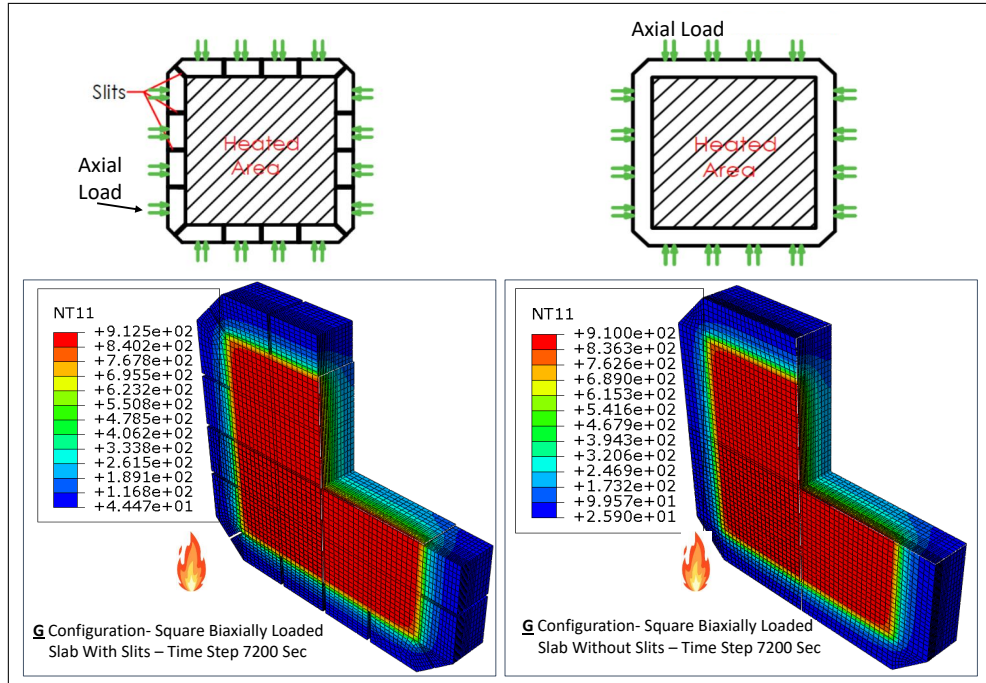


Figure 5.18: 3D section temperature Profile of the biaxially loaded samples with and without slits- G configuration

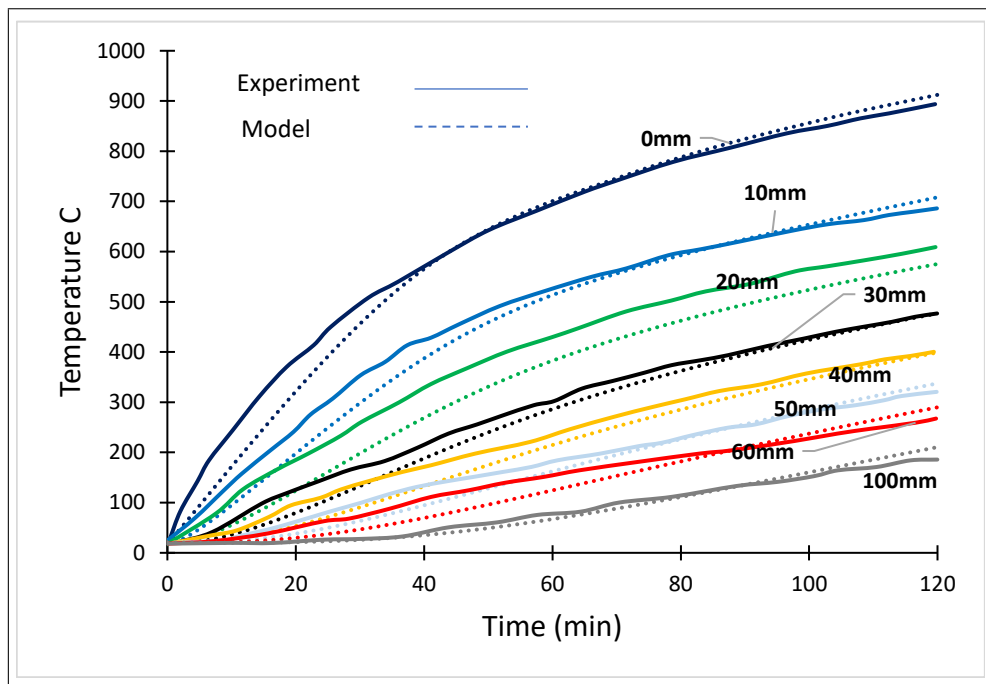


Figure 5.19: Temperature profiles at different depths of the bi-axially loaded sample

Profiles of minimum principal stress through the thickness of the samples at their centrelines,

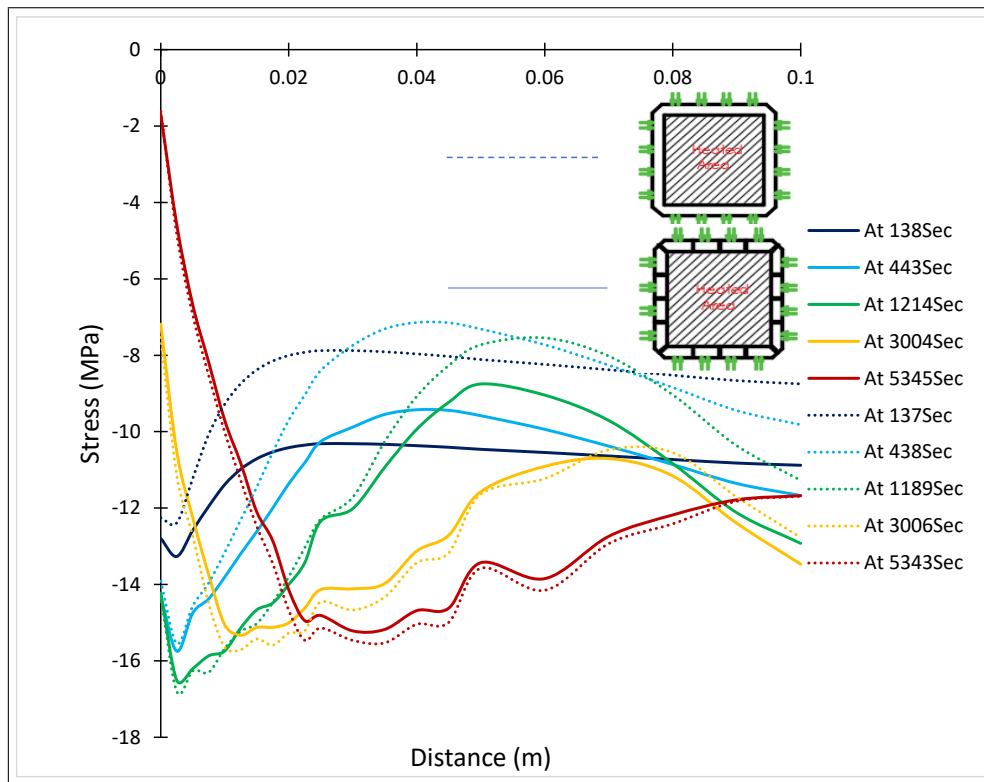


Figure 5.20: Minimum principal stresses through thickness of (G) configurations at different times

at different times are presented in Figure 5.20.

As with the uniaxially loaded sample discussed above, it can be seen that the initial effect of the load is to produce a strong compressive stress regime through the thickness of the sample. This is around 8 MPa for the intact sample and just over 10 MPa for the sample with slits. The lower stress in the intact sample may be a result of the effects of that circumferential ring acting to dissipate some of the stress, similar to the mechanism identified for Configuration (D) when frictional restraint was present. When the ring is cut by the slits, more of the load is transferred directly to the centre of the sample.

In both samples, this compressive stress dominates the behaviour during the earlier parts of the heating period (up to at least 1200 seconds) where, through much of the thickness, the stress in the intact sample remains lower than that in the samples with slits. However, right from the beginning of heating a spike in compressive stress is seen to develop near the hot face, as has been the case in all of the tests described so far. When the magnitude of this peak exceeds the initial stress then it dominates and the stresses in both samples are very similar and only separate in the cooler parts of the concrete deeper into the samples.

As time progresses, the concrete near the exposed face degrades due to the very high temperatures and loses much of its stress carrying ability. This is seen in the plots at 3000 seconds and 5300 seconds, where stresses near the face drop significantly. But, by this point, the compressive stress peak due to heating dominates much of the thickness of the sample, overcoming the biaxial stress state and both samples have very similar stress profiles throughout.

At this point, it may also be noted that the damage to the concrete near the hot face affects

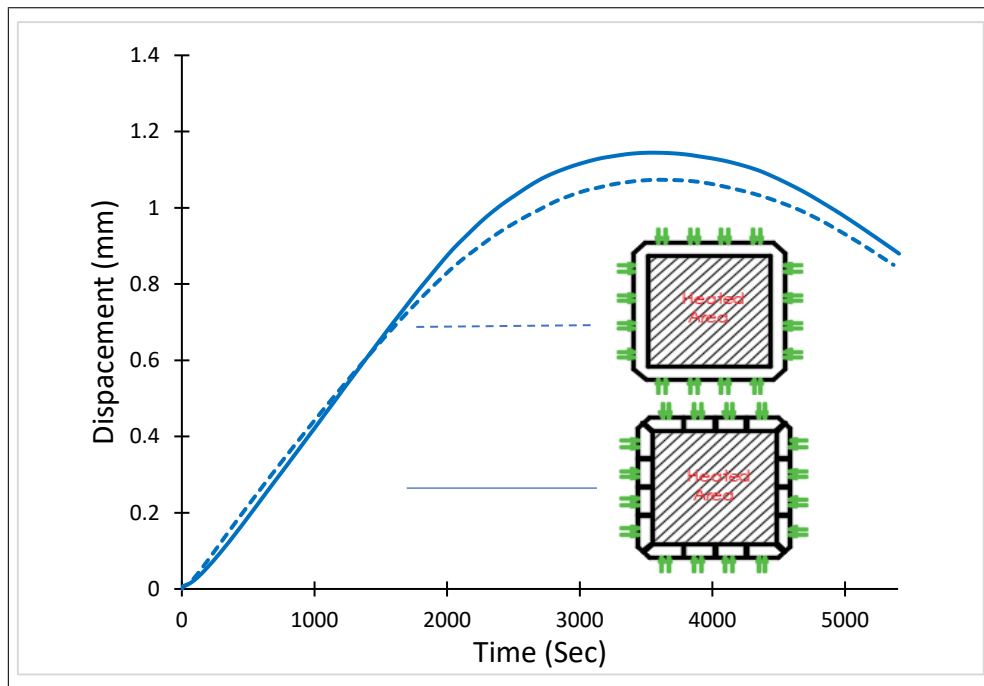


Figure 5.21: Simulated displacement results of a central point at the exposed surface through time for (G) configurations

the displacement of the samples. While the initial displacement at the centre of the slabs was towards the fire, as has been observed for other sample configurations, when stiffness is lost at the fire exposed face the neutral axis of these thin slabs shifts higher and the resulting eccentricity of the load causes the slab to deflect away from the fire. This behaviour was observed in the experimental work [37] and is well captured by the model (Figure 5.21).

These observations again suggest the sensitivity of the test results to the restraints and their mechanical characteristics, with clear influence from the applied loading and different sample configurations (with and without slits). Furthermore, the observed reversal of the displacement behaviour is attributed to the thickness of the samples. Where thicker samples were tested (Configurations (A-C)) no reversal of displacement was observed (Figure 5.6).

5.4 Conclusions

Mechanical restraint of concrete members has been investigated in this chapter as one of the most important factors affecting spalling behaviour in concrete under heating. This has been done through specific consideration of the details through which the restraints have been applied to experimental test samples and through consideration of different types of restraints.

The term restraint is used very broadly in the literature and covers a wide variety of different types and different configurations of restraint. It was found that these variations significantly affect test outputs and that therefore spalling results may be strongly associated with the test set ups under consideration and might not be generally applicable.

First, restraints applied mechanically by, for example, a steel ring or frame around the sample, were found to lessen the tensile stresses deeper in the sample, parallel and perpendicular to the

heated surface, in comparison to unrestrained samples. Corresponding to this, shallower spalling observed for the unrestrained sample in the test inferring severer tensile stress effects beyond the exposed surface comparing to the restraint samples. However, excessive restraint, for example by confining a sample over its full thickness was found to cause an increase in displacements of the concrete towards the fire when compared to unrestrained samples or samples restrained over only part of their thickness.

In contrast, samples restrained by the application of uniaxial load prior to heating, yield and spall much earlier than samples confined mechanically. Loaded samples are closer to plastic limit, even at ambient temperature, comparing to mechanically restrained samples. Therefore, upon heating, the applied load results in much higher stresses and significantly higher stress gradients than those developed gradually under passive restraint by a steel ring which delays spalling.

It may also be noted that the applied loads result in the development of significantly more transient thermal strain than develops under mechanical restraint [85] and this may affect the overall deformation behaviour of the samples including spalling.

Furthermore, the frictional forces between loading platens and samples must also be considered as high friction was found to create more severe stress gradients than low friction platens. This severe stress may surpass yielding limits in compression and tension and hence triggering sooner spalling comparing to the cases with less friction status. Similarly, the effect of friction between a sample and the supports on which it rests can also be significant with higher friction this time helping to reduce stresses and stress gradients.

Finally, in considering a biaxially loaded sample it was again seen that the applied loads could dominate the stress state in the sample causing high stresses and high stress gradients. However, the effects of maximum temperature and sample thickness were found to be as significant as the loads. Exposure to very high temperatures caused severe degradation of the material and a reduction in stress carrying capacity that then controlled the overall mechanical behaviour of the sample. This was exacerbated by the relatively thin sample that allowed bending deformations to occur very differently to the deformations seen in thicker samples.

These findings show that the type and configuration of restraint applied to a test sample can alter the test outputs significantly with restraint through applied load acting in opposition to passive restraint from a confining frame or ring and the dimensions of the sample and the heating regime determining the mechanical effect that the restraint will have.

Most importantly, generally these findings infer that testing of concrete as a material to find its behaviour under the sole effects of heating without presence of loading may be valid only for concrete applications in non-structural elements, such as in protection or decoration purposes. Results may not be valid for cases in which the concrete is used as a loaded structural members such as columns and shear walls. It is therefore recommended that tests be conducted to reflect the real conditions as closely as possible. While this seems demanding practically, with prior knowledge of the real applications of the concrete a test set up could be designed to reflect least real conditions especially in terms of load intensity and boundary conditions. This may

need further investigations to seek for any possible ways to simplify the test set ups without compromising test outputs.

Chapter 6

Effects of Sample Size on Concrete Behaviour and Spalling at High Temperatures

6.1 Introduction

In this chapter, sample size as another important parameter known arguably to have effects on concrete behaviour and spalling has been investigated. In most experimental works relating to heated concrete behaviour and spalling, sample size has been decided based on practical considerations or the limitations of the laboratory rather than with a focus on the implications the chosen size may have on the test outputs. Therefore, in this chapter, a parametric study using the ABAQUS model derived in **Chapter 3** has been performed. The main investigation parameter is sample size, more specifically sample thickness and span. Various samples tested with different test setups and boundary conditions from the literature have been chosen and simulated, then different size samples through altering either thickness or span of the original sample have been simulated under the same testing conditions. Simulated test results have been compared in terms of stresses and displacement states through the thickness and at the exposed surfaces of the samples. Through this, implications of using various sample sizes on test outputs in relation to concrete behaviour and spalling can be investigated in detail.

To investigate sample thickness, two different categories of test set up have been considered namely, unrestrained unloaded samples and restrained unloaded samples. For sample span investigation, loaded samples with different eccentricities have been considered.

The investigation results show that sample size can significantly alter the test outputs and the alteration varied appreciably per different test methodologies. It has been observed that increasing thickness of the unrestrained sample results in increasing spalling risk by imposing more intense stresses through the thickness. However, in the restrained samples, the dominant effects of the restraint eliminates effects of the increased thickness and reduces spalling risk comparing to their equivalents in unrestrained samples. This is through reducing the imposed stresses inside the sample, thereby decreasing stress transitioning steepness between compression and tension stresses.

These findings show that sample thickness can significantly alter the test outcomes and that the nature of the alteration depends on the boundary conditions. Therefore, while designing test set ups, the main challenges would be consideration of combined effects of the sample size and boundary conditions without compromising the test outputs.

Regarding sample span effects, the investigations conducted on loaded slabs with different eccentricities revealed that increasing the exposed span length has negligible effects on altering

the compressive and tensile stress state through the thickness of the sample under the adopted load intensity in this investigation. However, increasing the exposed span length affects the displacement of the exposed surface noticeably. In the longer span samples, higher deformations take place and this varies significantly depending on the load eccentricity. While these different deformations did not alter stress states of the samples, they may result in observing different spalling mode failures. That is observing less abrupt failure with increasing span regardless of the position of the load due to experiencing higher deformations. Even though there are differences in stress and displacement states between equivalent samples with different eccentricities, they are driven from the different test set ups rather than difference in sample span. While these observations may be more pronounced under higher applied loads, they emphasise the critical influences of sample size and test set up in controlling spalling test results.

All these findings conclude that one reason behind the contradictory results from the experimental work in the literature may be the adoption of varied sample sizes in different testing configurations. Therefore, it is strongly recommended to use a full sized sample representative to the real potential structural member in the experimental works. If it is not feasible, between span and thickness of sample, the former could be compromised since it seems to have much less effects in altering stress states and hence spalling and test outcomes. This is in addition to considering a test up capable to simulate the real sample's behaviour in terms of boundary conditions, loads and restraints otherwise the assessment based on the test results would be test specific and misleading if generalised.

6.2 Size configurations

Investigations in this chapter focus on effects of sample size on test outputs from two perspectives, thickness and span of the samples. The thickness has been considered to investigate how it can alter and control bending of the unloaded nonstructural sample under the sole effects of heating and hence change the overall behaviour and spalling potential. Meanwhile length has been considered in structural loaded samples to determine if it increases global bending of the sample and affects concrete behaviour and spalling potential. To perform thorough investigations covering structural and non-structural elements, three samples from the selections made in **Chapter 4** and shown in **Figure 4.1** have been selected and simulated with dimensions and set ups shown in **Figure 6.1**. The samples have been chosen to cover a wide range of methodologies in the literature, classified earlier into three categories, namely heated unloaded samples, restrained then heated samples, and loaded then heated samples. Unrestrained and restrained samples are considered here to represent concrete applications in unloaded nonstructural elements, such as for protection or decoration purposes, while the loaded samples to represent the cases where the concrete act as a structural element such as in columns or walls in buildings. The first sample (A sample) is an unrestrained unloaded sample set freely over a furnace. Its lower face, except the areas where the sample rests on the furnace walls, was subjected to the heating source as shown **Figure 6.1-A**. The dimensions of the sample were $L = 600$ mm, $W = 500$ mm & $T = 400$

mm. For the purpose of investigation in this chapter, specifically effects of sample thickness on test outputs, two more hypothetical cases with thicknesses 200 mm and 100 mm have also been simulated.

The second sample (B sample) is a partially restrained, unloaded sample tested in [4] with dimensions and test set up identical to the previous sample ($L = 600$ mm, $W = 500$ mm & $T=400$ mm). The sample was passively restrained externally by means of a 50 mm high circumferential steel ring as shown **Figure 6.1-B**. Again, to investigate effects of sample thickness but this time under restrained conditions, two more numerical samples have been derived, with thicknesses 200 mm and 100 mm respectively.

The third sample ((C) sample), which is employed to investigate effects of sample span on test outputs, is a loaded sample ($L = 1200$ mm, $H = 3500$ mm & $T = 300$ mm) aligned and loaded vertically while subjecting the front face to the heating source as shown in **Figure 6.1-C**. The sample is loaded eccentrically to 9.60% of its compressive strength (equivalent to 6.70MPa), with the load concentrated near the hot face. The rationale for selecting eccentric load is that almost all column in real structures are loaded eccentrically due to difference in adjacent span lengths and difference in live load at any floor of the building. The sample's entire height, except the uppermost 100 mm, was subjected to heating. This was to prevent the loading frame from being exposed directly to the heat source and left 3400 mm out of 3500 mm as the heated span. While simulating this sample, perfect friction on the platens at the top and bottom of the sample was considered. Furthermore, fixed displacement boundary conditions were used to prevent pushing back of the loading frame due to thermal expansion of the sample. Three more samples have been derived from this sample with heated spans of 1200 mm, 3900 mm and 5900 mm and with the other testing conditions identical to the original sample. Through this, the effects of sample span under loaded conditions will be investigated.

To consider the influence of span under different eccentricity of load, where the load is concentrated away from the hot face, a fourth hypothetical configuration has been developed (D sample). This is otherwise identical to the (C) sample as shown in **Figure 6.1-D**.

All samples have been exposed to the ISO834 fire curve through the hatched faces shown in **Figure 6.1**. Sample dimensions are shown in the same figure. The compressive strength of the restrained and unrestrained samples is 42 MPa and for the eccentrically loaded samples is 70 MPa. Same temperature dependant material properties have been used for the two concrete type, however different temperature boundary conditions have been considered. All these various samples and scenarios are compared in terms of stress and displacement states to understand how the results of a particular test configuration have been affected by changing the sample size.

6.3 Analysis results and discussions

As before, for the purpose of deciding the duration of the simulations, reported spalling times in the tests have been considered and followed accordingly in the ABAQUS model developed in Chapter 3 ([85]) for each simulation under consideration. The investigation consists of

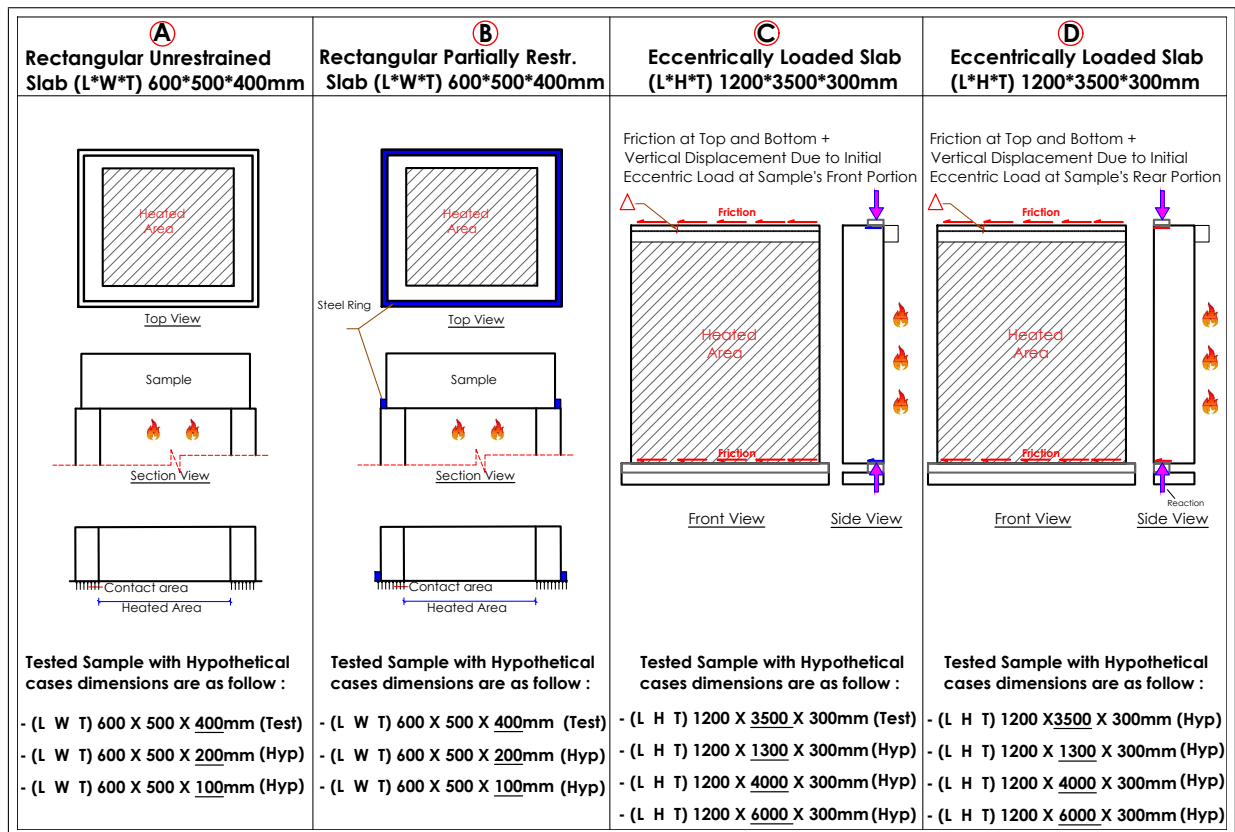


Figure 6.1: Different sample sizes with various boundary conditions

reproducing given experimental results, then performing parametric simulations through altering the sample size under the same testing conditions and comparing stress and/or displacement states.

6.3.1 (A) Samples- unloaded unrestrained

As discussed before, three samples with boundary conditions shown in **Figure 6.1-A** with different thicknesses (100 mm, 200 mm & 400 mm) have been considered under this category. These nonstructural samples are under the sole effect of heating, without the involvement of any loads or mechanical restraints.

The experimentally tested sample is the thickest sample, having dimensions $L = 600$ mm, $W = 500$ mm & $T = 400$ mm, which according to the reported test results spalled three times within a very short period after 660, 720 and 780 seconds of being exposed to heating. **Figure 6.2-b,c,d** shows the temperature profile (with a predicted maximum temperature of 331°C) along with cut-away views of the minimum and maximum principal stresses for the tested sample at first spalling time. **Figure 6.3** shows minimum and maximum principal stress profiles through the thickness of the samples at their centre line, for all three sample thicknesses at different times. Examining **Figure 6.2-c & d**, a yielded compressive zone (shown as black) and a yielded tensile zone (shown in grey) can be observed. As seen in **Figure 6.3-e & f**, the compressive zone is around 40 mm thick and evolves at the exposed surface before shifting immediately to the tensile zone deeper in the sample. As discussed in previous chapter, it may be observed that these high

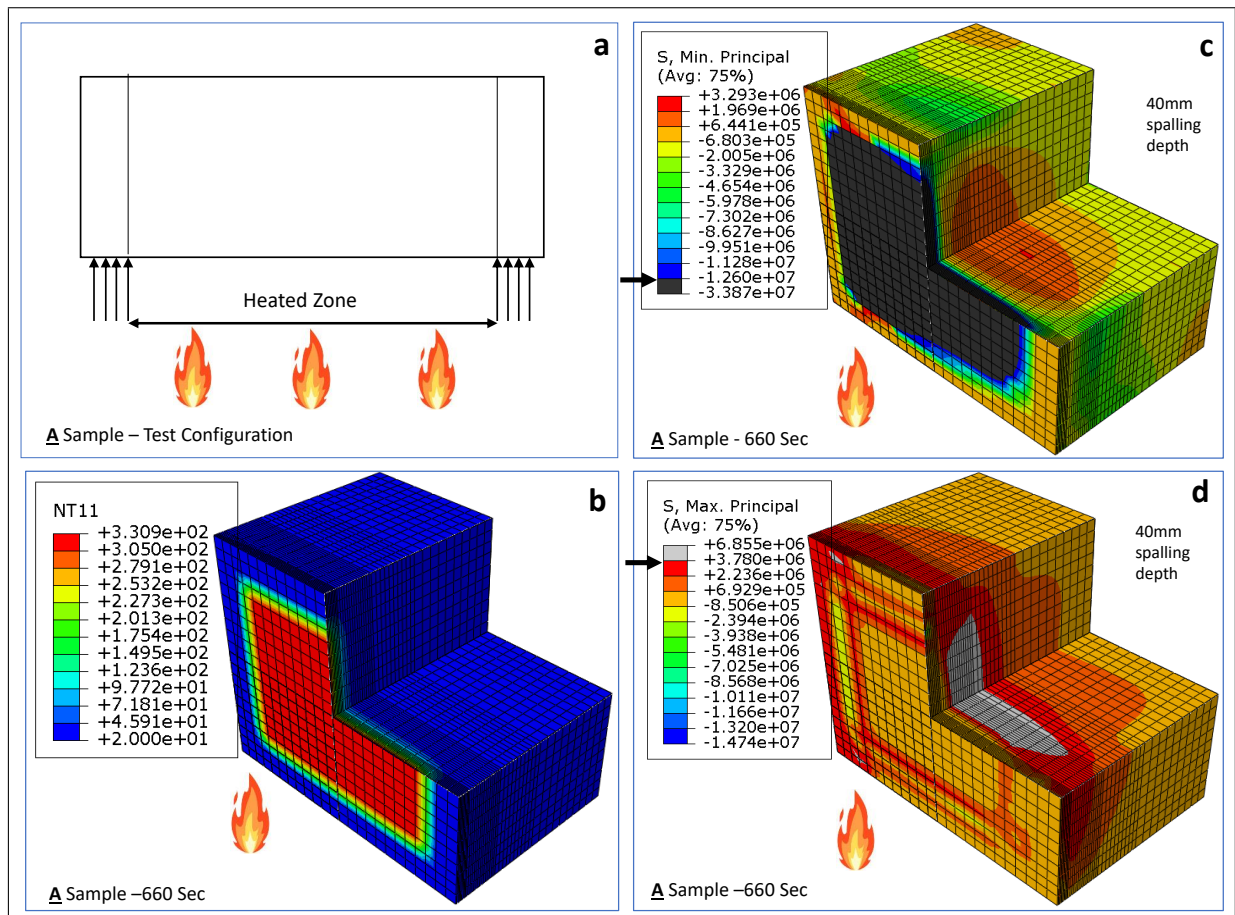


Figure 6.2: **a** Original test set up of sample (A) with 400 mm thickness, **b** Temperature profile of sample (A) at first spalling incidence, and **c**, **d** Minimum and maximum principal stress at first spalling incidence respectively

stress intensities and the very steep gradients in this transition correlate very closely both in time and location to the observed spalling mentioned earlier and may be inferred as a cause of the initiation especially they are higher than compressive yielding limit $0.3f'_c$ ($0.3 \times 42 \text{ MPa} = 12.6 \text{ MPa}$) and / or tensile yielding limit $0.09f'_c$ ($0.09 \times 42 \text{ MPa} = 3.78 \text{ MPa}$).

Regarding **Figure 6.3-a,c,e**, similar transitions from compression to tension can be observed for all of the samples throughout the heating time. The compressive stresses in all samples are very similar at the early heating phases. However, at later heating times, larger stresses can be observed in the thicker samples compared to thinner samples. Another compression zone nearby the cold face, furthest from the heating source, can also be observed in the three samples. However, in these second compression zones, the magnitude of stresses are higher in the thinner samples comparing to the thicker samples. This can be attributed to the difference in bending behaviour between thin and thick samples. The thinner samples bend easily towards the heating source, which relaxes the stresses at the exposed face. However, this is not the case in the thicker samples, which have higher stiffness that resists bending and leads to development of higher stresses in the hot region.

In terms of the tensile zones **Figure 6.3-b,d,f**, stresses in the three samples also develop and increase in time. In contrast to the compressive stresses, the stress intensities here are

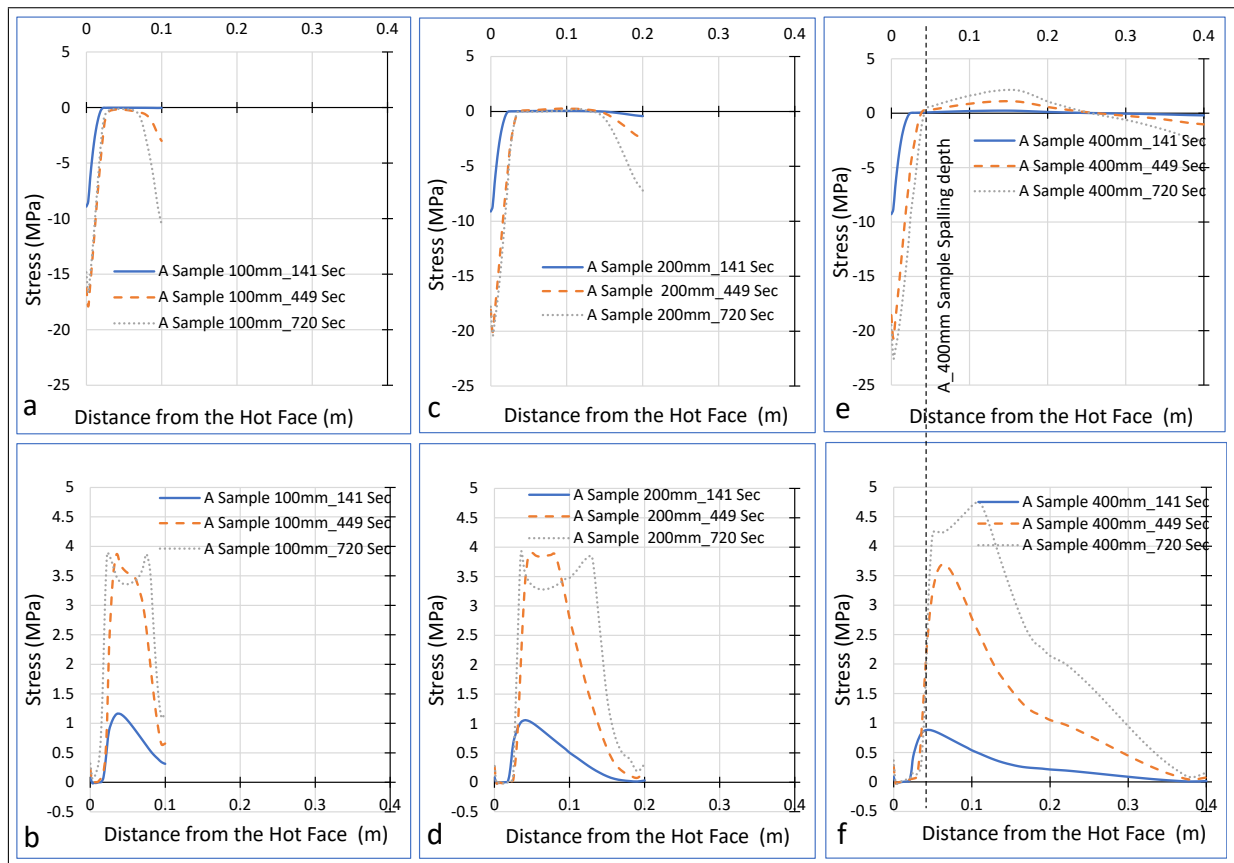


Figure 6.3: **a,c,e** Minimum and **b,d,f** Maximum principal stress profiles through the thickness of the samples at their centre line, for all three sample thicknesses at different times

almost equal for different thickness samples. In the thickest sample, the stress state turns to a completely tensile zone in a 150 mm portion starting 50 mm in from the heated face. This may be derived from the resistance of the thickest sample to bending. Considering the sharp stress transitions from compression to tension observed in each sample, the stress gradients become steeper with increasing thickness of the sample potentially increasing the risk of spalling in the thicker samples upon stress intensities surpassing either of the yielding limits mentioned before.

In terms of the exposed surface behaviours, 3D contour plots of the displacement component perpendicular to the heating source after 720 seconds of heating for the three unrestrained samples with 100 mm, 200 mm and 400 mm thickness respectively are shown in **Figure 6.4-a,b,c**. With increasing thickness of the (A) sample, the intensity of the displacement decreases noticeably. The magnitude of displacement is around 4 times less in the 400 mm thick sample **Figure 6.4-c** than in the 100 mm thick sample **Figure 6.4-a**. As discussed previously, this can be attributed to the combined effects of the sample bending and the effects of stiffness gain with increasing thickness of the sample. The thinner sample bends the most towards the heat source and hence displaces the most, while the thickest sample with the highest stiffness bends the least and therefore displaces the least.

Consistent with the displacement results, increasing thickness also affects the developed in-plane stresses at the exposed surfaces as shown in **Figure 6.5-a,b,c**. With increasing sample thickness, both the size of the yielded area and the in-plane stress intensity increase accord-

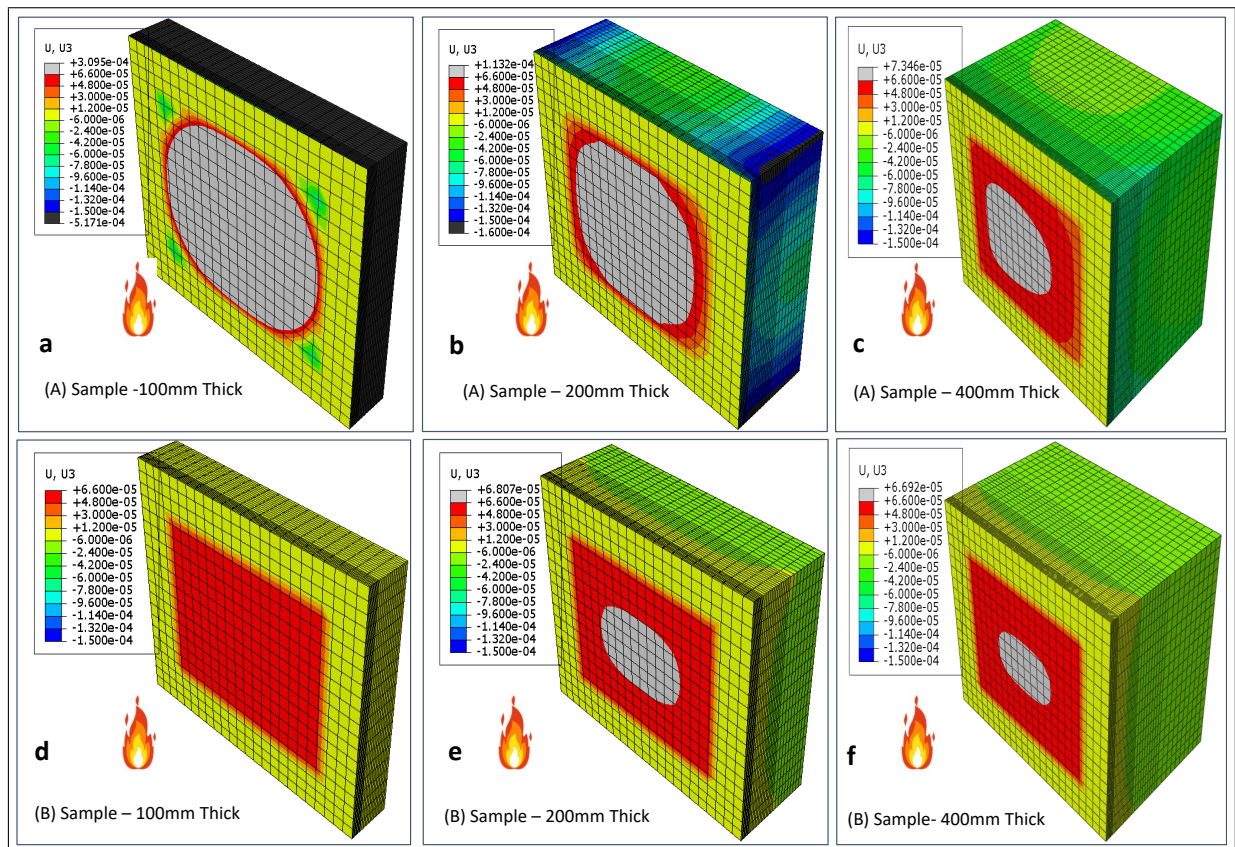


Figure 6.4: Displacement in meters toward the heating source: **a,b,c** for (A) Samples, and **d,e,f** for (B) Samples having 100mm, 200mm, 400mm thickness respectively at time step 720 seconds

ingly. Having the highest in-plane stress in the thickest sample indicates the highest in-plane deformation component and hence the least outward (toward the heating source) deformation component as observed in (Figure 6.4-c). The highest lateral expansion of the exposed surface also corresponds to the highest tensile stress developed in the cooler portions of concrete beyond the exposed surface as is clear in Figure 6.5-c (shown in grey). This is further consistent with the observations from Figure 6.3-e & f where it was seen that both maximum and minimum principal stresses were tensile.

Summing up all these aforementioned observations, it can be concluded that increasing thickness of unrestrained samples appears to create more severe stress states and hence may increase their spalling risk. It imposes more compressive and tensile stresses through the depth of the samples. Therefore it increases the sharpness of the switch from compression to tension, which seems to be correlated to the triggering of spalling upon surpassing yielding limits in compression and/ or tension discussed before.

With increasing sample thickness in-plane stress and hence lateral displacement increases while the displacement toward the heating decreases. This might lead to the anticipation of deeper and more abrupt spalling type failure, especially following the development of high tensile stresses in the inner portions of the samples. These findings agree with some findings from literature stating that explosive spalling increases with sample thickness [44]. However they seem counter to findings from [41] stating that thicker beam samples provide better stiffness and ductility when heated, hereby risk of explosive spalling decreased. This may imply that,

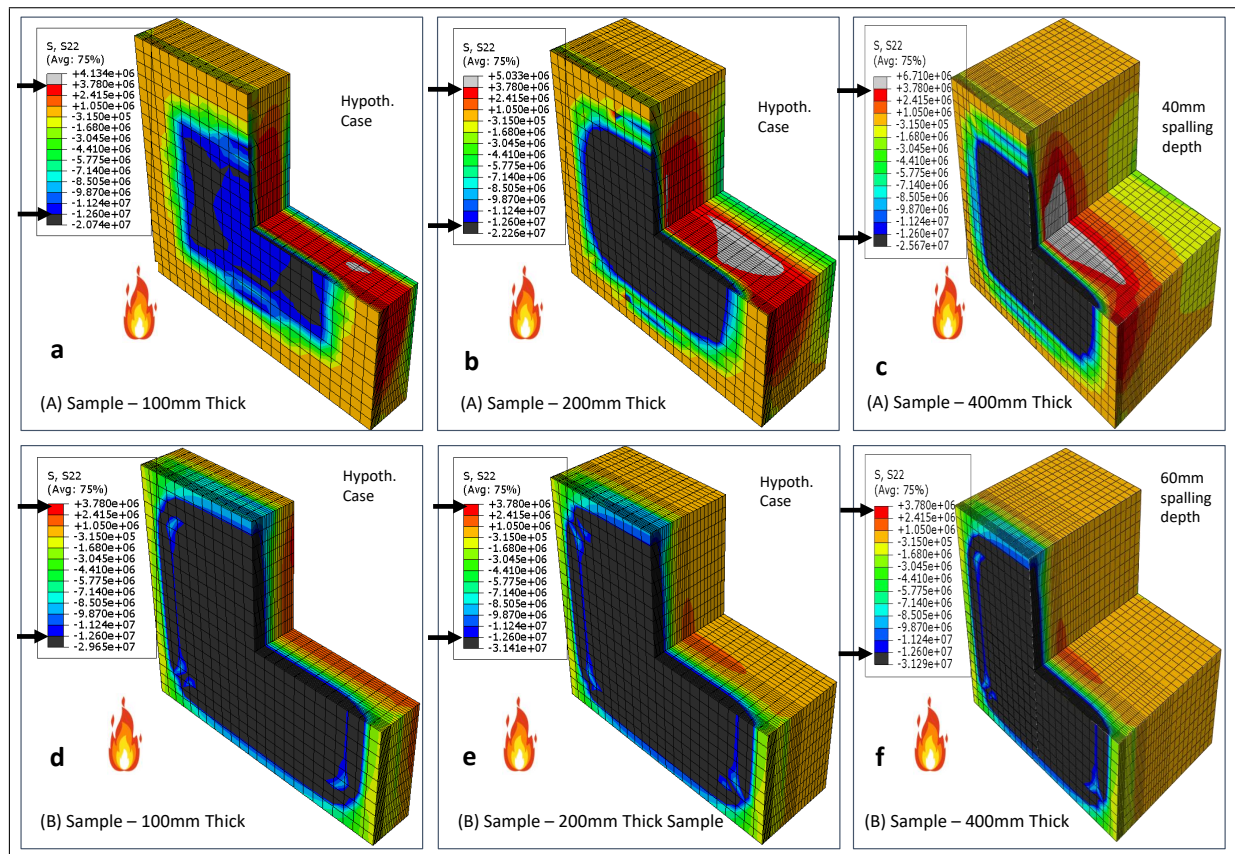


Figure 6.5: Developed in-plane stress at the heated surface: **a,b,c** for the (A) samples, and **d,e,f** for the (B) samples having 100mm, 200mm, 400mm thickness respectively at time step 720 seconds

even though sample thickness can alter sample behaviour significantly, the influence may be different under different test configurations relating to restraints and loads. Responding to this, in the next two sections, two different test set ups with restraints and loads will be considered and investigated for different size samples.

6.3.2 (B) Samples - unloaded partially restrained

A partially restrained sample shown in **Figure 6.1-B** identical to the unrestrained (A) sample in terms of dimensions, material properties and test configuration but different in boundary condition has been considered in this section. The effect of sample thickness under restrained conditions has been investigated. The experimentally tested sample was 400 mm thick and, as before, two more cases with thicknesses of 100 mm and 200 mm have been simulated to compare stresses and displacements. According to the reported experimental results, first spalling occurred at 10 minutes and was followed by two more spalling failures at 14 and 17 minutes of exposure to the heating source. 3D section views of minimum and maximum principal stresses at the nearest time step to the first spalling captured by the ABAQUS model (620 s), along with the temperature profile and the test set up are shown in **Figure 6.6**.

At the time of spalling the temperature reached 312°C at the central portion of the exposed surface (**Figure 6.6-b**), which in comparison to the (A) sample, means that the restrained sample

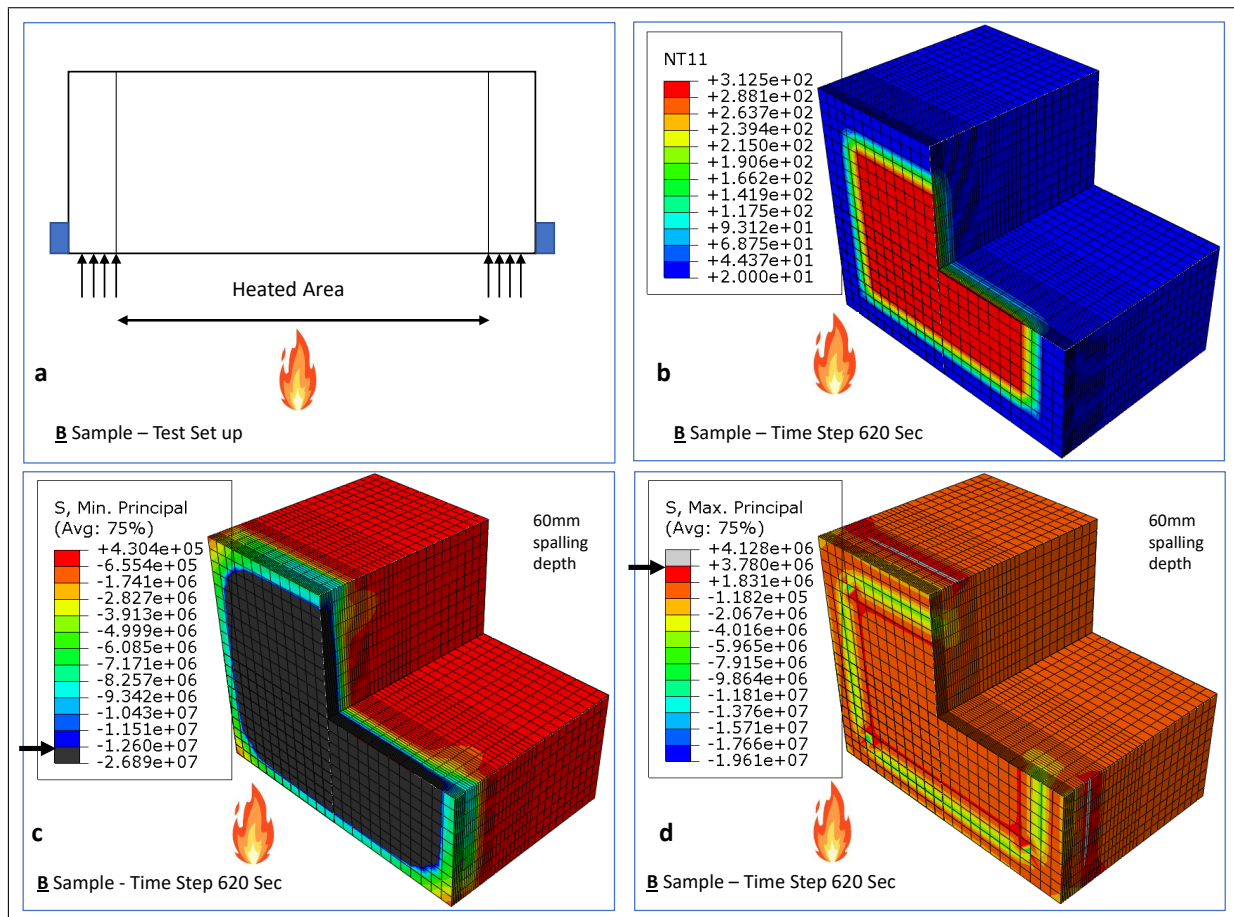


Figure 6.6: **a** Original test set up of sample (B) with 400 mm thickness, **b** Temperature profile of sample (B) at 620 seconds, **c** Minimum principal stress profile after 620 seconds, and **d** Maximum principal stress profile after 620 seconds

spalled at a lower temperature despite having the same material properties. As discussed for the tested sample in previous chapter, at the time of spalling, a compressive zone can be seen at the centre of the exposed surface (**Figure 6.6-c**) with stress values surpassing the yield limit of concrete in compression (black colour) which is $0.3f'_c$ ($0.3 \times 42 \text{ MPa} = 12.6 \text{ MPa}$). As with the unrestrained sample, this zone extended around 40 mm through the thickness of the sample and as before, this transitioned to a tensile zone deeper in the sample. But, unlike in the unrestrained (A) samples, the values were far smaller than the yielding limit in tension (**Figure 6.6-d**) which is $0.09f'_c$ ($0.09 \times 42 \text{ MPa} = 3.78 \text{ MPa}$). Compared to the (A) sample, the compressive yielded area at the exposed surface of the (B) sample covers a wider area and even reaches the unheated area at the outside of the sample. This can be attributed to the effects of the circumferential steel restraint (**Figure 6.6-a**) restricting lateral expansion and inducing more stress.

Through thickness, minimum and maximum principal stresses of the (B) sample with three thicknesses (100 mm, 200 mm & 400 mm) have been plotted for different heating times (**Figure 6.7**). For each sample individually, the peak values increase in time appreciably up to 446 seconds where they exceed the compression yielding limit (12.6MPa). Then less increase is seen up to 720 seconds and afterwards, the peaks do not increase noticeably even up to 1200 seconds time step, which is far longer than the spalling time. As discussed before, the steep

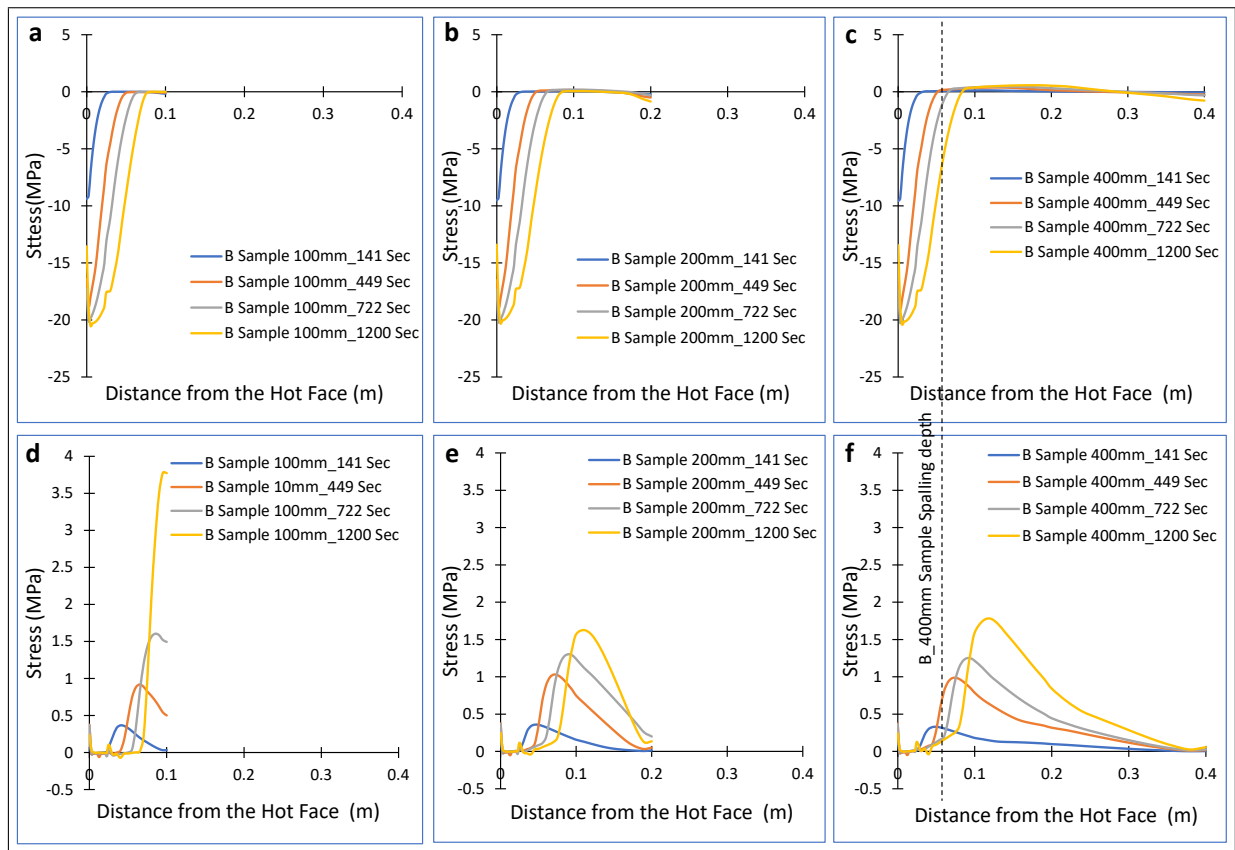


Figure 6.7: **a,c,e** Minimum and **b,d,f** Maximum principal stress profiles through the thickness of the samples at their centre line, for all three sample thicknesses at different times

transition from compressive to tensile stresses corresponds well with the timing and depth of the observed spalling and seems related to the triggering of spalling upon reaching concrete yielding values.

Generally, regarding compressive zones from (**Figure 6.7-a,b,c**), unlike the (A) samples, the compressive stress peaks behind the heated surface remain unchanged with increasing sample thickness at all heating time steps. This can be attributed to the role of the steel ring restraint provided over the first 50 mm of the sample thickness. The restraint confines almost all the deformations within the first 50 mm from the heated surface and it prevents global bending of the samples towards the heating source. Therefore, no noticeable balancing compressive stresses (the previously observed second compressive zone) develop at the rear cold portions of the restrained samples (**Figure 6.7-a,b,c**) compared to what has been observed in unrestrained samples (**Figure 6.3-a,b,c**) where bending causes squeezing of the rear cold portion of the sample. The dominant effect of the restraint is also valid in tensile stresses evolution of different sized samples (**Figure 6.7-d,e,f**). Again, increasing thickness does not noticeably change the tensile stress peaks at early time steps up to around spalling time. It seems that the restraint effects controls compression and tension behaviours and eliminates the size effects seen in the unrestrained sample. Even though tensile stress result of 100 mm sample at the latest time step (1200 seconds) seems inconsistent with other two thicker samples, it is well after the first spalling time, is still below yielding limit, and is not high enough to cause significant change. This discrepancy again is due to the effect of the restraint. In the restrained portion of the samples,

displacements are restricted to take place mostly perpendicular to the fire exposed face. Since the 100mm thick sample has the least stiffness along its thickness, it allows the highest peak tensile stress (**Figure 6.7-d**) to develop comparing to the other two stiffer samples (200mm and 400mm thick samples) under same displacement intensity. The peak stress here interact with the rear boundary of the sample where no concrete left to resist meanwhile in the thicker samples the stress peaks remain inside the samples' thickness and relaxed accordingly through the rest of the thickness. The tensile stress intensities here are noticeably lower than (A) samples. This means that the stress gradients are less steep between compressive and tensile zones thereby potentially reducing spalling risk along the thickness. All these different behaviours between the restrained and unrestrained samples suggest that sample thickness can significantly alter behaviour of the sample while subjecting to heating depending on boundary conditions. Incorporating other factors relating to test up such as restraints can override the thickness effects and control the test out puts

Comparing to the (A) samples, the behaviours of the (B) samples are quite different in terms of compressive and tensile stress intensities. First, the compressive stress peaks of the (B) sample with 100 mm thick shown in **Figure 6.7-a** are higher than the peaks of (A) sample with 100mm thick from **Figure 6.3-a** at same time steps, however this is opposite in tensile peaks up to the around first spalling if restrained sample **Figure 6.7-d** compared to unrestrained samples **Figure 6.3-d**. Secondly, the stress peaks of the 200 mm thick sample in compression are very similar for both (A) and (B) samples as is clear in **Figure 6.3-b** and **Figure 6.7-b** respectively despite existence of balancing compressive stress at the rear portion of the (A) sample. However, the tensile stress is lower noticeably in the restrained sample (**Figure 6.7-e**) comparing to the unrestrained samples **Figure 6.3-e**. This suggests that the actions of the steel ring in the (B) sample are equivalent to those balancing compressive stresses in the 200 mm thick samples, and at the same time are beneficial in tensile stress decrement. Finally, the compressive stress peaks of the 400 mm thick (B) sample (**Figure 6.7-c**) are lower than those in the unrestrained 400 mm thick (A) sample shown in **Figure 6.3-c**. This is also true in tensile stresses if the restrained sample (**Figure 6.7-f**) compared to the unrestrained samples **Figure 6.3-f**. This means that the efficiency of the restraint in improving fire resistance of the restrained samples increases in the thickest sample. Summing all together, it seems that the restraint effects eliminate effects increased thickness might have. Even though some improvement trend can be observed in the thickest sample through simultaneous effects of the restraint and the increased thickness, it is not significant because steep transitioning from compression to tension is still valid and can trigger spalling. In general, tensile stress decrement can be observed in the three restrained samples in comparison to the unrestrained samples, but this is mostly due to the restraint rather than thickness effects.

Regarding the exposed surface, displacement and in-plane stresses are taken into consideration here. For the former, from **Figure 6.4-d,e,f**, different behaviours from what have been observed for the (A) sample can be noticed here. It seems that in restrained samples the exposed surfaces are behaving very similarly. Almost the same, very low displacement intensities under

the effects of the heating can be observed, which are not appreciably affected by the thickness of the sample.

Through comparing the displacement of the exposed surface towards the heating source for (A) and (B) samples shown in **Figure 6.4**, it can be observed that the displacement intensity difference in thinner samples is quite obvious. With increasing sample thickness (potentially increasing the sample stiffness) it becomes almost negligible. For the 100 mm thick restrained (B) sample, the displacement intensity (**Figure 6.4-d**) is almost 5 times lower than the 100 mm unrestrained (A) sample (**Figure 6.4-a**). For the latter sample, alongside the steep stress transitioning from compression to tension as the main reason of spalling, the effects from sample's freedom to displace, its lower stiffness and therefore the highest bending tendency toward the heating are more conducive to trigger less abrupt spalling comparing to the restraint sample. For the 200 mm thick (B) sample, the displacement difference has fallen to half that of the unrestrained (A) sample under the effects of the higher stiffness the sample gains through the increased thickness. Through further increasing the thickness to 400 mm, the displacement difference between the unrestrained (A) and restrained (B) samples becomes negligible (it is less than 10%). Here the displacement of the exposed surface and sample's global bending toward the heating have been eliminated. This is due to the increased thickness (potentially stiffness) in the unrestrained samples, and through increased thickness and the steel restraint in the restrained samples. However, still steep stress transition from compression to tension is available in both samples at deeper portions which triggers spalling accordingly. The similarity in behaviour of the two thickest samples can be also evidenced by considering the first spalling time from the test results in which both restrained and unrestrained samples started to spall at very close time, the former spalled at 10 min and the latter at 11 minutes.

Comparing the developed in-plane stresses for the three restrained (B) samples shown in **Figure 6.5-d,e,f**, unlike the unrestrained (A) samples discussed previously and shown in **Figure 6.5-a,b,c**, the yielded areas and stress intensities here are very similar for the different thicknesses. As discussed before, this can be attributed to the effects of the restraint in eliminating the global bending of the samples regardless of their thickness. Therefore no appreciable balancing compressive stress develop at the rear end to relax the stress develops at front face as observed in the unrestrained samples. Also the restraint restricts the displacement to take place in the same manner in all samples, and it eliminates lateral displacement again regardless to the thickness.

To sum up, it can be concluded that restraint can override almost all influences that increasing the sample thickness might have. It effectively controls and stabilizes the behaviour of the sample by retaining the tensile and compressive stresses at certain values regardless of the sample thickness. Restraint effects may be slightly undermined, showing higher tensile stress in very thin samples due to lower stiffness, however this is still too small to cause significant change comparing to other samples.

6.3.3 (C) Samples - eccentrically loaded samples

In the last two sections, a nonstructural sample under the sole effects of the heating and another one under the combined effects of the heating and mechanical restraint have been investigated to consider the influence of different sample thickness. In this section, a structural member sample under the combined actions of heating and load applied prior to heating has been considered to explore the effects of increasing bending span on changing stress states and general behaviour of the sample. As discussed before eccentrically loaded sample was chosen considering that almost all columns and walls are eccentric due to reasons as difference in adjoining spans and live loads from floors. The tested sample, with dimensions $L = 1200$ mm, $H = 3500$ mm and $T = 300$ mm, was aligned vertically and loaded eccentrically to 6.70 MPa (equivalent to around 9.60% of its compressive strength). It was heated from the front face as shown in **Figure 6.1-C**. Fixed platens with perfect friction at the top and bottom of the sample were considered (i.e. the platens cannot move and resist the thermal expansion of the sample). This has been achieved in the analysis by imposing a vertical displacement boundary condition designed to achieve the initial applied load at ambient temperature. Three more cases extended from this configuration with heights of 1300 mm, 4000 mm and 6000mm were also considered to investigate the influence of span. Considering the relationship between eccentricity of the applied load and the span of the sample, all these cases have been re-simulated considering another hypothetical scenario where the eccentric load is applied on the rear, cold portion of the sample, as shown in **Figure 6.1-D**. The (C) sample, with the eccentric load near to the heated surface, is the experimentally tested case, which per the test results spalled 72mm depth at 420 seconds of exposure to the heating source. At the nearest time step (463 seconds) to the spalling time captured by the ABAQUS model, the temperature at the exposed surface reached 139°C as shown in the 3D section view of the sample in **Figure 6.8**. Thus, even though this sample has higher compressive strength (70 MPa) compared to the previous two samples (42 MPa), it spalled much sooner under the combined effects of applied loading and heating. To examine the compressive zone through the

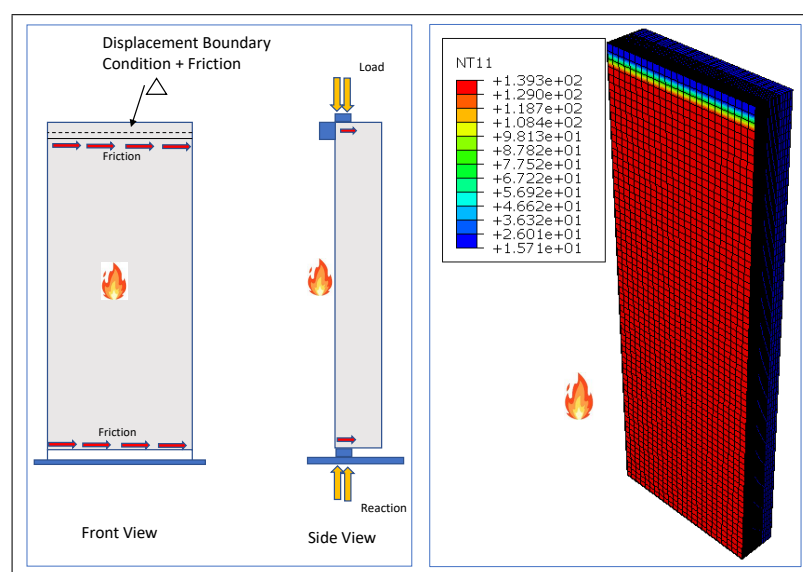


Figure 6.8: Test set up and temperature profile of (C) sample at nearest time step to spalling

thickness of the different size samples, minimum principal stresses are plotted in **Figure 6.9**. With increasing exposed span no appreciable difference can be observed in the peak values of the compressive stress zones near the hot face of the (C) or (D) samples. At the last time step (720 seconds) a slight flattening in the middle of the compressive zone of the three larger (C) samples can be observed **Figure 6.9-b,c,d**. This is not noticeable for the smallest, 1300

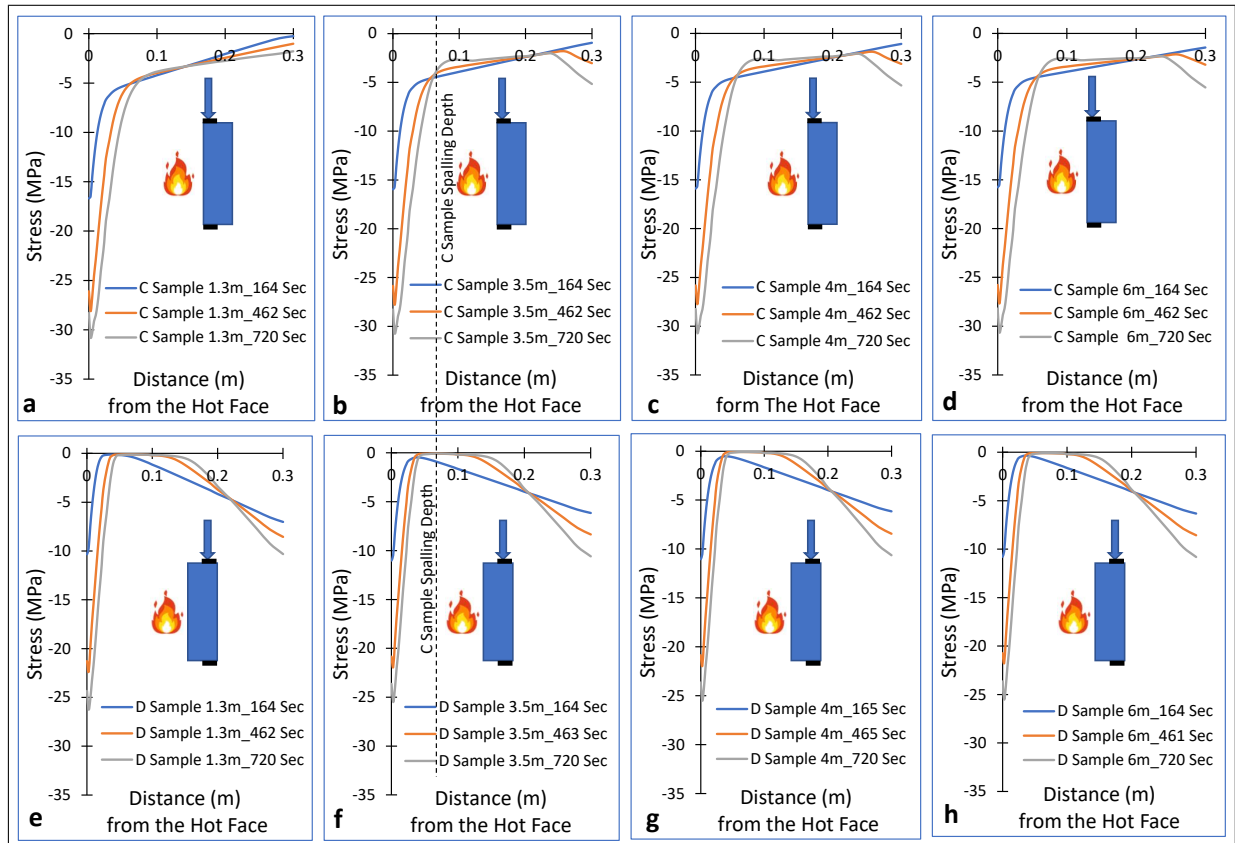


Figure 6.9: **a,b,c,d** Minimum principal stress of the (C) samples, and **e,f,g,h** Minimum principal stress of the (D) samples at different heating times through their thickness, having 1.30m, 3.50m, 4.00m, 6.00m heated span respectively

mm sample (**Figure 6.9-a**). However, the difference is within a very small stress range and is unlikely to cause significant changes in the sample's overall behaviour after spalling. All peak values starting from spalling time and onward are larger than the yielding limit of the concrete in compression ($0.3 \times 70MPa = 21MPa$) and they transition toward tensile zone steeply, deeper in the samples.

Examining tensile zone of the different span samples (**Figure 6.10**), the tensile stress peak of the smallest (C) sample (**Figure 6.10-a**) is slightly lower than the three larger samples (**Figure 6.10-b,c,d**) and this is true for the (D) samples too. Interestingly, the stress values for the three larger samples are almost identical in (C) and (D) samples. For the original experimental sample, represented in **Figure 6.10-b**, the tensile stress at the nearest time step to the time of spalling is still below the tensile yielding limit of the concrete ($0.09 \times 70MPa = 6.30MPa$). For the same sample, compressive stress at time step 462 seconds, as shown in **Figure 6.9-b**, exceeded compression yielding of concrete ($0.3 \times 70MPa = 21MPa$). Together, they result in a steep transition from compression to tension which correlates well with the location and time of

spalling and seems related to the triggering of spalling due to surpassing compressive yielding limit of the concrete. In terms of differences deriving from different eccentricities, comparing

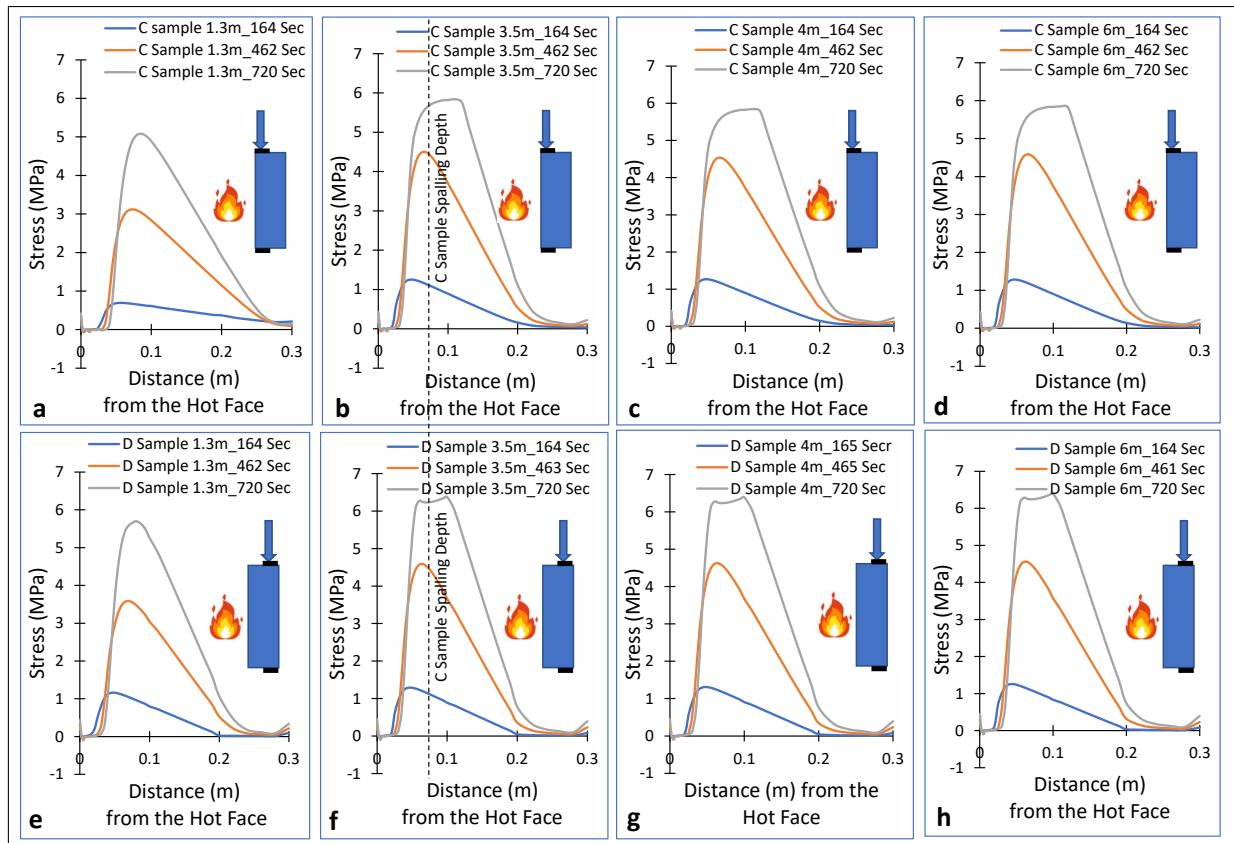


Figure 6.10: **a,b,c,d** Maximum principal stress of the (C) samples, and **e,f,g,h** Maximum principal stress of the (D) samples at different heating times through their thickness, having 1.30m, 3.50m, 4.00m, 6.00m heated span respectively

peak stress values in the compressive zone near the heated face of the (C) samples shown in **Figure 6.9-a,b,c,d** to the (D) samples shown in **Figure 6.9-e,f,g,h**, lower peaks can be noticed for the latter group regardless of the span of the sample. However, this is opposite in tensile stress peaks, the (D) samples (**Figure 6.10-e,f,g,h**) are subjected to slightly higher tensile stresses compared to (C) samples (**Figure 6.10-a,b,c,d**) regardless of the size of the sample. This is because of the greater deflection (D) samples experienced towards the heat source due to the combined actions of the heating and the rear eccentric load **Figure 6.11**. The rear eccentric load bowed the sample toward the heat source, this combined with the tendency for the concrete to expand towards the fire. At the same time the rear eccentric load in the (D) samples causes higher compressive stresses at the rear portion of the samples that act as a balancing force, similar to what observed in (A) samples discussed before, reducing the compressive stress developed at the front heated portion but causing higher tensile stresses accordingly, deeper in the samples. Despite of all these differences, steep transition from compression to tension can be observed in all samples regardless of the span and eccentricity conditions. If heating pursued, the stresses intensify further surpassing significantly yielding limits in compression and tension. Therefore the transition steepness increases too and more significant spalling failures would be anticipated accordingly.

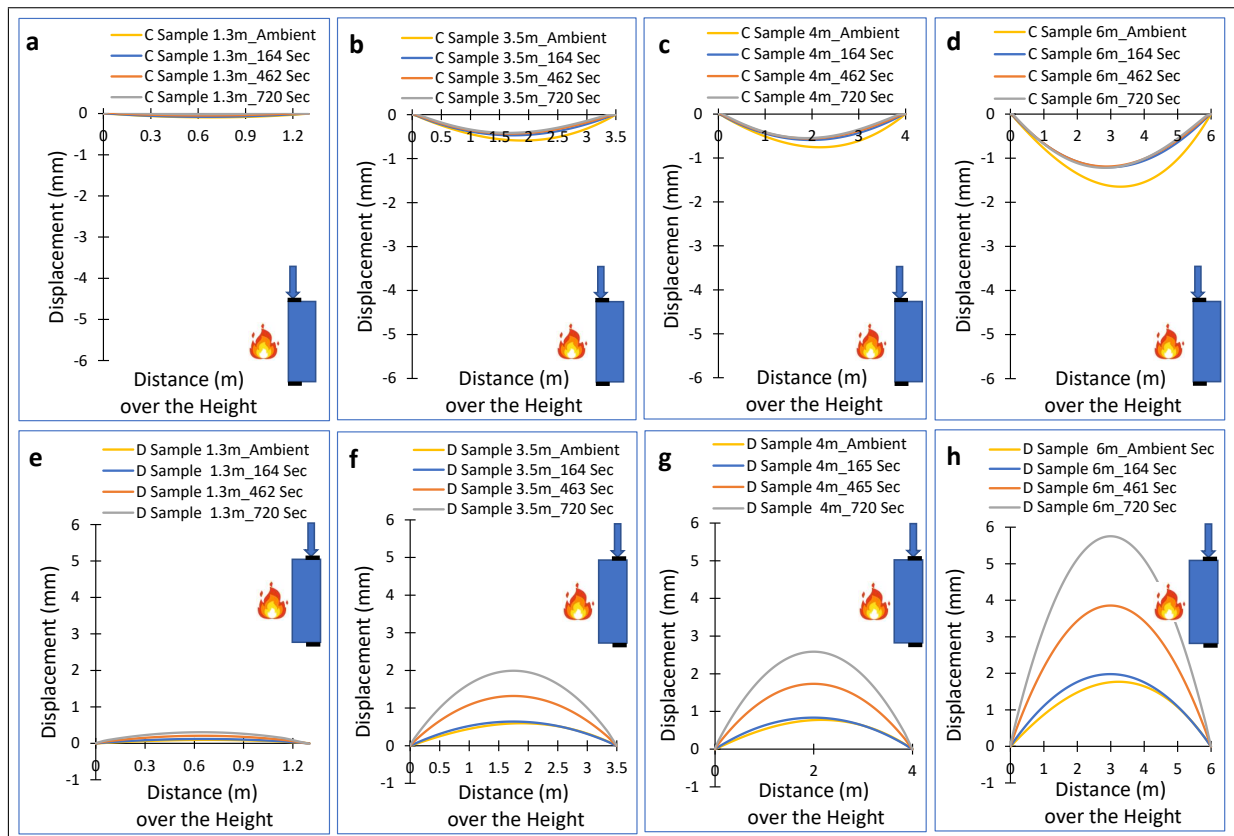


Figure 6.11: **a,b,c,d** Displacement of the (C) samples, and **e,f,g,h** Displacements of the (D) samples toward the heating source over the samples' height at different heating times, for samples with 1.30m, 3.50m, 4.00m, 6.00m heated span

Now turning to investigate the exposed surfaces of the samples, displacements perpendicular to the heat source over the height of the different span samples considering different eccentricities have been plotted in **Figure 6.11**. For the (C) samples shown in **Figure 6.11-a,b,c,d**, the samples at ambient temperature have already displaced away from the heating source due to the frontward eccentric load. With increasing heating time the samples tend to displace toward the heating source, thereby decreasing the overall displacement accordingly, but remaining concave to the heat. This becomes more noticeable with increasing span, with larger changes in displacement taking place.

In contrast, the displacement of the (D) slabs towards the heat source increases with increasing heating time (**Figure 6.11-e,f,g,h**) and this becomes more noticeable with increasing span. Here the initial displacements due to the eccentric load at ambient temperature are towards the heating source and as heating continues the exposed surface tends to displace further toward the heating source. Comparing the initial values at the ambient temperature, displacements increase by around three times in the 1300 mm sample, four times in the 3500 mm sample, 5 times the 4000 mm sample and 6 times in the largest 6000 mm sample. Comparing to (C) samples, these displacements are significantly higher for all samples with different spans, reaching almost six times at the largest span. However, considering that the stress states are very similar for different span samples in (C) and (D) samples, it seems that these displacement intensities do not cause significant alteration in overall behaviour of the samples. Possibly the only difference would be

observing less abrupt failure in (D) samples comparing to the (C) sample especially at the largest span samples due to having higher displacement.

These results imply that increasing span is not effective in altering the behaviour of the samples. The observed results are due to different eccentricities which are even not dramatic, possibly due to low intensity of the initial applied load. More pronounced observations might be observed if intenser initial load would be used, for this more investigations are recommended.

Examining further the exposed surface, significantly more severe stress in the direction of the loading can be anticipated compared to the horizontal direction (across the slab width). Therefore, the effect of span on the evolution of the vertical component of in-plane stresses have been investigated. Results at different heating times along a centroidal axis run over the exposed height of the different samples for both eccentricity scenarios have been shown in **Figure 6.12**. For the (C) slabs shown in **Figure 6.12-a,b,c,d**, almost all of the exposed surfaces of the different

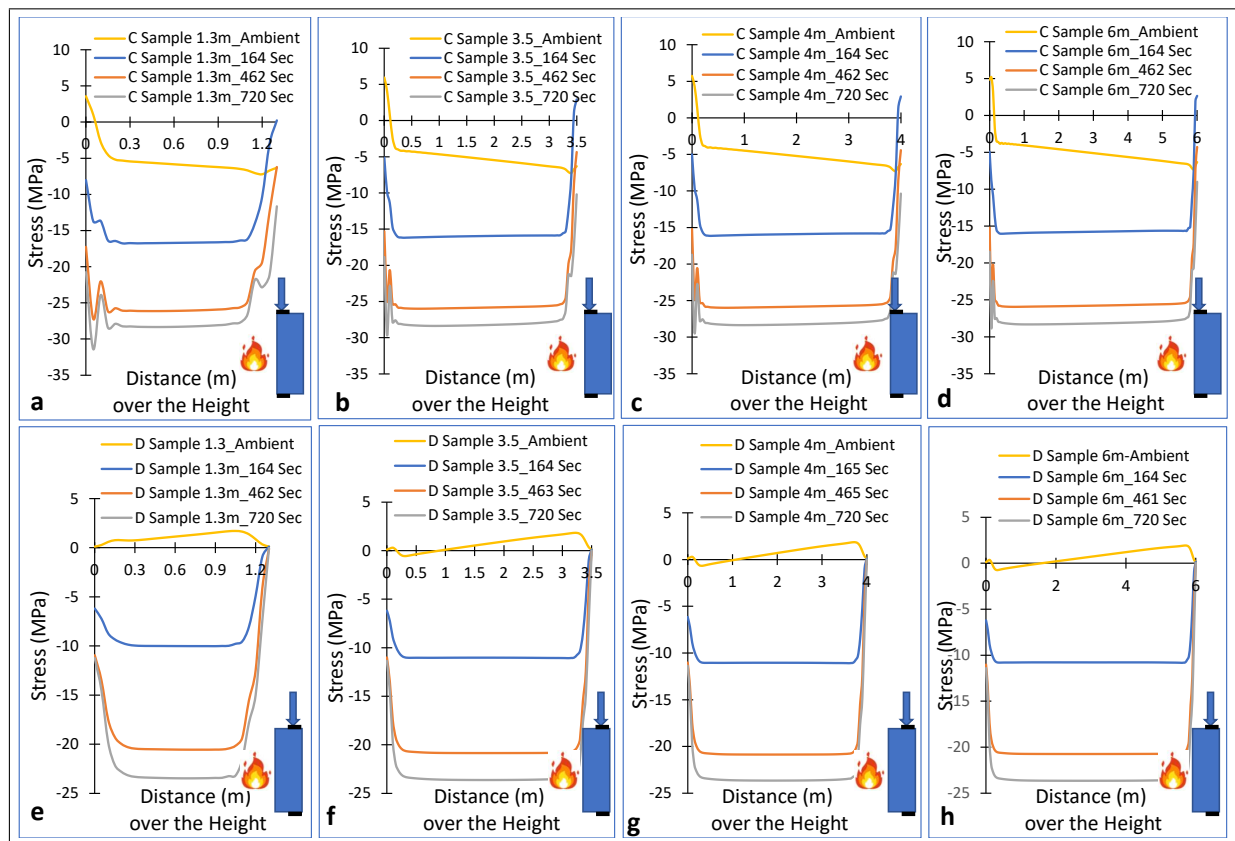


Figure 6.12: **a,b,c,d** Developed in-plane stresses of (C) samples, and **e,f,g,h** Developed in-plane stresses of (D) samples over the height of the different size samples, with the direction of the initial applied load, at different heating times

size samples at ambient temperature are under compressive stress by the sole action of the initial eccentric applied load. However, some small portions near the bottom of the samples are under tensile stress due to fixity of the platens. With increasing heating time, the compressive stress increases exceeding the yielding limit early on. However, with increasing size of the samples, no noticeable differences in terms of behaviour and peak values is observed. This can be attributed to the dominating effects of the thermally derived stresses over the initial applied stress, which is only 9.6% of the concrete strength. Thermally induced stresses even dominate the effects of

increased span where there are no differences in stress states for all samples. This is further confirmed by the rapid disappearance of the tensile stress at the lower portion of the sample and by the deformation of the sample towards the heating source as discussed above. It may however be inferred that different behaviour might be observed if intenser initial load were applied.

Regarding in-plane stresses in the (D) slabs shown in **Figure 6.12-e,f,g,h**, different behaviours from what have been observed for the frontward loaded (C) slabs can be observed at ambient temperature. The exposed surfaces at ambient temperature are mostly in tension except for a small portion near the lower end of the three larger samples, which are in compression (**Figure 6.12-f,g,h**). As with the (C) samples, as heating goes on, the tensile stresses are eliminated and the heated surface remains solely under compression while it displaces towards the heat source, as discussed before. As an effect of overcoming the tensile stresses, the values of the developed compressive stresses are lower than those observed in the frontward loaded (C) slabs, which means that the initial tensile stresses caused by the rear eccentric load improves spalling resistance of the samples.

To sum up, even though sample span may not change the stress state behaviour of the eccentrically loaded samples, it alters displacement behaviour at the exposed surfaces noticeably. First, for each eccentricity under consideration, increasing the exposed span of the samples does not affect compressive stress development through the depth and at the exposed surfaces of the samples. However, in 1300 mm sample tensile stresses is slightly lower than other three larger samples having very similar peaks. This is more pronounced in (C) samples than (D) samples. While it could be relating to position of the initial load, the difference is too small to cause dramatic change, especially there are still steep transitioning from compression to tension in all (C) and (D) samples. Second, for each eccentricity under consideration, increasing the exposed span of the samples increases displacement toward the heating source. This is more pronounced in (D) samples compared to the (C) samples because of the effects of the initial rearward applied load in displacing the sample toward the heating prior heating. Under the load intensity investigated here, these displacements in both (C) and (D) samples are not high enough to change overall behaviours of the samples because stress states remained unchanged for different span samples. These observations might vary if higher initial load would be used. Higher displacements of (D) samples might cause observing less abrupt failure comparing to (C) samples and again would be more pronounced if higher initial load would be used. Third, the exposed surface of the (D) sample is subjected to lower in-plane stress, in the direction of the applied load, compared to the (C) sample and increasing the sample size does not alter the stress. Fourth, in general increasing the exposed span results in less abrupt failure regardless of the position of the load due to experiencing higher deformations. Finally, observing these different results between samples with different eccentricities is a clear indication how test set up crucially affects test outputs regardless of the size of the samples. These observations may be more pronounced under higher applied loads, therefore it is recommended to test samples representative to reality as much as possible otherwise the results remain test specific. Between the span and thickness of the samples, compromising span is found to have less effect on results

under the load intensity employed in this investigation.

6.4 Conclusions

To investigate how the results of concrete spalling experiments are sensitive to sample size, specifically thickness and span of the sample, a series of numerical investigations were performed using a validated FE model developed in ABAQUS. The study considered examples of common test methodologies available in the literature. Focusing on sample thickness, experimental results have been chosen to represent unrestrained unloaded slab samples and restrained unloaded samples. Considering the sample span, experimental results from loaded samples with different load eccentricities have been chosen.

Along with the simulation of each selected test case, parametric studies based on the test case have been conducted using different sample sizes simulated under the same testing conditions. Based on the observed results from these simulations, it is clear that the sample size is an important factor in influencing test outputs and that the affect varies based on the test configuration. This may therefore be one reason behind the lack of consensus among spalling researchers. Test results found to be more sensitive to thickness of the samples rather than their span.

First, considering sample thickness effects, in unrestrained unloaded slab samples, increasing sample thickness impairs spalling resistance by inducing higher compressive and tensile stresses through the sample thickness thereby steepening the stress gradients in the transition between compression and tension zones. Thinner samples have less stiffness and therefore bend more towards the heating source when heated causing squeezing in the rear cold portion and the development of compressive stress there. This compressive stress equilibrates and relaxes the compressive stresses that develop near the heated surface. Therefore, the gradient steepness between compression and tension stress relaxes and reduces spalling risk accordingly. In contrast, thicker samples are stiffer and bend less, leading to increased compressive stress near the heated surface and more axial deformation through the sample's thickness, thereby increasing tensile stress as well. As a result of these, the gradient of the stress transition becomes steeper and more spalling could be anticipated. On the other hand, the displacement of unrestrained samples towards the heating source decrease significantly with increasing thickness, this might lead to the anticipation of deeper and more abrupt spalling type failure in thicker samples, especially following the development of high tensile stresses in the inner portions of the samples.

Considering sample thickness effects in the restrained samples, observed behaviours are controlled by the restraint essentially overriding the effects of thickness. It eliminates the global bending of the sample toward the heating source observed in the unrestrained samples and effectively controls the stress state development regardless of the sample thickness. No noticeable increase in stress state development observed through increasing thickness which means transition gradient between compressive and tensile stresses remained unchanged. Restraint effects may be slightly undermined in very thin samples that develop slightly higher tensile stress due to the lower stiffness of the sample, however this is too small to trigger different behaviour. The

dominant effects of the restraint effects is valid also in the exposed surface displacement toward the heating source. Almost the same, very low displacement intensities under the effects of the heating can be observed, which are not appreciably affected by the thickness of the sample.

Generally, compared to unrestrained samples, potential improvements in spalling resistance can be noted for the restrained concrete samples. This mainly due to the dominate action of the restraint over the negligible effects of the thickness in lowering compressive and tensile stresses through the sample thickness. This decreases the steepness of the gradient between compressive and tensile zones thereby potentially limiting a possible trigger for spalling. While both samples have potential of spalling due to this steep transition, the mode of failure could be different, less abrupt failure in unrestrained sample comparing to the restrained samples. Finally, observing negligible displacement difference between the unrestrained and restrained samples with increasing sample thickness implies the dominate action of the restraint over the negligible effects of the thickness.

Second, regarding sample span effects, increasing span of the eccentrically loaded samples does not changes the compressive stress development through the depth of the sample irrespective of the position of the eccentric load. This is also true for tensile stress development where no appreciable difference capable in changing behaviour of the samples can be observed through the depth. While there are differences in stress and displacement intensities between samples with different load eccentricities, they are mostly relating to different test ups rather than being dependant on the span of the sample. The only effect might sample span have is observing less abrupt failure with increasing span regardless of the position of the load. This is due to experiencing higher deformations, and according to this, in general less abrupt failure may be anticipated in rear loaded eccentric samples comparing to the frontward loaded samples.

In summary, sample thickness and sample span can affect concrete behaviour, the thickness effects seem to be more crucial comparing to the span effects. The effects can vary depending on test set up, restraints and loading configuration. Therefore, to reach a reliable test output, realistic conditions of the members in the real structures should be reflected in the test ups. Otherwise the assessment based on the test results would be test specific and potentially misleading if generalized. Between span and thickness of the samples, compromising span is found to have less effect on results under the load intensity employed in this investigation. While this may be helpful in designing experimental specimen size, and considering that has been concluded under low intensity load here, more investigation under severer load intensities are recommended.

Chapter 7

Effects of Load on Concrete Behaviour and Spalling at High Temperatures

7.1 Introduction

In the literature, load has been found to be one of the most influencing factors that can change behavior and cause spalling of concrete under effects of elevated temperatures. However, adopting different load types, load intensities, and various load application methods in the experiments have led to different test outputs and therefore lack of consensus among researchers regarding the exact correlation between loads and spalling under heating effects. An important question which is whether the test methodologies and test set up details have been a factor behind these scattered test results has not been focused on well in the literature, therefore it is addressed in this chapter. To do this, in spite of investigating concrete behaviours under different load types, other parameters like load intensity, load application methods, factors relating to test methodologies such as friction, test configuration, and boundary conditions have been also investigated thoroughly to find out whether there are any other underlying physical phenomena beyond the so far known factors that can control test outputs.

The numerical ABAQUS model developed in Chapter 3 has been used to simulate and investigate selected tests from the literature as they are, then some other hypothetical simulations have been extended from these tests for the purpose of the investigations. The results showed that loads can affect sample's behavior in very different ways based on whether they have been applied directly as static loads prior heating or they have been developed during heating by the actions of end restraints. Further more, it has been found that load intensity significantly alters samples' fire resistance under different boundary conditions and it accelerates spalling occurrence accordingly. Additionally, methods of load application whether it is concentric or eccentric and most importantly the location of the eccentricity with respect to the heating source can alter the test results significantly for the same sample under the same load intensity.

Further to these findings, testing conditions such as availability of friction between samples' contact areas with the testing apparatus and ways of maintaining the load application during the test have been found effective in altering test results. Based on the results of this study, it is not a reliable approach to simply assess fire resistance of a structural member based on results from a particular test in which real conditions of the member has not been reflected precisely. It is strongly recommended to incorporate real conditions of the structural members in terms of boundary conditions, load type, and its intensity and application method into the test set ups. Ensuring these along with highly controlled testing environment would produce more reliable

results upon its structural members could be assessed more confidently.

7.2 Load configurations

As previously explained, the source and intensity of the loading and details of how it has been applied onto the samples are taken into consideration in this chapter. Following the same procedure adopted in previous chapters, samples selected here also cover structural and nonstructural elements. Three samples from the selections made in **Chapter 4** and shown in **Figure 4.1** have been selected and simulated with dimensions and set ups shown in **Figure 7.1**. They cover a wide range of methodologies in the literature, following the same pattern classified

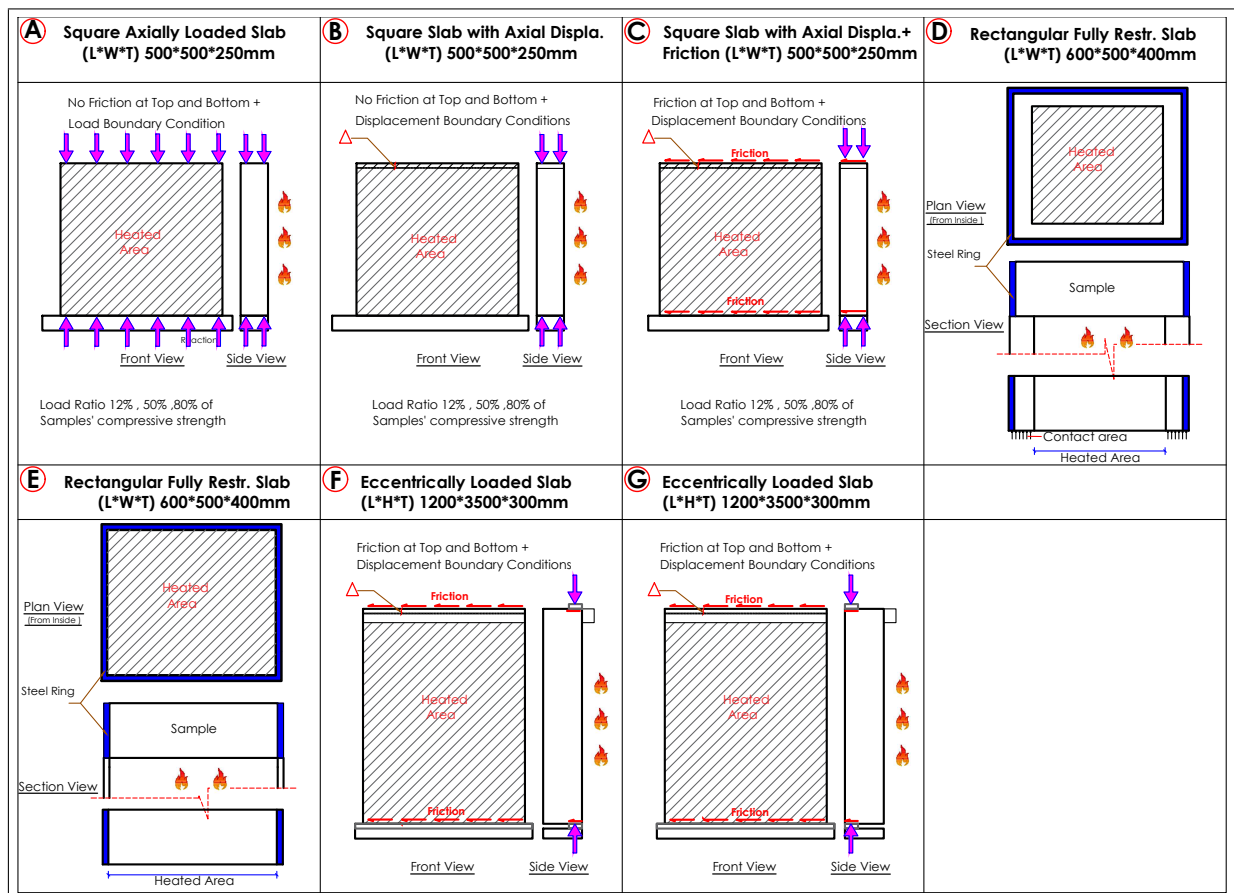


Figure 7.1: Work program and sample boundary conditions

earlier as restrained then heated samples, and loaded then heated samples, for both concentric and eccentric load configurations with various load intensities. Where necessary, hypothetical scenarios have been incorporated, extending the experimental tests parameters in order to conduct parametric studies.

Configurations (A), (B) & (C) concern a square loaded slab aligned vertically and with load applied concentrically perpendicular to its thickness prior to subjecting the front face to the heating source as shown in **Figure 7.1-A, B & C**. The original, experimental test was stressed to 12% (5MPa) of its compressive strength at ambient temperature. Two more load ratios 50% (21MPa) and 80% (33.6MPa) have also been simulated to investigate the effects of load intensity.

Furthermore, to investigate the effects of the way in which the load is applied under different load intensities, three possible loading conditions have been considered as shown in **Figure 7.1-A,B,C**. (A) sample represents test case in which framing load pushing back is possible due to the sample's expansion while heated. (B) sample represents test case in which framing load pushing back is not possible due to the sample's expansion when heated. (C) sample represents the test case in which framing load pushing back is not possible due to the sample's expansion and there is perfect friction at the top (with the loading plate) and at the bottom (with the supporting frame) of the sample. Effect of friction investigated in **Chapter 5**, here the investigation extended to consider different load intensities. Moreover, a different friction level has been incorporated, (A) sample is extremely loose case comparing to the no friction (B) sample and the extreme friction (C) sample cases. For (A) sample load boundary condition but for (B) and (C) samples displacement boundary condition will be applied to control load framing pushing back as it will be explained in later sections.

Configurations (D) & (E) concern a passively loaded rectangular sample fully fixed around its perimeter by a steel ring covering the entire sample's thickness. These configurations have been extended as a hypothetical case from a partially fixed tested sample chosen in **Chapter 4**. It has been simulated to investigate the effects of the loads originated from restraints rather than being directly applied. The sample was put on an oven and the central portion of the sample's lower face was heated. This way unheated ring around the heated zone at the sitting areas where samples rest on the oven configured as shown in **Figure 7.1-D**. This configuration has been a typical applicable experimental configuration in some tests in the literature to simplify resting the sample on the oven. Providing cold rim can be found also in so many works in the literature and some researchers understood it acts as a self-restrainer capable of imposing more stresses to the heated portion as [33]. From this simulation, another simulation has been extended with the only difference being that its entire lower face has been heated and no sitting area is available as shown in **Figure 7.1-E**. This configuration might be difficult practically but it is possible in numerical simulations. Through comparing these two configurations, developed stresses from restraints having different stiffness can be investigated. The heated area in (D) sample (**Figure 7.1-D**) is restrained with the unheated concrete ring then the steel ring (concrete stiffness is lower than the steel ring). However in (E) sample, the heated area is directly restrained with the steel ring without any cold rim in between as shown **Figure 7.1-E**. In **Chapter 5**, a similar investigation has been conducted on ring samples in which both samples had cold ring, here rectangular samples have been considered, one of them without cold rim to facilitate maximum possible reaction from very stiff steel ring.

Configurations (F) & (G) consider an eccentrically loaded sample from the same test chosen in **Chapter 4**, loaded to 9.60% of its compressive strength (equivalent to 6.70MPa). This eccentric case has been chosen since, as discussed before, columns and walls in buildings are usually eccentric due to difference in adjoining spans meeting on the columns and variation in live loads in different floors. The eccentric load had been applied through a plate covered 100mm out from 300mm of the sample's thickness at the front portion of the sample as shown in **Figure 7.1-F**.

Then its front face (except 100mm from the top to protect the loading equipment from the heating source) was subjected to the heating source. For this simulation, perfect friction at top and bottom of the sample has been considered between the sample and the apparatus. A displacement controlled loading platen to prevent pushing back due to the sample's expansion throughout the testing time has been considered. From this simulation, another scenario has been extended with the only difference being that the eccentricity has been provided at the rear portion of the sample as shown in **Figure 7.1-G**, all other testing conditions remain as before.

All samples were exposed to fire curve ISO834 through the hatched faces shown in **Figure 7.1**. Sample dimensions are shown in the same figure and the compressive strength of all samples was 42 MPa except for the eccentrically loaded samples (F) & (G), which was 70 MPa. All these different samples and scenarios are compared in terms of stress and displacement states to understand how the test results have been affected.

7.3 Analysis results and discussions

As in previous chapters, reported first spalling times in the tests was considered and followed accordingly in the ABAQUS model for each simulation under consideration.

7.3.1 Axially loaded samples

In this section, three samples (A,B, and C configurations from **Figure 7.1**) with different boundary conditions have been investigated under different load intensities (12%, 50%, and 80% of their compressive strength). Since exact boundary conditions relating to the load application details are unknown, parametric studies have been considered considered three possible ways mentioned before. For the (A) sample, vertical load boundary condition technique has been imposed in the ABAQUS model which allows pushing back the applied load vertically during analysis due to expansion of the heated sample. The displacements at the other two directions(perpendicular to the load direction) at top and bottom of the sample were not restrained to represent lack of friction for this configuration. For the (B) sample, an initial vertical displacement boundary condition has been applied with an amount equivalent to that produced by the initial applied load at ambient temperature. This prevents any vertical pushing back effects during the analysis which means the initial load value maintained. The displacements in the other two directions at the top and bottom of the sample were left unrestrained, representing a lack of friction. However for (C) sample, in addition to locking the vertical displacement, as for (B) Sample, the displacements in the other two directions at the top and bottom of the sample have been restrained too representing full friction condition which maintains in time.

For the experimentally tested sample, which was loaded to 12% of its strength, three spalling failures were reported at 360 seconds, 540 seconds, and 640 seconds with 9mm, 10mm and 11mm depth respectively. To visualize stress states of each configuration shown in **Figure 7.1-A,B,C** at the time of first spalling for 12% load, 3D section views of minimum and maximum principal stresses along with the test configurations have been presented in **Figure 7.2**. For different

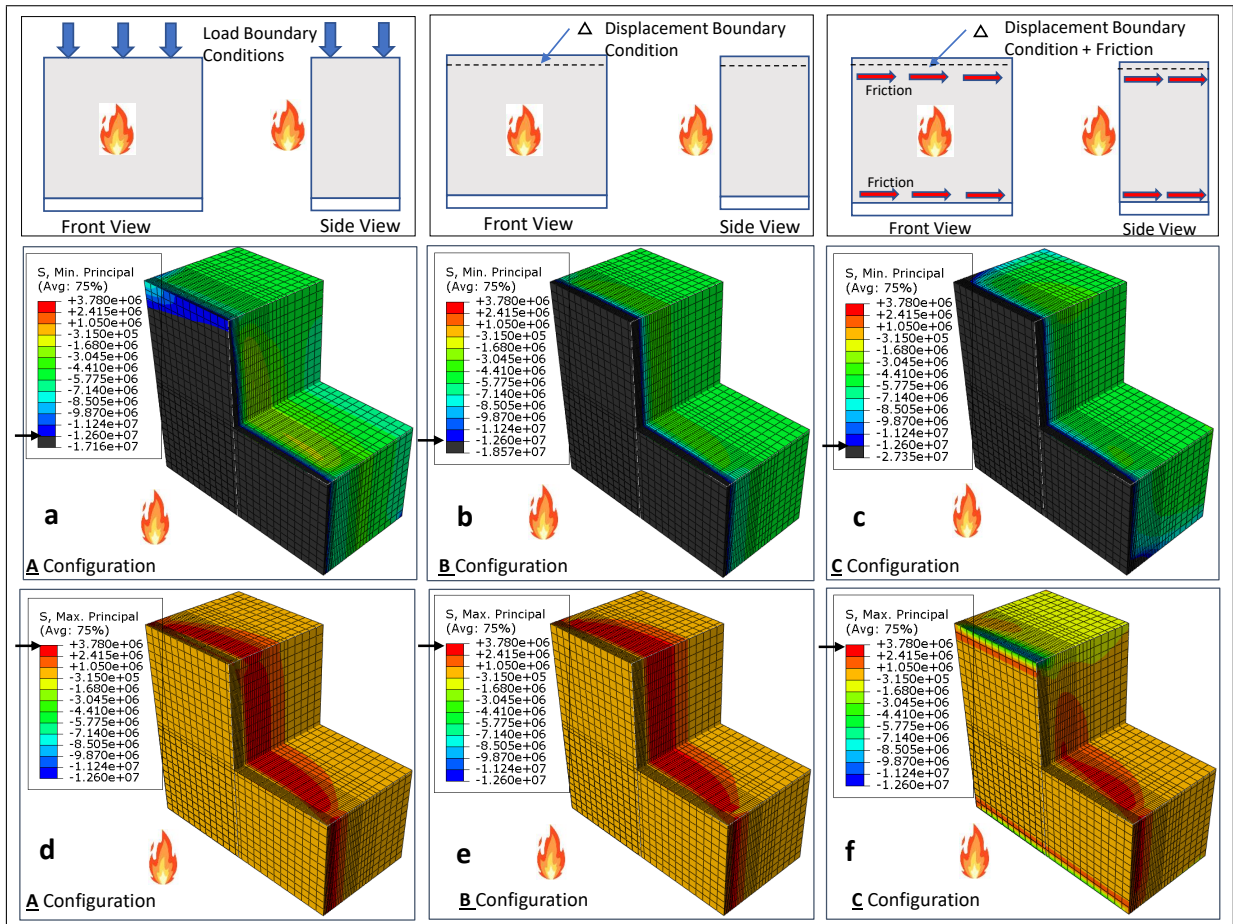


Figure 7.2: **a,b,c** Minimum principal stress and **d,e,f** Maximum principal stress at spalling time for A,B,C configurations shown in Figure 7.1 loaded to 12% of their compressive strength

load ratios, plots showing minimum and maximum principal stresses through the centreline thickness of the samples at different heating times considering the three aforementioned boundary conditions are shown in **Figure 7.3**.

As a general trend, a highly stressed compressive zone can be observed from the heated surface. Directly behind this, in the centre of the samples, there is a zone stressed with combined compressive and tensile stresses. The tensile stresses dissipate towards the cold face of the sample where again the stress field is largely compressive and associated with the ambient applied load (5MPa, 12MPa, or 33.6MPa). In the loaded samples, the loads predominately control and pronounce the behaviors. Here the compressive stress is vertical and the tensile stress are horizontal perpendicular to the heated face.

Regarding the compressive zone, as shown in black (**Figure 7.2-a,b,c**), the stress values over the entire exposed surfaces of the samples (A, B, and C) have exceeded the compression yielded limit ($0.30 \times 42\text{MPa} = 12.6\text{MPa}$) except in a very small area near to the top of the (A) sample. It may also be noted that the yielded layer is thinner in the (A) configuration than in the (B) and (C) samples. Additionally, the stress intensity of the (C) configuration (**Figure 7.2-c**) is significantly higher than the other two samples, which have similar stress intensities. Therefore, it can be implied that maintaining the load intensity (preventing its pushing back due to expansion of the sample upon heating) and frictional effects can cause more compressive stress in the samples.

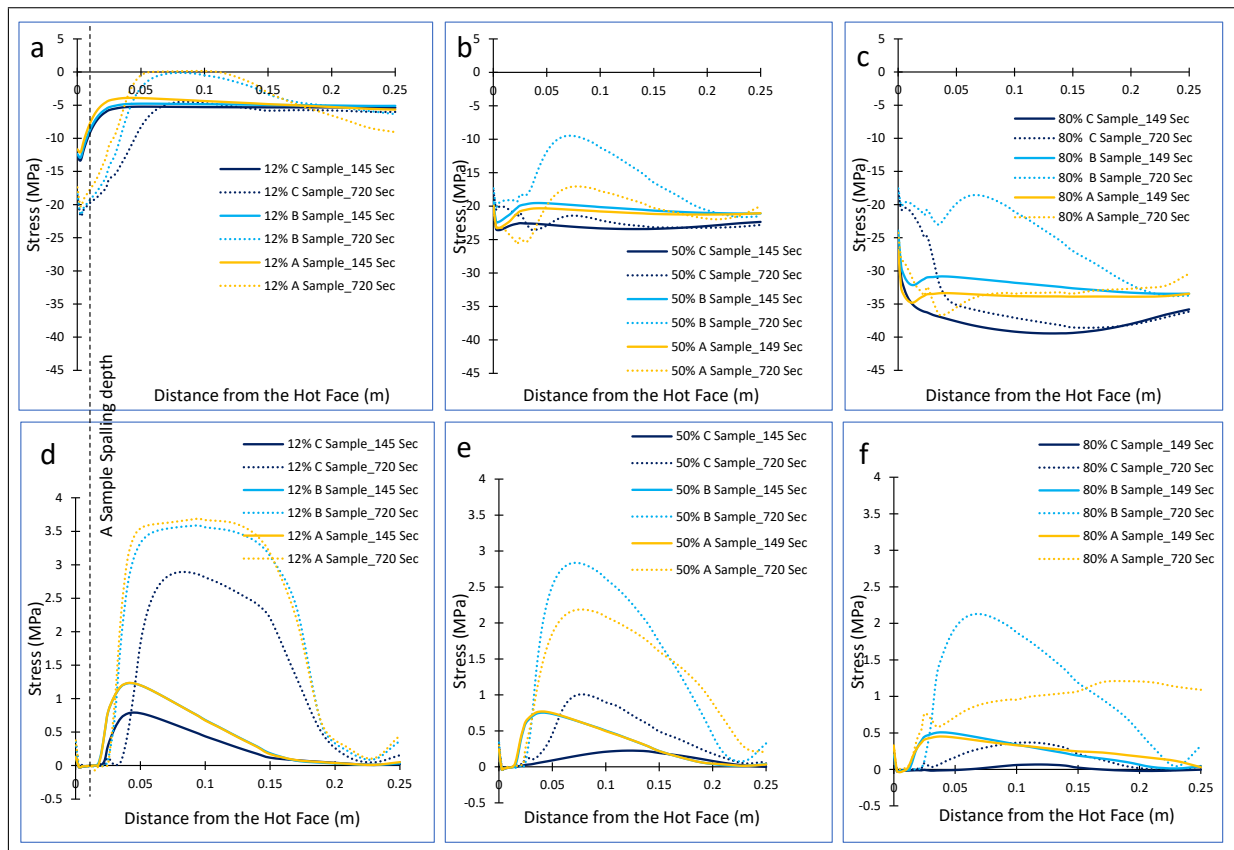


Figure 7.3: **a,b,c** Minimum principal stress and **d,e,f** Maximum principal stress through thickness of the square sample loaded to 12%, 50%, 80% of their compressive strengths respectively

Regarding the tensile zone of the three samples shown (**Figure 7.2-d,e,f**), the stress values are below the tension yielding limit of concrete ($0.09 \times 42\text{MPa} = 3.78\text{MPa}$) and no significant difference can be noticed stemming from various boundary conditions and friction. Considering these results together with the compressive stress results, steep stress gradient transitioning from compressive zone to tensile zone developed in the samples with the highest steepness in (C) sample. This causes spalling potentially due to surpassing compressive yielding limit (12.6 MPa) and tensile yielding limit (3.78 MPa).

Looking through the thickness of the samples, for the 12% load ratio (**Figure 7.3-a**), compressive stresses at the early time step (145 seconds) for the samples under the three boundary conditions are almost identical in terms of their development and intensity. Through most of the thickness except regions nearby the heating, the stress intensity represents the initial stress (5MPa). However, regarding tensile stresses from **Figure 7.3-d** at the same time step, the behaviour of the (C) sample is noticeably different from (A) and (B) samples. The friction in (C) sample improves the resistance of the concrete by lowering the tensile peak comparing to (A) and (B) samples. Due to the effect of the heating in increasing the compressive stress nearby the heated surface, the initial compression stress increases significantly and therefore tensile stress evolution develops quite deeper in the sample. The compressive peak values near to the exposed surfaces even at this early time exceed the compression yielding limit ($0.30 \times 42\text{MPa} = 12.6\text{MPa}$) and they significantly increase with increasing heating time. However tensile stresses at the same time step are quite below yielding limit but they also increase in time. At 720 seconds, the

compression peaks are approximately 1.7 times higher than at 145 seconds while tension peaks increase up to 3 times reaching values close to the yielding limit ($0.09 \times 42\text{MPa} = 3.78\text{MPa}$) especially in (A) and (B) samples. With increasing heating time and distancing from the heating source, obvious differences stemming from the friction effects can be observed in compressive stresses. Frictional confinement avoids stress relaxation and its transition toward tensile zone comparing to if no friction is available. Therefore, less steeper shifting toward tension zone for (A) and (B) samples comparing to (C) sample can be observed hereby larger portion through the depth of (C) sample remain highly stressed accordingly. Ultimately, the stress for the (C) sample rests at the initial applied compressive stress value (5MPa) meanwhile for (A) and (B) samples the stresses reach a zero plateau then plunge toward the compression zone again.

By increasing the initial applied load ratio to 50% and 80% (**Figure 7.3-b,c**), equivalent to 21 MPa 33.6 MPa respectively which are beyond the yielding limit of the concrete in compression, the overall aforementioned compression behaviours in the 12% load case have changed noticeably. From the early stages of heating (145 seconds), the (C) sample has higher stress compared to the (A) and (B) samples, and this is more pronounced in 80% load intensity case. Furthermore, with increasing load ratio, stress peak distances farther through the thickness, locating around 130mm from the heating source in the 80% load case (C) sample. Interestingly, at the later times, the stress peaks near the heated surfaces show a decrease, rather than an increase, for the (B) and (C) samples while the (A) sample's peak increases, even slightly, at the same zone. Regarding tensile behavior (**Figure 7.3-e,d**, with increasing load intensity the observations seen in 12% samples pursued, that is further lowering in stress peaks in all samples.

These results imply that, first with increasing applied load, tensile stresses tend to diminish. The peak values are much lesser than yielding limit especially for the (C) sample in which the tensile stress almost diminished even at the later step (720 s) and the sample became a purely compression member. Tensile stress decrement with increasing imposed loads does not lead to improving overall fire resistance of the samples. While the tensile peaks decrease, the compressive peaks at the same time increases much more significantly. Therefore still steep stress gradient would be available to cause potential dramatic spalling accordingly due to yielding in compression. Second, with increasing load intensity, more diffused stress pattern can be observed through thickness of all samples which means less stress fluctuation with respect to the highest peak near to the heated surface. The highest stress peaks distancing farther from the heating source in 50% and 80% loaded samples in comparison to 12% samples. They locate around 30mm to 50mm except for (C) sample with 80% load in which the peak shifted significantly deeper through thickness to around 200mm, whereas all peaks were only around 10 mm away in the previous 12% load ratio case. A possible reason for this is the yielding status of the concrete under the initial applied load. In lower loaded samples, the concrete at the exposed surface has not yielded and therefor can withstand stress imposed by the heating. Through this, maximum deformation takes place nearby the heated surface and therefore observing highest stress peak there. With increasing initial applied load, this behavior becomes less noticeable because the concrete at the exposed surface has yielded already and can not withstand more stress. As a

result, the deformations take place more uniformly across the thickness of the sample causing peak stresses to develop deeper comparing to the lower loaded samples. Third, it seems that heating effect in samples with higher initial load ratio does not increase noticeably the peak compression stresses, as the dominant stress regime, comparing to samples with lesser load ratio. In (C) samples for instance, for the 12% load ratio (**Figure 7.3-a**) the initial applied stress (5MPa) has been increased by 340% because of the heating meanwhile for the 50% and 80% load ratios from (**Figure 7.3-b,c**) no noticeable increment can be observed, it is only around 17% of the initial applied load (33.6MPa) for the 80% sample. This is again relates to the yielding status of the concrete. In higher intensity loads, the concrete has already yielded even before the application of the heating and can not withstand more stress due to the heating. Therefore the thermal action in imposing more stress is less pronounced for higher stressed samples compared to the 12% load case. Finally, the differences in peak values between samples with and without friction increases with the load ratio. As discussed before, this is due to the confinement effects of friction in avoiding stress relaxation across the thickness of the samples, and obviously higher loads are more conducive to this behavior comparing to lower loads.

These findings suggest that decisions based on test results with non representative boundary conditions to the reality would be problematic. This is also true and crucial while investigations based on experimental results are pursued numerically. Considering lesser friction suggests members impose to less compressive stresses. Therefore decisions based on this would be unsafe for compression members if the friction condition are severer in reality, for example through end restraints. On the other hand, exaggeration in friction suggests more compressive stress. Therefore decisions based on this would be too conservative and leads to uneconomic design. These observations are highlighting challenges relating to boundary conditions and load intensities that should be taken into consideration precisely while configuring tests for loaded members under heating effects and even afterwards while numerical investigations are pursued. On one hand special attention is required in assigning right test boundary conditions and maintaining them throughout the testing time. On the other hand well predicted load intensity for the member under consideration is required to be represented in the test. Through ensuring these, more reliable test outcomes can be obtained to be used in assessing real structural members.

7.3.2 Passively restrained rectangular Sample

In the previous section, the investigations were based on samples loaded directly through initial applied load prior heating. In this section, samples loaded passively through restraints with different stiffness under effects of heating have been investigated and compared to the initially loaded samples prior heating. In restrained samples, load develops only when the concrete is subjected to heating and the restraint prevents its expansion. The load becomes gradually intenser in time with heating due to the restraint reaction and this may vary depending on the restraint stiffness. Therefore, two restrained samples shown in **Figure 7.1-D-E** have been considered in this section considering two different restraint stiffness. They are restrained externally through a very stiff steel ring covering their entire thickness and are identical in terms of dimensions

and material properties. As mentioned before, these configurations have been extended from a partially restrained sample, and they are designed to have different restraint stiffness. In (D) sample, there are unheated zones around the perimeter of the exposed surface of the sample. This has been a typical applicable experimental configuration in the literature to simplify resting the sample on the oven. The cold zone surrounding the heated area can be considered as a restraint, with lesser stiffness than the steel ring, between the heated zone and the stiff steel ring. While in (E) samples, which may be practically demanding, all lower surface is heated and therefore the heated zone is directly restrained by the stiff steel restraint. The stiff steel restraint has been represented in the analysis through fixing all displacements at the restrained external sides along the perimeter of the samples.

According to the reported spalling results, the partially restrained sample from which the full restrained sample has been extended spalled after 600 seconds of being exposed to the heating. To investigate stress states at the first spalling time, minimum and maximum principal stresses for (D) and (E) samples at 620 seconds as the nearest time step to the spalling captured by the model are shown in **Figure 7.4**. For the (D) sample, a yielded compressive stress zone (black in colour-surpassing 12.6 MPa yielding limit) covering the exposed surface excluding the circumferential cold rings can be observed in **Figure 7.4-a**. However for the (E) sample a yielded compressive zone covering the entire exposed surface of the sample can be observed in **Figure 7.4-b**. The stress intensity of the (E) sample at the exposed surface is higher than the (D) sample and the complete yielded region has extended from the exposed surface through its thickness. However, in terms of tensile stress zones, no appreciable difference can be noticed from the cut views shown in **Figure 7.4-c,d**. The values have not exceeded yielded limit of concrete in tension (3.78 MPa) but still steep transition between compression and tension is available in both samples within which the spalling occur due to concrete compression failure. Despite different compressive stress intensities at the exposed surface resulting from different restraint stiffness, no appreciable difference can be observed in compressive and tensile stress states through the thickness of the (D) and (E) sample at different heating times as clear in **Figure 7.5-a,b**. Even though some severity due to the existence of cold rim can be observed in (D) sample, it does not alter the steepness of the transition between compressive and tensile zone as the main spalling trigger. Even at 1200 seconds which is almost twice the spalling time, the difference is barely 0.2 MPa. This suggests that the spring effect of the cold ring is effective only in reducing load intensity at the exposed surface and may not have effects on spalling, especially both samples have almost same transitioning steepness between compression and tension stress through their thickness. To examine to what extend the different compressive stress intensities change behavior at the exposed surface, developed in-plane stresses at different heating times along an axis across the centre of the exposed surface are presented in **Figure 7.6**. At the central exposed surface, higher stresses at some portions of the sample can be observed in (E) sample compared to (D) sample at different heating times compatible to what discussed before. This is even valid at later time steps after spalling where the stresses at both samples start to decrease due to concrete yielding and its incapability to withstand more load. However, in the vicinity

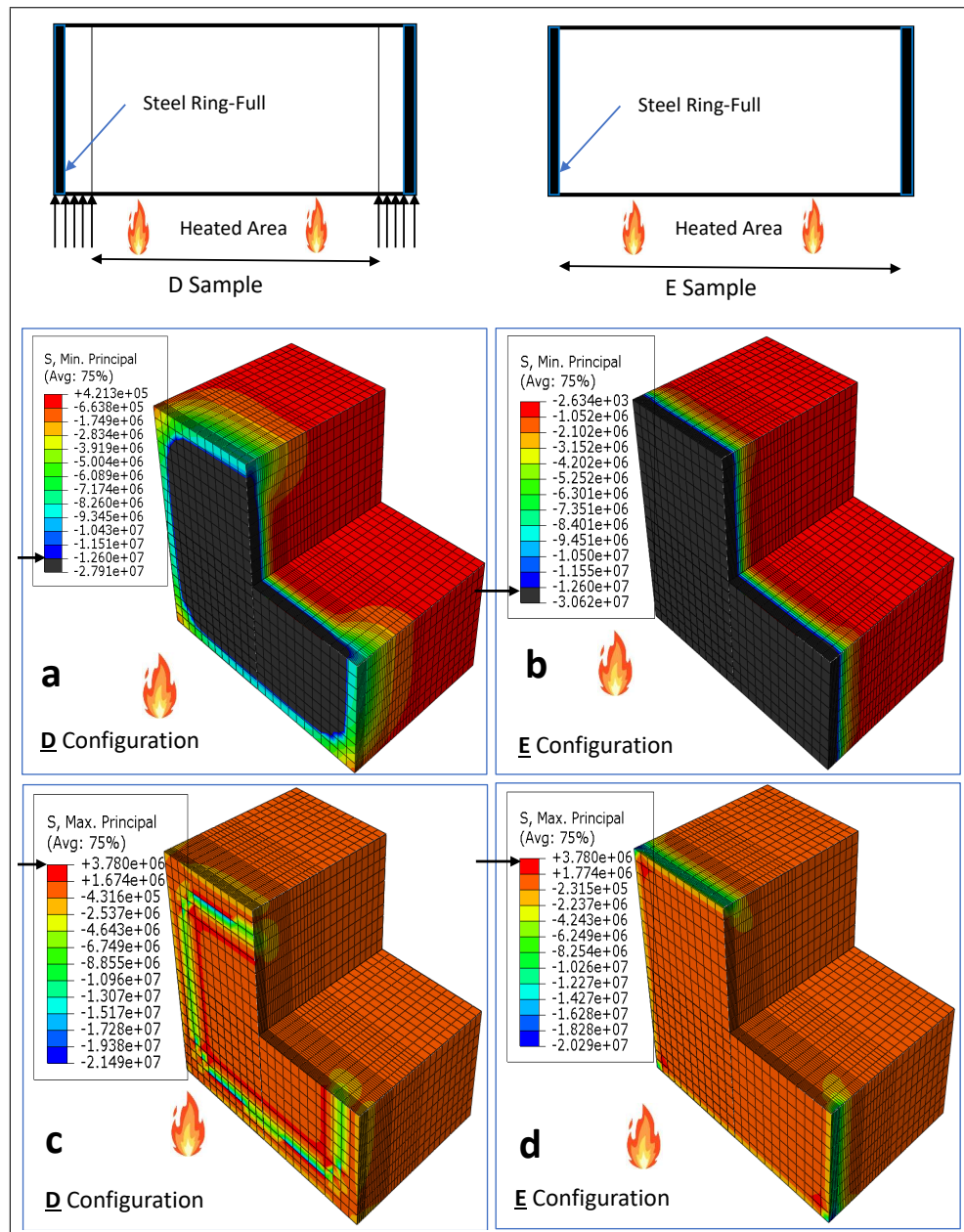


Figure 7.4: **a,b** Minimum principal stress and **c,d** Maximum principal stress at spalling time for D,E configurations shown in Figure 7.1

of the sample edges, different stress concentrations can be noticed. While the stresses increase persistently in time without reversal in (D) sample, reversal can be observed in (E) sample after spalling. The unheated zones in the (D) sample have not been damaged by the heating and are acting as a spring between the steel ring and the heated zone. This spring zone reduces stress concentration at the steel ring by deforming and absorbing higher stresses in the undamaged material. Therefore, stresses in this zone from spalling time and onward are higher than the central portion, and also higher than (E) sample too (**Figure 7.6**).

Linking to previous loaded sample groups, despite longer heating time simulation here, which is around four times longer than the loaded samples, the highest peak of the minimum principal stresses from **Figure 7.5-a** is almost equal to the peak values of the 12% loaded samples from **Figure 7.3-a**. Additionally, the peak tensile stress in (D) and (E) samples from **Figure 7.5-b** are

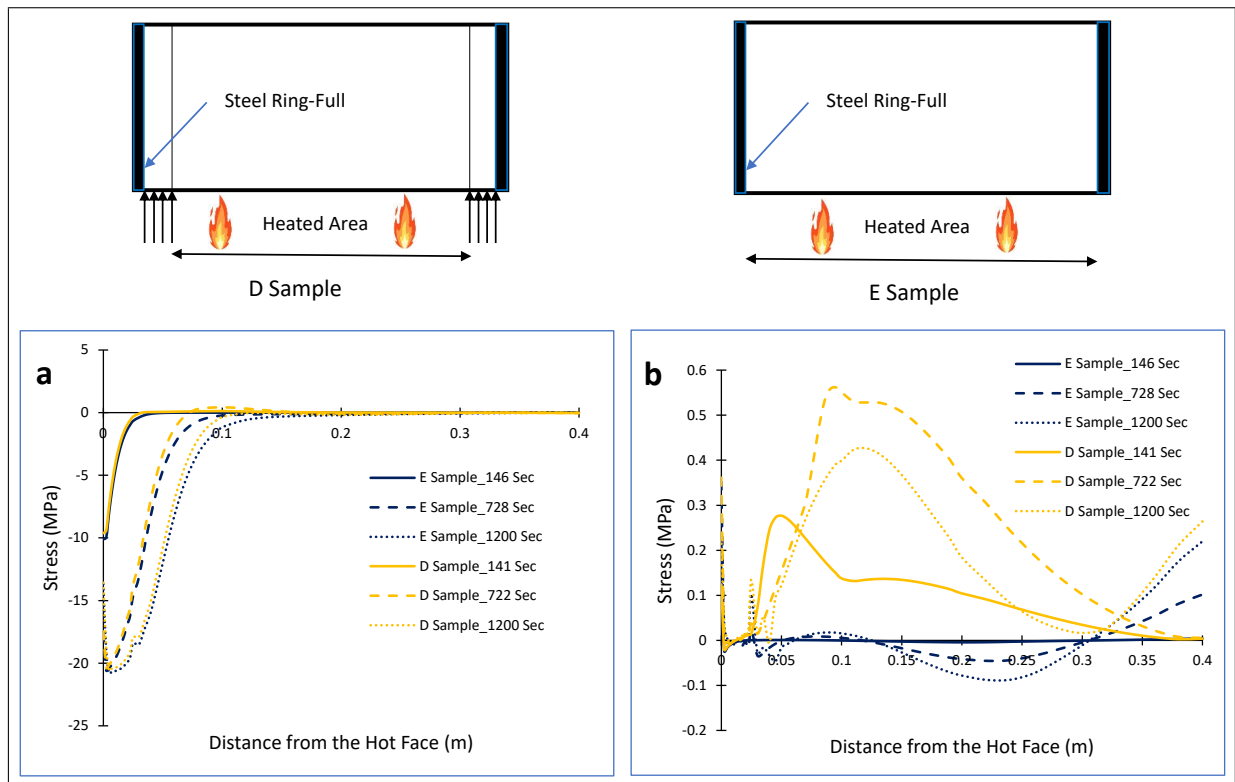


Figure 7.5: **a** Minimum principal stress and **b** Maximum principal stress through thickness of the restrained sample at different heating times

significantly smaller than 12% loaded samples shown in **Figure 7.3-d**. This suggests that testing unloaded samples under the effects of only passive restraint might give unrepresentative results in the context of assessing loaded samples. This is because, first, structural members would always be loaded to values larger than 12% from service dead and live loads and the effects of transient thermal strain would not be manifested accurately in the test outputs. Second, The gradual development of the stresses with heating due only to passive restraints would lag the true effects of transient thermal strain in these tests compared to samples loaded prior to heating. Third, the steepness of the stress transition between compression and tension is much lower than 12% loaded samples. While steepness of this transition is the trigger of the spalling, this has been underestimated in the restrained samples and this significantly misleads the test outputs.

To sum up, it seems that in restrained samples the load intensity through the thickness of the sample is not affected by the cold spring ring which is preferable to simplify experimental tests, however some effects can be observed at the exposed surface which may not affect stress state gradients and therefore potential spalling. The restrained samples are not a good representative sample to be used in assessing members that may be subject to initial loads in reality. Lagging of transient thermal strain development in restrained samples affects the results significantly and may mislead the assessment accordingly.

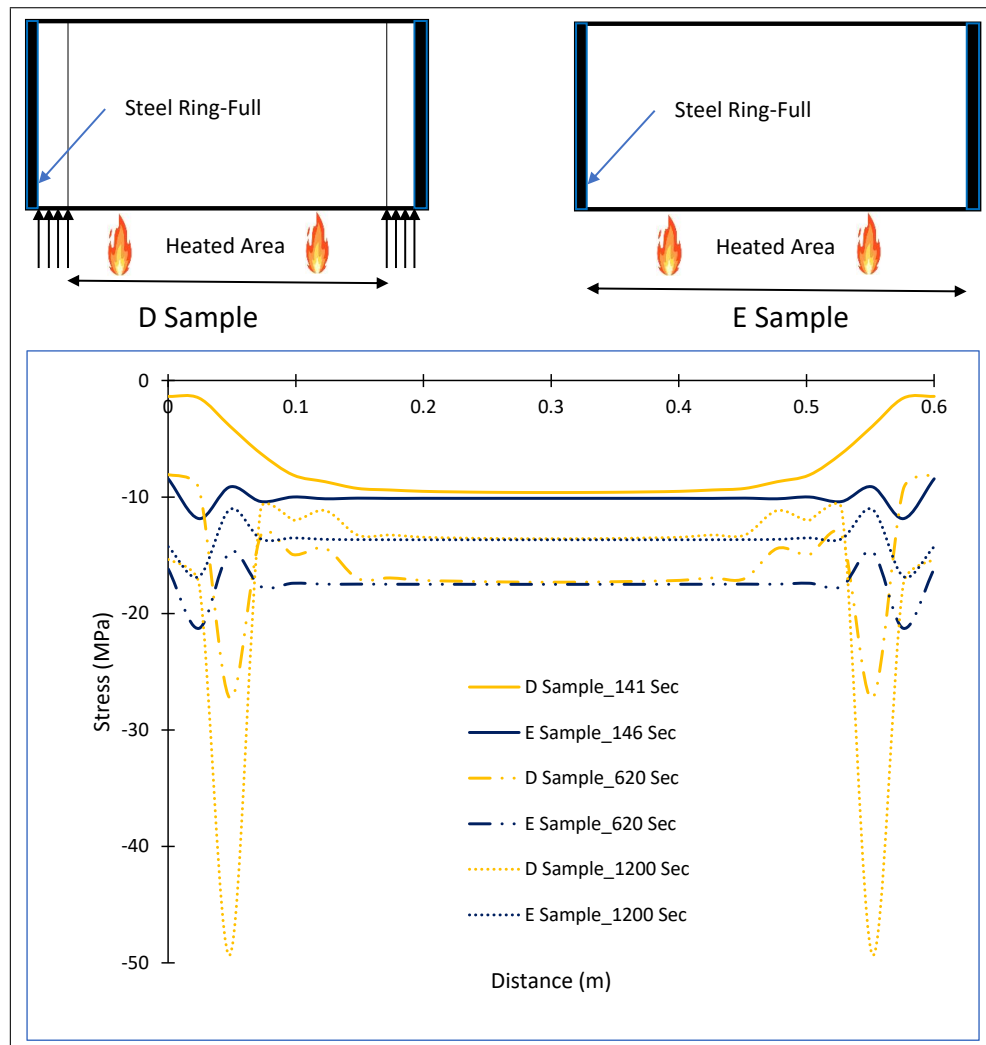


Figure 7.6: In-plane stresses at the exposed surface along a central axis with the length of the sample for restrained samples (D and E samples shown in Figure 7.1) at different time steps

7.3.3 Eccentrically loaded samples

Eccentricity cannot be predicted precisely for compression members in structures. It may arise for various reasons like difference in span of beams supported by a compression member or due to variation in live loads during the service life of the structure. This is particularly critical in multistory buildings where variations at any storey can cause transference of the applied loads eccentrically. To investigate eccentricity effects, two samples loaded to 9.60% of their compressive strength (6.70 MPa) but with the load placed eccentrically from different sides as shown in **Figure 7.1-F,G** have been investigated. The platens at the top and bottom of the sample are considered to exhibit perfect friction and to resist pushing back of the loading frame due to thermal expansion of the sample. To achieve this in the ABAQUS model, an initial vertical displacement was applied as the vertical boundary condition, with an amount equivalent to that caused by the initial applied load at ambient temperature and the displacements in the other two directions were restrained. The (F) sample, with the eccentric load near to the exposed surface shown in **Figure 7.7**, is the experimentally tested case, which according to the test results first spalled at 420 seconds of exposure to the heating source. At the nearest model time step to the

spalling time (463 seconds) the temperature at the surface reached 139°C as shown in the 3D section view of the sample in **Figure 7.7**. Results of minimum and maximum principal stresses

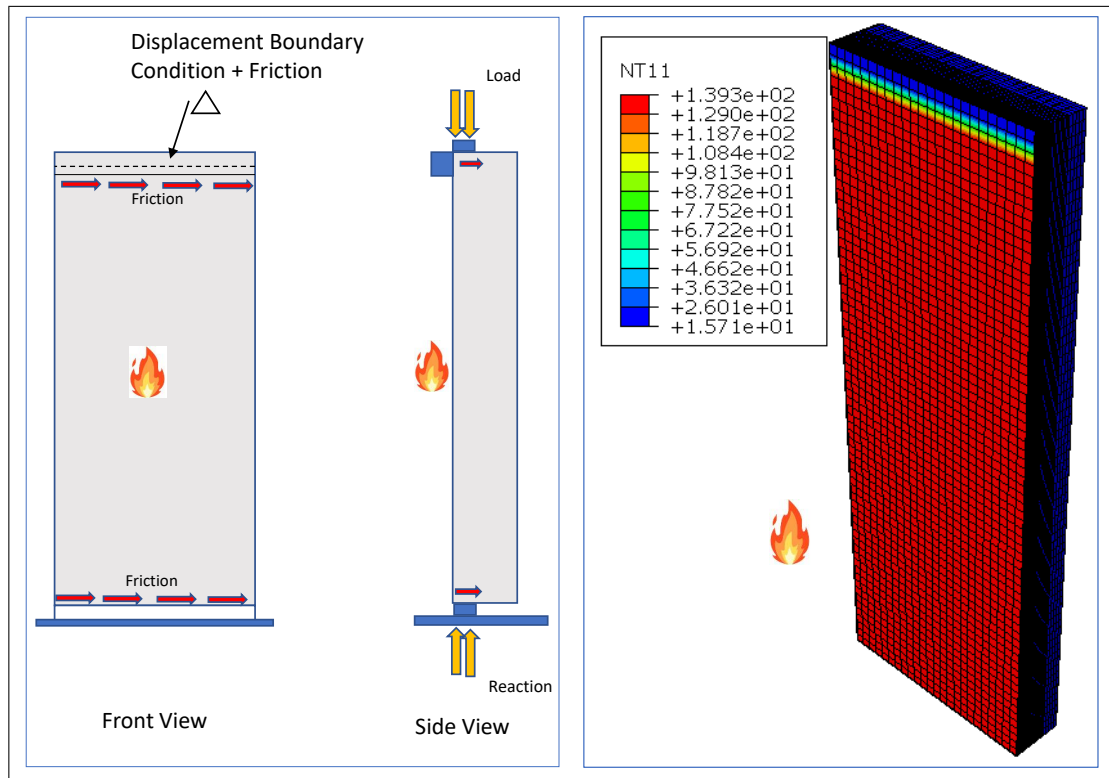


Figure 7.7: Test set up and temperature profile of (F) Sample at nearest time step to spalling

through sample thickness at the centre before spalling, at spalling and after spalling time (even it is unrealistic) are shown in **Figure 7.8-a-b** respectively. In the compressive zone near the hot face, different behaviour can be seen starting from early on depending on the location of the load with respect to the heating (**Figure 7.8-a**). Up to 164 seconds, for both samples, the stress peaks just beyond the heated surfaces are below the yielding limit of concrete in compression. Around the spalling time (463 seconds), the stress value for the (F) sample near the heated surface has considerably exceeded the compressive yielding limit ($0.30 \times 70\text{MPa} = 21\text{MPa}$) in comparison to the (G) sample, which is just below the limit. Beyond the spalling time, stress peaks for the (F) sample are much higher than the values for the (G) sample. At all time steps, the stress values in the (F) sample are higher than in the (G) sample all through to the middle of the sample where the situation is reversed. That is, the peaks in the (G) sample become more severe towards the rear of the sample while a significant reduction in stress can be seen for the (F) sample. Furthermore, the (G) sample stresses have a tendency to shift towards a tensile state between 50 mm & 150 mm from the heated surface while for the (F) sample compressive behaviour remains dominant. It is also worth noting that for both samples, unlike what has been observed in the concentrically loaded samples discussed before, at deeper portions of the sample thickness the results do not rest at the initial applied value (6.70 MPa). This is due to the deformations that the samples experience due to the combined effects of the eccentric load and the heating.

It seems that test set ups and more particularly initial displacement states at the ambient temperature play crucial roles in directing these different behaviors in the samples. At ambient

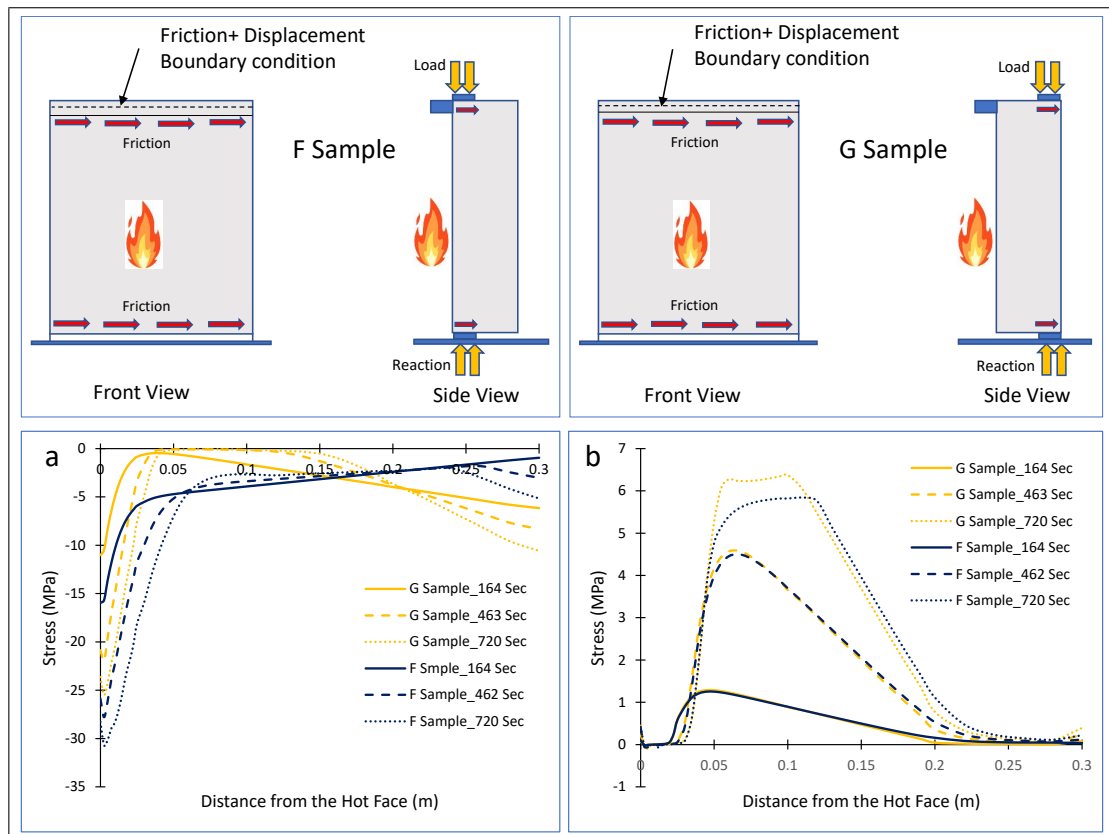


Figure 7.8: **a** Minimum principal stress, and **b** Maximum principal stress of through thickness of the eccentrically loaded samples

temperature, both samples have the same initial displacement but with different directions depending on the location of the initially applied eccentric loads as shown in **Figure 7.9**. For the (F) sample, the initial displacement is away from the heating source. As heating progresses, the exposed surface tends to displace toward the heat source. Therefore the overall displacement decreases with increasing heating time but the surface stays concave to the fire. Conversely, for the (G) sample, the initial displacement is towards the heating source and with progressive exposure to heat the surface tends to displace further in the same direction. Therefore, the overall displacement increases with increasing heating time resulting in bending the sample further towards the heating source. Consequently, the front hot face stretches meanwhile the cold face squeezes resulting in second compression stress peak generation at the rear cold zone (**Figure 7.8-a**). This second compression peak stress, which increases in time and has intensity higher than the initial applied stress, relaxes the compression peaks in the hot front zone at all heating time steps.

Regarding the tensile zone seen in the middle of the sample, interestingly in the early stages of heating up to 462 seconds there is very little difference in the stress results for the (F) and (G) samples **Figure 7.8-b** and the peaks are below the yielding limit in tension ($0.09 \times 70\text{MPa} = 6.30\text{MPa}$). However, in the later stages of heating (720 seconds) the (G) sample has higher tensile stress with the peak reaching the yielding limit while the peak of the (F) sample remains just below it. In both samples, the sharp rise in the maximum principal stress corresponds with the position that the minimum principal stress sharply reduces **Figure 7.8-a** and

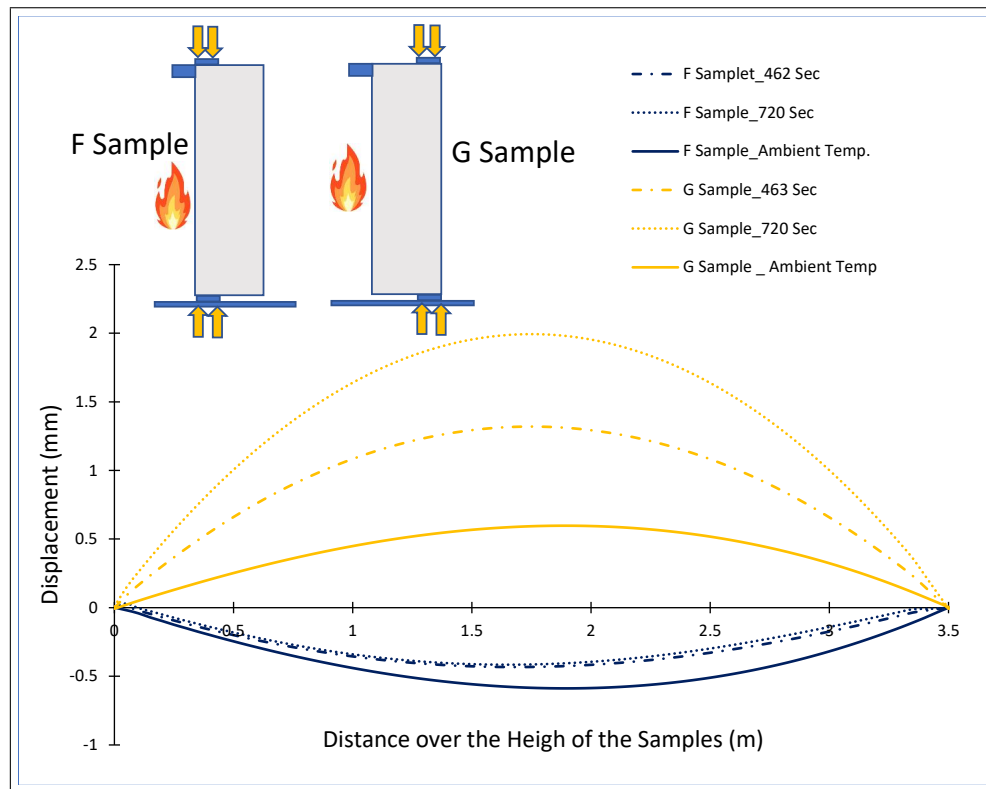


Figure 7.9: Displacement at the exposed surface along a central axis passing through the height of the samples with front and rear eccentric loads at different time steps

this makes a steep transition zone favourable to trigger spalling upon exceeding compressive (21 MPa) and/or tensile (6.3 MPa) yielding limits. Based on these observations and those from the compression zone, it seems likely that the (F) sample, with a more drastic stress transition, would be more susceptible to spalling than the (G) sample and that the differences in stress state are due only to the different test set up. Unlike to compression zone, test set ups and more particularly initial displacement states at the ambient temperature seems to affect less noticeably the tensile stress development. Tensile stresses stays with very little differences at both samples up to around spalling time and with very small progress afterwards, inferring that the compression failure cause spalling within the stress transition zone.

Alongside with the observed different behaviors derived from different initial displacement states, it is worth mentioning that displacement change in time is more pronounced in (G) sample comparing to (F) sample (**Figure 7.9**). In the former, the change in intensity up to four times of the ambient temperature can be noticed at 720 seconds, while in the latter the change is half of the ambient intensity. This means that the (F) sample behaves in a stiffer manner under the combined actions of the static and heating loads meanwhile the latter one can behave in a more softer way. These observations may be more pronounced if higher initial applied load would have used.

These outcomes should be taken into consideration while designing a test set up because they may significantly affect the stress state results and therefore potential for spalling. Assessments based on the results from particular eccentricity scenario would be inaccurate if they are applied for a member with different eccentricity due to underestimating the stress states and hence

spalling potentials.

These outcomes are stemmed only from the testing set up and the way the samples have been loaded. They emphasize on the cruciality of test set up in altering test outputs. Therefore it is strongly recommended that the expected real behaviours would be reflected in the testing configuration aiming to have more reliable test outcomes. In case of more than one possibility due to factors like shifting eccentricity from one side to another of the sample, the most critical outcomes from different scenarios can be chosen to ensure a more conservative assessment.

7.4 Conclusions

Load type, its intensity, and factors relating to test ups and the load application have been investigated numerically in this chapter. This is to understand how crucial are they in changing the behaviour, stress states and therefore potential of spalling of concrete samples upon exposure to elevated temperatures. Some experimental methodologies incorporating different load ratios, various boundary conditions and test configuration have been chosen from the literature to be simulated and investigated in this work. Some more hypothesis cases, to cover various different boundary conditions and test configurations, extended from the adopted experimental tests have also been simulated.

Some important conclusions have been drawn that should be taken into consideration while testing loaded samples under the effects of elevated temperatures. Some of these relate to the test methodologies and some relate to the details relating to ensuring precise boundary conditions and maintaining them during the entire test duration.

In terms of test methodologies, load type, load intensity and the way it is applied are found to significantly affect the test outputs. Samples loaded prior heating behave quite differently and seem to have the potential to spall much earlier than samples loaded through restraints where the load develops and intensifies gradually with heating progress. Additionally, increasing load intensity in pre-loaded samples also alters sample behaviour significantly and potentially accelerates spalling due to increasing steepness in transitioning compression stress to tension stress. On the other hand, samples loaded concentrically experience different behaviours compared to those loaded eccentrically. Most importantly the eccentric samples themselves behave very differently if the eccentricity shifts from one side to another side of the sample under same load intensity. Eccentric loads near by the heating source make the sample to behave in a stiffer way comparing to a softer behavior if the eccentric load is on the cold side of the member.

Apart from test methodologies, details relating to boundary conditions and test configurations can also have significant effects on the results. For example, maintaining the load intensity during test through preventing its pushing back due to expansion of the sample, providing full friction in the test set up between the sample at its contact areas with the testing apparatus can significantly alter the samples behaviour and hence the test outputs. While this may be practically hard to measure precisely, in numerical simulations this has significant impact on the results if investigations are extended numerically. Friction adds more compressive strength to the sample

meanwhile relaxes the developed tensile stresses.

To sum up, in order to have a more reliable test output, it is very crucial to choose a test methodology that can represent the real structural member condition in relation to load intensity and the way it has been applied. This is in addition to providing correct boundary conditions and maintaining them during the test. Otherwise, assessments based on the results from a test with particular methodology and configuration would be unsafe or irrelevant to be applied on other cases having different behaviours or load intensities from what have been reflected in the test.

Chapter 8

Effects of Cold Rim on Concrete Behaviour and Spalling at High Temperatures

8.1 Introduction

Cold rim is an unheated area surrounding the heated area of a sample that is considered may act as a self restrainer imposing stresses in the heated concrete and therefore triggering spalling. In this chapter, effects of cold rim on concrete behavior and its spalling have been investigated in details.

In real cases, cold rims might appear where structural elements partially heat during a fire incident. However, in laboratories cold rims have been modeled in different ways, often resulting from practical considerations of test set up, where the sample necessarily rests on the walls of a furnace and the periphery is consequently unheated.

Cold rim effects have not been intensively investigated in the literature, besides so far findings are still inconclusive and questionable. It is not clear enough if the observed results are relating to the mechanical characteristics of the cold rim or its heating status or both.

In this chapter, cold rim effects have been investigated thoroughly considering different tests from the literature utilizing the coupled thermo mechanical ABAQUS model developed in Chapter 3. Test results have been simulated first, then different scenarios proposed and investigated under the same testing conditions to investigate the cold rim effects in details through comparing stress and displacement states.

Investigation results show that cold rim effects can not be confirmed most of the times, and they are very sensitive to other factors relating to the boundary conditions, sample size, sample shape, test configuration, and test methodology. Results also show that cold rims do not change behaviour across the thickness of the samples, even though in few cases cold rim has found to have some superficial effects only at the exposed surface, they are specific to the test under consideration and can not be generalised.

8.2 Cold rim configurations

Following the same procedure adopted in previous chapters, samples selected here also cover loaded structural and unloaded nonstructural elements. Six samples from the selections made in **Chapter 4** and shown in **Figure 4.1** have been selected and simulated with dimensions, test set ups, and extended cases used in investigations shown in **Figure 8.1**. They cover common cold rim configurations observed in the literature [4, 3, 37, 50, 33, 38] falling within the three

main literature categories discussed before in **Chapter 3**, namely heated then loaded samples, restrained then heated samples, and loaded then heated samples.

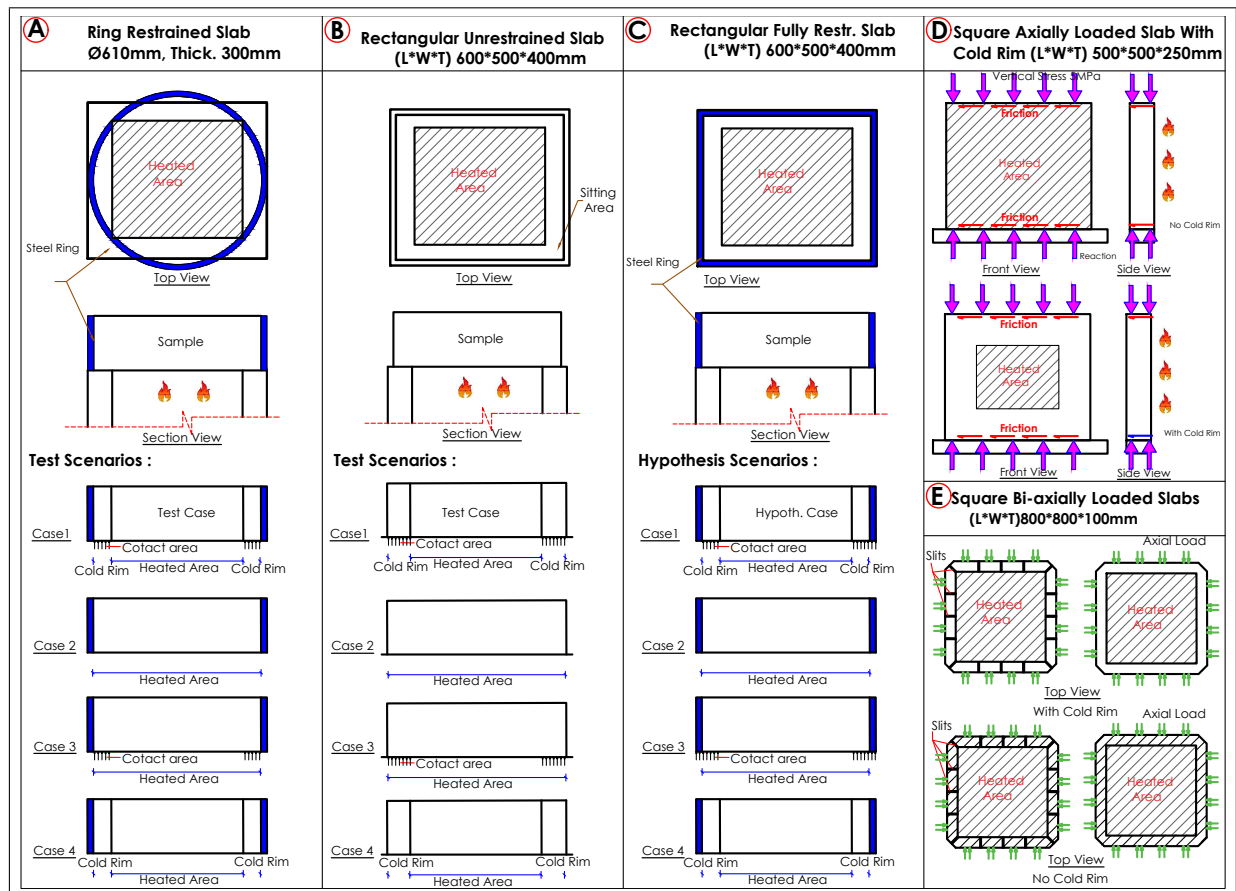


Figure 8.1: Cold rim configurations showing heated areas, mechanical restraints, loading, and different hypothetical test scenarios

Some of these configurations were considered in previous chapters for different reasons, such as to investigate how they ease effects of stiff external steel restraint on heated concrete. Here, a holistic cold rim investigation is the aim, therefore different shape samples recalled and more scenarios have been added for each case to investigate whether the cold status or mechanical status of the cold rim may affect the results and whether sample shape and various boundary conditions may contribute too.

The first sample (Figure 8.1-A) is a ring sample fully restrained inside a steel ring having cold rim around its perimeter along the furnace walls where the sample rests. Case 1 shown is the experimentally tested scenario from which, for the purpose of the parametric investigations, three more cases have been derived as labelled in the Figure (Cases 2, 3 & 4). Case 2 is the sample without cold rim to expose its entire lower surface to the heating. Through comparing this to Case 1, cold rim effect can be observed. Case 3 is identical to the tested case but with heating the restrained sitting area, this is practically hard but can be achieved numerically. Through this, effects of heating status of the restrained sitting area can be investigated. Case 4 is again identical to the tested case but the sitting area is cold and unrestrained. Through this, restrain status of the cold rim can be investigated. Ultimately, through all these cases, concerns whether cold rim, which is usually artefact in experimental tests, may act as self restrainer can be investigated.

It can be determined whether the heating status of the restrained sitting area or its mechanical characteristics or both may change behaviour of the sample.

The second sample (Figure 8.1-B) is an unloaded rectangular sample that sits on the furnace walls freely with a cold rim at the contact zone. As for the A samples, three more cases labeled as Case 2, 3 & 4.

The third sample (Figure 8.1-C) is a rectangular sample fully restrained by a steel frame around its circumferences (similar to the A sample) and again Cases 2 to 4 are also considered. This sample was originally tested as a partially restrained sample in which only a portion of its thickness restrained, however hypothetical scenarios have been considered here with all the thickness restrained to be consistent with A sample. Investigating these three configurations (A, B, and C) allow the effects of cold rims to be isolated, if exists, from sample shape and mechanical restraint effects.

The fourth sample, which is to investigate cold rim effects in initially loaded samples, is a uniaxially loaded sample aligned vertically with its front face subjected to the heating source as shown in Figure 8.1-D. It is loaded with 5 MPa of stress (12% of the sample's strength) applied vertically over its thickness prior to exposure to heating. The concentric rather than eccentric load sample considered here to minimize complications and intensify the cold rim effects in an ideal state. For the purpose of the investigations another testing scenario has been derived in which only the central 250 mm × 250 mm portion of the sample's front face is heated (Figure 8.1-D) and the rest area will remain as cold rims surrounding the central heated area. A displacement controlled boundary was applied, with the assumption of perfect friction between the platens and sample.

The fifth configuration, which is to investigate cold rim effects in biaxially loaded samples, considers two biaxially loaded samples (loaded through 10 MPa stress (17% of the sample's strength)). One has a cold rim around its circumference where it rests on the furnace walls, while the other has slits cut across the cold rim to eliminate the transmission of circumferential loads as shown in Figure 8.1-E. For the purpose of the investigation, the same two samples have also been simulated under a scenario where their entire lower surfaces are subjected to the heating source, i.e. no cold rim.

The concrete material used in these samples covers NSC and HSC with compressive strength 42 MPa for the unloaded rectangular samples (B & C) and the loaded square sample (D), 70 MPa for the ring sample (A) and 60 MPa for the biaxially loaded samples (E). The standard ISO834 fire curve was applied in the tests for all samples considering the hatched area as the heat exposed area in all figures.

8.3 Analysis results and discussions

As in previous chapters, for the purpose of the analysis in this chapter, a coupled thermo mechanical finite element model developed in Chapter 3 [85] has been adopted. A brief summary from other chapters for each tested sample have been restated here to ease comparison for newly

proposed cases in this chapter.

8.3.1 Unloaded restrained ring sample

As a recap from previous chapters for the tested sample, the ring sample test set up and boundary conditions are shown in Figure 8.1-A-Case1. As reported in [4], under experimental testing it experienced two spalling events with depths of 73 mm and 80 mm at the same time after 540 seconds of exposure to the standard ISO834 fire curve. The temperature profile at a depth of 50 mm from the exposed surface was also recorded and is shown in Figure 8.2-a along with the model prediction of the same. Considering this an accurate capturing of the thermal response of the sample, the temperature at the exposed surface at the nearest time step to the time of spalling was predicted to be just over 150°C (Figure 8.2-b). 3D cut views of minimum and maximum

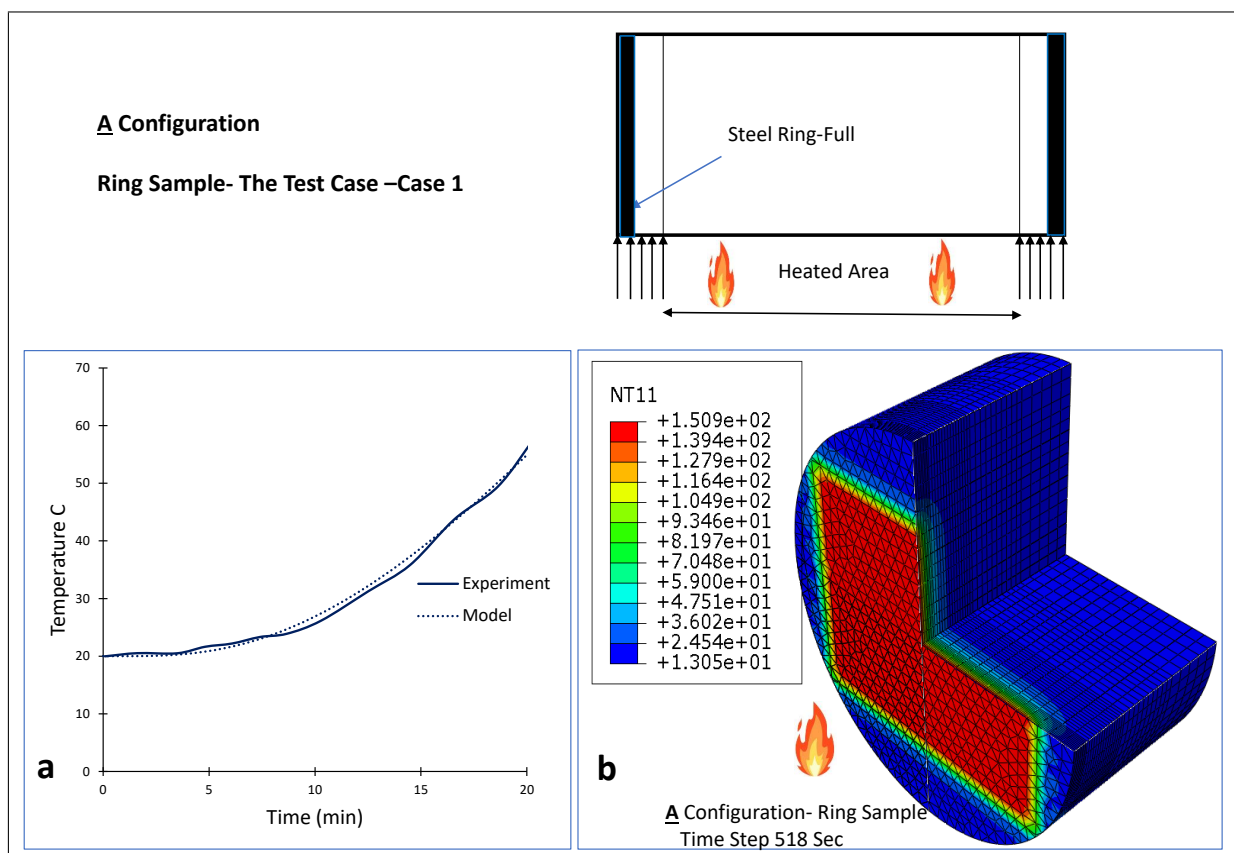


Figure 8.2: a) Temperature profile in time, 50 mm from the heated surface of the ring sample (configuration (A)), b) 3D section showing the temperature profile in the ring slab (configuration (A)) at closest time step to time of spalling (540 s)

principal stresses at the nearest time step to the spalling for Case 1 and Case2 samples from Figure 8.1-A have been presented in Figure 8.3. Case 1 is the experimental test case, while Case 2 is the extended scenario in which there is no cold rim and the entire lower face of the sample is heated. Furthermore, plots showing the minimum and maximum principal stresses along their center lines at different times are presented in Figure 8.4. Considering the compressive zone seen in the minimum principal stress, which is highly stressed up to 10-15 mm from the exposed surface surpassing compressive yielding limit ($0.30 \times 70MPa = 21MPa$), no appreciable

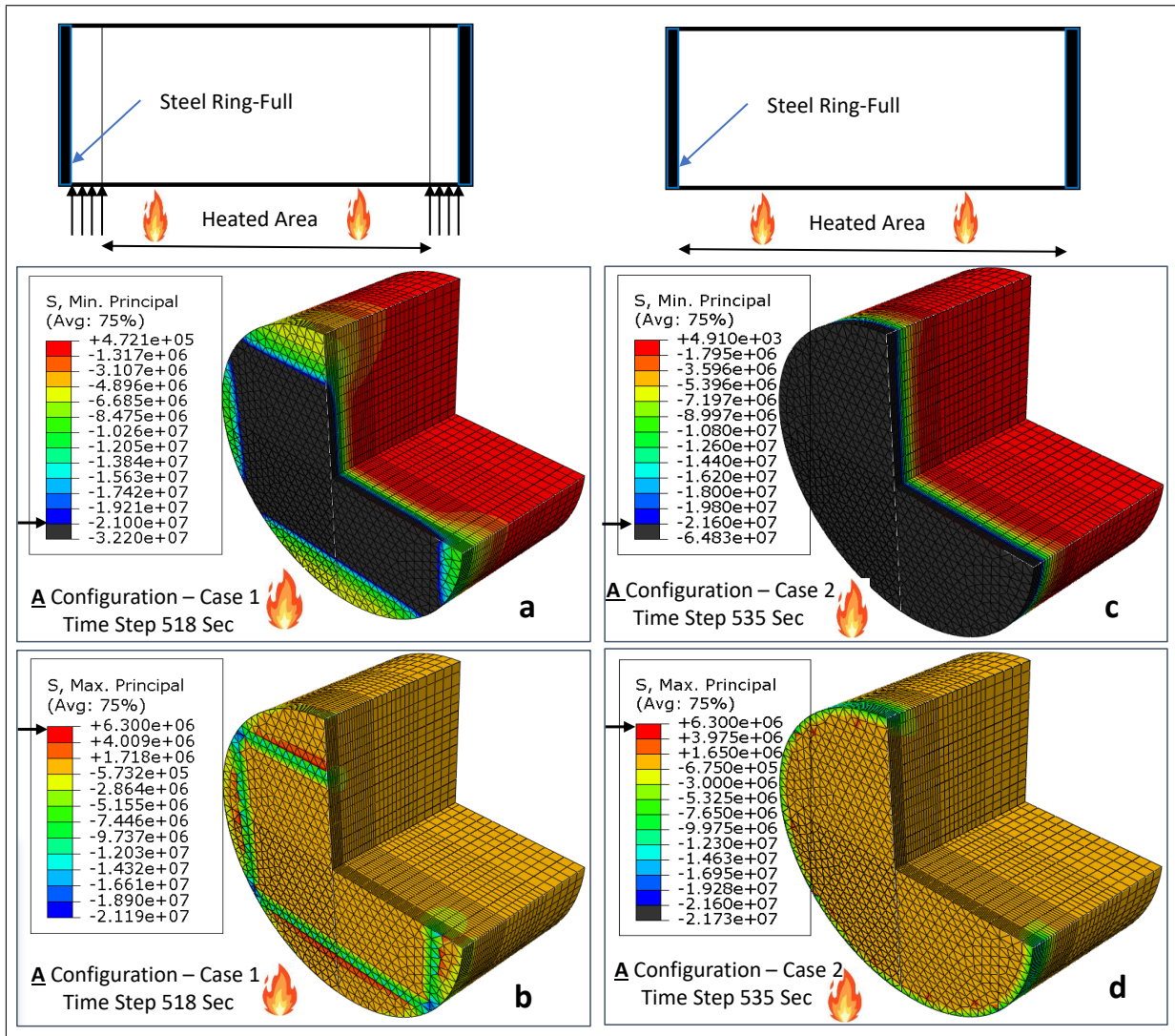


Figure 8.3: 3D sections of minimum and maximum principal stress profiles as close as possible to time of spalling in a), b) configuration (A) Case 1 & c), d) configuration (A) Case 2

difference can be seen with or without a cold rim (Figure 8.4-a). Just beyond the exposed surface, very similar stress peaks develop in both cases, increasing in time then transition toward the tensile zone, deeper from the exposed surfaces.

Unlike to the stress profiles at the centre of the samples, noticeable differences in compressive stress behaviours can be observed over the exposed surfaces. As is clear from the 3D views (Figure 8.3-a,c), a yielded compressive zone (black colour) covering the entire lower exposed surface of the sample can be seen for the A Sample Case 2 (Figure 8.3)-c in comparison to the the A Sample Case 1 in which the cold regions remain at relatively low stress and only the central area of the exposed face has yielded (Figure 8.3)-a. In both cases, the stresses are higher than compressive yielding limit 21 MPa. For the Case 2 sample the stress intensity at the exposed surface is almost twice the Case 1 value which can be attributed to the different test configurations adopted for the two samples relating to the availability of cold rims. For the Case 2 sample with its entire lower surface heated, the entire surface deteriorates and its strength capacity is undermined under the combined actions of the heating, entire surface expansion, and the reaction from the stiff steel restraint around the outside of the sample. However, for the Case

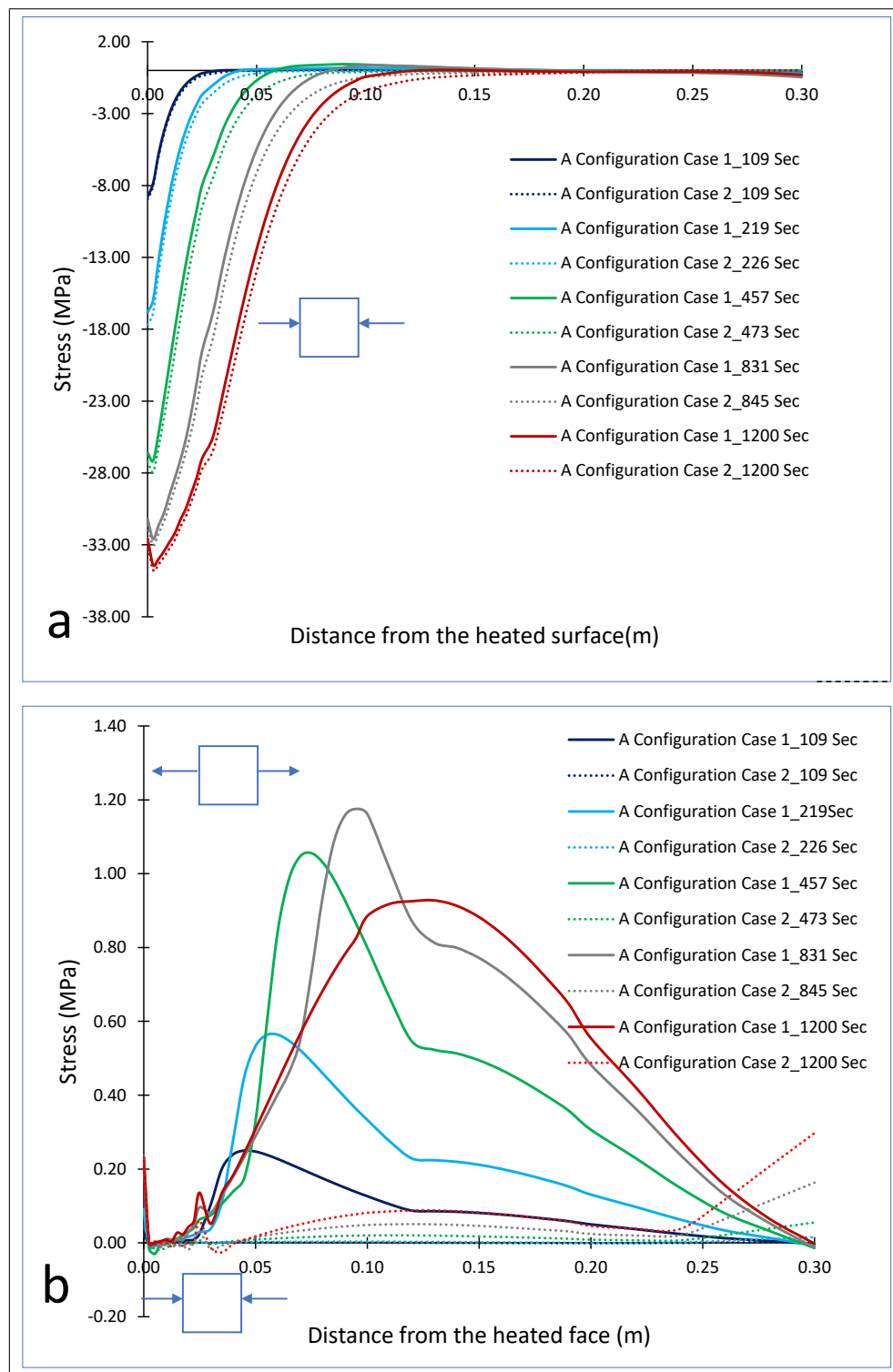


Figure 8.4: a) Minimum and b) maximum principal stress profiles through the centreline thickness of the ring sample (configurations (D) Cases 1 & 2 at different times

1 sample only the central area of the lower exposed surface yielded and the cold rim between the heated zone and the restraint ring remained intact. This region can be considered to act as a spring with less stiffness than the restraint steel and so relaxing the severity of the reaction against the lateral expansion of the exposed face under heating. This means that, where a stiffer steel restraint is present around the sample, a cold rim would act to lessen the developed stresses at the exposed surface. This is contradictory to the literature where it is suggested that a cold

rim imposes more stress on the sample. Therefore, to spall the whole surface of the the Case 1 sample, more time and intenser stress would be required.

Now considering the tensile zone seen in the maximum principal stress, even though it can be observed from Figure 8.4-b that the existence of a cold rim results in more tensile stress, the magnitudes and hence the actual difference is likely too small and well below tensile yielding limit ($0.09 \times 70MPa = 6.3MPa$) to cause any significant change in behaviour or cause spalling. Furthermore, existing of cold rim makes the tensile stress to increase in time (up to around 830 sec) until reaches certain value then decreases toward compression zone meanwhile if cold rim is omitted, the tensile stress vanish and becomes negligible. Observing tensile stresses with intensities far smaller than than yielding limit in tension even at higher temperatures is another indication confirming that the cold rim effects are negligible in imposing stress severe enough to change the concrete behaviour significantly. Likewise, from (Figure 8.3-b,d) no significant alterations caused by the cold rim can be noticed at the exposed surface except shifting of the compressive stress ring at the vicinity of the sample contact with the furnace walls to the outer most region under the steel ring, again with values far below the yielding limit (6.3 MPa) to cause change in behaviour. Recalling compressive stress profiles seen in Figure 8.4-a, in both cases the recorded spalling depths match well with the sharp transition from compression to tension seen in the stress profiles through the thickness of the samples (Figure 8.4) around the spalling time. The compressive yielding limit has been surpassed significantly indicating spalling due to compression failure, starting from the exposed surfaces.

From the observed results it seems that, in this scenario, cold rim effects are negligible through the sample's thickness but might have some influences on the exposed surface. To investigate this in more details, in-plane stress developed in time along the sample's diameter parallel to the exposed surface for Case 1 and Case 2 samples are potted Figure 8.5. Over the 200 mm central length of the exposed surface, there is no appreciable difference in stress values between Case 1 & Case 2. However, looking from the centre towards the edges, the difference becomes more noticeable. A high stress zone can be observed in Case 2 within an approximately 30 mm circumferential strip directly attached to the external restraint ring because of the reactions from the very stiff steel ring. However, in Case 1, the unheated sitting zones have not deteriorated and can act as a spring between the steel ring and the central heated zone. While this spring area, being of relatively lower stiffness than the steel ring, relaxes stress concentration at the very outside of the sample, it causes stress concentration at areas where the cold and hot zones meet. While these results imply that the cold rim might trigger surface spalling at the exposed surfaces nearby the cold zones, the observed behaviours may also be affected by or derived from the mechanical characteristics and boundary conditions of the sitting (cold) area rather than its heating status. To investigate this, two more hypothetical scenarios, named Case 3 and Case 4 (Figure 8.1) have been considered. Case 3 is extended from Case 1 considering its entire lower surface heated but keeping the sitting area restrained in representation of fricitonal effects and Case 4 is extended from Case 1 with the removal of frictional restraint between the sample and the supporting walls of the furnace while keeping the contact area cold. In-plane

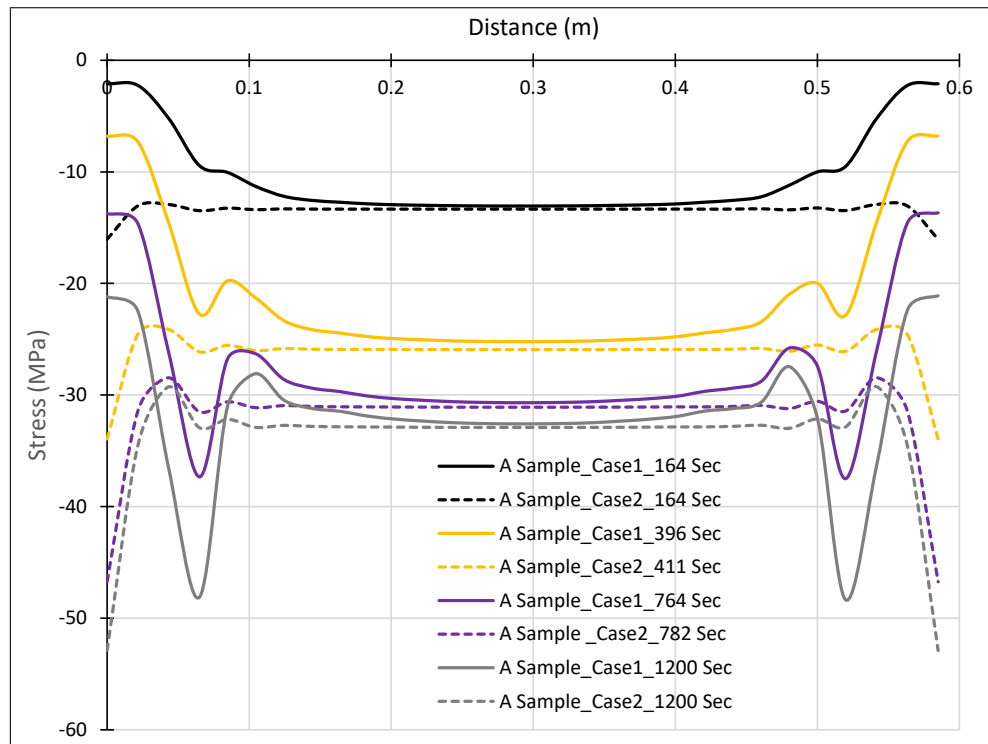


Figure 8.5: In-plane stress at the exposed surface of A samples Case 1 & Case 2 at different times

stress around the spalling time for the four scenarios are shown in Figure 8.6. It can be observed that it is not only the effect of the heating status of the cold rim that could change the stress development in the exposed area. The boundary conditions may alter the developed stress state too. For example, even though Case 1 and Case 4 have same exposed area and cold zones, lower stress intensity can be observed in Case 1 due to the frictional restraint effect between the sample and the supporting furnace wall, which makes the cold rim area dissipate more stress compared to if friction is not available. The effectiveness of frictional restraints at sitting areas can also be evidenced through comparing Case 2 and Case 3, which have the same exposed area with no cold zone but with different sitting area boundary conditions. Again lower stress intensity can be noticed for Case 3 due to the frictional restraint effects at the sitting area with the underlying furnace walls. Similarly, lower stress intensity can be observed if Case 1 is compared to Case 2. This is also true if Case 1 is compared to Case 3 where relaxation of stresses is seen in the presence of the cold zone. Through comparing Case 2 and Case 4, it appears the cold rim has the same effect, relaxing the intensity instead of imposing more stress as might be suggested in the literature [33]. Restraint effects due to friction on the sitting areas, even if heated, can have almost the same effect as a cold rim can have in relaxing the stress intensities as it is clear if Case 3 is compared to Case 4. These observations confirm that the explicit effects of the cold rim are hard to distinguish from the rest of the boundary condition effects and sometimes the cold rim acts in contradiction to what has been observed in literature. Therefore the observed behaviours cannot be associated only with the heat status of the cold rims.

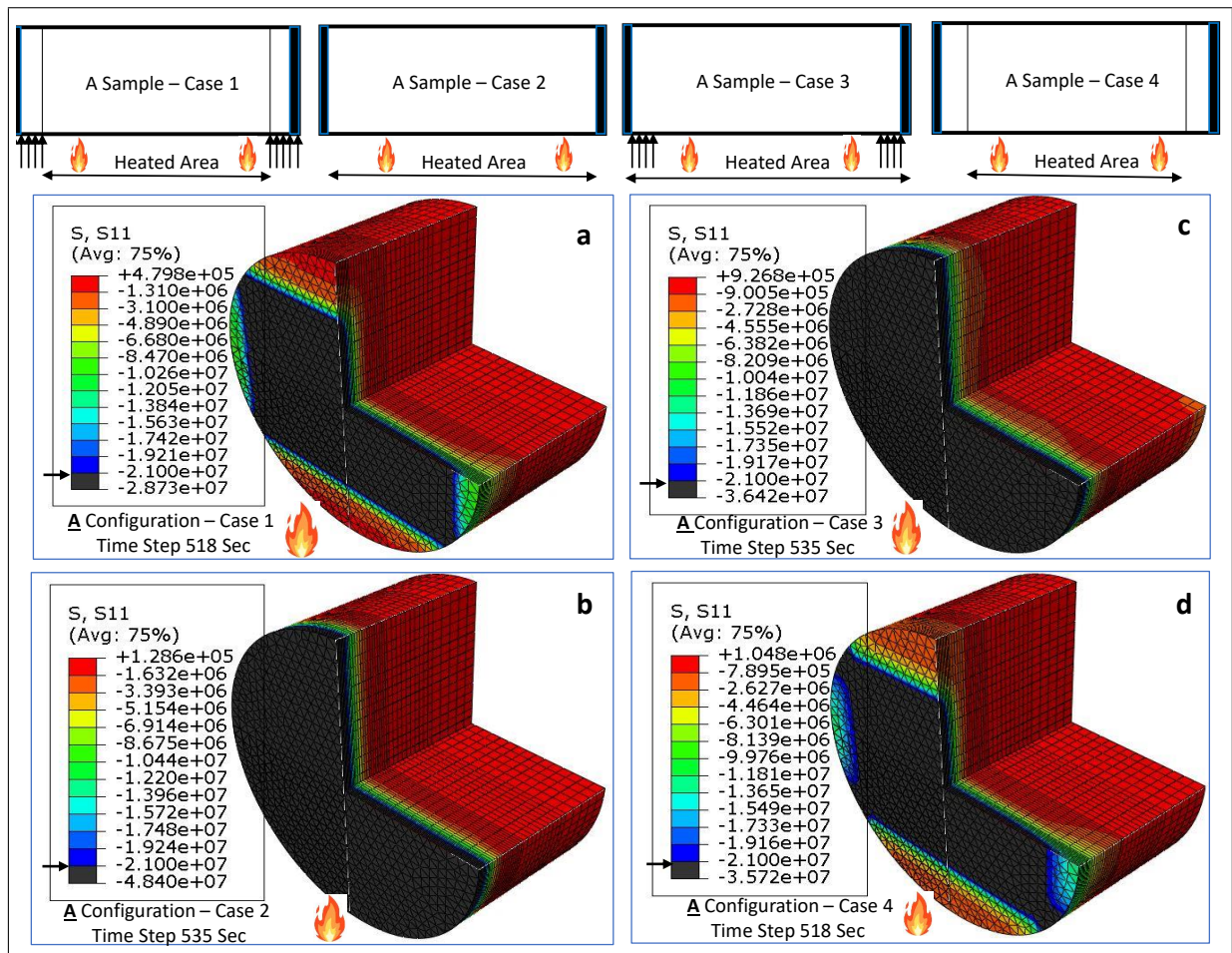


Figure 8.6: In-plane stress as close as possible to time of spalling at the exposed surface of A samples a) Case 1, b) Case 2, c) Case 3, & d) Case 4

8.3.2 Unloaded rectangular slabs

The unloaded unrestrained samples (Figure 8.1-B) and unloaded fully restrained sample, with a steel frame surrounding it (Figure 8.1-C) have been considered in this section. As for the ring sample, a brief summary from previous chapters have been recalled for each sample here then more scenarios are added to investigate whether cold rim heat status and/or its mechanical characteristics may affect the samples behaviours. The samples are identical in terms of geometry and material properties but different in boundary conditions. The Case 1 scenario shown in the figure for each B and C samples is the original experimental test set up from which other scenarios have been derived. The reported experimental temperature profile [4] at 30mm depth from the hot surface along with the model simulation is shown in Figure 4.3-a. Again, this is considered an accurate capturing of the thermal behaviour and accordingly, the surface temperature at the centre of the fire exposed area at the time of spalling for configuration (B) (reported as 660 seconds) is predicted to be 331°C and for the restrained sample (time of spalling reported as 600 seconds) is 304°C.

The depth of first spalling for each sample is reported to be 40 mm for the B Sample and 60 mm for the C Sample. To investigate the cold rim effects, the Case 2 scenario, which is without cold rim and the entire lower surface heated, has been incorporated into the investigations

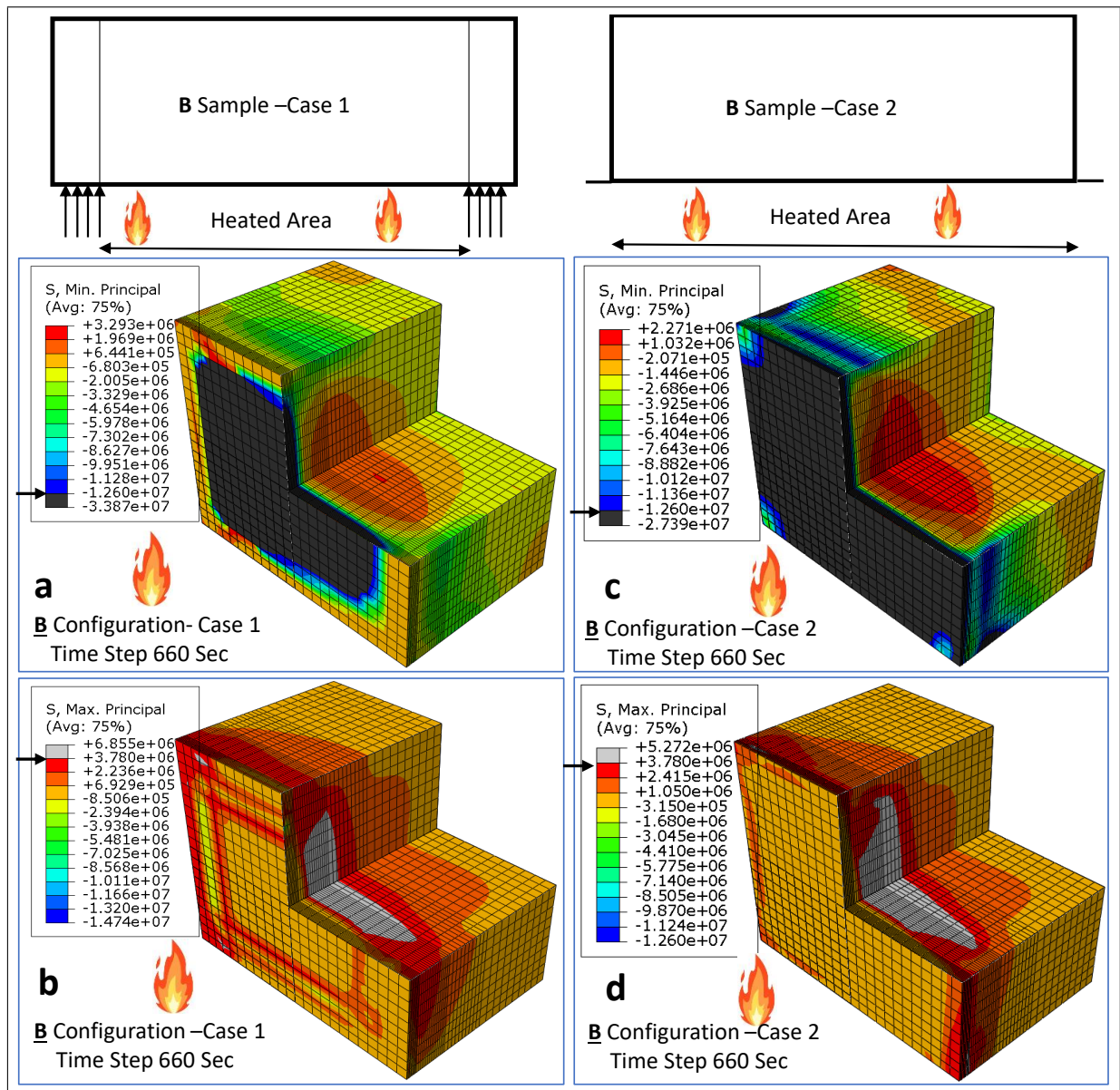


Figure 8.7: 3D sections of minimum and maximum principal stress profiles as close as possible to time of spalling in a), b) configuration (B) Case 1 & c), d) configuration (B) Case 2

for both B & C samples. 3D views of minimum and maximum principal stresses as close as possible to the time of spalling for both samples are plotted in Figure 8.7 and Figure 8.8 respectively. Furthermore, plots showing minimum and maximum principal stresses developed in time through the thickness of B and C samples (for Case 1 and Case 2) at their centerlines are shown in Figure 8.9. As it can be seen, for both B and C samples a yielded compressive zone with stress intensity surpassing compressive yielding limit ($0.30 \times 42\text{MPa} = 12.6\text{MPa}$) developed at the hot face with a tensile zone immediately behind it, deeper in the samples. For the B samples, the compressive stress intensity of the sample with a cold rim (Case 1) is slightly higher than for Case 2 (Figure 8.7-a,c) while for the C samples the opposite is true (Figure 8.8-a,c). Through the sample thickness, in general, for B & C samples no significant difference in compressive stress states can be observed from derived from lack or existence of cold rims Figure 8.9-a,c. These observations implying that while the cold rim has negligible effect through

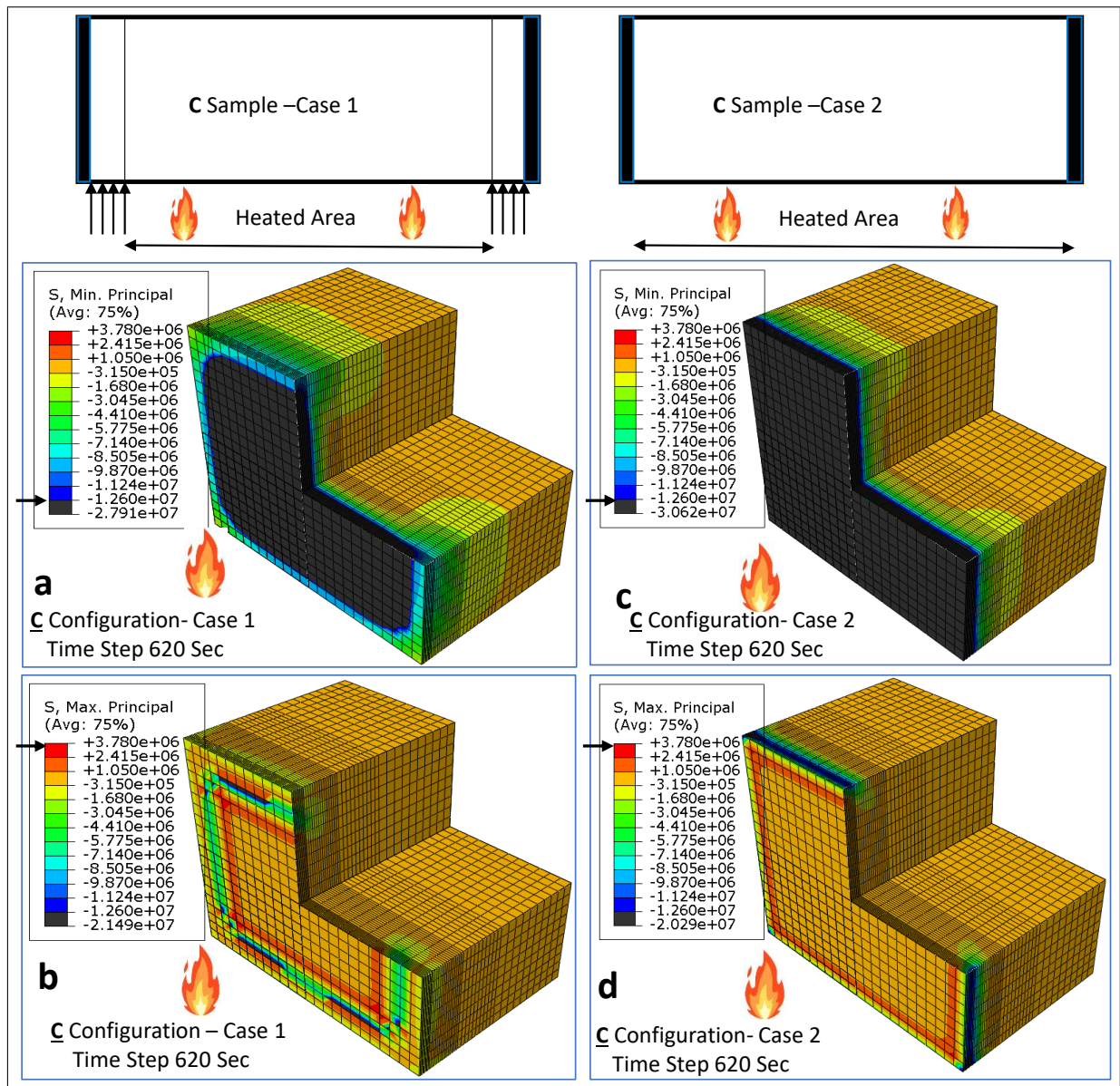


Figure 8.8: 3D sections of minimum and maximum principal stress profiles as close as possible to time of spalling in a), b) configuration (C) Case 1 & c), d) configuration (C) Case 2

the sample thickness, it may have some minor effects at the exposed surface depending on the boundary conditions of the samples. In the unrestrained sample (B Sample-Case 1), the cold rim may be acting as a restraint slightly increasing the stress at the exposed surfaces consistent with observation from the literature [33]. However, in the C samples any effect of the cold rim has been overwhelmed by the effects of the steel restraint and the cold rim actually relaxes developed stresses.

Regarding the tensile zone, different behaviours can be observed between B & C samples depending again on the boundary conditions of the samples (whether the sample is restrained or not). In the unrestrained B samples, a relatively narrower but more intense yielded tensile zone (grey colour around 70 mm wide), surpassing tensile yielding limit ($0.09 \times 42\text{MPa} = 3.78\text{MPa}$), can be observed just beyond the exposed surface for the sample with cold rim (Case 1) Figure 8.7-b compared to the relatively wider (around 100 mm) but less intense yielded zone in Case 2

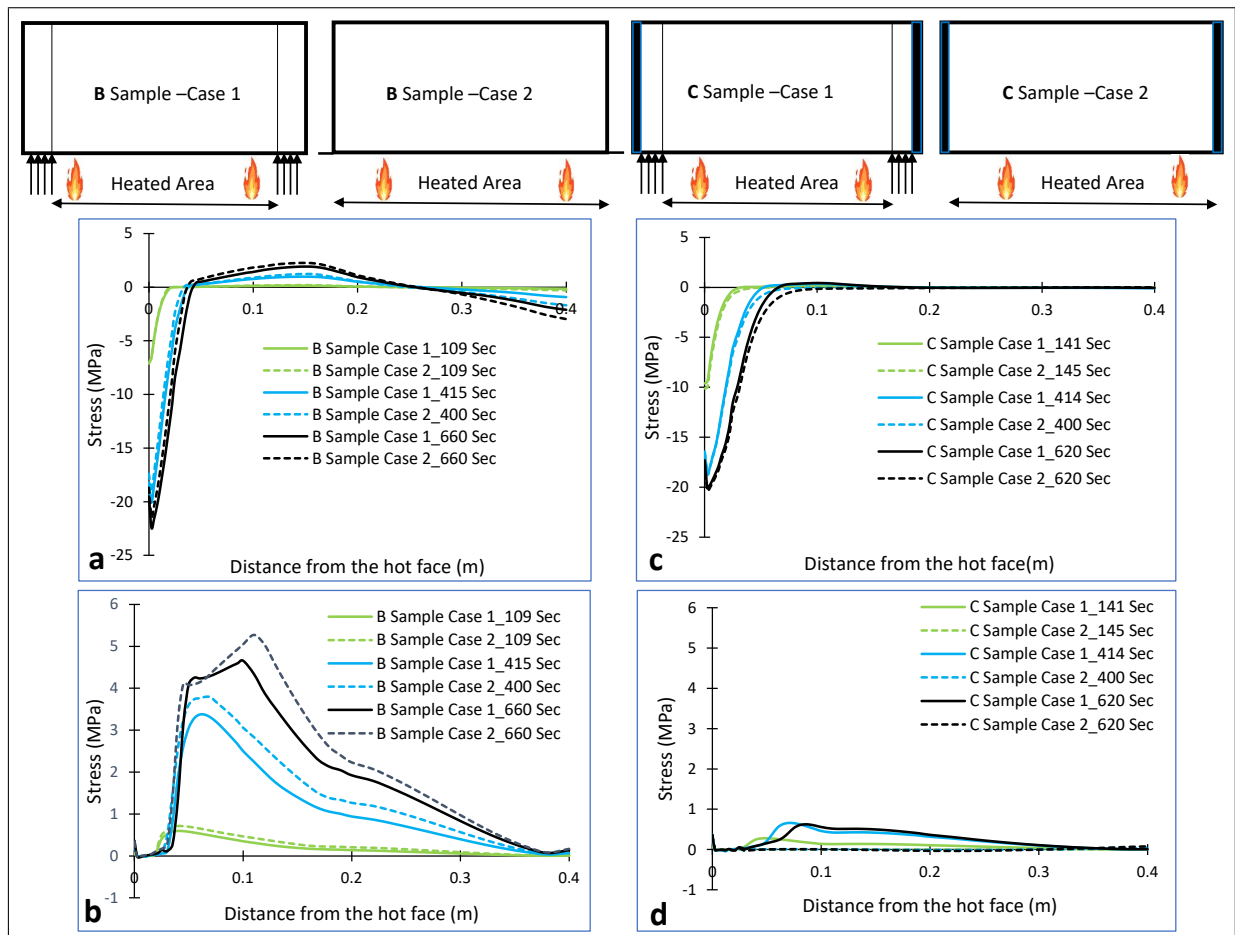


Figure 8.9: a) Minimum and b) maximum principal stress profiles through the centreline thickness of the B and C samples (Cases 1 & 2) at different times

(Figure 8.7-d). However, for the restrained C samples cold rim does not have appreciable effects compared to B Samples. Almost equal tensile stress intensity can be observed for Case 1 and Case 2 accompanied by a compressive area around the cold rim in Case 1 and a more pronounced circumferential compression strip at the outer sample boundary, under the steel retraining frame, for Case 2 (Figure 8.7-b,d). In slight contrast to this, some difference is seen in the tensile stress profiles through the thickness of the samples. Again apparently contradictory to the literature, the cold rim in the B sample reduces the developed tensile stress, reaching a maximum difference between Cases 1 & 2 of around 1 MPa at the time of spalling (660 seconds) (Figure 8.9-b). Given that the magnitude of the stresses are close to the yielding limit of the concrete (3.78 MPa), this difference could change the behaviour of a sample with a cold rim potentially moderating the likelihood of spalling.

The behaviour is different again in the C samples where the cold rim tends to impose around 0.5 MPa more tensile stress at the sample at spalling time (Figure 8.9-d). However, the cold rim effects may be considered negligible for the C samples given that the values are far below the yielding limit in tension (3.78 MPa).

It is worth mentioning that, for the B and C samples, the transition location from compression to tension around the time of first spalling fits well with the recorded spalling depth of the samples Figure 8.9, and in general, the developed compressive and tensile stresses for the B

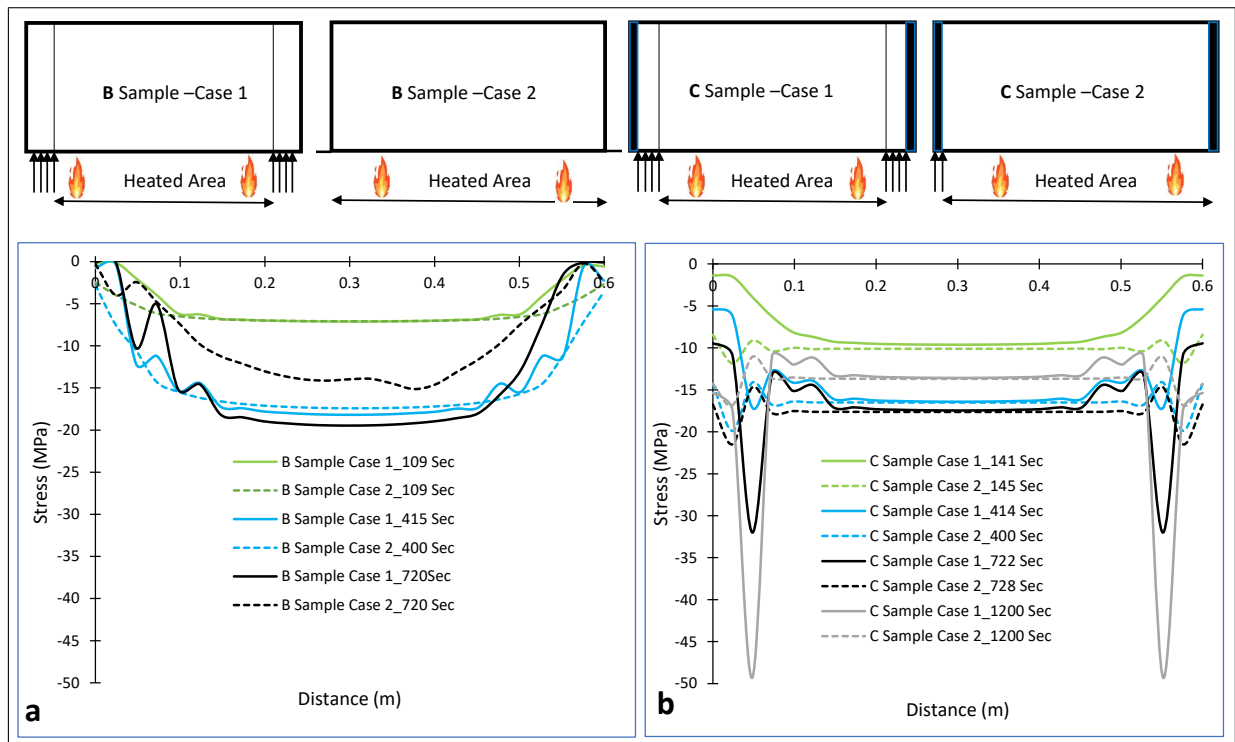


Figure 8.10: In-plane stress at the exposed surface of a) B Samples Case 1 & Case 2 b) C samples for Case 1 & Case 2 at different times

samples are higher than those in the C samples through the sample thickness. Spalling occurred in both sample, for the former both compressive and tensile yielding limit have been surpassed meanwhile for the later the compressive yielding has been severely surpassed.

All these observations, as it was observed in A samples as well, imply that the cold rim effects are very sensitive to the boundary conditions and its effects cannot be distinguished easily. While it has negligible effects on the stress development through B and C sample thickness, it seems to have some effects at the exposed surfaces, although these are dependent on other boundary conditions such as external restraints.

To investigate the exposed surface in details at different times, as has been done for the ring samples (A samples) in the previous section, in-plane stresses for Case 1 and Case 2 for each B and C sample along the length of the exposed surface parallel to the heating source are shown in Figure 8.10. Significant differences can be observed between the stress states depending on the boundary conditions and presence or lack of a cold rim. For the unrestrained B Samples (Figure 8.10-a), in the sample with a cold rim (Case 1) stress develops in time, while in Case 2 after the time of first spalling, a decrease in the stress intensity can be noticed (Figure 8.10-a). This behaviour may not relate to the spalling occurrence because as observed before, However, for the restrained C Samples (Figure 8.10-b), both Case 1 and Case 2 develop stress in time with almost equal values in the central exposed area. Similar to B sample Case 2, after spalling occurrence the stress intensity starts to decrease in both Case 1 and Case 2 but only at the central exposed area of the samples. In Case 1 the cold rim remains intact and can resist more hereby resulting in more severe stress concentration within the cold rim. The cold rim in B Sample Case 1 concentrates less stress compared to C Sample Case 1 because of the action of the steel

restraint; in the former the exposed surface can deform more laterally and hence less stress is concentrated at the cold rim, while in the latter the restraint prevents the expansion leading to higher stress concentration at the cold rim.

Recalling what has been observed for the ring samples (Figure 8.5), it seems that the decrease in stress intensity at the exposed face after spalling is more specific to rectangular samples. This can be attributed to the way the stresses develop in the samples. In rectangular samples they develop in two perpendicular directions whereas in the ring samples they develop in radial and circumferential directions. Tensile hoop stresses developed at the circumference of the ring sample confine the sample and relax the radial compressive stress, thereby giving the sample more resistance to the effects of heating as a whole. However, stresses in two perpendicular directions in the rectangular samples develop with different intensities depending on the dimensions of the sample, thereby one direction of the sample would be more prone to fail than the other due to more severe stress concentration which consequently weakens the overall strength of the sample.

To further extend the investigation of the sensitivity to boundary conditions, two additional cases (Cases 3 & 4) shown in Figure 8.1), are incorporated into the investigations for the B and C samples. 3D views of in-plane stresses at the spalling time for B and C samples have been plotted in Figure 8.11 and Figure 8.12 respectively. The effect of the cold rim can be

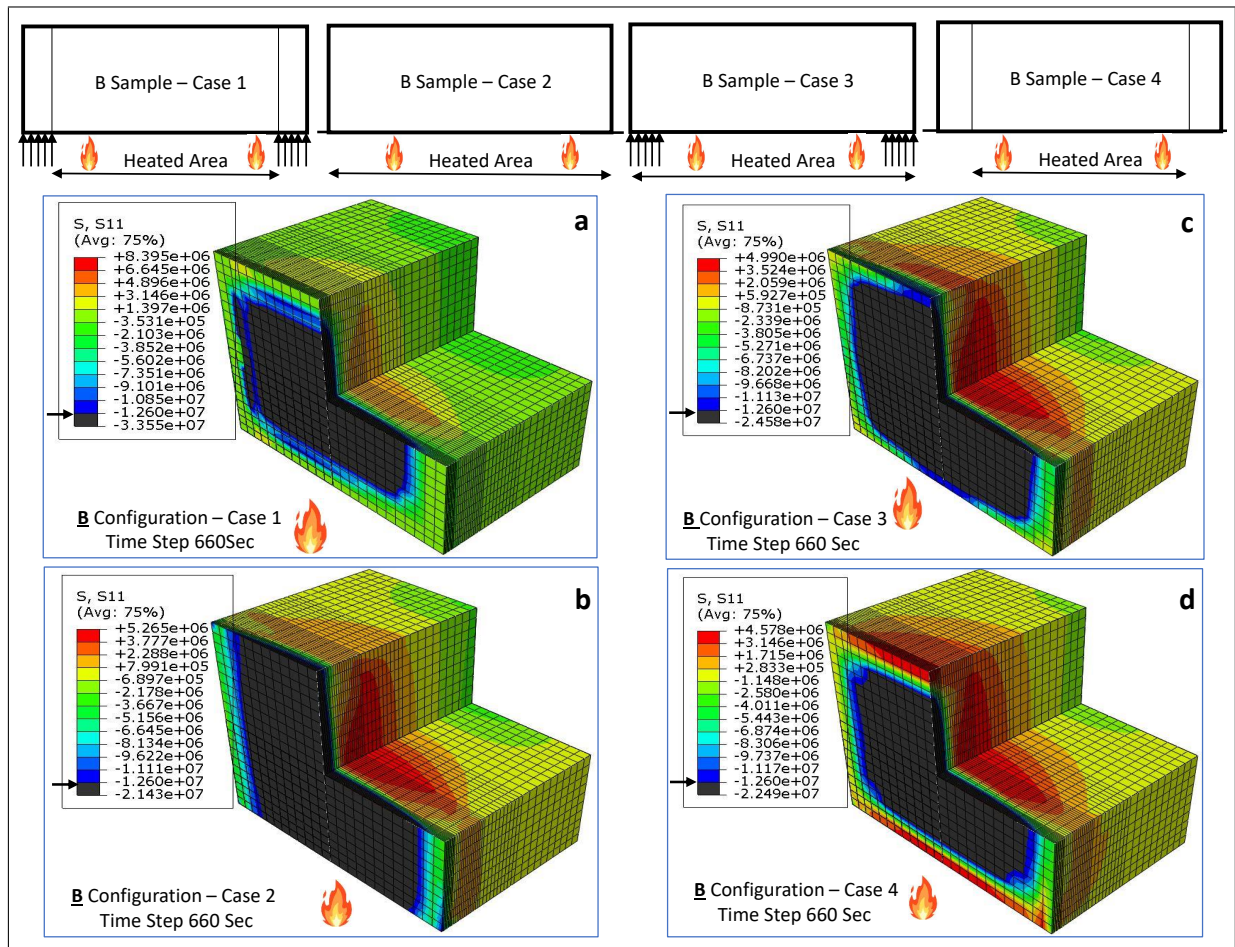


Figure 8.11: In-plane stress as close as possible to time of spalling at the exposed surface of B samples a) Case 1, b) Case 2, c) Case 3, & d) Case 4

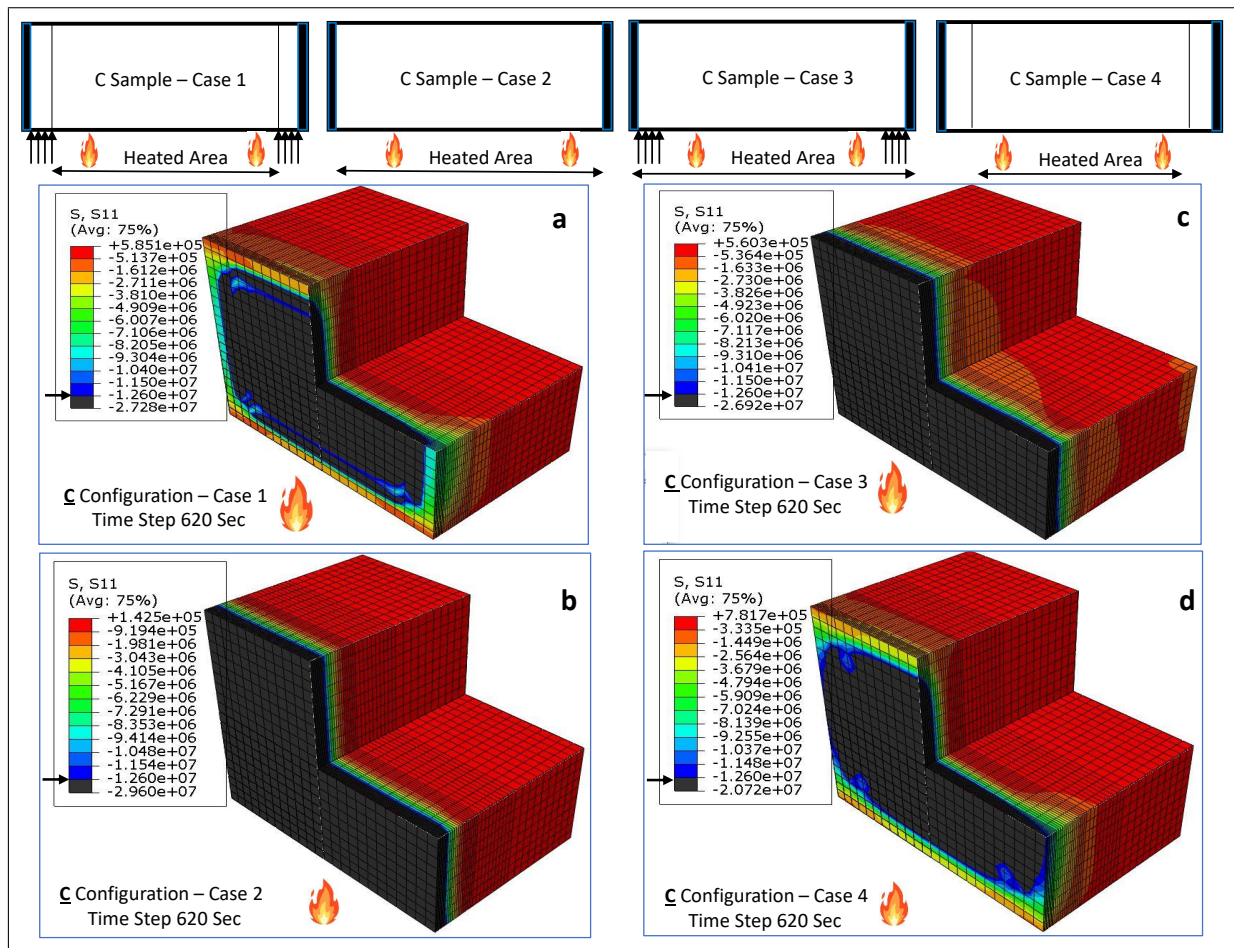


Figure 8.12: In-plane stress as close as possible to time of spalling at the exposed surface of C samples a) Case 1, b) Case 2, c) Case 3, & d) Case 4

noticed in the B sample by comparing Case 1 and Case 2 samples (Figure 8.11-a,b) where more compressive stress concentrated in the sample with cold rim, and this is also true if Case 1 is compared to Case 3 (Figure 8.11-a,c). However, through comparing Case 1 and Case 4, which have the same cold rim area but different restraint conditions, it appears that frictional restraint of the sitting area is the cause of the higher compressive stress in Case 1 rather than its coldness (Figure 8.11-a,d). This can be further evidenced through comparison of Case 2 and Case 4 where almost same stress intensity develop regardless of the cold rim (Figure 8.11-b,d). Most importantly, through comparing Case 2 and Case 3 it appears that restraint can impose stress in the samples even in hot conditions (Figure 8.11-b,c), which is also true if Case 3 is compared to Case 4 (Figure 8.11-c,d).

Now regarding the C samples (Figure 8.12), the external steel restraint introduces different behaviours to the samples and overrides some of the behaviour observed in the B samples. Here the cold rim effects cannot be observed if Case 1 is compared to Case 3 (Figure 8.12-a,c) because almost identical compressive stress intensities develop regardless of the heating status of the sitting area. Through comparing Case 2 and Case 4 (Figure 8.12-b,d), it appears the effect of the cold rim has been mitigated by the external steel ring and in fact the cold rim relaxes the stress intensity rather than increasing stress as has been suggested in the literature [33]. This

is also true if Case 1 is compared to Case 2 where the cold rim in the former relaxes the stress intensity (Figure 8.12-a,b). Comparing Case 1 to Case 4 it can be inferred that the intenser stress of the former case is derived from the frictional restraint effects at the sitting area rather than from being cold (Figure 8.12-a,d) and this is also true if Case 3 is compared to Case 4 (Figure 8.12-c,d). Finally, it seems that the effects of frictional restraint on the sitting area can also be mitigated by the direct reaction of the stiff external steel ring, which causes the restraint area to act as spring, slightly relaxing the compressive stresses as can be observed if Case 2 is compared to Case 3 (Figure 8.12-b,c).

From these investigations, the reported effects of cold rims in imposing more stress on a sample cannot be confirmed in most of the investigated cases and boundary conditions relating to restraints can significantly alter or even reverse the cold rim effects, contradicting findings in the literature [33]. As discussed before, the observed differences between the rectangular B and C samples can be attributed to the act of the steel ring in altering the overall sample behaviour. However, the differences between the A and C samples, which are both restrained, can be related to the shape of the samples.

8.3.3 Uniaxially loaded slab

Considering that in the case of accidental fires partial heating of structural members is possible and that members are always loaded from dead and imposed loads, a uniaxially loaded sample is therefore investigated here with two different heating scenarios as shown in Figure 8.1-D. The only difference between the two given samples is provision of a cold rim around a central heated area of the front exposed surface.

The original experimental test scenario was without the cold rim for which three spalling failures were recorded ([4]); the first with 9 mm depth after 360 seconds of exposure to the standard ISO834 fire curve, the second with 10 mm depth after 540 seconds and the third with 11 mm depth after 640 seconds. The same concrete mix used for the unloaded rectangular samples previously discussed (Configuration (B)) was used also used in casting the D sample and therefore had identical temperature dependent material properties. As in Figure 8.13, the maximum temperature at first spalling was predicted to be just above 190°C at the exposed surface of the samples. 3D cut views showing minimum and maximum principal stress as close as possible to the time of first spalling for both D sample scenarios are presented in Figure 8.14 and profiles representing principal stresses at different heating times through the thickness of the samples are shown in Figure 8.15.

A yielded zone of compressive stress (larger than 12.6 MPa compressive yielding limit) can be seen covering the entire exposed surface of the sample without a cold rim (Figure 8.14-a) with higher stress intensity compared to the compression zone of the sample with cold rim, yielded only at the central exposed area (Figure 8.14-c). This is because in the former sample, thermal gradient from the entire heated surface conducts to the concrete leading to higher deformations and stress development compared to the latter case, which has a smaller heat exposed area.

Deeper in the samples, a tensile zone in both samples can be observed with wider and slightly

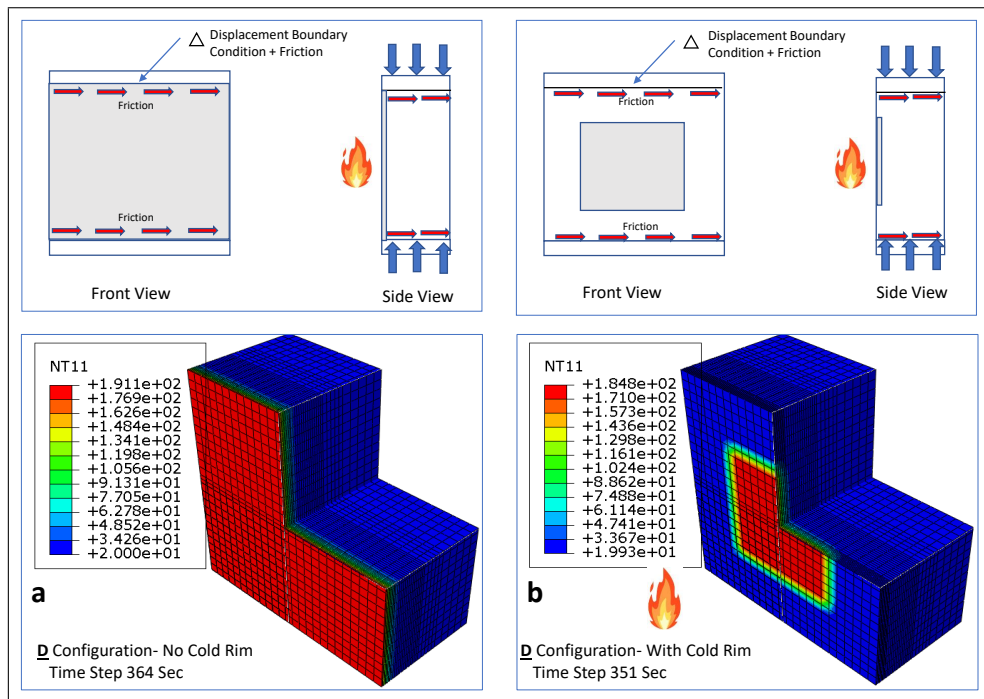


Figure 8.13: a) 3D section showing the temperature profile in D sample without cold rim at closest time step to time of spalling (364 s), b) 3D section showing the temperature profile in D sample with cold at closest time step to time of spalling (351 s)

higher magnitude for the case without a cold rim (Figure 8.14-b,d). This may be attributed to the higher expansion taking place at the exposed surface of the sample with no cold rim, which consequently exerts tensile stress in the adjacent layer, deeper in the sample. Again, these results are not compliant with the literature observations [33] because no stress increase derived from the cold rim can be noticed.

Similarly, through the the thickness of the samples (Figure 8.15-a), no increase in compressive stress values resulting from cold rim effects can be observed. In fact, lower peaks (by around 2 MPa) can be seen in the region near to the heating source for the sample with the cold rim. The stress peak values in both cases around spalling time are higher than the compressive yielding limit and they start to decrease, deeper in the sample, resting at the initial applied load (5MPa).

In terms of tensile stresses through the thickness of the D samples (Figure 8.15-b), the existence of cold rim does not change the evolution of the stress values significantly at any time before or after spalling.

Now turning to investigate the exposed surface of the samples, which may be the main region where cold rim could have effects. Displacement contours in different directions, namely the in-plane displacement component transverse to the axial load direction and the out of plane displacement component toward the heating source, both at spalling time are shown in Figure 8.16. Regarding the in-plane displacement component, the sample with no cold rim has freedom to expand laterally while the unheated area of the sample with the cold rim restricts the expansion of the central heated area. Therefore, for the sample with no cold rim the maximum value of displacement occurs at the edges (Figure 8.16-a) whereas for the sample with the cold rim the highest displacement zone is located where the cold and hot regions meet (Figure 8.16-c). The

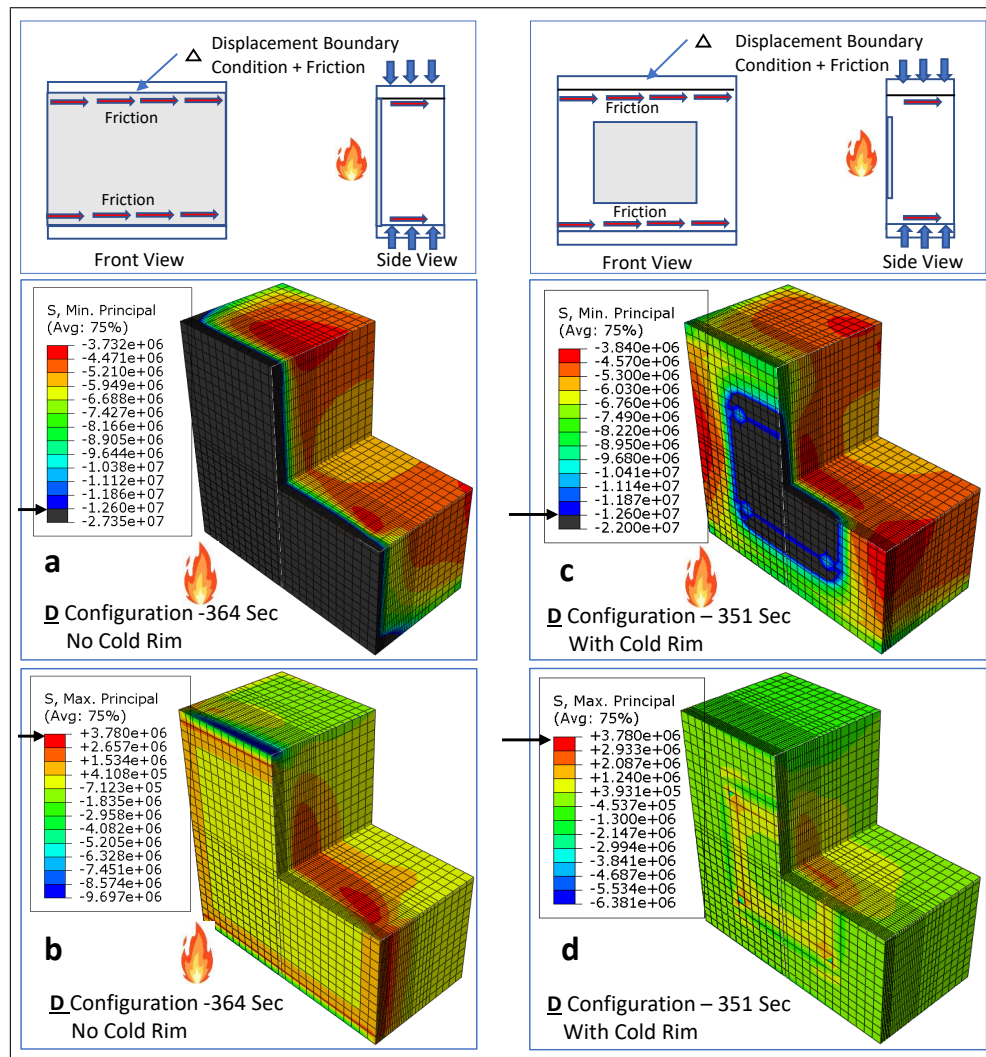


Figure 8.14: 3D sections of minimum and maximum principal stress profiles as close as possible to time of spalling in a), b) configuration (D) without cold rim & c), d) configuration (D) with cold rim

maximum displacement value for the sample without the cold rim is higher than the maximum value developed in the sample with the cold rim.

In terms of the out-plane displacement component toward the heating source, interestingly, identical maximum intensities can be observed for both samples (Figure 8.16-b,d). However, a wider area in the sample without the cold rim displaces severely, which in turn potentially increases the spalling risk across a wider area of the exposed surface. Considering both displacement components together, it is possible for the sample without cold rim to experience severe edge spalling at the edges and less severe surface spalling at the central portion. However, in the sample with the cold rim, surface and edge spalling are expected but with the same severity considering equal in-plane and out-plane displacements of the exposed surface.

Summing up all these results it can be concluded that in loaded samples the cold rim effects cannot be confirmed as causing extra stresses through the thickness of the sample. Even though a cold rim alters the displacement pattern of the exposed surface, it still it does not increase the displacement intensity and hence spalling risk.

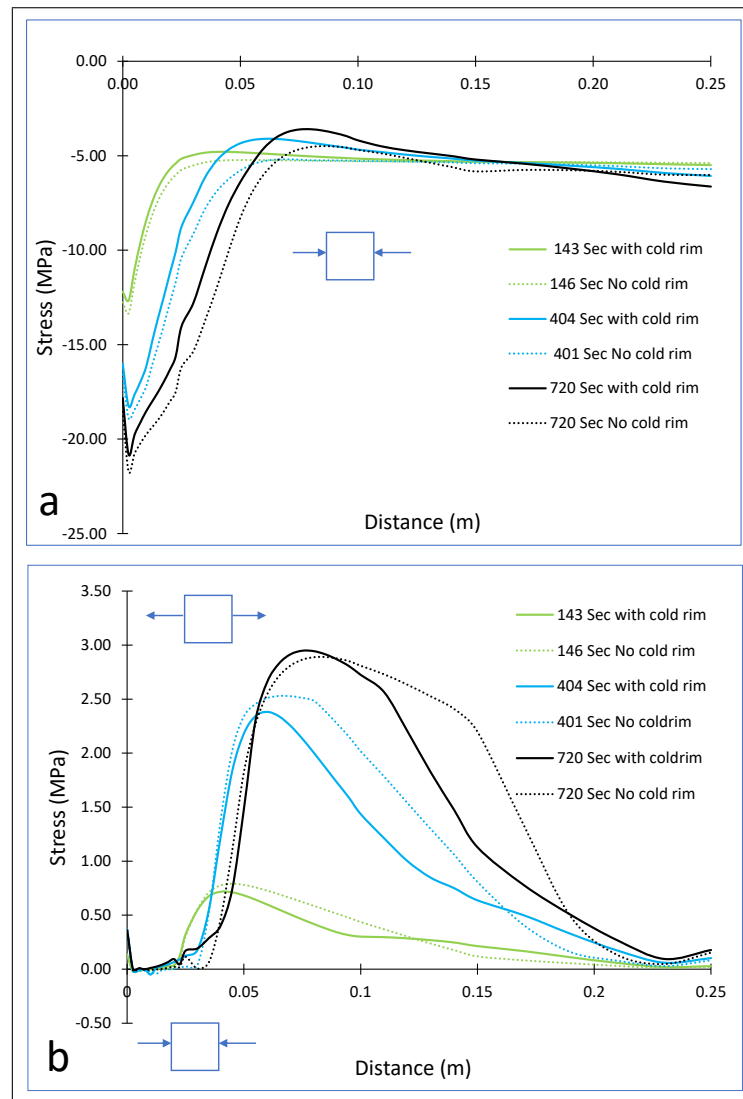


Figure 8.15: a) Minimum and b) maximum principal stress profiles through the centreline thickness of the D samples with and without cold rims

8.3.4 Biaxially loaded slabs

The last sample group covers the samples loaded biaxially while heat was applied perpendicular to the loading direction. Two thin samples from [37] with circumferential cold rims at the sitting areas, where the samples were put on the furnace, have been considered. The samples are identical in material properties and geometry except one has slits across the outer cold circumference as shown in Figure 8.1-E. The slits are provided in an effort to limit the hypothesised restraint effects of the outer cooler zone and to reduce its ability to transmit load by cutting its mechanical continuity. For the purpose of the cold rim investigations, the same two samples have been considered in another scenario in which their entire lower surface was heated (shown as the hatched zones in the figure). Reported experimental test results relating to the temperature profiles and displacements have been captured by the model satisfactorily as shown in Figure 8.17-c and according to Figure 8.17-a,b the temperature at the exposed surface of the samples after 7200 seconds was 910°C . Furthermore, it was observed in the experiment that the tested samples first displaced (sagged) toward the heat source, then after stiffness was lost, they displaced away

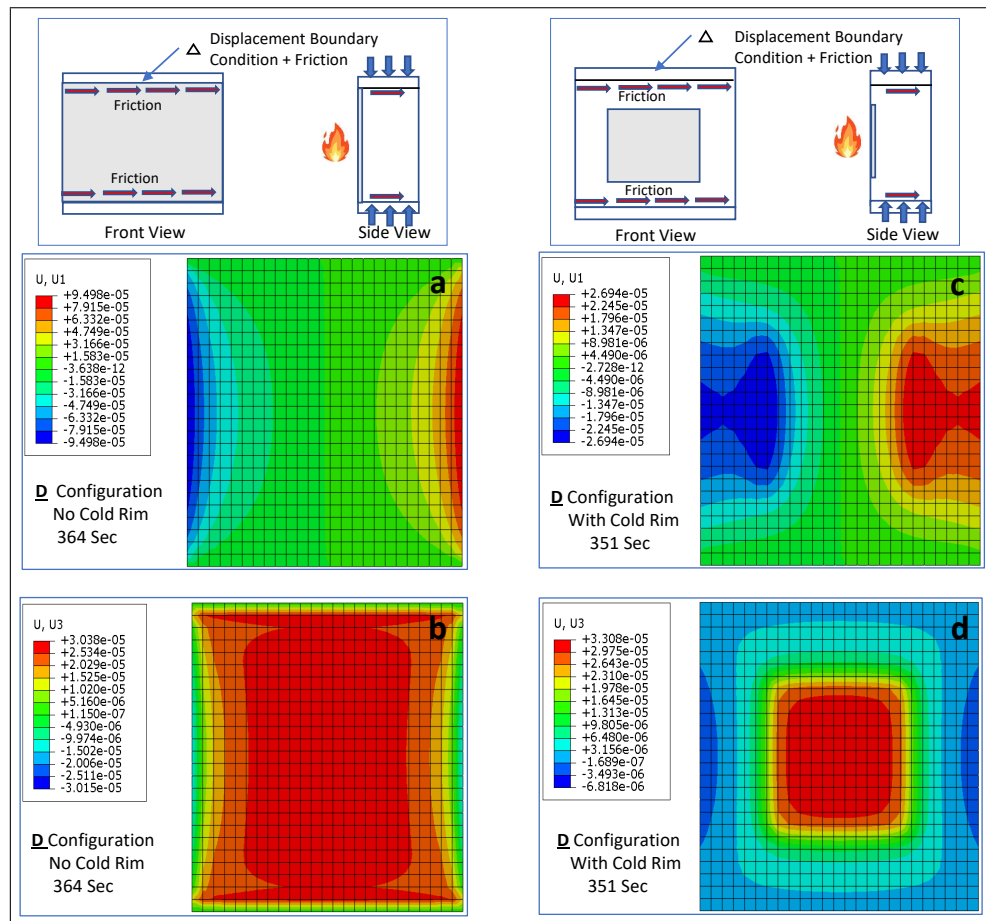


Figure 8.16: Exposed surface displacements a) toward the heating source , b) transverse to the uniaxial loading direction for sample with no cold rim, and c) toward the heating source, d) transverse to the uniaxial loading direction for sample with cold rim

from the fire (hogged). This was attributed to the action of the offsetting of the bi-axial load eccentricity and the shifting of the stiffness centre towards the cold zone after spalling [37]. This behaviour has also been captured very well by the model as shown in Figure 8.17-d and the same behaviour has been captured for the extended cases with their entire surfaces heated, which as shown in Figure 8.18 increases the displacements appreciably.

As for the previous samples, the sensitivity of cold rim effects to different boundary conditions have been investigated by comparing minimum principal stress states through the sample thickness and displacement at the exposed surfaces. Four possible boundary condition sets have been considered in the investigations; (Figure 8.19-a) is to investigate cold rim effects in intact samples, (Figure 8.19-b) is to extend the cold rim investigation to samples with slits and (Figure 8.19-c) and (Figure 8.19-d) are to investigate the effects of the mechanical characteristics of the circumferential area in different heating statuses (i.e with and without a cold rim). Starting from samples without slits with and without cold rims (Figure 8.19-a), two stress development behaviours can be observed. The stresses up to time frame 3000 seconds, which show distinct peaks near the hot face, correspond to the displacement toward the heating source while the stresses developed after 3000 seconds, which show a reduction in stress near the hot face, correspond to the displacement away from the heating source. It seems that the cold rim

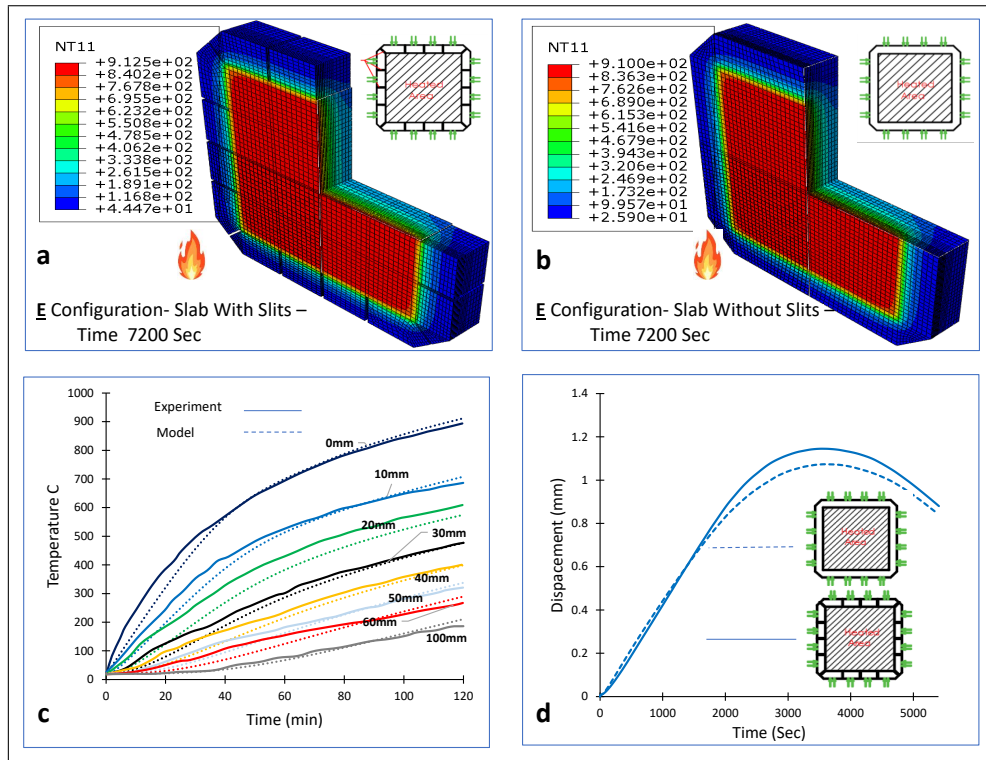


Figure 8.17: a,b) 3D section temperature profile of the E samples with and without slits, c) Temperature profiles at different depths of the sample, and d) Sagging and hogging phase displacement of a central point at the exposed surface in time for the both tested E samples

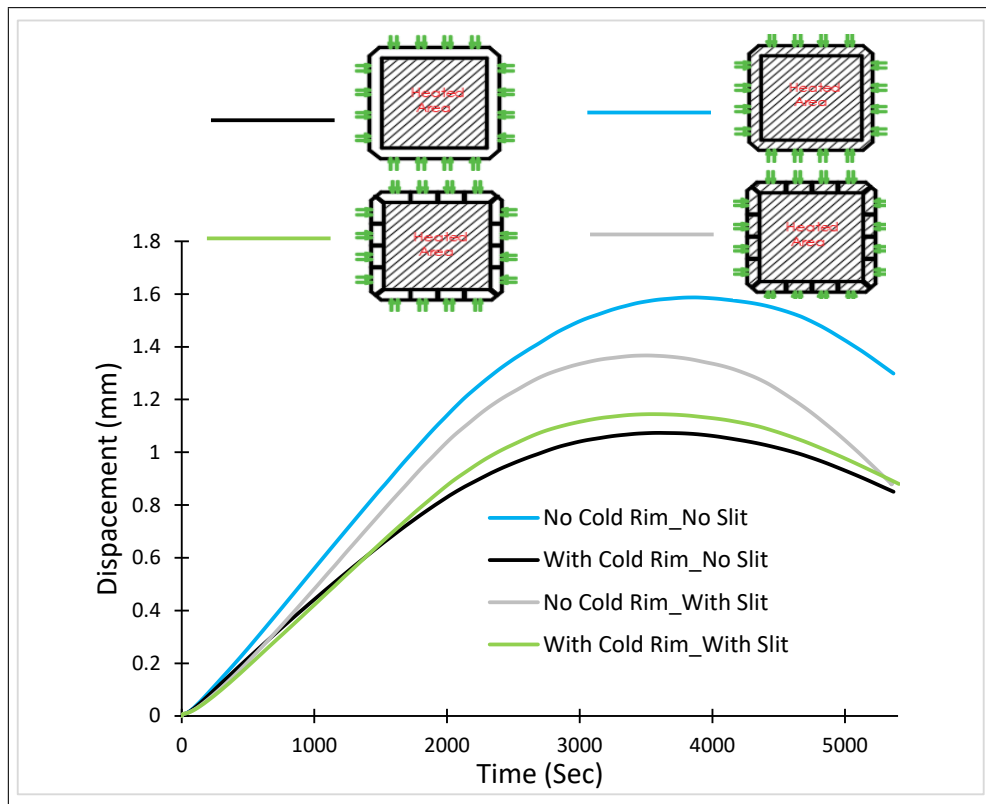


Figure 8.18: Simulated displacement results of a central point at the exposed Surface in time for different configurations of the E sample group

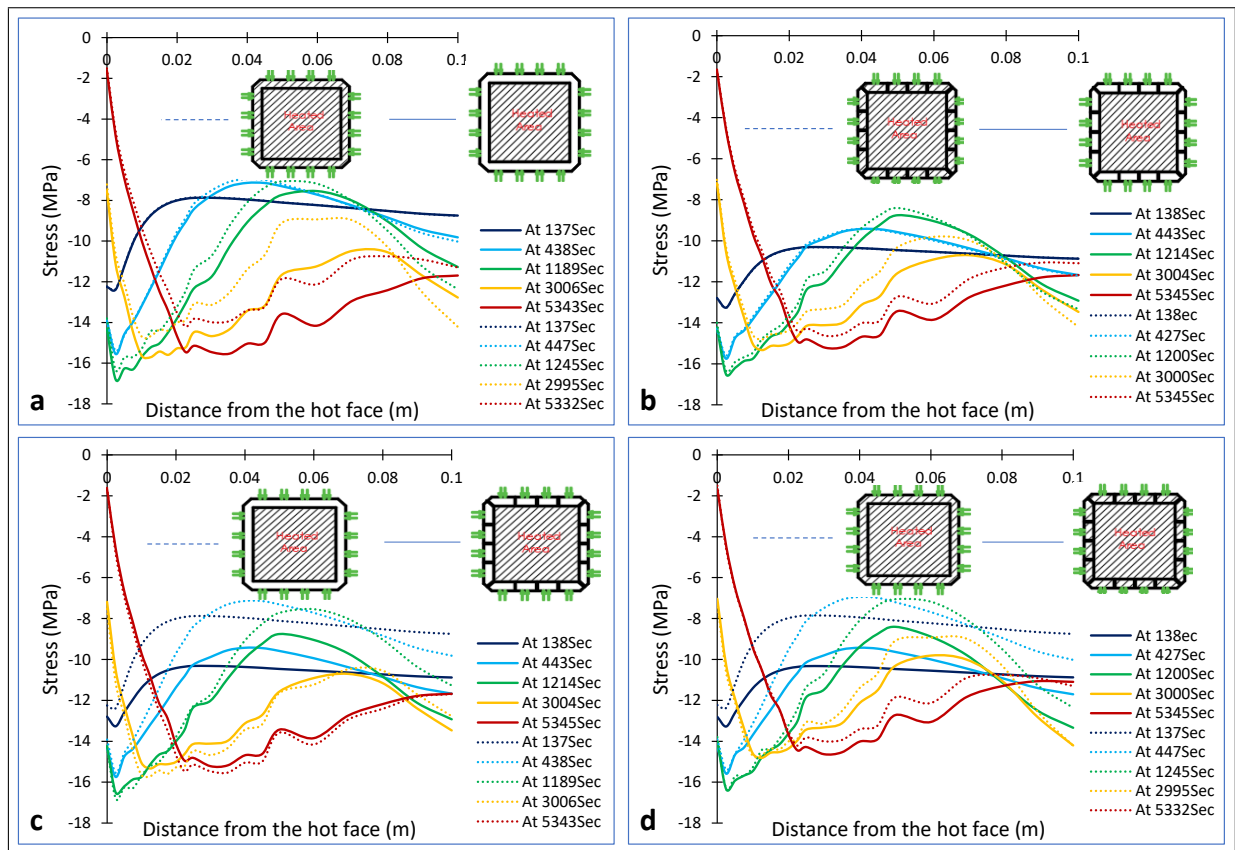


Figure 8.19: Minimum principal stresses through thickness in times for a) Samples without slits, b) Samples with slits, c) Samples with cold rims, and d) Samples without cold rims

effects are negligible up to 1200 seconds, but after that seem to be significant in the development of higher stress, especially deeper in the colder regions of the concrete. This is because both samples deteriorate in the first half of the heating duration until the stiffness almost destroyed at the exposed surfaces but, in the sample without a cold rim the whole exposed surface deteriorates while only the central exposed portion deteriorates in the sample with a cold rim. Therefore, the intact cold rim constrains lateral thermal expansion, which results in the development of tensile hoop stresses around the circumference and radial compression stress in the central zone.

Turning to how slits change these observations (Figure 8.19-b), unlike in the previous case, the effects of a cold rim cut by slits are not significant throughout the heating duration and the thickness of the sample with only a small difference in the results with and without a cold rim. Both samples have slits, which means thermal expansion is not resisted as before and therefore the stresses develop in a similar manner and the samples behave almost identically. Comparing these results with the previous case it can be inferred that the slits had weakened the ring action provided by the cold rim, cutting through its mechanical continuity.

Comparison is also made of the stress states in samples with cold rims but with different mechanical characteristics, one with slits and one without (Figure 8.19-c). In the first half of the heating duration, where the exposed surface sags towards the fire, the sample with slits develops higher stresses while in the second half of the heating duration both samples develop very similar stresses. This is because in the samples without slits the cold rim develops hoop

stress that dissipate radial stresses that would be transmitted to the heated portion. But, in the samples with slits the hoop stresses are much reduced and hence most of the stress from the biaxial load transmits directly to the central heated portion. As heating goes on, the concrete at the exposed surface is degraded significantly and the neutral axis shifts towards a cooler depth, which results in a reversing of the displacement away from the heating source and a loss of most of concrete's stress carrying capacity. By this time, after 3000 seconds, only a small portion of the slab thickness, which is by this time dominated by the compressive stresses caused by the very high temperatures, remains in both samples and they therefore act identically.

However, through reconsidering the same two previous samples but this time with their entire lower surfaces exposed to heating (Figure 8.19-d), almost the same stress development can be observed, which may imply that the results relate to the mechanical characteristics of the cold circumference rather than its heating status. This again suggests that cold rims do not have very much effect on the stress state in heated concrete samples.

From all these comparisons on the biaxially loaded slabs, it can be concluded that, as in previous samples, effects derived from the cold rim cannot be confirmed in most of the cases. In samples without slits cold rim effects appear after significant deterioration of the concrete has taken place and spalling has occurred at the exposed surface (Figure 8.19-a). This delay before additional stresses are seen lessens concerns regarding any effect cold rims might have as a trigger of spalling. Also the mechanical characteristics of the cold rim seem to affect more decisively the behaviour of the samples rather than its heating status.

8.4 Conclusions

The role of a cold rim in controlling the behaviour of heated concrete samples through self-restraint that may impose increased stresses in the heated concrete and hence trigger spalling has been investigated. Different tests from literature have been considered to investigate cold rim effects thoroughly taking into account different parameters relating to the samples and the adopted test ups. Investigation results do not confirm the cold rim as a parameter capable of changing concrete behaviour significantly or causing spalling under heating.

In thick samples, the cold rim effect is negligible and has very little influence of the development of stresses through the thickness of the samples. Even though in unrestrained samples cold rims seem to impose slightly more stress at the exposed surface, this observation is reversed in restrained samples with the same geometry and material properties. This means that cold rim effects are very sensitive to the boundary conditions and more specifically to restraints and their stiffness.

Observing decrease in stress intensity at the exposed face after spalling in rectangular samples comparing to persistent intensity increase in the ring samples indicates that shape of the samples can have effect in altering cold rim effects at the exposed surfaces.

Similar to the thick rectangular samples, in uniaxially loaded samples the effectiveness of the cold rim can not be observed in the development of the stress state under heating and in fact

cold rims tend to relax stresses. Additionally, even though the exposed surface displacement is affected noticeably by the cold rim, it does not seem likely to lead to increased spalling risk.

Results from thin biaxial samples clearly conclude that it is the mechanical characteristic of the cold rim rather than its heating status that changes stress development in the samples. It can be also concluded that observations of a reversal of the displacement behaviour from sagging to hogging during heating are the consequence of using thin samples and remain specific to this test configuration.

In summary, cold rim effects are not found to change the stress development or behaviour of concrete samples under heating. Furthermore, its precise role is highly sensitive to many parameters relating to sample shape, sample size, boundary conditions, test and loading configurations, and the test methodologies. Although in few cases a cold rim has been found to have some superficial effects at the exposed surface, they are specific to the test under consideration and can not be generalised.

Chapter 9

Conclusions

The aim of this thesis is to investigate how underlying factors relating to test methodologies can control concrete behaviours and its spalling under effects of heating and therefore alter test outcomes. To do this, a wide range of the literature experimental investigations have been considered and classified according to the adopted methodologies and test setups. Samples include loaded structural and unloaded non-structural elements which can be classified into three main classes per their test methodologies, namely heated unloaded samples, restrained then heated samples, and loaded then heated samples. To investigate all these thoroughly, five tested sample have been considered in the parametric studies conducted in this thesis, unrestrained samples, restrained samples, uniaxially loaded samples, biaxially loaded samples and eccentrically loaded samples.

Alongside this, influencing parameters relating to test methodologies that may have effects on concrete behaviour and its spalling have been highlighted. The parameters are sample size, applied load type, applied load intensity, restraint types and their stiffness and other details relating to test ups such as friction between the samples and the testing apparatus.

A sophisticated thermo-mechanical model was developed and demonstrated to be versatile in simulating experimental tests with various boundary conditions and test setups. It was found that restrictions relating to the associated test setups in the literature have reflected in the derivation of the provisions relating to temperature dependant material properties of concrete. Therefore, it is very challenging for numerical modellers to adopt consistent sets of concrete property models, especially for the coefficient of thermal expansion and transient thermal strain of concrete. Most importantly, it was found that the pore pressure stress, resulting from hygro thermo reactions of concrete during heating, has negligible effects on the parametric study results conducted throughout this thesis utilizing the thermo-mechanical model.

It was found that alongside material properties of concrete, underlying aforementioned factors relating to test methodologies and test setups can control significantly concrete behaviours and its spalling under effects of elevated temperatures.

Regarding sample size, sample thickness was found to be most significant, with thicker samples likely to have less resistance to spalling than more flexible thinner samples. The effects can vary depending on test set up, restraints and loading configuration. However, sample span was found to have less effect on results since it does not effect appreciably stress states developed through the sample thickness.

Load type, load intensity and the way it is applied are found to significantly affect the test outputs. Samples loaded prior to heating behave quite differently and seem to have the potential to spall much earlier than samples loaded through restraints where the load develops and intensifies gradually with heating progress. Additionally, increasing load intensity in pre-loaded

samples also alters sample behaviours significantly due to increasing steepness in stress gradients transitioning from compression stress at the exposed surface to tension stress deeper in the sample. On surpassing stresses intensities in this steep transition either of concrete yielding limit in compression or concrete tensile capacity or both, spalling occurs. On the other hand, samples loaded concentrically experience a different compressive regime compared to those loaded eccentrically. Details relating to boundary conditions and test configurations can also have significant effects on the results. Providing full friction in the test set up between the sample at its contact areas with the testing apparatus can significantly alter the sample behaviour and hence the test outputs.

Regarding restraint, this term is used very broadly in the literature and covers a wide variety of different types and different configurations of restraint. Type and configuration of restraint applied to a test sample can alter the test outputs significantly. Samples restrained through applied load act in opposition to samples passively restrained through a confining frame or ring. Additionally, the dimensions of the sample, the heating regime, and details of test set up such as friction between a sample and the supports on which it rests determine the mechanical effect that the restraint will have. While mechanically restraining a sample can improve resistance to spalling, samples with the entire thickness restrained were found to have less resistance than those with only part of the thickness restrained.

The role of a cold rim as self restraint in controlling the behaviour of heated concrete samples through self- restraint cannot be confirmed as a parameter capable of changing concrete behaviour significantly or causing spalling under heating. Its precise role is highly sensitive to many parameters relating to sample shape, sample size, boundary conditions, test and loading configurations and the test methodologies. Although in a few cases a cold rim has been found to have some superficial effects at the exposed surface, they are specific to the test under consideration and cannot be generalised.

Some literature test outcomes conducted on concrete under effects of elevated temperatures are test specific results. Moreover, test outcomes based on particular test setup may not be generalized to be used in assessing fire resistance of members experiencing different boundary conditions than those adopted in the test. Loaded structural and unloaded non-structural elements could be used in testing but with considerations of the real case. In all cases, the thickness cannot be compromised, however the length found to be flexible. Non-structural member results may not be reliable for structural members, therefore real boundary conditions in terms of loading and restraints are required, which may be demanding. While length compromising may help in easing test set up, load is recommended to be represented as close as possible, further investigations also are recommended to find more suitable but reliable methods.

Finally, the dominant effects from these factors investigated in this thesis can change test outcomes and this may have been a reason behind literature disagreement regarding concrete spalling. Reflecting real conditions relating to size, loading and restraints in the test set up is strongly recommended to ensure representative results.

Bibliography

- [1] C. Davie, C. Pearce, and N. Bićanić, “A fully generalised, coupled, multi-phase, hygro-thermo-mechanical model for concrete,” *Materials and Structures*, vol. 43, no. Supplement 1, pp. 13–33, 2010.
- [2] D. Gawin, F. Pesavento, and A. G. Castells, “On reliable predicting risk and nature of thermal spalling in heated concrete,” *Archives of Civil and Mechanical Engineering*, vol. 18, no. 4, pp. 1219–1227, 2018.
- [3] K. Hertz, “Limits of spalling of fire-exposed concrete,” *Fire Safety Journal*, vol. 38, no. 2, pp. 103–116, 2003.
- [4] L. Boström, R. McNamee, J. Albrektsson, and P. Johansson, “Screening test methods for determination of fire spalling of concrete,” 2018.
- [5] R. McNamee, “Fire spalling of concrete: Theoretical and experimental studies,” Ph.D. dissertation, 10 2013.
- [6] R. Jansson, “Fire spalling of concrete—a historical overview,” in *MATEC Web of Conferences*, vol. 6. EDP Sciences, 2013, p. 01001.
- [7] C. Pearson and N. Delatte, “Ronan point apartment tower collapse and its effect on building codes,” *Journal of Performance of Constructed Facilities*, vol. 19, no. 2, pp. 172–177, 2005.
- [8] W. A. Webb, “Effectiveness of automatic sprinkler systems in exhibition halls,” *Fire Technology*, vol. 4, pp. 115–125, 1968.
- [9] R. M. Tavares, “An analysis of the fire safety codes in brazil: Is the performance-based approach the best practice?” *Fire Safety Journal*, vol. 44, no. 5, pp. 749–755, 2009. [Online]. Available: <https://www.sciencedirect.com/science/article/pii/S0379711209000289>
- [10] Y. Fu and L. Li, “Study on mechanism of thermal spalling in concrete exposed to elevated temperatures,” *Materials and Structures*, vol. 44, no. 1, pp. 361–376, 2011.
- [11] M. Zeiml, R. Lackner, and H. A. Mang, “Experimental insight into spalling behavior of concrete tunnel linings under fire loading,” *Acta Geotechnica*, vol. 3, no. 4, pp. 295–308, 2008. [Online]. Available: <https://doi.org/10.1007/s11440-008-0069-9>
- [12] F. Ali, D. O’Connor, and A. Abu-Tair, “Explosive spalling of high-strength concrete columns in fire,” *Magazine of Concrete Research*, vol. 53, no. 3, pp. 197–204, 2001.
- [13] J.-C. Liu, K. H. Tan, and Y. Yao, “A new perspective on nature of fire-induced spalling in concrete,” *Construction and Building Materials*, vol. 184, pp. 581–590, 2018.

- [14] E. W. Klingsch, “Explosive spalling of concrete in fire,” Ph.D. dissertation, ETH Zurich, 2014.
- [15] F. L. Monte, R. Felicetti, and M. J. Miah, “The influence of pore pressure on fracture behaviour of normal-strength and high-performance concretes at high temperature,” *Cement and Concrete Composites*, vol. 104, p. 103388, 2019.
- [16] H. Zhang and C. Davie, “A numerical investigation of the influence of pore pressures and thermally induced stresses for spalling of concrete exposed to elevated temperatures,” *Fire Safety Journal*, vol. 59, 2013.
- [17] C. Davie, C. Pearce, and N. Bićanić, “Aspects of permeability in modelling of concrete exposed to high temperatures,” *Transport in porous media*, vol. 95, no. 3, pp. 627–646, 2012.
- [18] Y. Wang, Y. L. Dong, and G. C. Zhou, “A fire test on continuous reinforced concrete slabs in a full-scale multi-story steel-framed building,” *Fire Safety Journal*, vol. 61, pp. 232–242, 2013.
- [19] S. Lian, Z. Wang, Q. Wang, L. Wang, and J. Jiang, “Experimental and analytical study on ultimate load capacity of rc columns in the subway stations under high-temperature gas fume effects,” *International Journal of Civil Engineering*, vol. 16, no. 2, pp. 147–154, 2018.
- [20] M. Ahmad, “Behavior of reinforced concrete beams when partially exposed to fire,” *Inter. Journal of advances in Mech. and Civil Eng.*, vol. 3, no. 2, 2016.
- [21] Q. Xu, C. Han, Y. C. Wang, X. Li, L. Chen, and Q. Liu, “Experimental and numerical investigations of fire resistance of continuous high strength steel reinforced concrete t-beams,” *Fire Safety Journal*, vol. 78, no. C, pp. 142–154, 2015.
- [22] H. Hajiloo, M. F. Green, M. Noël, N. Bénichou, and M. Sultan, “Fire tests on full-scale frp reinforced concrete slabs,” *Composite Structures*, vol. 179, pp. 705–719, 2017. [Online]. Available: <http://www.sciencedirect.com/science/article/pii/S026382231730243X>
- [23] D. Gawin, F. Pesavento, and B. Schrefler, “Modelling of hygro-thermal behaviour of concrete at high temperature with thermo-chemical and mechanical material degradation,” *Computer Methods in Applied Mechanics and Engineering*, vol. 192, no. 13, pp. 1731–1771, 2003. [Online]. Available: <https://www.sciencedirect.com/science/article/pii/S0045782503002007>
- [24] S. Serega, “Effect of transverse reinforcement spacing on fire resistance of high strength concrete columns,” *Fire Safety Journal*, vol. 71, pp. 150–161, 2015.
- [25] C. Calmeiro dos Santos and J. P. Rodrigues, “Compressive strength at high temperatures of a concrete made with recycled tire textile and steel fibers,” vol. 6, 09 2013.

-
- [26] G. L. Albuquerque, A. B. Silva, J. P. C. Rodrigues, and V. P. Silva, "Behavior of thermally restrained rc beams in case of fire," *Engineering Structures*, vol. 174, pp. 407–417, 2018.
- [27] R. K. S. Al Hamd, M. Gillie, H. Warren, G. Torelli, T. Stratford, and Y. Wang, "The effect of load-induced thermal strain on flat slab behaviour at elevated temperatures," *Fire Safety Journal*, vol. 97, pp. 12–18, 2018.
- [28] Y. Anderberg and S. Thelandersson, *Stress and deformation characteristics of concrete at high temperatures: experimental investigation and material behaviour model*. Lund Institute of Technology Lund, Sweden, 1976.
- [29] P. Kalifa, G. Chéné, and C. Gallé, "High-temperature behaviour of hpc with polypropylene fibres - from spalling to microstructure," *Cement and Concrete Research*, vol. 31, no. 10, pp. 1487–1499, 2001.
- [30] M. M. Hossain, M. K. Hassan, S. K. Shill, and S. Al-Deen, "Mechanical and thermo-chemical degradation of concrete exposed to simulated airfield conditions," *Road Materials and Pavement Design*, pp. 1–21, 2022.
- [31] L. Phan, J. Lawson, and F. Davis, "Effects of elevated temperature exposure on heating characteristics, spalling, and residual properties of high performance concrete," *Materials and Structures (France)*, vol. 34, no. 236, pp. 83–91, 2001.
- [32] Y.-S. Heo, C.-G. Han, and K.-M. Kim, "Combined fiber technique for spalling protection of concrete column, slab and beam in fire," *Materials and Structures*, vol. 48, pp. 3377–3390, 2015.
- [33] K. Mróz, I. Hager, and M. Tekieli, "Effect of cold rim on extent and type of concrete fire spalling," *Proceedings from the 5th International Workshop on Concrete Spalling At: Borås, Sweden,*, 2017.
- [34] M. B. Dwaikat and V. K. R. Kodur, "Response of restrained concrete beams under design fire exposure," *Journal of Structural Engineering*, vol. 135, no. 11, pp. 1408–1417, 2009.
- [35] Y. Wang, G. Yuan, Z. Huang, J. Lyv, Z.-Q. Li, and T.-Y. Wang, "Experimental study on the fire behaviour of reinforced concrete slabs under combined uni-axial in-plane and out-of-plane loads," *Engineering Structures*, vol. 128, no. C, pp. 316–332, 2016.
- [36] C. G. Bailey and W. S. Toh, "Small-scale concrete slab tests at ambient and elevated temperatures," *Engineering Structures*, vol. 29, no. 10, pp. 2775–2791, 2007.
- [37] F. L. Monte and R. Felicetti, "Heated slabs under biaxial compressive loading: a test set-up for the assessment of concrete sensitivity to spalling," *Materials and Structures*, vol. 50, no. 4, pp. 1–12, 2017.

- [38] F. L. Monte, R. Felicetti, and C. Rossino, "Correction to: Fire spalling sensitivity of high-performance concrete in heated slabs under biaxial compressive loading," *Materials and Structures*, vol. 53, no. 4, pp. 1–1, 2020.
- [39] M. Dwaikat and V. Kodur, "Response of restrained concrete beams under design fire exposure," *Journal of Structural Engineering*, vol. 135, no. 11, pp. 1408–1417, 2009.
- [40] G. L. Albuquerque, A. B. Silva, J. P. C. Rodrigues, and V. P. Silva, "Behavior of thermally restrained rc beams in case of fire," *Engineering Structures*, vol. 174, pp. 407–417, 2018.
- [41] E. Ryu, Y. Shin, and H. Kim, "Effect of loading and beam sizes on the structural behaviors of reinforced concrete beams under and after fire," *International Journal of Concrete Structures and Materials*, vol. 12, no. 1, pp. 1–10, 2018.
- [42] A. H. Shah and U. Sharma, "Fire resistance and spalling performance of confined concrete columns," *Construction and Building Materials*, vol. 156, pp. 161–174, 2017. [Online]. Available: <https://www.sciencedirect.com/science/article/pii/S0950061817317750>
- [43] S. H. Buch and U. K. Sharma, "Fire resistance of eccentrically loaded reinforced concrete columns," *Fire Technology*, vol. 55, no. 5, pp. 1517–1552, 2019.
- [44] V. K. R. Kodur and L. Phan, "Critical factors governing the fire performance of high strength concrete systems," *Fire Safety Journal*, vol. 42, no. 6, pp. 482–488, 2007.
- [45] T. Hulin, C. Maluk, L. Bisby, K. Hodicky, J. Schmidt, and H. Stang, "Experimental studies on the fire behaviour of high performance concrete thin plates," *Fire Technology*, vol. 52, no. 3, pp. 683–705, 2016.
- [46] P. Kalifa, F.-D. Menneteau, and D. Quenard, "Spalling and pore pressure in hpc at high temperatures," *Cement and concrete research*, vol. 30, no. 12, pp. 1915–1927, 2000.
- [47] L. T. Phan, J. R. Lawson, and F. L. Davis, "Effects of elevated temperature exposure on heating characteristics, spalling, and residual properties of high performance concrete," *Materials and structures*, vol. 34, no. 2, pp. 83–91, 2001.
- [48] J. P. C. Rodrigues, L. M. Laím, and M. Korzen, "Fire behaviour of circular concrete columns with restrained thermal elongation," *Journal of advanced concrete technology*, vol. 12, no. 9, pp. 289–298, 2014.
- [49] I. Rickard, N. Gerasimov, L. Bisby, and S. Deeny, "Predictive testing for heat induced spalling of concrete tunnel linings—the potential influence of sustained mechanical loading," in *5th International Workshop on Concrete Spalling due to Fire Exposure, 12-13 October 2017, Bors, Sweden*, 2017, pp. 337–344.
- [50] T. Tanibe, M. Ozawa, R. Kamata, R. Sato, and K. Rokugo, "Thermal stress estimation in relation to spalling of hsc restrained with steel rings at high temperatures," in *MATEC Web of Conferences*, vol. 6. EDP Sciences, 2013, p. 01004.

- [51] L. Boström, U. Wickström, and B. Adl-Zarrabi, “Effect of specimen size and loading conditions on spalling of concrete,” *Fire and Materials: An International Journal*, vol. 31, no. 3, pp. 173–186, 2007.
- [52] H. Yang, F. Liu, and L. Gardner, “Performance of concrete-filled rhs columns exposed to fire on 3 sides,” *Engineering structures*, vol. 56, pp. 1986–2004, 2013.
- [53] L.-y. Li and J. Purkiss, “Stress–strain constitutive equations of concrete material at elevated temperatures,” *Fire Safety Journal*, vol. 40, no. 7, pp. 669–686, 2005.
- [54] U. Schneider, “Modelling of concrete behaviour at high temperatures,” *Design of structures against fire*, pp. 53–69, 1986.
- [55] M. J. Terro, “Numerical modeling of the behavior of concrete structures in fire,” *ACI Structural Journal*, vol. 95, pp. 183–193, 1998.
- [56] V. Kodur, “Properties of concrete at elevated temperatures,” *International Scholarly Research Notices*, vol. 2014, 2014.
- [57] A. M. Neville *et al.*, *Properties of concrete*. Longman London, 1995, vol. 4.
- [58] D. P. Thanaraj, N. Anand, G. Prince Arulraj, and E. Zalok, “Post-fire damage assessment and capacity based modeling of concrete exposed to elevated temperature,” *International Journal of Damage Mechanics*, vol. 29, no. 5, pp. 748–779, 2020.
- [59] T. T. Lie, T. Rowe, and T. Lin, “Residual strength of fire-exposed reinforced concrete columns,” *Special Publication*, vol. 92, pp. 153–174, 1986.
- [60] K. D. Hertz, “Concrete strength for fire safety design,” *Magazine of Concrete Research*, vol. 57, no. 8, pp. 445–453, 2005.
- [61] V. Kodur, T. Wang, and F. Cheng, “Predicting the fire resistance behaviour of high strength concrete columns,” *Cement and Concrete Composites*, vol. 26, no. 2, pp. 141–153, 2004.
- [62] M. Bastami, F. Aslani, and O. M. ESMAEILNIA, “High-temperature mechanical properties of concrete,” 2010.
- [63] Y.-F. Chang, Y.-H. Chen, M.-S. Sheu, and G. C. Yao, “Residual stress–strain relationship for concrete after exposure to high temperatures,” *Cement and concrete research*, vol. 36, no. 10, pp. 1999–2005, 2006.
- [64] J. Xiao and G. König, “Study on concrete at high temperature in china—an overview,” *Fire safety journal*, vol. 39, no. 1, pp. 89–103, 2004.
- [65] A. Khennane and G. Baker, “Uniaxial model for concrete under variable temperature and stress,” *Journal of Engineering Mechanics*, vol. 119, no. 8, pp. 1507–1525, 1993.

- [66] T. Lie, “Fire resistance of circular steel columns filled with bar-reinforced concrete,” *Journal of structural engineering*, vol. 120, no. 5, pp. 1489–1509, 1994.
- [67] B. En, “1-2: 2004 eurocode 2: Design of concrete structures-part 1-2: General rules-structural fire design,” *European Standards, London*, 2004.
- [68] T. Lie and V. Kodur, “Thermal and mechanical properties of steel-fibre-reinforced concrete at elevated temperatures,” *Canadian Journal of Civil Engineering*, vol. 23, no. 2, pp. 511–517, 1996.
- [69] R. de Borst and P. P. Peeters, “Analysis of concrete structures under thermal loading,” *Computer methods in applied mechanics and engineering*, vol. 77, no. 3, pp. 293–310, 1989.
- [70] C. J. Pearce, C. V. Nielsen, and N. Bićanić, “Gradient enhanced thermo-mechanical damage model for concrete at high temperatures including transient thermal creep,” *International journal for numerical and analytical methods in geomechanics*, vol. 28, no. 7-8, pp. 715–735, 2004.
- [71] Q. X. Le, J. L. Torero, and V. T. Dao, “Understanding the effects of stress on the coefficient of thermal expansion,” *International Journal of Engineering Science*, vol. 141, pp. 83–94, 2019. [Online]. Available: <https://www.sciencedirect.com/science/article/pii/S0020722519303660>
- [72] M. Youssef and M. Moftah, “General stress–strain relationship for concrete at elevated temperatures,” *Engineering structures*, vol. 29, no. 10, pp. 2618–2634, 2007.
- [73] T. Gernay, “Effect of transient creep strain model on the behavior of concrete columns subjected to heating and cooling,” *Fire technology*, vol. 48, no. 2, pp. 313–329, 2012.
- [74] C. Nielsen, C. Pearce, and N. Bićanić, “Theoretical model of high temperature effects on uniaxial concrete member under elastic restraint,” *Magazine of Concrete Research*, vol. 54, no. 4, pp. 239–249, 2002.
- [75] Y.-Y. Xu and B. Wu, “Fire resistance of reinforced concrete columns with l-, t-, and +-shaped cross-sections,” *Fire Safety Journal*, vol. 44, pp. 869–880, 08 2009.
- [76] O. Bahr, P. Schaumann, B. Bollen, and J. Bracke, “Young’s modulus and poisson’s ratio of concrete at high temperatures: Experimental investigations,” *Materials & Design*, vol. 45, pp. 421–429, 2013.
- [77] V. Birtel and P. Mark, “Parameterised finite element modelling of rc beam shear failure,” in *ABAQUS users’ conference*, 2006, pp. 95–108.
- [78] J. Lubliner, J. Oliver, S. Oller, and E. Oñate, “A plastic-damage model for concrete,” *Int. J. Solids and Structures*, 1989.

- [79] J. Lee and G. L. Fenves, “Plastic-damage model for cyclic loading of concrete structures,” *Journal of engineering mechanics*, vol. 124, no. 8, pp. 892–900, 1998.
- [80] M. Smith, *ABAQUS/Standard User’s Manual, Version 6.9*. United States: Dassault Systèmes Simulia Corp, 2009.
- [81] B. En, “1-2: 2002 eurocode 1: Actions on structures—part 1-2: General actions—actions on structures exposed to fire,” *British Standards*, 1991.
- [82] S. Thelandersson, “Modeling of combined thermal and mechanical action in concrete,” *Journal of Engineering Mechanics*, vol. 113, no. 6, pp. 893–906, 1987.
- [83] Z. P. Bažant and B. H. Oh, “Crack band theory for fracture of concrete,” *Matériaux et construction*, vol. 16, no. 3, pp. 155–177, 1983.
- [84] C. T. Davie, C. J. Pearce, and N. Bićanić, “Fully coupled, hygro-thermo-mechanical sensitivity analysis of a pre-stressed concrete pressure vessel,” *Engineering Structures*, vol. 59, no. C, pp. 536–551, 2014.
- [85] A. M. Abubaker and C. T. Davie, “A generalised model for direct prediction of stresses in concrete at high temperatures,” *Magazine of Concrete Research*, pp. 1–34, 2022.